



The  
University  
Of  
Sheffield.

**Development of 2D-LC for the analysis of oligonucleotide therapeutics and their associated manufacturing impurities.**

**Christina Jayne Vanhinsbergh**

A thesis submitted in partial fulfilment of the requirements for the degree of  
Doctor of Philosophy

The University of Sheffield  
Faculty of Engineering  
Department of Chemical and Biological Engineering

Submission Date: June 2020

## Acknowledgements.

Throughout my PhD research and the writing of this thesis I have received a great deal of support and assistance. I would first like to thank my supervisor Professor Mark Dickman, for his experienced advice on disseminating my work and invaluable expertise in formulating the research strategy. I will be forever grateful for the research opportunities Mark presented to me. I would also like to thank my industrial supervisors at GSK; Dr Elliot Hook and Dr Nicola Oxby for their input into my research. Especially for supporting me during my internship at the Stevenage site, as I learned a lot about industry and the analytical environment therein. I am truly grateful for their inclusive and welcoming approach. In addition, I would like to thank the BBSRC and GSK for funding the research at the University of Sheffield and The Chromatographic Society for awarding a John Dolphin Fellowship to attend HPLC 2019.

I would like to acknowledge my research group and academic colleagues from the University of Sheffield Chemical and Biological Engineering Department, in particular Dr Caroline Evans, Dr Philip Jackson and James Grinham. Thank you for providing the opportunities to learn how to maintain and fix equipment and for your experimental collaboration. You supported me greatly and were always willing to help me.

Alongside my research I focused on developing my skills as an educator and was able to achieve Fellow status with the Higher Education Academy. I would like to thank all of the academic staff that employed me as a graduate teaching assistant or facilitator, which helped me gain teaching experience. In particular, thank you to Professor Rachel Horn for her support during my application for Fellow.

I was supported to continue with studies in my late 20's by my family and I would like to express my gratitude to them for believing in me. I would like to note that my father's encouragement to do what makes me happy is what made me think I could carry out postgraduate research, for that I am thankful to him – the *late* Stephen Vanhinsbergh. My sisters and grandparents have also been a great support; whether it was feigning interest in my work, financial assistance or an experienced mind guiding me through the scientific landscape- thanks to Rusty and Mac McIntyre, Sheila Vanhinsbergh, Kate Vanhinsbergh and Lucy Marks.

I'd also like to acknowledge my friends for their encouragement, ability to keep me grounded and happily distracted when I needed to give my mind a rest. Thank you in particular to Owen Robbins for keeping me smiling and Rebecca Braganza and Helen Rafferty for their support during my final writing up stage.

You become a small family with your academic peers during PhD research, tumbling through the good, bad, chaotic, stressful and elating periods together. I'd like to honour them in being there together and I look forward to seeing them progress in life and career. In particular I would like to recognise Dr John Howard, Josie McQuillan, Giulia Lambiase and Joanna Harley for being great friends and collaborators.

I hope I have managed to give good coverage to those that contributed to my work and mind-set during the project. There are so many more people I could thank, however, to save space I'd just like to say cheers to anyone who helped me get there. Finally, thank you for reading this work!

## **Abstract.**

Oligonucleotide (OGN) therapeutics are an emerging class of pharmaceuticals that control gene expression, splicing events and bind to target ligands. High performance liquid chromatography (HPLC) is widely used for the analysis of OGN therapeutics and their related manufacturing impurities. Two-dimensional HPLC (2D-LC) couples orthogonal separations to improve peak capacity and resolution of complex samples. The aim of this thesis was to develop 2D-LC methods for the analysis of OGN therapeutics and their manufacturing impurities, with the objective of reducing the reliance on mass spectrometry (MS) for impurity characterisation, and providing an automated method that reduces operational complexity.

OGN separations were optimised using a range of HPLC modes in conjunction with OGN models. By optimising analytical parameters, separation mechanisms were manipulated towards either size or sequence dominance. Optimised orthogonal HPLC modes were subsequently coupled to develop 2D-LC methods for the analysis of unmodified and phosphorothioated (PS) OGNs and OGN therapeutics provided by GlaxoSmithKline. 2D-LC methods were developed by studying OGN retention behaviour and orthogonality, which facilitated the design of offline and online heart-cut 2D-LC workflows. In addition, an OGN reference mapping strategy was used in conjunction with UV detection and confirmed by MS, to characterise OGNs and their impurities.

Increasing OGN chemical complexity reduced accuracy of the reference mapping approach when identifying key impurities for PS OGNs and OGN therapeutics. 2D-LC methods resolved a proportion of chemically complex OGN impurities; however, MS analysis was required for full impurity characterisation. 2D-LC methods developed in this study demonstrated improvements in peak capacity and could potentially be coupled to MS to further improve the analysis of OGN impurities by reducing the sample complexity prior to analysis.

# Table of Contents.

	<i>Page</i>
<b>Acknowledgements</b> .....	2
<b>Abstract</b> .....	3
<b>Table of Contents</b> .....	4
<b>Table of Figures</b> .....	9
<b>Figure Acknowledgements</b> .....	13
<b>Table of Tables</b> .....	14
<b>Abbreviations</b> .....	18
<b>Declaration</b> .....	20
<b>Manuscripts in preparation</b> .....	20
<b>Chapter 1: Introduction</b> .....	21
<b>1.1 Nucleic Acids</b> .....	21
<b>1.1.1 Antisense therapeutics</b> .....	22
<b>1.1.2 siRNA therapeutics</b> .....	27
<b>1.1.3 Aptamer therapeutics</b> .....	29
<b>1.1.4 Other OGN therapeutics</b> .....	30
<b>1.1.5 The OGN therapeutics market</b> .....	30
<b>1.2 OGN manufacturing</b> .....	31
<b>1.2.1 OGN solid phase synthesis</b> .....	31
<b>1.2.2 OGN chemical modifications</b> .....	32
<b>1.2.2.1 Modifications to the OGN backbone</b> .....	32
<b>1.2.2.2 Modifications to the OGN ribose</b> .....	33
<b>1.2.2.3 Modifications to the OGN bases</b> .....	35
<b>1.2.3 Impurities caused during the manufacturing process</b> .....	35
<b>1.2.4 OGN manufacturing analysis strategies</b> .....	37
<b>1.2.4.1 Regulatory governance</b> .....	37
<b>1.2.4.2 Analytical approaches for OGN physicochemical characteristics, structure and sequence</b> .....	38
<b>1.2.4.3 Analytical approaches for impurities</b> .....	39
<b>1.3 Analysis of nucleic acids using liquid chromatography</b> .....	41
<b>1.3.1 Analysis of OGNs using anion exchange liquid chromatography</b> .....	41
<b>1.3.2 Analysis of OGNs using ion-pair reversed-phase liquid chromatography</b> .....	46
<b>1.3.2.1 IP-RP HPLC analysis of nucleic acids using ‘weak’ ion-pair reagents</b> .....	48

	<b>Page</b>
1.3.2.2 IP-RP HPLC analysis of nucleic acids using ‘strong’ ion-pair reagents.....	50
1.3.2.3 IP-RP HPLC analysis of nucleic acids using acidic modifiers alongside ion-pair reagents.....	53
1.3.3 Analysis of OGNs using size exclusion liquid chromatography.....	54
1.3.4 Analysis of OGNs using mass spectrometry.....	56
1.3.5 Challenges of 1D HPLC for the analysis of OGNs- statement and summary.....	58
1.3.6 Two-dimensional HPLC.....	59
1.3.6.1 Orthogonality metrics for 2D-LC.....	61
1.3.6.2 Applications of 2D-LC.....	62
1.4 Summary of findings and project aims.....	65
1.4.1 Project aim and objectives.....	67
<b>Chapter 2: Materials and Methods.....</b>	<b>69</b>
2.1 Materials.....	69
2.1.1 Equipment and HPLC columns.....	69
2.1.2 Chemicals and reagents.....	69
2.1.3 OGN sample preparation.....	70
2.1.4 HPLC Mobile phases.....	73
2.2 HPLC analytical equipment - configurations.....	76
2.2.1 HPLC equipment- fractionation. ....	77
2.2.2 2D-LC (Configuration 1).....	79
2.2.3 HPLC data analysis.....	80
2.2.3.1 Resolution.....	80
2.2.3.2 Efficiency.....	80
2.2.3.3 Selectivity.....	81
2.2.3.4 Fractionation efficiency.....	81
2.2.4 2D-LC Orthogonality.....	82
2.3 LC-MS analysis.....	83
2.3.1 MS data analysis.....	84
<b>Chapter 3: Optimisation of size and sequence dependent separations of OGNs using HPLC.....</b>	<b>85</b>
<b>Abstract.....</b>	<b>85</b>
3.1 Introduction.....	86

<b>3.2</b> Optimisation of size and sequence based separations of OGNs using ion-pair reversed-phase HPLC.....	88
<b>3.2.1</b> Optimisation of weak ion-pair reversed-phase chromatography for analysis of OGNs .....	88
<b>3.2.1.1</b> Size dependent separations of OGNs using weak IP-RP HPLC.....	89
<b>3.2.1.2</b> Sequence dependent separations of OGNs using weak IP-RP HPLC.....	92
<b>3.2.2</b> Optimisation of strong ion-pair reversed-phase chromatography for the analysis of OGNs.....	96
<b>3.2.2.1</b> Size dependent separations of OGNs using strong IP-RP HPLC.....	96
<b>3.2.2.2</b> Sequence dependent separations of OGNs using strong IP-RP HPLC....	100
<b>3.2.3</b> Optimisation of hexafluoroisopropanol modified ion-pair reversed-phase liquid chromatography for the analysis of OGNs .....	101
<b>3.2.3.1</b> Size dependent separation of OGNs using HFIP modified IP-RP HPLC.	101
<b>3.2.3.2</b> Sequence dependent separation of OGNs using HFIP modified IP-RP HPLC .....	105
<b>3.2.4</b> Summary of work using IP-RP HPLC for OGN analysis.....	107
<b>3.3</b> Optimisation of size and sequence separations of OGNs using strong anion exchange HPLC .....	108
<b>3.3.1</b> Optimisation of strong anion exchange chromatography for the analysis of OGNs - using sodium chloride as eluotropic salt.....	108
<b>3.3.1.1</b> Size dependent separations of OGNs using SAX HPLC in conjunction with NaCl.....	109
<b>3.3.1.2</b> Sequence dependent separations of OGNs using SAX HPLC in conjunction with NaCl.....	111
<b>3.3.2</b> Optimisation of strong anion exchange for the analysis of OGNs- using sodium perchlorate as eluotropic salt.....	112
<b>3.3.2.1</b> Size dependent separations of OGNs using SAX HPLC in conjunction with NaClO <sub>4</sub> .....	112
<b>3.3.2.2</b> Sequence dependent separations of OGNs using SAX HPLC in conjunction with NaClO <sub>4</sub> .....	114
<b>3.3.3</b> Summary of work using SAX HPLC for OGN analysis.....	115
<b>3.4</b> Optimisation of size dependent separations of OGNs using size exclusion HPLC.....	115

<b>3.4.1</b> Optimisation of size dependent separations using SEC HPLC for the analysis of OGNs .....	115
<b>3.4.2</b> Summary of work using SEC HPLC for OGN analysis.....	121
<b>3.5</b> Conclusions.....	121
<b>Chapter 4: Optimisation of two-dimensional Liquid-Chromatography for the analysis of unmodified OGNs</b> .....	124
<b>Abstract</b> .....	124
<b>4.1</b> Introduction.....	125
<b>4.2</b> Analysis of OGN retention behaviour in 1D HPLC.....	126
<b>4.3</b> Orthogonality assessments of 2D-LC workflows for analysis of OGNs.....	130
<b>4.4</b> Mobile phase compatibility using 2D-LC for the analysis of OGNs.....	134
<b>4.4.1</b> Analysis of OGNs using (strong IP-RP)-(weak IP-RP) 2D-LC.....	134
<b>4.4.2</b> Analysis of OGNs using (strong IP-RP)-(SAX) 2D-LC. ....	135
<b>4.4.3</b> Analysis of peak capacity in 2D-LC analysis of OGNs.....	137
<b>4.5</b> Optimisation of offline 2D-LC and a reference mapping strategy for 2D-LC method development.....	137
<b>4.5.1</b> Offline 2D-LC of OGN test sets in conjunction with reference mapping and mass spectrometry validation.....	139
<b>4.5.1.1</b> Mass spectrometry analysis of first dimension fractions of OGNs.....	144
<b>4.6</b> Optimisation of an online heart-cut 2D-LC workflow for analysis of OGNs.....	148
<b>4.7</b> Conclusions.....	151
<b>Chapter 5: Optimisation of 2D-LC for the analysis of phosphorothioated oligonucleotides</b> .....	153
<b>Abstract</b> .....	153
<b>5.1</b> Introduction.....	154
<b>5.2</b> Analysis of PS OGN retention behaviour in 1D HPLC.....	156
<b>5.2.1</b> Orthogonality assessments of 2D-LC workflows for analysis of PS OGNs.....	162
<b>5.3</b> Mobile phase compatibility using 2D-LC for the analysis of PS OGNs.....	162
<b>5.3.1</b> Analysis of PS OGNs using (strong IP-RP)-(HFIP modified IP-RP) 2D-LC.....	165
<b>5.3.2</b> Analysis of PS OGNs using (HFIP modified IP-RP)-(strong IP-RP) 2D-LC. ....	167
<b>5.4</b> Optimisation of offline 2D-LC and a reference mapping strategy for 2D-LC method development .....	169
<b>5.4.1</b> Offline 2D-LC of PS OGN test sets in conjunction with reference mapping.....	169

	<b>Page</b>
5.4.2 Mass spectrometry analysis of first dimension fractionation of PS OGNs.....	172
5.5 Optimisation of an online heart-cut 2D-LC workflow for analysis of PS OGNs.....	176
5.6 Conclusions.....	178
<b>Chapter 6: Optimisation of two-dimensional liquid chromatography for the analysis of OGN therapeutics</b> .....	<b>180</b>
<b>Abstract</b> .....	<b>180</b>
6.1 Introduction.....	181
6.2 Analysis of OGN therapeutic retention behaviour in 1D HPLC.....	182
6.2.1 Orthogonality assessments of 2D-LC workflows.....	188
6.3 Mobile phase compatibility using 2D-LC analysis of OGN therapeutics.....	190
6.4 Optimisation of offline 2D-LC and a reference mapping strategy for 2D-LC method development .....	192
6.4.1 Offline (strong IP-RP)-(SAX) 2D-LC for the analysis of OGN therapeutics.....	192
6.4.2 Offline (HFIP modified IP-RP)-(SAX) 2D-LC for the analysis of OGN therapeutics.	197
6.5 Online heart-cut 2D-LC analysis of OGN therapeutics.....	202
6.6 Conclusions.....	208
<b>Chapter 7: Conclusions and future directions</b> .....	<b>211</b>
7.1 Summary of contribution to the field.....	211
7.2 Directions for future research.....	214
<b>Appendix 1: Methods supplements</b> .....	<b>219</b>
<b>Appendix 2: Data Supplements</b> .....	<b>221</b>
A2.1 Chapter 3 data supplements.....	221
A2.2 Chapter 4 data supplements.....	222
A2.3 Chapter 5 data supplements.....	225
A2.4 Chapter 6 data supplements.....	230
<b>Bibliography</b> .....	<b>236</b>

## Table of Figures.

	<i>Page</i>
<b>Figure 1.1:</b> Structure of DNA and RNA.....	21
<b>Figure 1.2:</b> OGN therapeutic types and function.....	23
<b>Figure 1.3:</b> Phosphoramidite solid phase synthesis of DNA OGNs showing the cyclic process of nucleotide addition to the DNA OGN polymer.....	31
<b>Figure 1.4:</b> Typical OGN chemical modifications.....	34
<b>Figure 1.5:</b> GalNAc–siRNA conjugates.....	37
<b>Figure 1.6:</b> Mechanism of retention during anion exchange chromatographic separation of OGNs.....	42
<b>Figure 1.7:</b> Mechanism of retention during ion-pair reversed-phase chromatographic separation of OGNs.....	47
<b>Figure 1.8:</b> Chemical structure of various IPRs used for the analysis of OGNs under IP-RP HPLC conditions.....	51
<b>Figure 1.9:</b> Analysis of a full PS OGN 15-mer and its related impurities using strong IP-RP HPLC.....	52
<b>Figure 1.10:</b> Mechanism of retention during HFIP modified ion-pair reversed-phase chromatographic separation of OGNs.....	53
<b>Figure 1.11:</b> Mechanism of elution during size exclusion chromatographic separation of OGNs.....	55
<b>Figure 1.12:</b> Fragmentation nomenclature of nucleic acids as described by McLuckey and Habbibi-Goudarzi [274].....	58
<b>Figure 1.13:</b> Comprehensive and heart-cut 2D-LC.....	60
<b>Figure 1.14:</b> Comprehensive (HILIC)x(IP-RP) analysis of 27 polymeric dA, dC, dT OGNs showing mass spectra of specific OGNs.....	64
<b>Figure 2.1:</b> Graphical representation of Thermo Scientific U3000 fractionation configuration.....	78
<b>Figure 2.2:</b> Graphical representation of Thermo Scientific U3000 online heart-cut 2D-LC set-up.....	79
<b>Figure 3.1:</b> Orthogonal OGN separations within a 2D-LC workflow aim to separate on a size basis or a sequence basis.....	87
<b>Figure 3.2:</b> Optimisation of flow rate and elution gradient using weak IP-RP HPLC .....	91
<b>Figure 3.3:</b> Optimisation of analysis temperature using weak IP-RP HPLC .....	94
<b>Figure 3.4:</b> Separation of PS variant OGNs using weak IP-RP HPLC .....	95
<b>Figure 3.5:</b> Strong IPR comparisons and improved chromatographic effect on full PS OGN using strong IP-RP HPLC .....	97

<b>Figure 3.6:</b> Optimisation of analysis temperature, elution gradient and stationary phase for analysis of OGNs using strong IP-RP HPLC .....	99
<b>Figure 3.7:</b> Optimisation of elution gradient and analysis temperature under HFIP modified IP-RP HPLC conditions .....	103
<b>Figure 3.8:</b> Optimised analysis of PS OGNs using HFIP modified IP-RP HPLC.....	104
<b>Figure 3.9:</b> Optimisation of HFIP modified IP-RP mobile phase for analysis of OGNs .....	106
<b>Figure 3.10:</b> Optimisation of temperature, elution gradient and mobile phase for analysis of OGNs by SAX HPLC .....	110
<b>Figure 3.11:</b> Analysis of 50 picomole sample of 16-mer PS variants using SAX HPLC in conjunction with NaCl .....	112
<b>Figure 3.12:</b> Optimisation of SAX HPLC using NaClO <sub>4</sub> as eluting salt for OGN analysis .....	113
<b>Figure 3.13:</b> Optimisation of SEC HPLC for the analysis of OGNs .....	117
<b>Figure 3.14:</b> Optimisation of flow rate for analysis of oligonucleotides using SEC HPLC .....	118
<b>Figure 3.15:</b> Optimisation of SEC HPLC mobile phase for analysis of OGNs .....	120
<b>Figure 3.16:</b> Conclusions for size or sequence based separations of OGNs using IP-RP, SAX and SEC HPLC.....	122
<b>Figure 4.1:</b> Analysis of retention behaviour of 19-22-mer size and sequence variants analysed using SAX and IP-RP HPLC.....	128
<b>Figure 4.2:</b> Comparison of OGN size verses retention time using strong IP-RP (TBuAA), weak IP-RP (TEAA), SAX (NaClO <sub>4</sub> /MeCN and HFIP modified IP-RP (TEAA:HFIP) HPLC conditions.....	129
<b>Figure 4.3:</b> 2D-LC scatter plots of normalised retention times for 2D-LC workflows.....	133
<b>Figure 4.4:</b> Offline 2D-LC feasibility analysis of OGNs using strong IP-RP HPLC to weak IP-RP or SAX HPLC.....	136
<b>Figure 4.5:</b> Offline 2D-LC using strong IP-RP to SAX HPLC to analyse test set 1.....	140
<b>Figure 4.6:</b> Offline 2D-LC using strong IP-RP to SAX HPLC to analyse test set 1.....	141
<b>Figure 4.7:</b> Offline 2D-LC using strong IP-RP to SAX HPLC to analyse test set 2.....	142
<b>Figure 4.8:</b> Offline 2D-LC using strong IP-RP to SAX HPLC to analyse 1000 picomole sample of a 20-mer unmodified oligonucleotide therapeutic and its 17-21-mer associated manufacturing impurities added at 1.5% concentration.....	143
<b>Figure 4.9:</b> Online 2D-LC analysis of OGNs using strong IP-RP to SAX HPLC.....	150
<b>Figure 5.1:</b> PS OGN structure. Comparison of phosphodiester bond with a PS bond.....	154

<b>Figure 5.2:</b> Elution order assessment of Model A PS OGN and associated impurities using SAX, strong IP-RP and HFIP modified IP-RP HPLC conditions.....	159
<b>Figure 5.3:</b> Elution order assessment of Model B PS OGN and associated impurities using SAX, strong IP-RP and HFIP modified IP-RP HPLC conditions.....	160
<b>Figure 5.4:</b> Feasibility assessment for (strong IP-RP)-(HFIP modified IP-RP) 2D-LC of PS OGNs.....	166
<b>Figure 5.5:</b> Feasibility assessment for (HFIP modified IP-RP)-(strong IP-RP) 2D-LC of PS OGNs.....	168
<b>Figure 5.6:</b> Offline HFIP modified IP-RP to strong IP-RP 2D-LC analysis of Model A and B PS OGNs.....	171
<b>Figure 5.7:</b> LC-MS analysis of model A and B PS OGN 1st dimension fractions.....	173
<b>Figure 5.8:</b> Online heart-cut HFIP modified IP-RP to strong IP-RP 2D-LC analysis of PS OGN Model A and B samples.....	177
<b>Figure 6.1:</b> Elution order assessment of the therapeutic OGN and associated impurities analysed using SAX, HFIP modified IP-RP and strong IP-RP HPLC conditions.....	185
<b>Figure 6.2:</b> Elution order assessment of the conjugated therapeutic OGN and associated impurities analysed using SAX, HFIP modified IP-RP and strong IP-RP HPLC conditions.....	187
<b>Figure 6.3:</b> Feasibility analysis- testing OGN therapeutic retention in a range of diluents using SAX HPLC conditions.....	191
<b>Figure 6.4:</b> Offline (strong IP-RP)-(SAX) 2D-LC analysis of 1000 picomole sample of the therapeutic OGN and its associated manufacturing impurities.....	193
<b>Figure 6.5:</b> Offline (strong IP-RP)-(SAX) 2D-LC analysis of 1000 picomole sample of the conjugated therapeutic OGN and its associated manufacturing impurities.....	194
<b>Figure 6.6:</b> Offline (HFIP modified IP-RP)-(SAX) 2D-LC analysis of 1000 picomole sample of the therapeutic OGN and its associated manufacturing impurities.....	199
<b>Figure 6.7:</b> Offline (HFIP modified IP-RP)-(SAX) 2D-LC analysis of 1000 picomole sample of the conjugated therapeutic OGN and its associated manufacturing impurities.....	200
<b>Figure 6.8:</b> Online heart-cut (HFIP modified IP-RP)-(SAX) 2D-LC analysis of 1000 picomole samples of OGN therapeutics and their associated manufacturing impurities.....	204
<b>Figure 6.9:</b> Online heart-cut (HFIP modified IP-RP)-(SAX) 2D-LC analysis: Zoomed view of 2nd dimension analysis of the therapeutic OGN and its associated manufacturing impurities using SAX HPLC.....	206
<b>Figure 6.10:</b> Online heart-cut (HFIP modified IP-RP)-(SAX) 2D-LC analysis: Zoomed view of 2nd dimension analysis of the conjugated therapeutic OGN and its associated manufacturing impurities using SAX HPLC.....	207

<b>Figure A2.1:</b> Weak IP-RP HPLC analysis of full PS 16-mer OGN at 30-70 °C.....	221
<b>Figure A2.2:</b> SAX HPLC analysis (using NaSCN) of 19-24-mer dT OGNs at 30-70 °C.....	221
<b>Figure A2.3:</b> Strong IP-RP HPLC analysis of 1650 picomole sample of 19-22-mer OGN size and sequence variants to calculate fractionation efficiency.....	222
<b>Figure A2.4:</b> Offline 2D-LC using strong IP-RP to SAX HPLC to analyse 1000 picomole samples of 19-22-mer size and sequence variant OGN mixture (replicate 2).....	223
<b>Figure A2.5:</b> Online 2D-LC analysis of OGNs using strong IP-RP to SAX HPLC (replicate 2).....	224
<b>Figure A2.6:</b> Minimum convex hull area of 2D-LC workflows for analysis of Model A PS OGN.....	225
<b>Figure A2.7:</b> Minimum convex hull area of 2D-LC workflows for analysis of Model B PS OGN.....	226
<b>Figure A2.8:</b> Spiking experiments analysis of PS OGNs using HFIP modified IP-RP HPLC.....	227
<b>Figure A2.9:</b> Offline HFIP modified IP-RP to strong IP-RP 2D-LC analysis of Model A and B PS OGNs (replicate 2).....	228
<b>Figure A2.10:</b> Online heart-cut HFIP modified IP-RP to strong IP-RP 2D-LC analysis of PS OGN Model A and B samples (replicate 2).....	229
<b>Figure A2.11:</b> Minimum convex hull area of 2D-LC workflows for analysis of the therapeutic OGN and its associated manufacturing impurities.....	230
<b>Figure A2.12:</b> Minimum convex hull area of 2D-LC workflows for analysis of the conjugated therapeutic OGN and its associated manufacturing impurities.....	231
<b>Figure A2.13:</b> Mass spectrometry analysis of fractions of a 1st dimension separation (fractionated under strong IP-RP HPLC conditions).....	232
<b>Figure A2.14:</b> MS analysis of fractions of the 1st dimension the therapeutic OGN separation (fractionated under HFIP modified IP-RP HPLC conditions).....	233
<b>Figure A2.15:</b> MS analysis of fractions of the 1st dimension of the therapeutic OGN-conjugate separation (fractionated under HFIP modified IP-RP HPLC conditions) .....	234
<b>Figure A2.16:</b> Offline (HFIP modified IP-RP)-(SAX) 2D-LC analysis of 1000 picomole sample of OGN therapeutics and their associated manufacturing impurities (replicate 2).....	235
<b>Figure A2.17:</b> Online heart-cut (HFIP modified IP-RP)-(SAX) 2D-LC analysis of 1000 picomole samples of OGN therapeutics and their associated manufacturing impurities (replicate 2).....	236

## Figure Acknowledgements:

**Figure 1.3:** Phosphoramidite solid phase synthesis of DNA OGNs showing the cyclic process of nucleotide addition to the DNA OGN polymer. Reprinted by author permission from MDPI: *Molecules*: Open access. *Synthesis of DNA/RNA and Their Analogs via Phosphoramidite and H-Phosphonate Chemistries –Scheme 2*. S. Roy and M. Caruthers (2013).

**Figure 1.5:** GalNAc–siRNA conjugates. Reprinted by permission from Springer: *Nature Materials*. *Delivery materials for siRNA therapeutics- Figure 6*. R. Kanasty, J. R. Dorkin, A. Vegas and D. Anderson. Copyright (2013).

**Figure 1.9:** Analysis of a full PS OGN 15-mer and its related impurities using strong IP-RP HPLC. Reprinted by author permission from Elsevier: *Journal of Chromatography A*: Open access. *Nucleic acid separations using superficially porous silica particles- Figure 6*. E.D. Close, A.O. Nwokeoji, D. Milton, K. Cook, D.M. Hindoch, E.C. Hook, H. Wood and M.J. Dickman (2016).

**Figure 1.14:** Comprehensive (HILIC)x(IP-RP) analysis of 27 polymeric dA, dC, dT OGNs showing mass spectra of specific OGNs. Reprinted by permission from Elsevier: *Journal of Chromatography A*. *Comprehensive hydrophilic interaction and ion-pair reversed-phase liquid chromatography for analysis of di- to deca-oligonucleotides- Figure 5*. Q. Li, F. Lynen, J. Wang, H. Li, G. Xu and P. Sandra. Copyright (2012).

## Table of Tables.

	<i>Page</i>
<b>Table 1.1:</b> ASO therapeutics being used in phase I to phase III clinical trials and registered ASO therapeutics.....	25
<b>Table 1.1 continued...:</b> ASO therapeutics being used in phase I to phase III clinical trials and registered ASO therapeutics .....	26
<b>Table 1.2:</b> siRNA therapeutics being used in phase I to phase III clinical trials and registered siRNA therapeutics .....	28
<b>Table 1.3:</b> Aptamer therapeutics being used in phase I to phase III clinical trials and registered Aptamer therapeutics .....	29
<b>Table 1.4:</b> Nomenclature of multidimensional liquid chromatography terms [281, 282].....	60
<b>Table 2.1:</b> Equipment and HPLC columns.....	69
<b>Table 2.2:</b> Chemical and reagents.....	69
<b>Table 2.2 continued...:</b> Chemical and reagents.....	70
<b>Table 2.3:</b> Model OGNs used for evaluation of size and sequence dependent separations in Chapter 3. OGNs are described by size in nucleotide length (nt), sequence and monoisotopic mass .....	71
<b>Table 2.4:</b> Unmodified OGNs utilised for 2D-LC method development in Chapter 4. Size/sequence variant OGNs and 1st generation model OGN therapeutic and its associated manufacturing impurities are described by impurity type, size in nucleotide length (nt), OGN sequence and monoisotopic mass.....	71
<b>Table 2.4 continued...:</b> Unmodified OGNs utilised for 2D-LC method development in Chapter 4. Size/sequence variant OGNs and 1st generation model OGN therapeutic and its associated manufacturing impurities are described by impurity type, size in nucleotide length (nt), OGN sequence and monoisotopic mass. ....	72
<b>Table 2.5:</b> Phosphorothioated OGNs utilised for 2D-LC method development in Chapter 5. Model A and B OGNs are two fully phosphorothioated OGN sequences and their associated manufacturing impurities are described by size in nucleotide length (nt), OGN sequence and monoisotopic mass. ....	72
<b>Table 2.6:</b> Therapeutic OGNs utilised for 2D-LC method development in Chapter 6. Unconjugated and conjugated OGNs are two fully phosphorothioated OGN sequences (with additional 2'-O-MOE modifications) and their associated manufacturing impurities are described by size in nucleotide length (nt), OGN sequence and mass by manufacturing certificate of analysis specification. ....	73
<b>Table 2.7:</b> HPLC mobile phases used for optimisation of HPLC analysis of OGNs.....	75
<b>Table 3.1:</b> Characteristics of DNAPac RP and Accucore C18 columns.....	89

<b>Table 3.2:</b> Model OGNs used for evaluation of size and sequence dependent separations. OGNs are described by size in nucleotide length (nt), sequence and monoisotopic mass. ....	90
<b>Table 3.3:</b> Comparison of stationary phases DNAPac and Accucore C18 under two gradients and two analysis temperatures.....	100
<b>Table 3.4:</b> Characteristics of the DNAPac PA 200 Rs column.....	109
<b>Table 3.5:</b> Characteristics of Advance BioSEC column.....	116
<b>Table 3.6:</b> Estimations of orthogonal modes of chromatography for analysis of OGNs.....	123
<b>Table 4.1:</b> Optimised chromatographic conditions employed for 1D HPLC analysis and sequential retention behaviour assessment of size and sequence variant OGNs.....	126
<b>Table 4.2:</b> Unmodified OGNs utilised for 2D-LC method development. Size/sequence variant OGNs and 1st generation model OGN therapeutic and its associated manufacturing impurities are described by impurity type, size in nucleotide length (nt), OGN sequence and monoisotopic mass. ....	127
<b>Table 4.3:</b> Normalised retention values for 1D HPLC analyses of size and sequence variants in a range of chromatographic modes.....	131
<b>Table 4.4:</b> Orthogonality of each 2D-LC workflow analysed using the bin counting method and the minimum convex hull method.....	132
<b>Table 4.5:</b> OGNs used for Test set 1 (size and sequence variant OGNs).....	138
<b>Table 4.6:</b> OGNs used for Test set 2 (size and sequence variant OGNs).....	138
<b>Table 4.7:</b> OGNs used for first generation OGN therapeutic model set (with manufacturing N-x/N+1 impurities).....	138
<b>Table 4.8:</b> LC-MS identification of OGN masses in each fraction of the 1 <sup>st</sup> dimension analysis of test set 1.....	145
<b>Table 4.9:</b> LC-MS identification of OGN masses in each fraction of the 1 <sup>st</sup> dimension analysis of test set 2.....	146
<b>Table 4.10:</b> LC-MS identification of OGN masses within each fraction of the 1 <sup>st</sup> dimension analysis. Sample of the 1 <sup>st</sup> generation (unmodified) OGN and manufacturing N-x/N+1 impurities at 94% and added 1.5% total sample concentration respectively.....	147
<b>Table 5.1:</b> Optimised chromatographic conditions employed for 1D HPLC analysis and sequential retention behaviour assessment of PS OGNs.....	156
<b>Table 5.2:</b> Fully phosphorothioated model A OGN and its associated manufacturing impurities described by size in nucleotide length (nt), OGN sequence and monoisotopic mass. ....	157

<b>Table 5.3:</b> Fully phosphorothioated model B OGN and its associated manufacturing impurities described by size in nucleotide length (nt), OGN sequence and monoisotopic mass .....	157
<b>Table 5.4:</b> Analysis of PWHH, nc, resolution and selectivity for separations of model A and B sample sets under SAX, strong IP-RP and HFIP modified IP-RP HPLC.....	161
<b>Table 5.5:</b> Orthogonality measurements for OGNs of Model Set A and B using the bin counting and minimum convex hull methods.....	163
<b>Table 5.6:</b> LC-MS identification of OGN masses within each fraction of the 1 <sup>st</sup> dimension analysis of PS OGN Model A and its associated manufacturing impurities added at 1.5% total sample concentration.....	175
<b>Table 5.7:</b> LC-MS identification of OGN masses within each fraction of the 1 <sup>st</sup> dimension analysis of PS OGN Model B and its associated manufacturing impurities added at 1.5% total sample concentration.....	175
<b>Table 6.1:</b> Optimised chromatographic conditions employed for 1D HPLC analysis and sequential retention behaviour assessment of OGN therapeutics.....	183
<b>Table 6.2:</b> Unconjugated therapeutic OGN and its associated manufacturing impurities are fully phosphorothioated OGN sequences (with additional 2'-O-MOE modifications) -described by OGN/impurity type and mass by manufacturing certificate of analysis specification .....	183
<b>Table 6.3:</b> GalNAc conjugated therapeutic OGN and its associated manufacturing impurities are fully phosphorothioated OGN sequences (with additional 2'-O-MOE modifications) -described by OGN/impurity type and mass by manufacturing certificate of analysis specification. ....	183
<b>Table 6.4:</b> Resolution between the FLP therapeutic OGN and its associated manufacturing impurities in SAX, strong IP-RP (using TBUAA) and HFIP modified IP-RP (using TEAA:HFIP) HPLC.....	184
<b>Table 6.5:</b> Resolution between the FLP of the therapeutic OGN-conjugate and its associated manufacturing impurities in SAX, strong IP-RP (using TBUAA) and HFIP modified IP-RP (using TEAA:HFIP) HPLC.....	188
<b>Table 6.6:</b> Orthogonality analysis of potential mode couplings in 2D-LC by minimum convex hull method: OGN therapeutic sample sets.....	188
<b>Table 6.7:</b> LC-MS identification OGN masses within each fraction of the 1 <sup>st</sup> dimension analysis (strong IP-RP HPLC) of the therapeutic OGN and its associated manufacturing impurities added at 1.5% total sample concentration .....	196

<b>Table 6.8:</b> LC-MS identification OGN masses within each fraction of the 1st dimension analysis (strong IP-RP HPLC) of the conjugated therapeutic OGN and its associated manufacturing impurities added at 1.5% total sample concentration.....	197
<b>Table 6.9:</b> LC-MS identification OGN masses within each fraction of the 1st dimension analysis (HFIP modified IP-RP HPLC) of the therapeutic OGN and its associated manufacturing impurities added at 1.5% total sample concentration. ....	201
<b>Table 6.10:</b> LC-MS identification OGN masses within each fraction of the 1st dimension analysis (HFIP modified IP-RP HPLC) of the conjugated therapeutic OGN and its associated manufacturing impurities added at 1.5% total sample concentration. ....	202
<b>Table A1.1:</b> Coefficient of peak area and retention time for HPLC columns.....	219
<b>Table A1.2:</b> Table A1.2: 2D-LC fraction sampling parameters between the 1st and second dimension separations.....	220
<b>Table A2.1:</b> Quality control calculations for fractionation efficiency and analysed fraction amount.....	222

## Abbreviations.

1D-LC	One-dimensional liquid chromatography	EDTA	Ethylenediaminetetraacetic acid
<sup>1</sup> D	First dimension separation	ESI-MS	Electrospray-ionisation Mass spectrometry
<sup>2</sup> D	Second dimension separation	F	Fluoro modification
2D-LC	Two-dimensional liquid chromatography	F <sub>coverage</sub>	Coverage of the separation space
5'-1	Shortmer impurity	FLP	Full length product
5'-2	Shortmer impurity	g	Grams
5'-3	Shortmer impurity	G	Guanine
α	Selectivity	GalNac	N-Acetylgalactosamine
A	Adenine	GCxGC	Comprehensive two dimensional gas chromatography
Abasic	Base loss impurity	GSK	GlaxoSmithKline
AC	Affinity chromatography	H <sub>12</sub> N <sub>3</sub> O <sub>4</sub> P	Ammonium phosphate
AEX	Anion exchange chromatography	HA	Hexylamine
ASO(s)	Antisense oligonucleotide(s)	HCL	Hydrochloric acid
BDMA	Butyldimethylamine	HFIP	Hexafluoroisopropanol
Bin	Portion of separation space	HFMIIP	Hexafluoromethylisopropanol
C	Cytosine	HIC	Hydrophobic interaction chromatography
CEX	Cation exchange chromatography	HILIC	Hydrophilic interaction chromatography
CID	Collision induced dissociation	HPLC	High performance liquid chromatography
CGE	Capillary gel electrophoresis	IPA	Isopropanol
°C	Degrees Celsius	IPR	Ion-pair reagent
Da	Daltons	IP-RP	Ion-pair reversed-phase chromatography
DEA	Diethylamine	KCL	Potassium chloride
DIPEA	Diisopropylethylamine	LCXGC	Two dimensional liquid chromatography-gas chromatography
DMBA	Dimethylbutylamine	LCxLC	Comprehensive 2D-LC
DMCHA	Dimethylcyclohexylamine		
DNA	Deoxyribonucleic acid		
Σ	Total or Sum		

LC-LC	Heart-cut 2D-LC	N-x	Shortmer impurity
LC-MS	Liquid chromatography mass spectrometry	N+x	Longmer impurity
LCXSFC	Two dimensional liquid chromatography-supercritical fluid chromatography	N [+o]	Addition of oxygen
LNA	Locked nucleic acid	N [+S-O]	Removal of oxygen, addition of sulphur
MALDI	Matrix assisted lazer desorption ionisation	nt	Oligonucleotide length in nucleotides
mAU	Milli absorbance units	n <sub>T</sub>	Total peak capacity
MeCN	Acetonitrile	OGN(s)	Oligonucleotide(s)
MeOH	Methanol	O-Me	Methoxy modification
min	Minutes	PA	Propylamine
miRNA	Micro RNA	Pmax	Maximal peak capacity
mL	Millilitre	P=O	Oxidated impurity
mM	Millimole	PS	Phosphorothioate
MMT	Monomethoxytrityl	PWHH	Peak width at half apex height
MOE	Methoxyethyl	QC	Quality Control
MS	Mass spectrometry	Q-TOF	Quadrupole time of flight hybrid
MS/MS	Tandem mass spectrometry	R <sup>2</sup>	Coefficient of determination
m/z	Mass to charge ratio	RISC	RNA induced silencing complex
N-1	Shortmer impurity	RNA	Ribonucleic acid
N-2	Shortmer impurity	Rp	PS diastereoisomer conformation
N-3	Shortmer impurity	RP	Reversed phase chromatography
N+1	Longmer impurity	Rs	Resolution
Na	Sodium	Rt0	Injection peak
NaCl	Sodium chloride	Rt	Retention time
NaClO <sub>4</sub>	Sodium perchlorate	Rt <sub>cur.pk</sub>	Retention time of current peak
NaH <sub>2</sub> PO <sub>4</sub>	Monosodium phosphate	Rti (norm)	Normalised retention time
NaOH	Sodium hydroxide	Rt min	Minimum retention time
NaSCN	Sodium thiocyanate	Rt max	Maximum retention time
n <sub>c</sub>	Peak capacity	Rt <sub>ref.peak</sub>	Retention time of a reference peak
NMR	Nuclear magnetic resonance	SAX	Strong anion exchange chromatography
NP	Normal phase chromatography		

SEC	Size exclusion chromatography	TEAA	Triethylammonium acetate
SFC	Supercritical fluid chromatography	tetBAA	Tetrabutylammonium acetate
siRNA	Short interfering RNA	tetBAB	Tetrabutylammonium bromide
SMD	Spinal Muscular Dystrophy	T <sub>g</sub>	Time of gradient
SMN1	Survival motor neurone gene 1	T <sub>m</sub>	Melting temperature
SMN2	Survival motor neurone gene 2	Tris	Tris (hydroxymethyl) aminomethane
Sp	PS diastereoisomer conformation	U	Uracil
SSO(s)	Splice switching oligonucleotide(s)	UHPLC	Ultrahigh performance liquid chromatography
T	Thymine	UHR	Ultra high resolution
TBA	Tributylamine	v/v	Volume by volume
TBuAA	Tributylammonium acetate	W	Peak width (at base)
TEA	Triethylamine	WAX	Weak anion exchange chromatography

## Declaration.

*I, the author, confirm that the Thesis is my own work. I am aware of the University's Guidance on the Use of Unfair Means ([www.sheffield.ac.uk/ssid/unfair-means](http://www.sheffield.ac.uk/ssid/unfair-means)). This work has not been previously been presented for an award at this, or any other, university.*

## Manuscripts in preparation.

- Vanhinsbergh. C.J, Oxby. N, Hook. E & Dickman. M (2020). *Optimization of 1D and 2D HPLC for analysis of oligonucleotides and their manufacturing impurities*. In preparation: Intended for submission to Journal of Chromatography A.
- Vanhinsbergh. C.J, Oxby. N, Hook. E & Dickman. M (2020). *Development of targeted 2D-HPLC methods for the analysis of phosphorothioated oligonucleotides and their manufacturing impurities*. In preparation: Intended for submission to Journal of Chromatography A.

# Chapter 1: Introduction.

## 1.1 Nucleic Acids.

In biology, nucleic acids are the chemical structures responsible for coding for life. The code they contain serves to translate into functional molecules within all biological lifeforms. Typically DNA is found within the nucleus of every cell and RNA is the transcript of the DNA code that is used for translation into proteins and construction of other molecules required for life. The DNA within the nucleus is segregated into 46 chromosomes with vast lengths of nucleic acid in each chromosome. All nucleic acids have a backbone structure formed of phosphodiester bonds between nucleotide monomer units. Nucleotides consist of a base (either a purine or a pyrimidine) and a ribofuranose sugar. The hydroxylation status of the 2' carbon of the ribofuranose gives the designation of deoxyribonucleic acid (DNA) or ribonucleic acid (RNA). In RNA the 2' carbon is hydroxylated. In addition, the pyrimidine thymine is only found in DNA and uracil is only found in RNA (see Figure 1.1). Double stranded nucleic acids contain complementary hydrogen bonding between purines and pyrimidines (adenine or guanine and cytosine or thymine or uracil) of opposite single stranded chains. Complementary hydrogen bonding is of the order guanine to cytosine and adenine to either thymine or uracil [1].

Oligonucleotides (OGNs) are small polymers of nucleotide monomers. Their chemistry is identical to all nucleic acids in that they participate in complementary hybridization between purines and pyrimidines, which can give rise to double stranded oligonucleotides in addition to single stranded molecules [1].

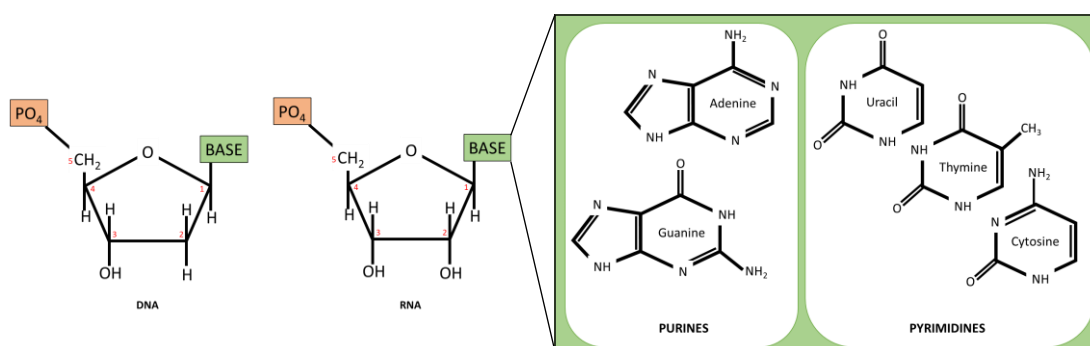


**Figure 1.1: Structure of DNA and RNA.** Showing ribose structure for RNA and DNA with chemical structures for purine and pyrimidine bases (adenine/guanine and uracil/thymine/cytosine respectively).

OGNs are commonly synthesized within the laboratory and can be used for a range of applications, such as assay probes, nucleic acid sequencing, genotyping, reference ladders, polymerase chain reaction primers, gene editing tools or use within microarray and molecular biology assays [2-10]. In addition, OGNs have also been used as pharmaceutical drugs, which are termed 'oligonucleotide therapeutics' that control gene expression, bind to ligands and stimulate the immune system [11].

The term OGN therapeutic covers a wide range of types of OGN structure and function. These OGNs include antisense OGNs, siRNAs, aptamers, splice-switching OGNs, antagomirs and immunoregulatory OGNs, among others [12]. The OGN therapeutic industry has been active for around 3 decades with modest progress in regulatory approvals until recent years [13]. Their potential was originally inferred from observations that antisense OGN sequences could inhibit mRNA translation and endogenous OGNs could affect gene expression in *C.elegans* by facilitating mRNA degradative pathways [14-16] (see Figure 1.2). Oligonucleotide therapeutics target specific gene transcripts and therefore are a form of precision medicine, where therapeutic OGNs can be tailored for multiple conditions or pathologies. This precise nature increases the probability of obtaining higher drug efficacy due to the potential reduction in off target effect. This targeted nature will no doubt be capitalised upon further as personalised medical treatments become more commonplace.

### **1.1.1 Antisense therapeutics.**

Most historical genetic therapies have focused on the alteration of gene expression using viral vectors to reduce disease phenotypes. This genome alteration approach remains bereft of challenges with safety, germ line effects and insertional mutagenesis [17]. More recently, targeted gene editing techniques using the CRISPR/Cas system have been discovered [18]. For the purposes of this work, CRISPR oligonucleotides will not be classified under the 'therapeutic oligonucleotide' umbrella term because they are gene editing tools, whereas oligonucleotide therapeutics alter expression without altering genomic sequence. In addition, exogenous mRNA can be introduced into the cellular environment to facilitate or upregulate protein production and act as a vaccine [19]. Although mRNA therapeutics are classified under the term 'oligonucleotide therapeutic', they are not considered within this research using smaller oligonucleotide therapeutic analytes (<100 base pairs or nucleotides in length). This is due to large differences in mRNA molecular weight and chemistry in comparison to smaller oligonucleotide therapeutics, which alters its chromatographic

behaviour in comparison to shorter oligonucleotide therapeutics. The mRNA transcript possesses higher accessibility than genomic DNA within the cell as it is not limited to containment within the nucleus. It serves as an accessible molecule for therapeutic manipulation of protein translation.

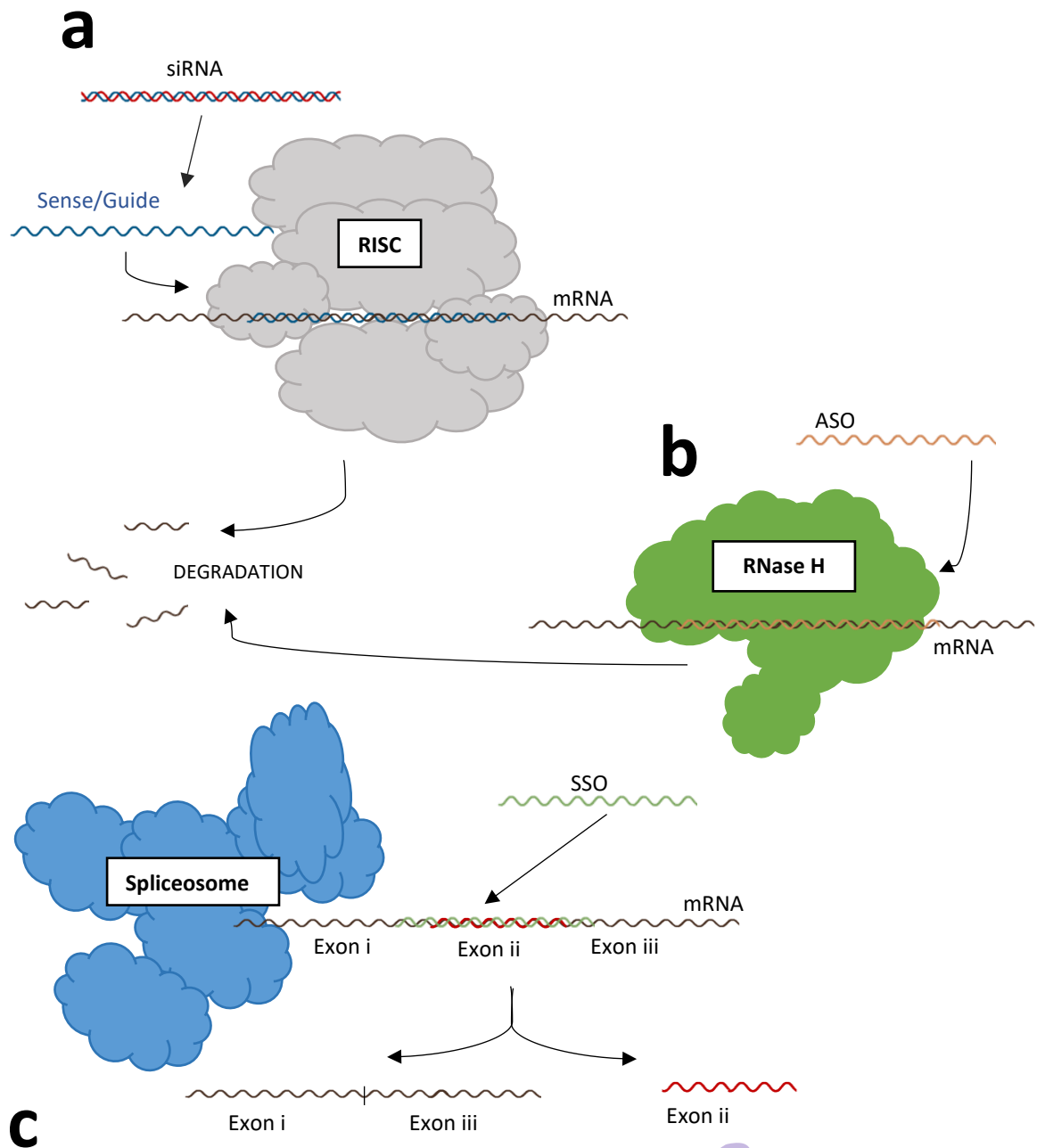
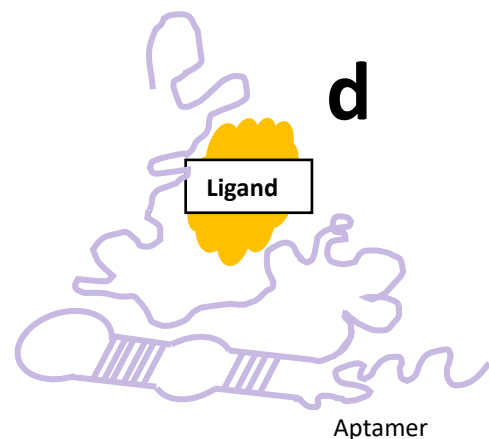


**Figure 1.2: OGN therapeutic types and function.** **a:** siRNA- the sense strand is loaded into the RNA induced silencing complex (RISC) and facilitates mRNA degradation. **b:** ASOs complementarily hybridize with mRNA to facilitate enzymatic degradation by RNase H. **c:** SSO's hybridize to target exons to facilitate alternative splicing pathways. **d:** Aptamers exhibit a 3D conformation to enable their binding to target ligands.



Antisense oligonucleotides (ASOs) are short (19-21-mers) single stranded nucleic acids that facilitate direct enzymatic degradation of mRNA and thus prevent disease associated proteins from being translated. First identified within the 1970's to inhibit viral protein translation [15], ASOs are of complementary sequence to an mRNA transcript and hybridize directly to it. Although the modern ASO is chemically modified to improve its own resistance to enzymatic degradation [20], it allows Ribonuclease H to cleave the duplex of mRNA-ASO (see Figure 1.2b). In an alternative strategy, some ASOs physically block protein translation due to chemically modified elements of their structure blocking ribosomes from accessing the mRNA transcript [21] (see Figure 1.2b). The first ASO to be developed and approved in the pharmaceutical market was Fomivirsen in 1998, which targeted cytomegalovirus retinitis in individuals with compromised immune systems, such as those with HIV [11, 15, 22].

More recently, splice switching OGNs (SSOs) were developed to interrupt protein translation and splicing events. These therapeutics aim to reduce net production of aberrant splice variants that cause disease phenotypes or produce substitute proteins where gene deletions lead to downregulation of expression [23, 24] (see Figure 1.2 c). Gene mutation and deletions create exon deletions and reading-frame shifts that prevent translation of functional proteins. An example of this is in individuals with spinal muscular atrophy (SMD) where mutations prevent production of motor neuron gene 1 (SMN1). An SSO (Spinraza®) was developed to complex with the mRNA transcript and alter the splicing of a paralogous gene (SMN2) to produce a near identical copy of the SMN1 protein [25]. The most recent approval of a SSO was for Golodirsen (Vyondys 53™), which is a phosphorodiamidate morpholino OGN. Golodirsen directs the splicosome to skip exon 53 of the dystrophin gene to produce an alternative form of dystrophin protein for the treatment of Duchenne muscular dystrophy [26].

One SSO has been used for personalised medicine to treat Batten disease. Named in honour of its target patient – Mila Makovec; Milasen targets a genetic mutation in Mila that results in the fatal neurodegenerative condition. Using genetic sequencing, a novel retrotransposon insertion site was located and linked to abnormal splicing of exon 6 of the MFSD8 gene into a cryptic splice acceptor site. 22-mer Milasen SSO targets the site to correct splicing of the MFSD8 gene [27]. It is the first example of an 'n-of-1' OGN therapy.

Challenges presented within ASO treatments are linked to delivery, stability and immunogenicity [12, 28, 29]. Improved delivery strategies include the conjugation to cell penetrating peptides, receptor ligands and GalNAc molecules [30-32], or modification of the 2' carbon of ribose units to facilitate uptake by cell membrane proteins [33]. There are more approved antisense therapies than

other types of therapeutic OGNs and clinical trials have focussed on treating diseases such as amyloidosis, cancers, Huntington’s disease and cystic fibrosis. Current approved antisense oligonucleotides are shown in Table 1.1 alongside selected clinical trials in various stages.

**Table 1.1: ASO therapeutics being used in phase I to phase III clinical trials and registered ASO therapeutics.**

<b>Antisense or splice switching Drug</b>	<b>Organisation</b>	<b>Medical Condition</b>	<b>Clinical Trial Phase</b>
IGF-1R/AS ODN	Thomas Jefferson University & Imvax	Malignant glioma	<b>1</b>
BP1002	Bio-Path Holdings, Inc	Advanced lymphoid malignancies	
ISTH0036	Isarna Therapeutics GmbH	Primary open angle glaucoma	
c-myb AS ODN	University of Pennsylvania	Hematologic malignancies	
ISIS 113715	Ionis Pharmaceuticals, Inc	Type 2 diabetes mellitus	
OGX-427	Vancouver Coastal Health	Bladder cancer	
QR-010	ProQR Therapeutics	Cystic fibrosis	
AVI-6002	Sarepta Therapeutics, Inc	Ebola hemorrhagic fever	
WVE-210201	Wave Life Sciences Ltd	Duchenne muscular dystrophy	
AVI-6003	Sarepta Therapeutics, Inc	Marburg hemorrhagic fever	
ION352	Astrazeneca	Kidney disease	
EGFR Antisense DNA	The University of Texas Health Science Center at San Antonio	Head and neck Cancer	<b>2</b>
G3139 - Oblimersen	University of Chicago & National Cancer Institute	Lung cancer, recurrent renal cell cancer and B-cell non-Hodgkin's lymphoma	
AVI-4658 (PMO)	Sarepta Therapeutics & Imperial College London	Duchenne muscular dystrophy	
IONIS-AGT-LRx	Ionis Pharmaceuticals, Inc	Mild hypertension	
BP1001	Bio-Path Holdings, Inc	Chronic myelogenous leukemia, Ph1-positive acute myeloid leukemia & myelodysplastic syndrome	
SPC2996	Santaris Pharma A/S	Chronic lymphocytic leukemia	
AP 12009	Isarna Therapeutics GmbH	Glioblastoma & anaplastic astrocytoma	
QR-421a	ProQR Therapeutics	Retinitis pigmentosa	
ISIS 104838	Ionis Pharmaceuticals, Inc	Rheumatoid arthritis	
Alicaforsen	Ionis Pharmaceuticals, Inc	Chrohn’s disease	
Genasense	Genta Incorporated	Chronic lymphocytic leukemia	
Lucanix	NovaRx Corporation	Lung neoplasm	
IONIS-STAT3Rx	Ionis Pharmaceuticals, Inc & AstraZeneca	Advanced cancers	
IONIS-PKK-LRx	Ionis Pharmaceuticals, Inc	Hereditary angioedema	
SB012	Sterna Biologicals GmbH & Co. KG	Ulcerative colitis	

Table 1.1 continued...: ASO therapeutics being used in phase I to phase III clinical trials and registered ASO therapeutics.

<b>Antisense or splice switching Drug</b>	<b>Organisation</b>	<b>Medical Condition</b>	<b>Clinical Trial Phase</b>
SB010	Sterna Biologicals GmbH & Co. KG	Asthma	<b>2</b>
GTX-102	GeneTX Biotherapeutics, LLC	Angelman syndrome	
WVE-120101	Wave Life Sciences Ltd	Huntington's disease	
Miravirsen	Santaris Pharma A/S	Hepatitis C	
DS-5141b	Daiichi Sankyo Co., Ltd	Duchenne muscular dystrophy	
QR-1123	ProQR Therapeutics	Autosomal dominant retinitis pigmentosa	
IONIS-MAPT-RX	Ionis Pharmaceuticals, Inc and Biogen	Alzheimers disease	
IONIS-ENAC-2.5RX	Ionis Pharmaceuticals, Inc	Cystic fibrosis	
Alicaforsen	Ionis Pharmaceuticals, Inc and Atlantic, Inc	Ulcerative Colitis	<b>3</b>
G3139-Oblimersen	National Cancer Institute (NCI)	Acute myeloid leukemia and melanoma	
ISIS 3521	Ionis Pharmaceuticals, Inc	Lung cancer	
RG6042	Hoffmann-La Roche	Huntingtons disease	
QR-110	ProQR Therapeutics	Leber's congenital amaurosis	
Tominersen	Ionis Pharmaceuticals, Inc & Roche	Huntingtons disease	
Tofersen	Ionis Pharmaceuticals, Inc & Biogen	Amyotrophic lateral sclerosis	
AKCEA-TTR-LRX	Ionis Pharmaceuticals, Inc & Akcea Therapeutics	ATTR amyloidosis	
AKCEA-APO(a)	Ionis Pharmaceuticals, Inc, Novartis & Akcea Therapeutics	Apolipoprotein(a) in cardiovascular disease	<b>Registered</b>
Formivisiren-Vitravene	Novartis Ophthalmics Europe Ltd	Cytomegalovirus retinitis	
Mipomersen-Kynamro	Ludwig-Maximilians - University of Munich	Hypercholesterolemia	
Exondys 51 - Eteplirsen	Sarepta therapeutics	Duchenne muscular dystrophy	
Spinraza - Nusinersen	Biogen	Spinal muscular dystropy	
Inotersen-Tegsedi	Akcea Therapeutics	Amyloidosis	
Aganirsen	Gene Signal SAS	Ischaemic central retinal vein occlusion & neovascular glaucoma	
Viltolarsen - Viltepso	NS Pharma Inc	Duchenne muscular dystrophy	
Milasen	Boston Children's Hospital	Batten Disease n-of-1	
Vyvondys 53-Golodirsen	Sarepta therapeutics	Duchenne muscular dystrophy	

### 1.1.2 siRNA therapeutics.

In the 1990's Fire and Mellow *et al.* discovered that mRNA could be targeted with double stranded RNA to manipulate gene expression by RNA interference. A complementary strand (sense) and homologous strand (antisense) duplex reduced unc-22 translation in *C. elegans* [14]. The approach has been further understood and developed for use in humans over the past three decades [34-36]. Alteration of gene expression functions via an mRNA degradative pathway involving the RNA induced silencing complex (RISC). The RISC is a small group of proteins that can enzymatically digest a target mRNA molecule. Small interfering RNA oligonucleotides or siRNAs are short duplex OGNs that associate within the RISC by loading the sense strand into it. The loaded strand is complementary to a specific mRNA sequence and so binds the mRNA within the RISC where it is finally digested by Argonaut 2 endonuclease [37] (see Figure 1.2 a).

Clinical trials involving siRNAs have been challenged with issues of immunogenicity, target cell delivery and stability *in vivo*; however, chemical modification of the OGN has facilitated better functionality [12], which is explained later in section 1.2.2. The inherent negative charge and high molecular weight of siRNAs inhibits cellular uptake [38]. Strategies to overcome these challenges have involved encasing the drug in a cationic lipid nanoparticle that promotes endocytosis [38, 39] or conjugation to cholesterol to facilitate cellular targeting [40]. Other strategies include embedding targeting ligands into conjugate molecules such as cyclodextrin based polymers and conjugation to aptamers [41, 42].

In 2018, the first siRNA drug was approved- Patisiran [43]. The pharmaceutical targets hereditary transthyretin amyloidosis by downregulating the production of transthyretin in the liver and thus decreasing the rate of amyloid deposition. The drug product Onpattro® is delivered using liposomes for hepatic targeting [44]. The recent approvals of other siRNA drugs, such as Givosiran and Lumasiran (for hepatic porphyria and primary hyperoxaluria respectively) shows that development scientists are overcoming some of the challenges presented within early clinical trials and gives promise to the future of the industry. Current clinical trials are focusing on treatments for a range of conditions such as ocular or skin diseases, kidney and liver disorders, cancer and hepatitis (see Table 1.2 for selected clinical trials).

**Table 1.2: siRNA therapeutics being used in phase I to phase III clinical trials and registered siRNA therapeutics.**

siRNA Drug	Organisation	Medical Condition	Clinical Trial Phase
TD101	Transderm, Inc	Pachyonychia congenita	1
AGN211745	Allergan and Sirna Therapeutics, Inc	Age-related macular degeneration	
Atu027	Silence Therapeutics GmbH	Advanced solid tumours	
siRNA-transfected peripheral blood mononuclear cells APN401	Wake Forest University Health Sciences	Melanoma, kidney or pancreatic cancer	
SLN124	Silence Therapeutics plc	Non-transfusion-dependent $\beta$ -thalassaemia and low risk myelodysplastic syndrome	
DCR-HBVS	Dicerna Pharmaceuticals, Inc	Hepatitis B, chronic	
Cemdisiran	Alnylam pharmaceuticals	Complement mediated diseases	
AGN211745	Allergan and Sirna Therapeutics, Inc	Choroidal neovascularization	2
Cand5	OPKO Health, Inc	Diabetic macular edema & macular degeneration	
STP705	Sirnaomics	Hypertrophic scar	
AMG 890	Amgen	Cardiovascular disease-lipoprotein(a)	
PF-04523655	Quark Pharmaceuticals	Choroidal neovascularization, diabetic retinopathy & diabetic macular edema	
OLX10010	Olix Pharmaceuticals, Inc	Scars	
SYL040012	Sylentis	Glaucoma	
ARO-ANG3	Arrowhead pharmaceuticals	Dyslipidemia	
JNJ-3989	Janssen	Hepatitis B	
Fitusiran	Alnylam Pharmaceuticals	Haemophilia and rare bleeding disorders	
Vutrisiran	Alnylam Pharmaceuticals	ATTR amyloidosis	3+
SYL1001-Tivasiran	Sylentis	Dry eye disease	
QPI-1007	Quark Pharmaceuticals	Optic atrophy & non-arteritic anterior ischemic optic neuropathy	
Inclisiran	Novartis	Homozygous familial hypercholesterolemia	
DCR-PHXC (Nedosiran)	Dicerna Pharmaceuticals, Inc	Primary hyperoxaluria	
QPI-1002	Quark Pharmaceuticals	Acute kidney injury & delayed graft function.	
Patisiran (Onpattro)	Alnylam Pharmaceuticals	Hereditary ATTR amyloidosis	Registered
Givosiran (Givlaari)	Alnylam Pharmaceuticals	Acute hepatic porphyria	
Lumasiran	Alnylam Pharmaceuticals	Primary hyperoxaluria	

### 1.1.3 Aptamer therapeutics.

By selective engineering, the sequence of an OGN can be utilised to participate in the overall 3D conformation of the molecule. Aptamers are OGNs that have a conformational 3D shape and interact with ligands according to their conformation. Those conformations that can specifically bind to a target are selected from a pool of randomised OGNs [45]. They bind to antigens, such as small molecules or proteins to function in a multitude of ways (see Figure 1.2 d). Aptamers have shown promise functioning as molecular biosensors [46], diagnostics for medical imaging [47], delivery molecules [42] and therapeutics [48]. Aptamers in some contexts are easier to produce due to a low variation between manufactured batches (in comparison to biological ligands such as antibodies). In addition, they are easier to chemically modify due to the synthetic synthesis process providing more control over molecule chemistry in comparison to production within a cellular environment (that may yield higher product molecule heterogeneity) [48]. There is only one approved drug on the market (Pegaptanib), which treats age-related macular degeneration by targeting vascular endothelial growth factor to reduce angiogenesis [49]. There is significant interest in developing new aptamers that treat ocular conditions (see Table 1.3 for a selection of clinical trials).

**Table 1.3: Aptamer therapeutics being used in phase I to phase III clinical trials and registered Aptamer therapeutics.**

<b>Aptamer Drug</b>	<b>Organisation</b>	<b>Medical Condition</b>	<b>Clinical Trial Phase</b>
REG1	National Heart, Lung, and Blood Institute	Blood anticoagulation	1
ARC19499	Baxalta now part of Shire	Hemophilia	
NOX-E36	NOXXON Pharma AG	Chronic inflammatory diseases, type 2 diabetes mellitus & systemic lupus erythematosus	2
Fovista	Ophthotech Corporation	Age-related macular degeneration	
ARC1779	Archemix Corp	Von Willebrand disease	
NOX-A12	NOXXON Pharma AG	Autologous & hematopoietic stem cell transplantation	
AS1411	Antisoma Research	Acute myeloid leukemia	
EYE001 anti-VEGF aptamer	Eyetech Pharmaceuticals	Macular degeneration & choroidal neovascularization	3
Zimura	Ophthotech Corporation	Idiopathic polypoidal choroidal vasculopathy, geographic atrophy & macular degeneration	
Lexaptepid pegol (NOX-H94)	NOXXON Pharma AG	Anemia & end stage renal disease	
Macugen (Pegaptanib)	Eyetech Pharmaceuticals	Age-related macular degeneration	Registered

#### **1.1.4 Other OGN therapeutics.**

Aptamers, ASOs and siRNA are just three types of OGN therapeutic. There are in fact many more being developed for clinical treatment of diseases. Micro RNA (miRNA) post transcriptional silencing in diseases such as cancer can be controlled by treatment with a complementary sequence to the miRNA (antagomirs or anti-mirs), which prevents it from negatively affecting gene expression [50, 51].

Other types of OGN therapeutic function to stimulate or ablate the immunological response *in vivo*. Although activation of toll-like receptors can be a negative outcome in treatment with more commonly found OGN therapeutics (ASOs) [52], the immunostimulatory response is capitalised upon when using OGN therapeutics as adjuvants or immunomodulators [53-55].

#### **1.1.5 The OGN therapeutics market.**

Although in a relatively infantile stage, the OGN therapeutics market is expected to grow in the coming decades. The global market is currently valued at \$2-2.5 billion with anticipated gain to \$8 billion by 2026 [56, 57]. Tables 1.1-1.3 demonstrate that a wide variety of diseases are being targeted with ASO, siRNA and aptamer therapeutic OGNs. The actual number of therapeutic OGNs in development is higher due to programs in pre-clinical phase, as well as the contribution of alternate types of therapeutic OGN. A recent review of the history of emerging technologies and the comparison of progress with the therapeutic OGN industry shows that the market has a promising future [13]. Continuing approvals of SSOs and siRNA therapeutics demonstrate that the medicinal chemistry of therapeutic OGNs is improving and indicates that progress is being made to overcome challenges of delivery and stability *in vivo* [20].

## 1.2 OGN manufacturing.

### 1.2.1 OGN solid phase synthesis.

Nucleic acids are typically synthetically manufactured in the laboratory using a technique called solid phase synthesis. This technique was developed by various groups between the 1950's to 1980's [58-61] and begins with a polystyrene or silica support bonded with the first nucleoside. The phosphoramidite method is summarised for DNA OGNs in Figure 1.3. This is a chain elongation process where phosphoramidite nucleosides are added using a cyclic elongation process.

The bonded starting monomer is protected with a dimethoxytrityl group at the 5' carbon and is first detritylated with trichloroacetic acid in dichloromethane to functionalize it for polymerization. Next, the sequential phosphoramidite nucleoside in the DNA sequence is introduced alongside a tetrazole activator to couple the two monomers via the 5' carbon of the first monomer and the 3' carbon of the second. The process of polymerisation thus travels from the 3' to the 5' direction. The next step in the cyclic process of polymerisation is the capping of unreacted 5' hydroxyl groups to prevent erroneous chain elongation. Next the phosphotriester bond is formed by oxidation and the cycle is repeated for each nucleotide in the OGN chain.

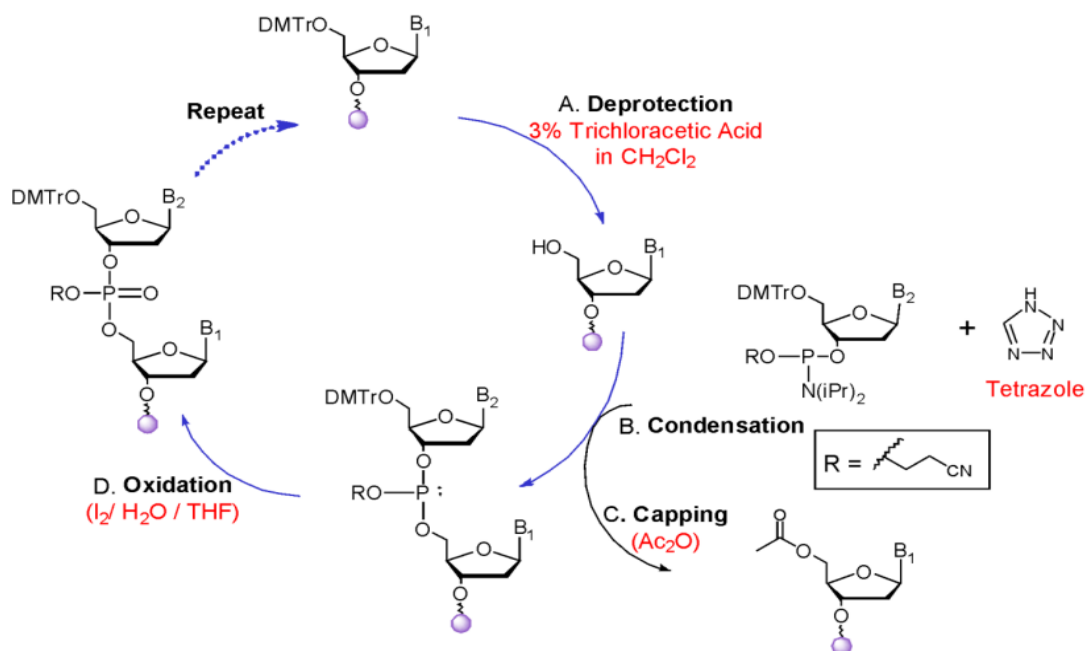


**Figure 1.3: Phosphoramidite solid phase synthesis of DNA OGNs showing the cyclic process of nucleotide addition to the DNA OGN polymer.** The next nucleoside is deprotected and coupled to the bound nucleoside. Uncoupled nucleosides are capped to prevent erroneous elongation. Next the phosphotriester bond is formed by oxidation and the cycle is repeated for each nucleotide in the OGN chain. Image re-printed with permission from Roy and Caruthers. MDPI: Molecules [62] (2013).

The capping step is performed using a mixture of acetic anhydride, pyridine and tetrahydrofuran with N-methyl imidazole in acetonitrile. The unreacted hydroxyl groups become acetylated and unable to be polymerised with another monomer. Next, the phosphite triester bond between monomers is oxidized using iodine in a mixture of water, pyridine and tetrahydrofuran to form a stable phosphotriester bond between the monomers. The cycle of detritylation > coupling > capping is repeated for each monomer in the sequence. The solid phase monomer linker molecule (usually a succinyl linker) is cleaved using ammonium hydroxide to free the OGN from the solid support and any protecting groups are removed (such as N-2-isobutyryl on guanine) to prevent further nucleophilic reaction) [62].

The process of RNA synthesis is similar to the DNA phosphoramidite method in that it is a cyclic process that functions to add monomer units to the growing polymer chain. The 2' carbon hydroxyl group of the ribofuranose is protected by a tert-butyldimethylsilyl group. This prevents hydroxyl migration during the synthesis process. The coupling step (addition of a new monomer in the RNA sequence) typically requires a longer duration due to steric hindrance of the tert-butyldimethylsilyl to the next monomer [62-64].

### **1.2.2 OGN chemical modifications.**

Chemical modifications increase the stability of the therapeutic OGN against nucleases, improve its pharmacokinetics and reduce its renal clearance rate whilst in the body. Early OGN therapeutic development studies highlighted that unmodified OGNs were rapidly cleared within the body and this led to reduced therapeutic effect [12]. There are many potential sites for chemical modification and many types of modification at each site [12, 20]. Chemical modification can be applied to the OGN backbone, ribofuranose sugar or base. Furthermore, the OGN itself may be conjugated to cell delivery molecules (see Figure 1.4). The most commonly used chemical modifications in OGN therapeutics are described in the following sections.

#### **1.2.2.1 Modifications to the OGN backbone.**

Modification to the OGN backbone is commonly seen in a diverse range of OGN therapeutics where a non-bridging oxygen of the phosphodiester bond is substituted (see Figure 1.4). The oxygen may be replaced with a sulphur, boron or methyl group to produce phosphorothioate (PS),

boranophosphate and methyl phosphonate bonds respectively. Phosphorothioation and boranophosphation demonstrate the same improvement to nuclease stability [65-68], although phosphorothioation has been linked to thrombocytopenia [69]. While methyl phosphonates exhibit reduced RNA affinity [20], phosphorothioated OGNs show improved pharmacokinetics by binding to plasma proteins, thereby decreasing renal clearance rate and interacting with cell surface stabilins to promote delivery [33, 70-72]. However, each modification reduces duplex complementarity affinity by 0.5°C [73] and can induce toxicity responses [52], which should be avoided.

PS linkages are commonly found on antisense OGNs and cover the span of the backbone as they do not inhibit RNase H activity [12]; however, in siRNA OGNs there is less PS modification to facilitate higher drug efficacy [74]. The PS bond itself creates chirality around the phosphorus centre to produce diastereomer bonds in 'Rp' and 'Sp' conformations. Experimental evidence demonstrates that the 'Rp' conformation exhibits higher binding affinity for the target and increases RNase H activity [75, 76], but is less resistant to nuclease degradation compared to the 'Sp' conformation [77]. Stereo selective synthesis methods have enabled more control over stereochemistry, although the balance of stereo-randomness to stereo-purity remains in question when assessing OGN functionality versus stability [77-79].

Alternative approaches to backbone modification are to modify the phosphodiester linkage to an amide or use of morpholino OGN structures (see Figure 1.4). Amide backbones reduce siRNA susceptibility to degradation by nucleases [80], which increases residence time within the body and reduces high dosage requirements. The replacement of the phosphodiester backbone and ribose for a phosphorothioate backbone and morpholino ring has demonstrated good antisense activity and has been utilised in SSOs to assist with exon skipping function [81, 82].

### **1.2.2.2 Modifications to the OGN ribose.**

Ribose modifications are also common among a diverse range of OGN therapeutics and can be combined to tune functionality and resistance of the molecule to enzymatic degradation [12]. In addition, they are readily combined with backbone modifications for further balancing the function and resistance to degradation [12, 20, 83].

An easily accessible site for chemical modification is the 2' carbon hydroxyl group, which can be substituted for methoxy (O-Me), methoxyethyl (O-MOE) or fluorine (F) moieties (see Figure 1.4).

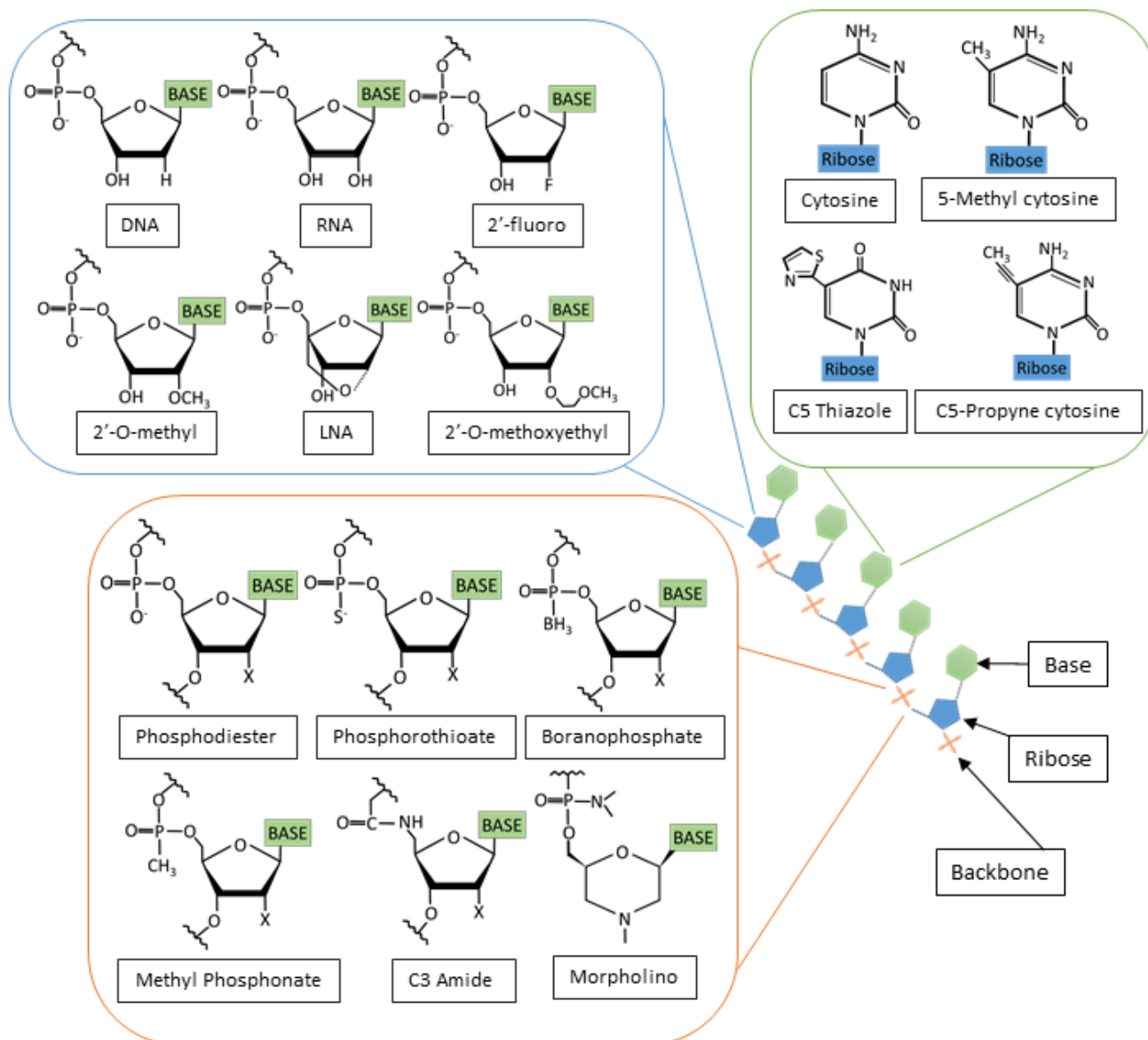


**Figure 1.4: Typical OGN chemical modifications.** OGNs can be chemically modified at the ribose sugar (blue box), base (green box) or backbone linkages (orange box). 'X' may be H (DNA) or OH (RNA).

These modifications have been shown to improve the affinity of the OGN for the complementary target sequence. In addition, the effect on nuclease resistance is modification specific; sterically larger modifications impart more resistance than smaller modifications [84]. The 2'-O-Me modification reduces off target effects and shows improved functionality at specific positions on siRNA (3' terminal of antisense) as it can interfere with RISC loading when placed at other positions on the strand [85]. The 2'-O-MOE modification is sterically the largest of the modifications described. Despite its size, it is commonly placed in most types of OGN therapeutic and is generally well tolerated on the sense strand of siRNA [83, 86]. The 2'-F modification is the substitution of the hydroxyl moiety with a fluorine atom, which imparts more electronegativity onto the OGN and is

well tolerated within double stranded OGNs as it does not affect complementary hydrogen bonding between bases [83]. When 2'-O-Me and 2'-F are sequentially alternated in siRNA, improvements in RISC loading and efficacy are demonstrated. However, 2'-F is usually only used on the antisense strand as 2'-O-Me modification reduces duplex affinity [87, 88]. Second generation antisense OGNs typically are chimeric RNA/DNA mixtures with a central DNA region and modified RNA flanks to improve resilience [12, 89].

Nucleotide ribose sugars are flexible and shift in pucker conformations (non-planar), with the two most stable conformations being the C-2' endo and C-3' endo conformation. However, chemically tuning nucleotides to be more rigid has shown that increased duplex binding affinity can be achieved. This is performed by locking the nucleotide ribose into conformation by linking the 2' carbon oxygen and 4' carbon together (see Figure 1.4). These locked nucleic acids (LNA) have shown that their complementary binding affinity increases by as much as 8°C per LNA modification [90, 91]; however, totally LNA modified OGNs are associated with liver toxicity so should be used in combination with other modification types [92]. A good example of LNA incorporation are in LNA-2'-O-Me-RNA antimirs with PS backbones [93].

### **1.2.2.3 Modifications to the OGN bases.**

One commonly found base modification is the methyl substitution on the 5-carbon of cytosine, which is observed in nature (see Figure 1.4). This modification, when incorporated into the OGN structure, decreases the immunogenic response and has inspired developers to create analogues. Base analogues, such as 5-propynyl or 5-thiazole, have demonstrated an ability to improve double stranded nucleic acid stability. However, most chemical modifications have had limited success due to complementary base pairing inhibition [20, 94, 95].

### **1.2.3 Impurities caused during the manufacturing process.**

Solid phase synthesis (outlined in 1.2.1) is a cyclic process of the addition of nucleotides to the growing OGN polymer with the coupling efficiency of each cycle reaching 95-99.5% [96]. The number of cycles needed to make a typical small OGN therapeutic strand (20 nucleotides = 20 cycles) results in a yield of final product at approximately 80% (termed the 'full length product', 'FLP' or 'N'). This yield decreases as the OGN gets longer [97], however, each cycle of the synthesis

process results in accumulation of failed OGN sequences-otherwise known as OGN impurities. It is important to understand what OGN impurities are created during the synthesis process, as these may lead to immunogenic or toxicological effects, off target effects or reduced drug efficacy [52]. In addition, it is important to understand the toxicological effects of the impurity cohort to make evaluations of drug safety. Characterisation of the level of product related impurities is also used to track batch to batch consistency and help optimise manufacturing. [98, 99].

The capping step (where uncoupled 5' terminal hydroxyl groups are acetylated) creates failed OGN sequences that are shorter than the desired product. These failed sequences, in addition to other shorter sequences formed by cleavage during ammonia treatment or aberrant structures from branching events, are termed 'shortmers' or 'N-x' [96, 100, 101]. Doublet coupling or the coupling of branched nucleotides to the OGN during the synthesis cycle may also occur, creating longmer OGNs which exhibit higher molecular weight than the FLP [102, 103]. Depurination (base loss of adenine and guanine) or incomplete deprotection of the trityl group also can occur during the synthesis process [98, 102, 104], as well as adduction (cyanoethyl adducts on thymine bases), deamination or chemical transformation of OGN moieties [105-107].

The synthesis of phosphorothioated OGNs and the chemical modification of OGNs adds to the cohort of manufacturing OGN impurities. As stated in section 1.2.2.1, the substitution of a sulphur for one of the non-bridging oxygens of the phosphate backbone is known as phosphorothioation. This is easily incorporated into the synthesis process [108-110], however can lead to OGN sequences that aren't fully phosphorothioated or oxidize to contain phosphodiester bonds, forming (P=O)<sub>x</sub> impurities [111]. Chemical modification of the 2' carbon of RNA OGNs with fluorine or methoxy groups can be lost by the substitution of a hydroxyl group [112], which can lead to loss of the function of the OGN therapeutic.

The chiral bond of each PS OGN creates diastereoisomerism to form an 'Rp' and 'Sp' conformation [108] and each bond that is phosphorothioated adds to the potential diastereoisomer cohort to give 2<sup>n-1</sup> OGN length possible diastereoisomers. A fully phosphorothioated OGN of 20 nucleotides in length would result in 2<sup>19</sup> or 524288 diastereoisomers. Although not officially categorised as an impurity, it is important to be aware that these exist within the cohort of OGN sequences within the manufacturing batch as stereoselectivity or stereorandomness may be required for OGN function [79, 113].

Further chemical modification of any of the available sites of the nucleotide can lead to OGN impurities from modification failure events, further isomerism (for example migration of an RNA 2' carbon hydroxyl group to the 3' carbon) or strand scission [114, 115]. As stated in section 1.1,

conjugation of various molecules to the OGN overcomes some of the challenges of cell delivery and renal clearance of the therapeutic OGN. However, the addition of an OGN to a delivery molecule such as N-Acetylgalactosamine (GalNAc) (see Figure 1.5) or cholesterol can create further manufacturing impurities by introducing conjugation failures [98, 99].

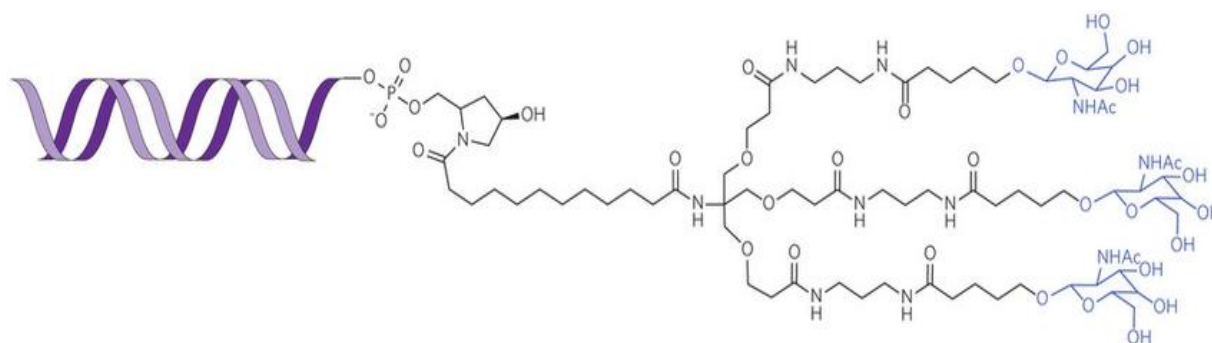


**Figure 1.5: GalNAc–siRNA conjugates.** Structure of the triantennary GalNAc–siRNA conjugate used in several drug candidates from Alnylam Pharmaceuticals. Image re-printed with permission as shown in Kanasty *et al.* [116] Springer: Nature Materials (2013).

## 1.2.4 OGN manufacturing analysis strategies.

### 1.2.4.1 Regulatory governance.

As OGN therapeutics are made by solid phase synthesis and not within a cell, they are not considered to be of biopharmaceutical classification [98]. However, they are far larger and more complex than small molecules to be classified under small molecule regulations. OGN therapeutics are excluded from ICH guidelines Q6A and Q6B (small molecules and biotech products respectively) [117, 118] as these were not written to consider OGNs manufactured by solid phase synthesis [98]. A number of attempts have been made to advise development scientists about attributes for monitoring and reporting [98, 99, 119, 120], but due to the vast diversity in structure, mechanism of action and toxicology profile of OGN therapeutics, regulatory bodies appear to remain in data collation mode to gather critical quality attribute information prior to producing defined regulatory guidelines. Development of analytical methods that are able to improve the characterisation of therapeutic OGNs and their associated impurities provides more data to regulatory bodies to help define guidance and governance.

The FDA has provided some pre-regulatory advice on OGN therapeutic characterisation for regulatory applications and their general consensus is that OGN therapeutics are more similar to small molecules than biomolecules due to their synthesis process [119]. Many of the guidelines for small molecules can be applied to the analysis of OGN therapeutics. Specifically, the FDA advises scientists to characterise the drug substance and drug product identification, potency, quality and purity, along with stability using validated analytical methods and work completed according to GxP. They advise to follow regulatory guidance in ICH Q3C (R6) for reporting residual solvents and ICH Q3D for reporting elemental impurities [121, 122]. In addition, USP salt policy guidelines should be followed to name and label drug products containing salt [123].

There is still some ambiguity in reporting limits and thresholds for qualification due to the complex chemical nature of OGN therapeutics. Advising groups suggest that reporting limits need to be higher than those for small molecules owing to higher limits of detection and quantitation in analytical methods. It is clear that preclinical and clinical data will feed into decision making processes for these acceptance criteria alongside risk assessments of chemistry derived toxicology [98, 99]. Additionally, improved analytical methods may help to overcome the challenges of higher limits of detection.

#### **1.2.4.2 Analytical approaches for OGN physicochemical characteristics, structure and sequence.**

The identity of the OGN is derived from an accurate molecular weight measurement, which can be obtained using multiple methodologies [124-128]. High resolution mass spectrometry establishes molecular mass by mass to charge detection and size exclusion liquid chromatography defines molecular weight by retention time agreement. Circular dichroism spectroscopy studies provide information on structure by analysing the conformation of the OGN [129] and moisture content analysis by Karl Fischer titration provides information for long term storage [98]. OGN conformation can also be determined by analysing the melting temperature ( $T_m$ ) of an OGN in duplex, this may either be applied to a double stranded OGN, such as an siRNA therapeutic or to a single stranded OGN therapeutic while in complex with its target sequence (usually another oligonucleotide mimicking the mRNA transcript target sequence). Melting temperature analysis is performed using nuclear magnetic resonance, circular dichroism spectroscopy or ultraviolet spectrophotometry [129-131]. Changes to the melting temperature can also give information on sequence isomerism and mismatches of the duplex [98].

Ensuring the OGN sequence has been correctly synthesised is important as mismatches and off target effects can occur from aberrant OGN sequences. Analysis using mass spectrometry (MS), either by a fragmentation approach using tandem mass spectrometry or by enzymatic digestion of the OGN prior to analysis, can fingerprint the OGN sequence for quality control of the final synthetic drug [132-134]. The OGN is fragmented to reveal sequential sized OGNs respective to the accumulating sequence that can be read from a mass spectrum. Quality control is analysed and confirmed by a range of complementary approaches. In addition to assessments of  $T_m$ , mass, sequence and moisture content, the elemental composition can be interrogated to identify changes between manufacturing batches. Nuclear magnetic resonance analysis (NMR) is used to identifying the ratio of phosphorothioate to phosphodiester bonds of the OGN backbone [135, 136] as it is a highly sensitive approach to determining differences in elemental composition. In addition, NMR can be used in a number of modes (and dimensions) to identify structural elements, such as hydrogen, carbon, fluorine and phosphorus containing moieties [99, 137-139]. OGN length can be confirmed by classical approaches such as capillary gel electrophoresis [140], however highly selective approaches using liquid chromatography can interrogate retention time of length and sequence isomers to identify the impurity profile, as explained in section 1.3.

#### **1.2.4.3 Analytical approaches for impurities.**

Inorganic impurities and residual solvents may arise from the manufacturing process or handling/storage of the product post-manufacture [98, 138]. Gas chromatography is an analytical method that separates volatile residual solvents and detects by retention time alignment [141]. Inductively coupled plasma-MS may be used to validate changes to the elemental composition identified by NMR studies, as well as the introduction of elemental impurities or counter ion sodium content [142]. It is crucial to identify product related organic impurities as these also may have been formed due to storage or during the manufacturing process. Characterisation of impurity levels can be used to monitor and optimise manufacturing processes. In addition, it is important to understand the impurity cohort from a toxicological perspective [98, 99].

The majority of analytical approaches for tracking impurity levels are based upon liquid chromatography [143]; however, due to the vast array of OGN structures, sequences and chemistry- a multimodal approach is best utilised for appropriate coverage of impurity types [99]. It also may not be practically possible to resolve all of the product related impurities in a single separation

method, requiring an orthogonal method to contribute further characterisation information on purity or assay characteristics [98]. Post-manufacturing, OGNs are commonly purified by column anion exchange chromatography (AEX), which removes the majority of OGN impurities from the sample [144-146]. Another purification approach is to delay the final OGN detritylation step, to capitalise upon the hydrophobic dimethoxytrityl moiety for OGN purification using reversed-phase chromatography. The reversed-phase method retains OGNs on the hydrophobic stationary phase using the hydrophobic dimethoxytrityl moiety, which is later cleaved post-purification [147]. For both approaches, closely related structures, such as the N-1 impurity are difficult to resolve and so the sample requires further analysis to understand the level and types of OGN impurities present. Alternative approaches include gel electrophoresis, perfluorination of the protecting group for affinity chromatography purification or use of azide or biotinylated photo cleavable moieties which can enable the 'catch' and 'release' of functionalised OGNs with photo irradiation [137, 148, 149].

The general consensus for reporting impurities is that they can be considered by assembling closely related structures into groups or classes as outlined in ICH Q3A for identification and qualification [98, 150]. There is a requirement for reporting specified, unspecified and total impurities, however due to broader chromatographic peaks caused by higher chemical complexity, advisory reporting thresholds have been altered to reflect higher limits of detection and quantification [99]. An example of a group type is the 'abasic' impurity where there is a loss of a specified base in any of the appropriate locations of the OGN. Alternatively, the P=O impurity is a transition of the phosphorothioate bond to a phosphodiester bond in any of the backbone linkages.

Characterisation of single stranded OGN impurities commonly precedes analysis of double stranded OGN therapeutics. However, completeness of annealing is defined by analysing the remaining single strand after complementary binding of the two strands [151]. Although the OGN impurity profile is characterised before chemical conjugation, the process of conjugation may introduce further product related impurities that require identification. Conjugate molecules are polydisperse in nature and this characteristic may also lead to difficulty in resolving impurities. Orthogonal chromatographic approaches may be required to first analyse the distribution of polymer-OGN molecular weights (polydispersity) and then impurities associated with each polymer-OGN identity. For example, size exclusion chromatography (SEC) coupled with a chromatographic mode that identifies changes in chemical nature [98].

### **1.3 Analysis of nucleic acids using liquid chromatography.**

High performance liquid chromatography (HPLC) is an analytical technique that separates molecules under high pressure [152]. Analytes separate according to their individual partitioning towards or adsorption to a stationary phase (held within a column) from a mobile phase. Analytes elute from the stationary phase due to differences in their affinity for it and are detected upon elution (as they exit the column). The chemical environment of the mobile phase can be altered under gradient conditions (change of pH, ionic strength, solvent polarity) to accelerate analyte elution and sharpen chromatographic peaks that are usually broadened by diffusion (under isocratic conditions). Detection can be performed by numerous approaches, however UV-VIS spectrophotometric detectors are commonly utilised to produce a data output in the form of a chromatogram. Application of high pressures facilitates improved resolution, as does the use of smaller stationary phase particle sizes by minimising diffusional pathways [153].

A range of chromatographic modalities are available for analysts to apply to molecular separations, including cation and anion exchange (CEX, AEX), reversed-phase, (RP), normal-phase (NP), hydrophobic interaction (HIC), size exclusion (SEC), hydrophilic interaction (HILIC), ion-pair reversed-phase (IP-RP) and affinity chromatography (AC). Each mode separates molecules using different retention mechanisms between analytes and the stationary phase, for example, by charge, hydrophobicity, polarity, molecular weight or chemical affinity. Many modes of chromatography have been applied to the analysis of OGNs, however, this literature review is centred on AEX, IP-RP and SEC modalities.

#### **1.3.1 Analysis of OGNs using anion exchange liquid chromatography.**

Ion exchange chromatography separates cations or anions using a stationary phase oppositely charged to the analytes. Charged analytes electrostatically interact with the stationary phase during retention and are competitively displaced by increasing concentrations of counter ions for elution. Counter ions are exchanged for the analyte ions to compete for immobilized, charged chemical groups within the stationary phase. The more strongly ionised the analyte, the stronger its retention to the stationary phase, as well as a requirement for higher salt concentration or pH for elution [153].

OGNs are negatively charged in aqueous solutions due to the phosphate backbone that links their nucleotides in the polymer chain, with each bond linkage contributing to the net ionisation of the OGN anion. This characteristic enables the separation of OGNs of varying lengths using anion exchange chromatography (AEX) and a cationic stationary phase. Larger OGNs are more strongly retained than shorter OGNs due to the net contribution of each phosphate bond to their anionic nature, enabling separation by OGN size [154]. The immobilization of charged amines on the stationary phase does not exhibit 100% coverage, resulting in secondary, non-ionic interactions to occur [143]. In respect to single stranded and double stranded nucleic acids, secondary interactions are more frequently observed with single stranded OGNs due to the availability of the bases for interaction, whereas double stranded OGNs occupy the interacting moieties of the bases by complementary hydrogen bonding of the two strands together [154]. Additionally, the bases of OGNs electrostatically interact with the stationary phase in a base specific manner, which results in separation by OGN sequence (see Figure 1.6). This enables OGNs of varying size and or base sequence to be resolved during SAX HPLC separations.

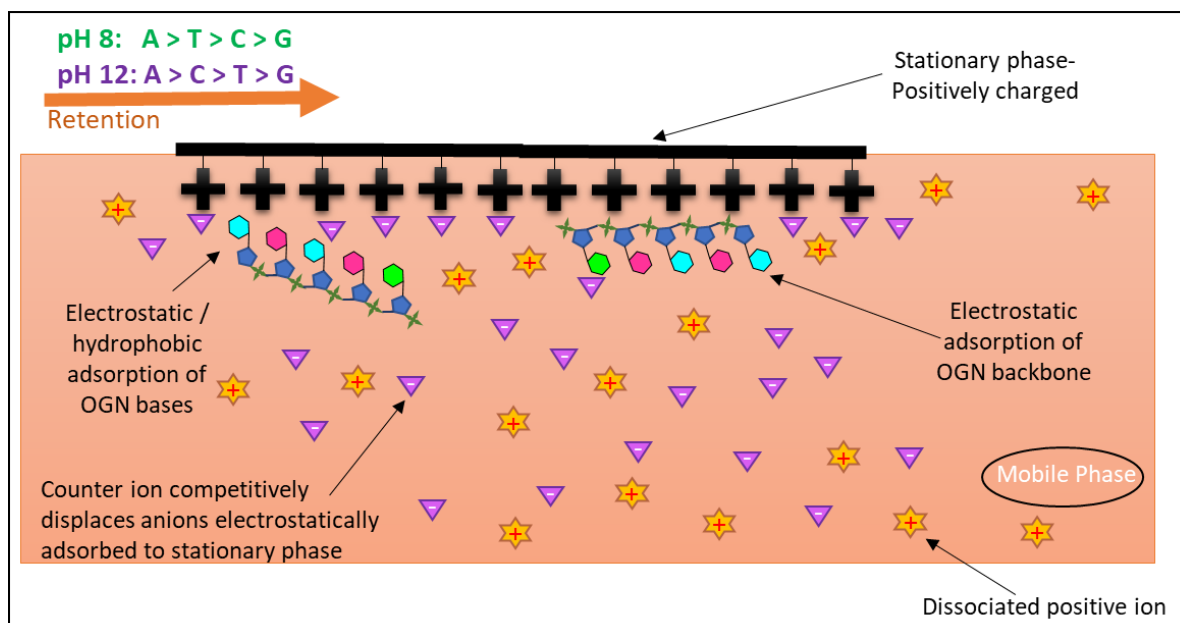


**Figure 1.6: Mechanism of retention during anion exchange chromatographic separation of OGNs.** OGN anions electrostatically adsorb to a positively charged stationary phase due to their negatively charged phosphate backbone. Secondary interactions between the OGN bases and stationary phase are also observed differentially between bases and in various mobile phase pH. OGNs are eluted with an eluotropic salt.

Anion exchange stationary phases are categorised as weak or strong exchangers in respect to the bonded charged group that facilitates electrostatic retention. Weak (WAX) phases are typically bonded with diethylaminoethyl groups and are liable to lose charge in contact with lower pH mobile phases (e.g. pH 6). Strong (SAX) phases are typically bonded with quaternary amines and are more resistant to losing their charge, which prevents secondary hydrophobic secondary interactions from occurring [154, 155]. Traditionally, the solid support of stationary phase consisted of agarose or cellulose, however modern phases use polystyrene based polymers for improved resilience to temperature, pH and pressure. It is well documented that smaller particle size and the utilisation of pellicular or fused core particles achieve improved resolution due to convective mass transfer rather than diffusional mass transfer processes [154, 156, 157]. Another novel stationary phase gaining attention is the use of monolithic columns- porous polymeric monoliths functionalized with the appropriate charged moiety. These monoliths also facilitate convective mass transfer (by reducing diffusional pathways) and reduce secondary interactions between the phase and the analytes due to having a more uniform chemical structure [156, 158].

The post-synthesis purification of synthetic OGNs aims to remove waste reagents and the majority of product and process related impurities. AEX is safer than alternative reversed-phase approaches due to the use of less hazardous salts (such as sodium chloride) in contrast to toxic organic solvents used in reversed-phase chromatography. However, high salt conditions require a desalting step prior to lyophilisation of the product [159]. Early studies on nucleic acids focused on developing stationary phases that exhibit improved resolution of OGNs and many groups have obtained single nucleotide resolution using WAX columns and salt gradient elution (using phosphate buffers and sodium chloride) [160-162].

Isocratic elution assisted with the beginnings of retention modelling, however the optimisation of gradient elution in place of isocratic separation facilitated improved resolution of smaller single stranded OGNs (1-30-mers), larger single stranded OGNs (74 and 128-mers) and double stranded DNA fragments from enzymatic digestion. Retention time changes between 21-mer sequence isomers suggested that there is sequence based selectivity under AEX conditions and that the bases also interact with the stationary phase. The addition of organic modifier to the mobile phase did not change the selectivity of sequence isomers but functioned to generally reduce secondary interactions between nucleic acids and the stationary phase [163].

Bunček *et al.* showed that utilisation of mobile phases above pH 8 prevents OGN depurination or strand scission, and reduces secondary structure formation by reducing hydrogen bonding - enabling WAX columns to retain their charge density [164]. Further studies using WAX stationary phases have

facilitated the purification of various isoforms of large plasmids and double stranded DNA ladders using sodium chloride gradients for size analysis [165, 166]. Additionally, analysis of the pharmacokinetics and tissue distribution of an 18-mer PS OGN therapeutic and its 16-mer metabolite has been demonstrated using a WAX stationary phase and lithium chloride gradient [167].

SAX stationary phases are functionalized with quaternary amines that are more adept at maintaining charge density over a larger range of mobile phase pH. This is due to their more strongly ionic nature in comparison to WAX diethylaminoethyl groups and results in better suitability for analysing OGNs of different sequences, as the mobile phase pH can be optimised to manipulate OGN selectivity. Mobile phases of higher pH ionise tautomeric guanine or thymine bases in the OGN sequence in addition to the phosphate backbone. These conditions also disfavour secondary structure formation and facilitate OGN sequence based separations. In contrast, mobile phases that are more neutral-slightly acidic pH reduce ionisation of the nucleobases and when coupled with the use of a stronger eluotropic salt (such as sodium perchlorate), the separation mechanism can be adjusted towards an OGN size basis [168, 169]. Use of stronger displacers are also useful for the analysis of modified OGNs that have PS backbones and other chemical modifications. Specifically, the PS bond results in longer retention times due to strong additional hydrophobic interactions with the stationary phase. Stronger eluotropic salts such as sodium perchlorate, sodium bromide, sodium iodide and sodium thiocyanate reduce secondary interactions and therefore retention time in comparison to elution under sodium chloride gradient conditions [157, 159, 170].

Increasing amounts of phosphorothioation on an OGN results in increasing retention [135]. In addition, the PS bond imparts chirality upon the phosphorous centre and creates conformational diastereoisomerism. The limitations of using SAX for the analysis of OGNs containing phosphorothioate bonds are that broad peak shapes are observed due to resolution of diastereoisomers and secondary interactions with the stationary phase. Pellicular SAX stationary phases have been demonstrated to separate 37-mer aptamer diastereoisomers, as well as siRNA diastereoisomers and single stranded RNA diastereoisomers [113, 157, 171]. AEX studies on the retention patterns of PS isomers have demonstrated that the 'Rp' conformation elutes before the 'Sp' conformation, exemplified by studies on DNA, RNA and ribozyme diastereoisomers [113, 172]. The study by Frederiksen *et al.* on RNA diastereoisomer elution order also described improved resolution of RNA diastereoisomers by complementary hybridisation to DNA OGNs and sequential removal of the DNA OGN by DNase digestion [113]. Although sodium chloride and sodium bromide gradients have demonstrated utility in separating phosphodiester (P=O) impurities from fully PS DNA OGNs [173], Bergot and Egan also described the use of stronger displacers (such as potassium

bromide or sodium thiocyanate) to resolve shortmer failure sequences and P=O impurities from synthetic phosphorothioated DNA OGNs [135].

AEX using sodium chloride and sodium perchlorate gradients has been utilised to study synthesis related side reactions and product related impurities, such as phosphoryl migration in RNA OGNs, strand scission and abasic impurities [174, 175]. Degradation analysis of RNA linkage isomers has demonstrated that sequence selective analysis at high pH can be performed without degradation of the analyte - as long as the run time is kept to under 20 minutes [174] (longer analysis time may facilitate on column degradation of the RNA at high mobile phase pH). In other studies, pellicular polymeric stationary phases were utilised to separate double stranded 2'-O-Me modified siRNA linkage isomers and large single stranded 2'-O-Me modified RNA OGNs [64, 114]. Duplex and single strand impurities can be identified by elucidating the stoichiometry of duplex to single OGN strand under the application of denaturing temperature gradients. This is an important application for understanding mismatching of duplexes [176].

Monolithic polymers have gained notoriety as anion exchange functionalized stationary phases as they shift mass transfer characteristics from diffusive to convective [177]. Monoliths have been utilised for retention studies of double stranded and single stranded DNA OGNs. Yamamoto *et al.* showed that single stranded OGNs elute earlier than double stranded OGNs due to lower levels of ionic interactive sites on the molecule. They described that all OGNs become harder to resolve as they increase in length [178]. Other studies have shown good stability of monolithic capillary phases when separating DNA OGNs in sodium chloride gradients at high pH and with the use of optimised gradients [158, 179]. Monolith SAX technology has also demonstrated utility in resolving large double stranded RNA fragments (58-1810 bp), siRNA OGNs recovered from a dicer reaction (post biological manufacture), RNA linkage isomers and DNA/RNA PS diastereoisomers [177, 180, 181]. The studies confirmed that selectivity can be controlled by mobile phase pH. Thayer *et al.* described that the retention pattern of linkage isomer positions on RNA OGNs is unpredictable. They demonstrated that linkage isomerism can be located with the use of endonucleolytical digestion by PDase-II [181]. This suggests that the UV detection approach to identify isomers that Thayer *et al.* used could be improved by using mass spectrometry detection.

Pharmacokinetic studies using SAX have been commonly performed using pellicular polymeric stationary phases. Earlier quantification approaches utilised lithium chloride or lithium bromide gradients in the presence of organic modifier to analyse levels of synthetic PS DNA and polyethylene glycol conjugated aptamers in serum or tissue extracts [182-184]. The addition of an organic modifier to the mobile phase, such as acetonitrile, increased recovery indicating that AEX

separation of OGNs has a mixed mode nature. Sodium chloride gradients demonstrated the ability to analyse the bioavailability of antisense morpholino OGNs in serum, liver tissue and malignant tumours [185, 186]. The bioavailability of siRNAs and their shortmer impurities in prostate cancer cells has also been studied using sodium chloride and potassium chloride gradients in conjunction with modern pressure resistant polymeric pellicular stationary phases [187]. McGinnis *et al.* showed that N-1 and N-2 metabolite impurities could be resolved from the precursor during quantification of siRNA uptake over time.

The limitations of utilising AEX as a technique when developing a new chromatographic method are that with some chemically modified OGNs, peak shapes may be broad. This lowers the limits of detection when analysing molecules at low concentration. In addition AEX mobile phases contain salts, which are not compatible with MS detection, thus requiring additional desalting steps within the analytical method.

### **1.3.2 Analysis of OGNs using ion-pair reversed-phase liquid chromatography.**

Within the reversed-phase mode of chromatography, a hydrophobic stationary phase is utilised to retain analytes by their inherent hydrophobicity. Analytes are separated by their differential hydrophobic partitioning toward or adsorption to the stationary phase while being introduced within an aqueous mobile phase. An organic solvent is applied either isocratically or within a gradient to elute the analytes and analytes that are polar or hydrophilic do not strongly interact with the stationary phase and are either not retained or elute early within the separation. Biomolecules that exhibit high polarity and hydrophilicity, such as OGNs are therefore, difficult to separate using reversed-phase due to low retention [153, 188].

A method of 'depolarising' analytes is to add reagents to the mobile phase that neutralise analyte inherent charge and impart hydrophobicity. For example, the addition of alkyl amines to the mobile phase reduces the negative charge caused by the OGN phosphate backbone. This enables the OGN-alkyl amine complex to retain on the stationary phase due to the hydrophobicity of the alkyl chain. This addition of reagents to reduce analyte polarity is called ion-pairing and defines a new mode of chromatography - ion-pair reversed-phase (IP-RP) HPLC. The more negative charges available on the OGN backbone provide more opportunity for complexes to form between the alkyl amine ion-pair reagent (IPR) and the OGN. Increasing ion-pairing results in increasing hydrophobicity of the complex and thus separation is based upon OGN length according to the number of nucleotides in the OGN

polymer [189]. As a result, IP-RP HPLC is used for the analysis of nucleic acids and synthetic OGNs [143].

The IP-RP mechanism of retention was contentiously discussed between the 1970's to 1990's and two models of retention arose. The 'ion-pair' model states that the neutralisation of analyte charge with the complexation of an IPR to the analyte causes hydrophobic adsorption of the analyte-IPR complex (or ion-pair) towards a hydrophobic stationary phase [190]. Alternatively, the 'dynamic ion-exchange model' describes a mechanism whereby the IPR itself has an affinity to the stationary phase and adsorbs to it to form a layer upon its surface. This secondary layer of IPR dynamically exchanges analyte ions in an electrostatic manner [191]. In fact, the two mechanisms occur simultaneously as studied and defined in partnership as the 'ion-interaction' model or more recently the 'electrostatic retention' model [192, 193] (see Figure 1.7).

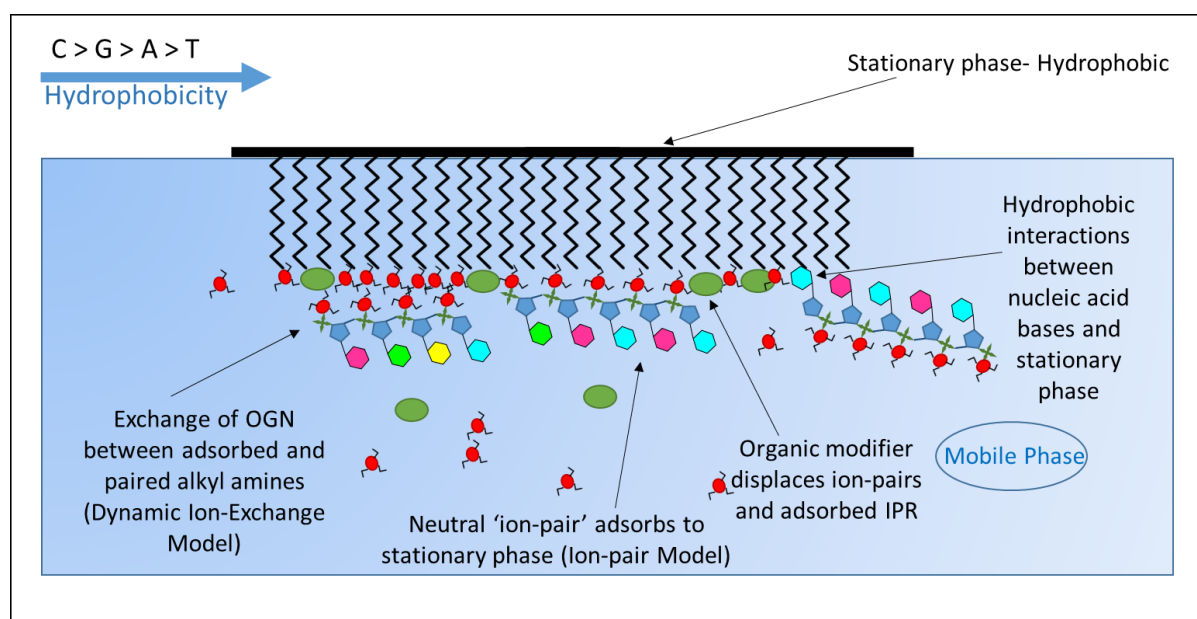


**Figure 1.7: Mechanism of retention during ion-pair reversed-phase chromatographic separation of OGNs.** The IPR associates with the OGN to impart hydrophobicity onto it, which results in hydrophobic interaction between the IPR-OGN and stationary phase. The IPR also adsorbs towards the stationary phase to dynamically exchange OGNs. In addition, the bases of the OGNs take part in secondary interactions with the stationary phase with hydrophobicity increasing from cytosine > guanine > adenine > thymine. OGNs are eluted with a gradient of organic solvent.

Traditional reversed-phase stationary phases consist of fully porous silica with bonded alkylsilanes, with octadecylsilane bonded phases most commonly used for OGNs [153, 194]. The improvement in chromatographic stationary phase chemistries has enabled the use of bonded polymeric phases and

hybrid silica-polymeric stationary phases for analysis of OGNs [195, 196]. Improvements in stationary phase chemistry, such as the development of alkylated poly(styrene-divinylbenzene) particles enabled higher resistance to extreme pH and operating temperatures [197] thus facilitating improved accuracy of nucleic acid size based analysis in comparison to slab based electrophoretic approaches. This demonstrated that IP-RP in conjunction with polymeric stationary phases was an accurate tool in respect to OGN analysis [198]. Additionally, monolithic and cholesterol bonded stationary phases have shown to improve resolution of PS OGNs due to improved mass transfer and alternate selectivity characteristics respectively [199, 200].

Reduction in particle size improves mass transfer by reducing diffusional pathways and thus improves resolution of closely related analytes [201]. Particles of 2.5-5 $\mu$ m are typically used in traditional HPLC. However, use of <2 $\mu$ m particles has been used for ultra-high-pressure liquid-chromatography (UHPLC) analysis [143, 202]. The adoption of solid core technology has also improved mass transfer by reducing eddy diffusion and thus having beneficial effects upon OGN chromatographic peak shape [154, 203]. OGN chemistry, structure or size can have an effect on resolution and so the choice of stationary phase is carefully chosen with analyte characteristics in mind [204]. Consideration of stationary phase characteristics, such as particle pore size can impact upon retention and thus separation efficiency of OGNs [205, 206].

#### **1.3.2.1 IP-RP HPLC analysis of nucleic acids using 'weak' ion-pair reagents.**

The majority of initial analyses of nucleic acids using IP-RP centred on the use of triethylammonium acetate (TEAA) as the IPR. Single stranded and double stranded DNA OGNs have been analysed and used to define optimal chromatographic conditions for improved resolution. Studies have shown that increasing amounts of TEAA improve retention and resolution. However, the stationary phase requires sufficient equilibration to achieve optimal separations [198, 207, 208]. DNA OGNs can be resolved using a temperature gradient elution approach for single stranded analytes and the use of high analysis temperature has a denaturing effect upon duplexes for analysis of their complementary strands, which can identify single nucleotide polymorphisms [197, 207, 209, 210].

The use of homopolymeric OGNs in IP-RP analysis has contributed to the understanding of their retention mechanisms, where in addition to retention by their nucleotide length (providing ion pair sites for the IPR reagent to contribute hydrophobicity) there is a sequence based retention mechanism occurring. This is due to differences in retention behaviour between homopolymers of

alternate sequences, such as poly dT or poly dA. The bases of each nucleotide are differentially hydrophobic and contribute towards the analytes adsorbing to the stationary phase in the order cytosine> guanine> adenine> thymine, although uracil is not as hydrophobic as thymine when applying the same approach to RNA OGNs [189, 211-213]. IPRs with the ability to separate OGNs by both size and sequence in this manner are defined here as 'weak' ion pairing agents as their lower hydrophobicity allows the OGN to access the stationary phase for base induced interaction.

Aiming to understand the impact of chromatographic parameters on OGN resolution; retention studies have shown that low flow rate in combination with a shallow gradient application of organic solvents (such as acetonitrile) can improve the resolution of OGNs due to enhanced mass transfer effects, however this becomes more difficult as the OGN increases in size due to the reduced net hydrophobicity difference between OGNs of similar size [189, 196, 211, 212]. Optimisation of IP-RP using TEAA has demonstrated that resolution of 1 nucleotide is achievable for sequence isomers and homopolymeric OGNs up to 60 nucleotides long, with enhanced resolution following the use of monolithic capillary columns or smaller particle sizes or optimised chromatographic parameters, such as gradient or flow rate [201, 214-216].

Azarani and Hecker demonstrated that OGN analysis at higher analysis temperature resulted in improved size based separations due to a denaturing and moiety exposing effect upon OGNs in duplex and as single strands respectively [217]. By default, the contrasting utilisation of low analysis temperature can conserve analyte conformation for structural analysis or separation by base sequence. Structural analysis of double stranded DNA Holliday junctions has been demonstrated using IP-RP in conjunction with TEAA, in addition to conformational analysis of single stranded RNA [188, 218]. McCarthy *et al.* analysed the annealing of siRNA OGNs using low temperatures for on column duplex formation and analysis [202]. The Impact of this is better understanding of mismatched duplexes due to isomerism and characterisation of nucleic acids adopting specific conformations.

Chemical modification of synthetic OGNs, such as those observed in OGN therapeutics, adds or chemically substitutes chemical groups to the molecule and this changes their steric dimensions, charge density and hydrophobicity [219]. Thiolation of the phosphate backbone increases the molecule net hydrophobicity and creates diastereoisomerism with each modification [220]. PS diastereoisomers exhibit differential retention to the stationary phase when analysed using IP-RP in conjunction with TEAA [221] due to base stacking differences between the isomers and steric differences in accessing the IPR or stationary phase. Although PS DNA and RNA OGN diastereoisomers have been resolved in OGNs of varying lengths [194, 221], as phosphorothioation

increases, chromatographic peaks become wider, which increases the limit of detection and reduces chromatographic efficiency [220]. Li *et al.* investigated UHPLC columns with octadecyl or phenyl chemistries to enable resolution of siRNA diastereoisomers containing up to 6 phosphorothioate bonds [222]. Another way of analysing PS OGNs with many phosphorothioate bonds using TEAA IP-RP is to desulfurize the OGN with an oxidation method prior to chromatographic separation [223].

TEAA can be used to analyse OGNs with other types of chemical modification. For example, 60 OGN isomers of 2'-fluoro and 2'-methoxy modified siRNA were analysed using 100 mM TEAA in combination with core shell column technology [203]. OGN resolution was improved in comparison to fully porous stationary phases. In respect to stationary phases, C18 and phenyl bonded phases have demonstrated the best selectivity for sequence isomers [224]. C18 and phenyl phases also showed high selectivity for PS OGNs, demonstrated during analysis of 18-26-mer PS DNA OGNs and PS siRNA [222, 225]. IP-RP in conjunction with 100 mM TEAA has also been demonstrated for OGNs with positional isomer adducts [219, 226] and dye labelled OGNs [227].

Other small IPRs have been used to separate and analyse OGNs, such as butyldimethylamine (BDMA), hexylamine (HA), diethylamine (DEA) or propylamine (PA). These IPRs have the same or lower amounts of carbon as triethylamine (TEA), but exhibit both linear to branched alkyl chains, which may enhance or suppress size based OGN separations respectively (see Figure 1.8). Linear IPRs elongate the distance between the OGN analyte and the stationary phase to reduce secondary interactions from OGN bases, as demonstrated with studies using 15 mM hexylamine to analyse a 20-mer 2'-O-Me PS OGN to identify low level synthesis impurities [126, 136]. An example of utilisation of a branched IPR is the analysis of crude RNA OGNs using 25 mM BDMA, which enabled the identification of a cyanoethyl adduct from synthesis [228]. Some studies have shown the utility of combining small alkylamines within the mobile phase for improved resolution, combinations of propylamine with triethylamine have demonstrated utility in the analysis of chemically modified siRNAs and other OGNs (2'-F, 2'-O-Me and PS) to identify modification failures, positional isomers, shortmers and longmers from synthesis [112, 229].

### **1.3.2.2 IP-RP HPLC analysis of nucleic acids using 'strong' ion-pair reagents.**

Utilisation of low hydrophobicity IPRs facilitates additional interactions to occur between the bases of the OGN and the stationary phase, thus they are termed 'weak' IPRs [206]. In order to prevent these secondary interactions from occurring, a 'strong' alkylamine is used within the mobile phase.

This results in improved peak shapes due to the reduction in sequence based separation. IPRs with longer alkyl chains and higher amounts of carbon are more hydrophobic and adsorb to the stationary phase more readily than 'weak' IPRs. This forms a more hydrophobic IPR stationary phase saturation layer and results in longer retention times during analysis of OGNs [230]. The relationship between IPR concentration and OGN retention is not linear, with optimal levels of 'strong' IPRs below 20 mM concentration [230-232].

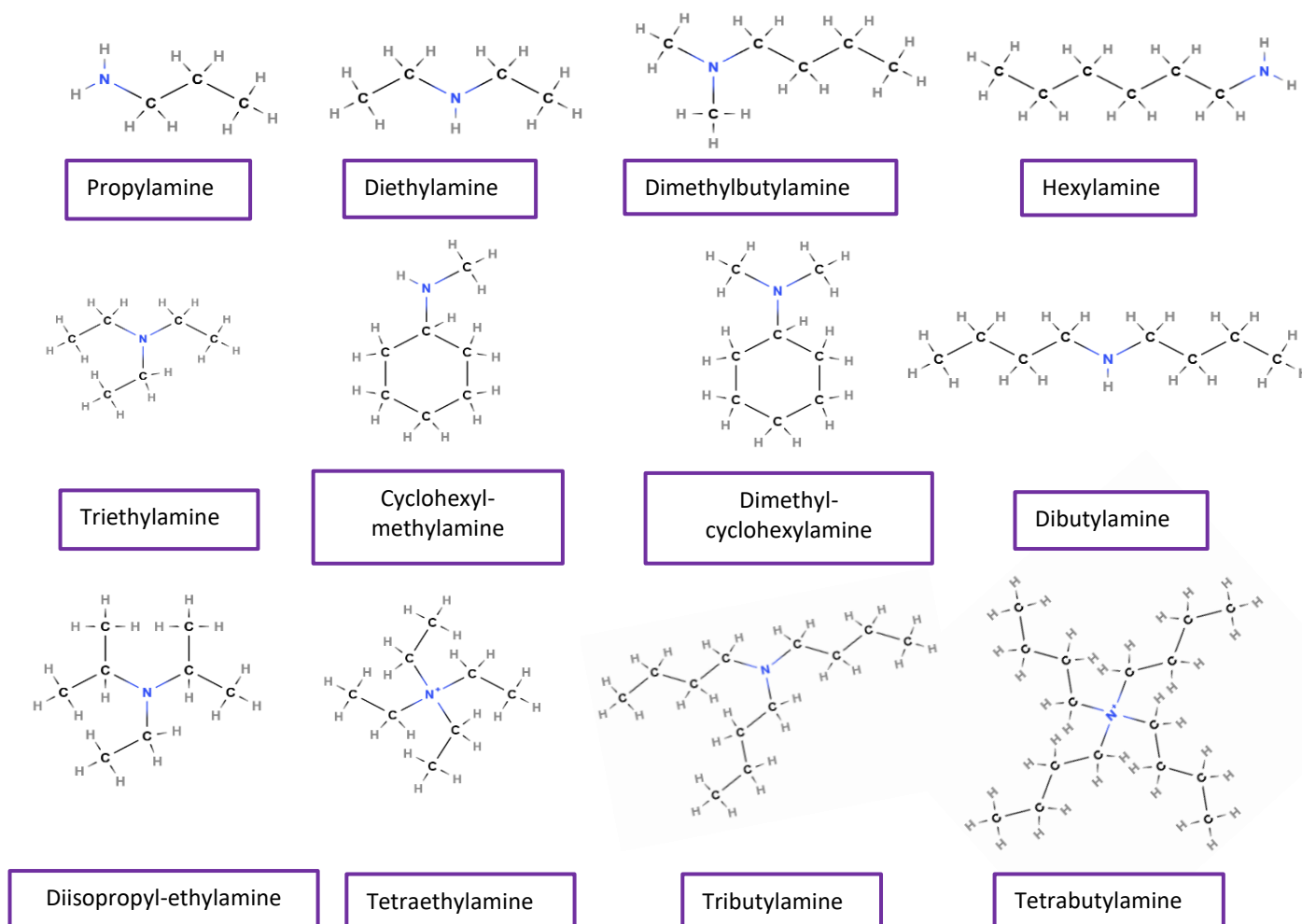


**Figure 1.8: Chemical structure of various IPRs used for the analysis of OGNs under IP-RP HPLC conditions.** Propylamine, diethylamine and triethylamine are generally considered to be 'weak' IPRs used for IP-RP of anions, such as OGNs (where sequence based separations are more prevalent). The remaining IPRs are generally considered to be 'strong' IPRs for IP-RP of OGNs and reduce secondary base interactions with the stationary phase (thus enabling more size dominant separations to occur). IPR 'strength' increases with increasing levels of alkylation.

Use of strong IPRs suppresses MS ionisation due to their lower volatility in respect to weaker IPRs. However, this effect is mitigated by the requirement for higher organic solvent elution conditions, which aids ionisation through increased volatility of the mobile phase [233]. Li *et al.* described that high concentrations of IPR can suppress mass spectrometric signal [234]. Thus the utilisation of strong IPRs at lower respective concentrations facilitates the interface of chromatographic separation and MS detection for improved characterisations of OGN impurities. An example of this approach is the use of 10 mM cyclohexyldimethylammonium acetate as a strong IPR for IP-RP HPLC analysis of DNA OGNs and the pharmacokinetic study of PS OGNs in rat plasma [231].

Strong IPRs facilitate more size dominant OGN separations, further examples of the use of strong IPRs are analysis of ribozymes that are 2'-O-Me modified along with the products of RNA foot printing and separation of fully PS OGNs using 2.5 mM tetrabutylammonium bromide [235] [206]. Additionally, 5 mM tributylammonium acetate (TBuAA) has been used in conjunction with IP-RP HPLC for the analysis of 20-mer PS OGNs [232, 236, 237]. The results demonstrated that peak shape improved and facilitated the identification of numerous synthesis related impurities such as high molecular weight species [236]. 20-mer 2'-O-Me PS OGNs were analysed using TBuAA IP-RP and MS detection. Synthesis impurities such as deamination products, shortmers and longmers are readily identifiable using strong IPRs in conjunction with IP-RP and high resolution techniques [232, 237].

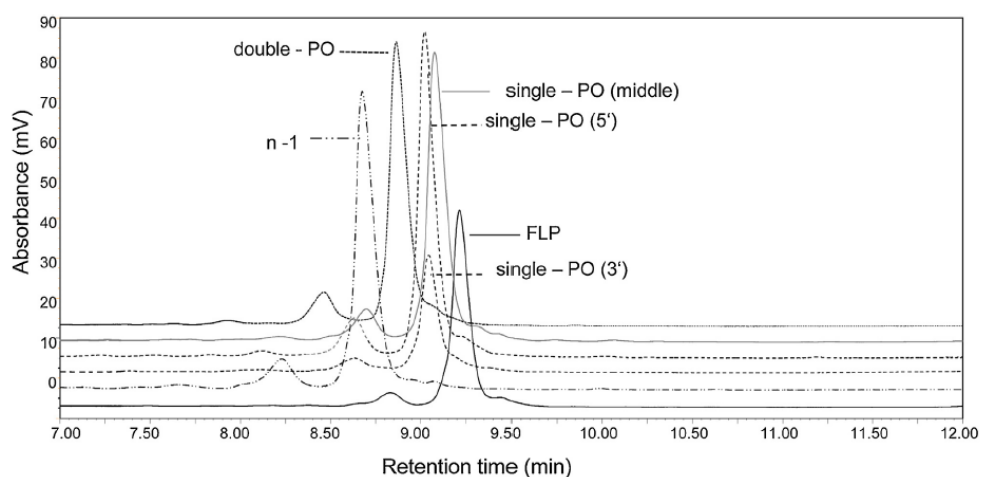


**Figure 1.9: Analysis of a full PS OGN 15-mer and its related impurities using strong IP-RP HPLC.** Analysis performed on an Accucore C18 column using 2.5 mM TetBAB and a gradient of 44-64 % MeCN at 50°C. Detected at 260 nm. 80 picomole samples of FLP overlaid with N-1, P=O (5' end, 3' end, centre and 3'/5' end P=O(2)). Re-printed with permission from Close *et al.* [206] Elsevier: Journal of Chromatography A (2016).

### 1.3.2.3 IP-RP HPLC analysis of nucleic acids using acidic modifiers alongside ion-pair reagents.

In 1997, Apffel *et al.* described the addition of hexafluoroisopropanol (HFIP) to a mobile phase containing low concentrations of IPR to facilitate improved sensitivity in MS analysis [238]. HFIP evaporates before the IPR whilst in the electrospray droplet, thereby increasing the droplet surface charge to improve OGN ionisation efficiency. [239]. Apffel *et al.* suggested that chromatographic efficiency must be balanced with MS sensitivity [238] and proposed that the HFIP drives stronger adsorption of the IPR to the stationary phase surface -thus reducing the need for higher concentrations of IPR in the mobile phase and shifting the separation more towards differences in OGN size (see Figure 1.10). The 400 mM HFIP mobile phase was titrated with 4.3 mM triethylamine to pH 7 for direct comparison to a mobile phase containing 100 mM TEAA at pH 7. However in later studies, chromatographic resolution was markedly improved with ratio of 16.3 mM TEA to 400 mM HFIP and enabled the identification of synthesis related adducts and retention modelling for OGNs of different size and sequence. HFIP addition was also shown to disrupt secondary structures and secondary interactions between OGN bases and the stationary phase [189, 214, 240].

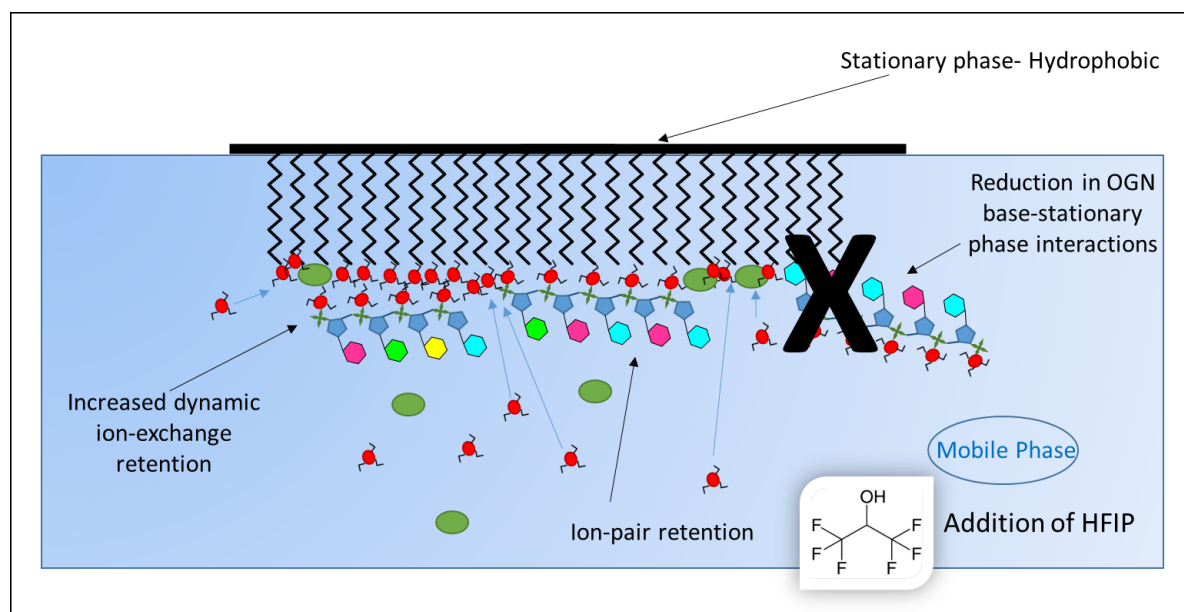


**Figure 1.10: Mechanism of retention during HFIP modified ion-pair reversed-phase chromatographic separation of OGNs.** Increased dynamic ion-exchange separation mechanisms occur due to increase IPR stationary phase layer formation. In addition, secondary interactions between OGN bases and the stationary phase are reduced.

Various groups have published pharmacokinetic data using a ratio of TEA: HFIP in the mobile phase for HFIP modified IP-RP analysis [241-245]. For example, 1.7 mM TEA:100 mM HFIP enabled the analysis of 21-mer 2'-fluoro/methoxy modified siRNA in human serum and liver microsomes, which identified shortmer impurities by denaturing the duplex at high analysis temperature [241]. This approach has also been demonstrated using higher concentrations of the two reagents at 16.3 mM TEA:400 mM HFIP to analyse siRNA in urine and tissue samples [242]. PS OGNs have also been pharmacokinetically analysed using different ratios of TEA and HFIP, as well as PS antagomirs containing LNA [243-245]. The benefits of coupling HFIP modified IP-RP to MS was demonstrated with the identification and characterisation of closely related structures such as sequence ladders of 2' modified siRNA and other RNA/DNA OGNs [246, 247]. Combinations of TEA and HFIP have demonstrated utility in the analysis of PS OGNs, 2' modified siRNA OGNs, RNA aptamers and PS OGN conjugates, where synthesis impurities (such as shortmers, oxidised products or adducts), degradation products (such linkage isomers and strand scission fragments), positional isomers and purity were characterised [114, 248-253], therefore this approach shows applicability across OGN types..

Investigations on other IPRs in conjunction with HFIP modified IP-RP HPLC have been performed [151, 233, 254, 255]. For example, combinations of HA with HFIP have shown utility in analysing siRNA duplex purity and synthesis related impurities and PS OGNs in liver microsomes [151, 256]. While, other studies have found that combinations of diisopropylamine (DIPA) with HFIP were able to resolve size variants of DNA and isomers of bridged DNA, PS OGNs and 2'-O-Me OGNs [257, 258], and combinations of dimethylbutylamine (DMBA) or dimethylcyclohexamine (DMCHA) and HFIP were able to resolve DNA sequence isomers, PS OGNs and their associated metabolites in serum or oxidative stress products [204, 255, 256, 259]. Furthermore, Basiri *et al.* assessed the impact of other fluorinated alcohols on separation of OGNs to elucidate if HFIP is unique in its balance of volatility and acidity for improved LC-MS analysis [260]. Their findings were that as the hydrophobicity of the IPR increases, so should the hydrophobicity of the fluoroalcohol, such as DMCHA with hexafluoromethylisopropanol and that this combination is useful in longer OGN separations.

### **1.3.3 Analysis of OGNs using size exclusion liquid chromatography.**

Size exclusion liquid chromatography (SEC) physically retains analytes by extending diffusional pathways in relation to decreasing size (see Figure 1.11). It is not desirable for the analyte to interact

with the stationary phase and this instead physically filters analytes based upon their molecular weight or hydrodynamic volume/size. The particles of the stationary phase are therefore, porous (commonly silica or a cross linked polymer) and analytes of decreasing size/volume are able to penetrate further into the pores in respect to their larger neighbours [156]. Therefore, larger analytes elute from the column first, followed by smaller analytes in a size order.

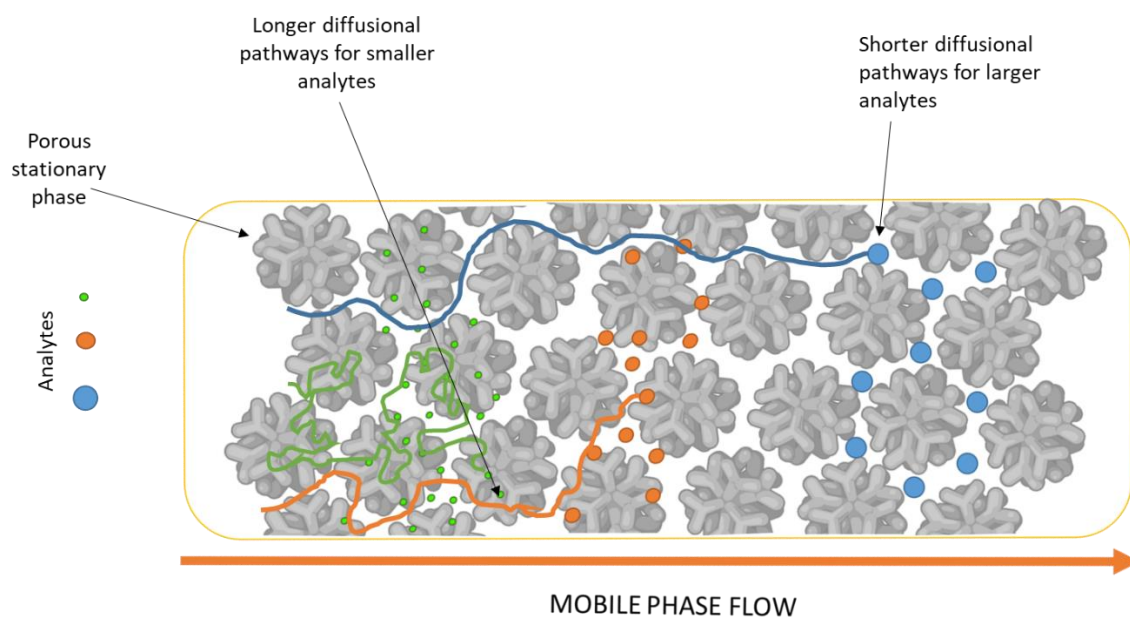


**Figure 1.11: Mechanism of elution during size exclusion chromatographic separation of OGNs.** Larger analytes do not enter into the stationary phase pores and thus elute first due to shorter diffusional pathways. Smaller analytes elute last.

Size exclusion mobile phases are typically aqueous salt containing solutions that facilitate native state conformations of OGNs [114] and commonly used salts for the mobile phase include sodium phosphate, tris(hydroxymethyl)aminomethane or ammonium acetate for the analysis of OGNs [261, 262]. Although the mode of SEC is well known to be a low resolution separation approach [262], there are examples of its application to analysis or purification of OGNs, particularly when applied prior to analysis by AEX or IP-RP HPLC, or as an alternative to gel electrophoresis purification [114, 124, 263-266].

It is important to understand OGN duplex formation during storage, and so SEC has been utilised to monitor OGN duplex stability during degradation studies with acid and base treatment [156]. SEC has been utilised to comprehensively study a range of DNA OGN conformations such as unstructured

strands, duplexes, triplexes and i-motifs and RNA hairpins [262]. In comparison to other modes of chromatography, such as AEX or IP-RP, resolution is not as high. For example, homogeneous dT OGNs were resolved by 10 nucleotides within a study by Wehr and Abbott. Other reports have demonstrated resolution of deoxythymine OGNs to 5 nucleotides [261], but this is not as high as the 1 nt resolution obtained in AEX and IP-RP. SEC has been compared to IP-RP HPLC for the analysis of duplex formation; although single strands are more resolved in IP-RP mode, SEC is a good tool for non-denaturing analysis of duplex formation of OGNs such as siRNAs [151].

Although a low resolution mode, Liu *et al.* showed that radiolabelled 25-mer morpholino OGN radiochemical purity could be analysed using SEC shift assays. Analytes bound to complementary OGNs and the radiochemical purity was defined by the proportion of shift in radioactivity from single strand to double strand under SEC conditions [267]. In other studies, conformation isomers and oligomers of a 15-mer aptamer were analysed using potassium phosphate within the SEC mobile phase and showed clear resolution of single stranded and double stranded OGNs [268]. Shimoyama *et al.* demonstrated that phosphorothioated OGNs demonstrate broader peaks under SEC conditions [269]. To mitigate this challenge the group added organic solvents to the mobile phase, which resulted in narrower peaks and less secondary interactions between the PS OGNs and stationary phase.

The stationary phase particle pore size essentially drives the efficiency of separations, whereby larger pores are more suited to larger analytes [261, 270]. Pore size can be sequentially reduced by the coupling of HPLC columns with particle pores reducing in size. This has been demonstrated to be of utility for the analysis of a large range of RNA OGNs – 20 to >1000 nucleotides in length [266].

### **1.3.4 Analysis of OGNs using mass spectrometry.**

Electrospray ionisation- mass spectrometry (ESI-MS) is often used in conjunction with a chromatographic separation for the analysis of OGNs. Its detection by mass enables accurate characterisation of analytes and their impurities caused during the manufacturing process [271, 272]. The process of ESI-MS of OGNs requires the delivery of OGNs to an ionisation source within a liquid phase and OGNs are ionised to prime them for traversing the mass spectrometer. The OGNs are delivered to a capillary needle under high potential and nebulised to form vapour droplets. An inert gas is used to dry the spray of droplets and help desolvate ionised analytes, which are then drawn in the gas phase towards a mass analyser inlet [273]. Alternatively, OGN samples can be

spotted onto a chemical matrix and ionised by matrix assisted laser desorption (MALDI) methods [127].

Within the mass analyser OGN ions travel along electric or magnetic fields to be separated by their mass to charge ratio ( $m/z$ ). There are a number of types of mass analyser, including quadrupoles, ion traps and time of flight mass analysers. Separation of ions within the mass analyser may be approached by the filtration of ions of no interest (outside a specified mass range) or by retention of specified ions (within a specified mass range), such as with quadrupoles or ion traps respectively. Time of flight mass analysers deliver pulses of ion packets that separate ions by velocity in respect to their mass. A detector produces a mass spectrum showing a range of ion  $m/z$  signals [152, 273].

ESI-MS analysis of OGNs is typically performed in negative mode where ions have multiple negative charges generated via the ESI source [271, 272]. Due to low salt and high organic solvent elution conditions, IP-RP HPLC is highly compatible with MS detection as it prevents adduction of salts to the OGN ions and thus gives higher analytical sensitivity in comparison to salt containing AEX or SEC mobile phases [132]. To circumnavigate challenges posed by AEX and SEC; it is possible to desalt samples prior to MS analysis or use volatile salts in the case of SEC separations with MS detection [181, 262]. Initial utilisation of IPRs for IP-RP ESI-MS resulted in a reduction in sensitivity as the IPR inhibits the ionisation of OGNs within the ESI droplet, however Appfel demonstrated that this challenge could be overcome by the addition of an acid modifier that acts as a less inhibitive counter ion (in comparison to the acetate in TEAA) and enhances ionisation (as it volatilises before the IPR and increases the surface chemistry of the ESI droplet in favour of ionisation) [238]. Optimisation of IP-RP HPLC ESI-MS conditions has resulted in a number of combinations of IPR with or without acid modifiers, such as HFIP for the analysis of OGNs [126, 238, 257, 260]. The focus of optimisation is predominantly balanced between chromatographic resolution/efficiency and MS sensitivity, which is hindered by high concentrations of IPR within the mobile phase. In addition to the requirement to maintaining this fine balance, there is also the potential for further ionisation suppression due to competitive ionisation processes. Analytes in higher concentration can have a matrix effect on those analytes in low concentration and inhibit their ionisation when present [274].

ESI ionisation is known as a 'soft' ionisation approach due to its ability to preserve the analyte structure during ionisation. Therefore soft ionisation techniques are readily adopted within a tandem mass spectrometry analytical workflow (MS/MS) where the ion is fragmented in a second dimension of analysis. The ion is collided with neutral gas molecules inducing its dissociation (collision induced dissociation or CID). OGNs dissociate into predictable fragment patterns (see Figure 1.12) [126, 275]. DNA OGNs tend to consistently and predictably fragment into 'w' and 'a-B'

ions while RNA OGNs tend to dissociate into 'c' and 'y' fragment ions [276, 277]. However, this consistency is lost as the OGN structure is chemically modified as chemical modifications change the way the OGN fragments and creates more complicated mass spectra [271].

Analysis of OGN synthesis impurities is enabled by calculating the mass of common impurities and identifying the analyte using extracted ion chromatograms under chromatographic co-elution conditions. Examples of impurity analysis using ESI-MS are identification of shortmers and adducts from crude synthesis mixtures of a 40-mer DNA OGN or 25-mer PS OGN [208, 240], pharmacokinetic studies of PS OGN and siRNA metabolites [242, 243], identification of siRNA structural isomers [247], P=O and adduct characterization from a PS OGN [250] and PS OGN depurination and deamidation [232, 259].

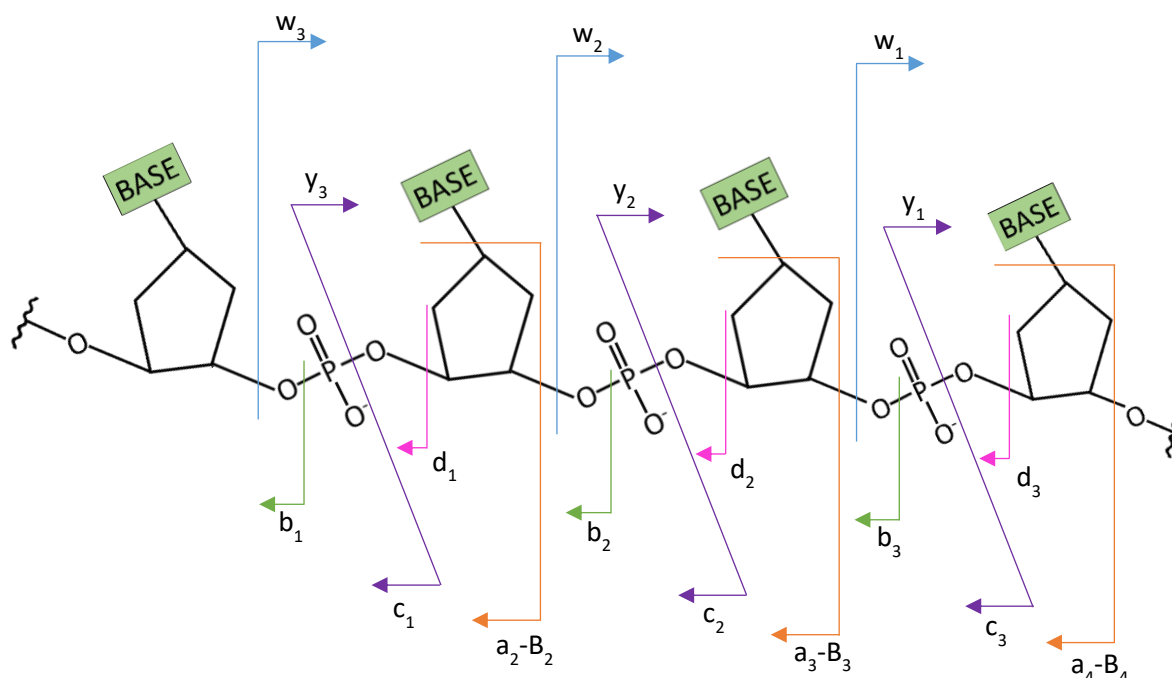


**Figure 1.12: Fragmentation nomenclature of nucleic acids as described by McLuckey and Habbibi-Goudarzi [275].** Using tandem MS analysis and collision induced dissociation, nucleic acids can be fragmented in a predictable manner. These fragments are termed the w and y ions from the 3' to 5' direction and b, c, d and a-B ions in the 5' to 3' direction. and are detected in a 2<sup>nd</sup> dimension mass spectrum.

### 1.3.5 Challenges of 1D HPLC for the analysis of OGNs- statement and summary.

One dimensional chromatography has clearly established its place within the OGN analytical landscape. Resolution of OGNs can reach up to 1 nucleotide for OGNs below 60 nucleotides in length

within AEX HPLC and IP-RP HPLC separations, decreasing to 5 nucleotides for SEC HPLC separations. The ability to separate the plethora of OGN impurities is not achievable under any 1D chromatographic mode. This is due to biased separation mechanisms and the inherent closely related chemical nature of chemically modified OGN therapeutics. Therefore, co-elution of the target OGN and impurities can occur, requiring the use of more specific detection such as MS to fully characterise peak identities.

The complexity of the mixtures requiring separation are increased further through chemical modification to OGN therapeutics with higher amounts of isomerism and a loss of chromatographic resolution (resulting in broad peaks) for highly modified OGNs- leading to higher limits of detection and co-elution of many impurities. Therefore, the requirement for native and denatured state analysis requires more than one analytical approach, providing an increasingly laborious analytical workflow that is undesirable for high throughput analysis.

### **1.3.6 Two-dimensional HPLC.**

Multidimensional chromatography has been a developing technique since the 1970's where studies demonstrated that the coupling of two dimensions of separation resulted in higher peak capacities than using a 1D approach [278]. Although early experiments suffered from long analysis times, the results showed that close or co-eluting analytes could be resolved using two-dimensional liquid-chromatography (2D-LC) methods [279]. Modern analytical methods are faster due to improvements in 2D-LC technology where fractions can be analysed in a second dimension simultaneous to sampling during the 1<sup>st</sup> dimension separation [280]. Table 1.4 describes the notation of multidimensional chromatography as defined in 2012 and now widely accepted to be standardized [281, 282].

The main aim of 2D-LC separations is increased peak capacity ( $n_c$ ), which is a term to describe the maximum number of resolvable compounds within an analytical separation [153, 283-285]. Peak capacity is defined by dividing the gradient separation time by the average peak width. In 2D-LC the 1<sup>st</sup> and 2<sup>nd</sup> dimension peak capacities are multiplied by each other to give the total peak capacity ( $n_T$ ) and can reach into the 1000's. This number however, is an overestimate of the real number of resolvable peaks due to exclusion zones, peak overlap, random peak placement and potential under sampling of the 1<sup>st</sup> dimension [280, 286-289]. The progress of stationary phase chemistries for 1D HPLC have resulted in smaller particle sizes, which has resulted in increased efficiency. In addition,

new bonded phases enable the separation of closely related analytes (such as enantiomers and diastereoisomers).

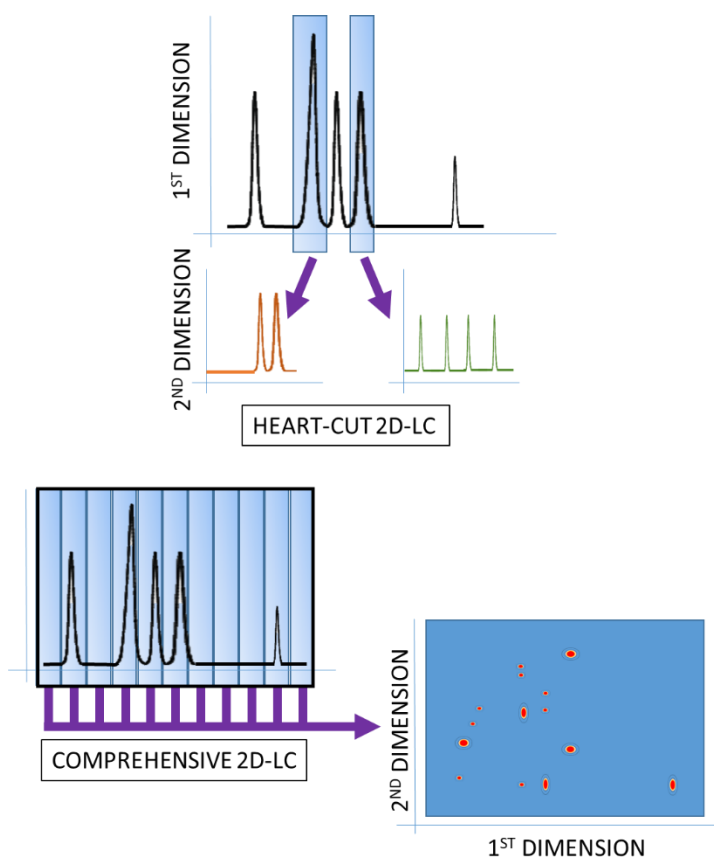


**Table 1.4: Nomenclature of multidimensional liquid chromatography terms [281, 282].**

Nomenclature Term	Description
<sup>1</sup> D	First dimension separation
<sup>2</sup> D	Second dimension separation
LCxLC	Comprehensive 2D-LC
LC-LC	Heart-cut 2D-LC
1D-LC	One dimensional liquid chromatography
2D-LC	Two dimensional liquid chromatography

**Figure 1.13: Comprehensive and heart-cut 2D-LC.** Heart-cut 2D-LC samples specific peaks in the 1<sup>st</sup> dimension, whereas comprehensive 2D-LC samples all peaks in the 1<sup>st</sup> dimension to create a contour plot of the 2D separation.

Despite this, there remains limits to the resolution of closely related analytes that differ by only a few elements in their composition, such as OGNs. The simple coupling of two columns in sequence doesn't necessarily overcome co-elution through differential column selectivity alone because serial column coupling does not fully overcome chromatographic peak overlap [288].

There are now a range of modes of 2D chromatography (GCxGC, LCxGC, LCxSFC), and in fact, two-dimensional gas chromatography (GCxGC) is a well-established technique for volatile compounds [280, 290]. 2D-LC also has a range of approaches - offline/online and heart-cut/comprehensive – to improve peak capacity and the resolution of complex sample mixtures [285, 287, 291]. In online 2D-LC the <sup>1</sup>D eluent is immediately introduced into the <sup>2</sup>D separation after sampling. However, offline

2D-LC facilitates the storage of 1<sup>st</sup>D fractions before 2<sup>nd</sup> dimension analysis to overcome sample processing or mobile phase incompatibility. Although the potential for achieving the highest resolution of analytes is reduced in online 2D-LC, it is more facile to perform in respect to offline 2D-LC where extra sample or system processing may be required e.g. desalting or column equilibration. When using a heart-cut 2D-LC method, a time period or specific peak is targeted for sampling and analysis in the 2<sup>D</sup>. The targeted area may be sampled over multiple fractions to resolve closely or co-eluting compounds (see Figure 1.13). Alternatively, comprehensive 2D-LC samples the entirety of the 1<sup>st</sup> dimension to maximise on the available peak capacity that 2D-LC offers [280].

Some of the challenges of 2D-LC are orthogonality, under sampling/sample remixing and low mobile phase compatibility [288]. In 2D-LC, orthogonal separations are achieved using different separation mechanisms between analytical dimensions. Orthogonality describes how different the two dimensions are to each other and is mathematically measurable using orthogonality metrics (explained in 1.3.6.1) [280, 292]. Theoretically orthogonal separations need to be experimentally optimised to understand if the mobile phases of each dimension are compatible with each other. For example, mobile phase incompatibility may lead to reduced retention or degradation to the stationary phase in the 2<sup>nd</sup> dimension [292, 293]. The rate of sampling must also be optimised to prevent resolved peaks from the 1<sup>st</sup> dimension re-mixing before they have been introduced to a second dimension analysis [294, 295]. The sampling rate is dependent on the number and complexity of peaks in the sample and their corresponding peak widths.

#### **1.3.6.1 Orthogonality metrics for 2D-LC.**

There are numerous orthogonality metric approaches for the analysis of chromatographic orthogonality described within the literature. Metrics assess the coverage and spread of chromatographic peaks in a 2D-LC separation space and remain the same regardless of the direction of analytical flow between dimensions [296, 297]. Non-discretized orthogonality measurements, such as calculating the correlation between retention vectors [298] or using the R<sup>2</sup> value of a 2D separation space [299] can define the correlation between retention in different dimensions. Low correlation values associate with orthogonality [285, 298]. Non-discretized calculations indicate that no scaling or segregating into 'binned' areas has been performed on retention data. Liu *et al.* proposed a geometric approach to identify the correlation between dimensions and effective separation space, justifying space that was not accessible to analytes within the 2D-LC separation. Another non-discretized orthogonality measurement is the creation of a graph that

outlines the convex hull relative area, which is a reflection of separation surface coverage [300]. Although there are many strategies to calculate  $F_{\text{coverage}}$  (coverage of the separation space), such as minimum convex hull, convex hull peel and k-nearest neighbour convex hull, Rutan *et al.*, concluded that the minimum convex hull was the most effective and simplistic approach.

However, discretized orthogonality metrics, as described within a recent review by Schure and Davis [296], are those that divide the separation space into area fractions. Information theory is a discretized measurement that can statistically describe orthogonality through mutual information, information entropy and information similarity [301]. Slonecker *et al.*, related different separation mechanisms to retention behaviour and estimated the probability of retention in a 2D separation space by computing the informational entropy of scaled retention values and how these contribute to a percent synentropy. Gilar *et al.* outlined a discretized geometric approach for visualising orthogonality of 2D-LC peptide separations [302]. Using the geometric occupancy approach peptide retention times were normalised and retention data was visualised within a scatter plot of chromatographic space (divided into bins totalling the peak capacity of separation). The occupation of the 2D separation space indicated the orthogonality of a 2D-LC workflow, although it did little to identify the level of compatibility between the two modes (in relation to retention or mobile phase miscibility).

### 1.3.6.2 Applications of 2D-LC.

2D-LC approaches have been widely used for the analysis of a range of analytes [303]. Comprehensive 2D-LC has been demonstrated as a useful method for the analysis of natural medicines plant metabolites, intact proteins, pharmaceuticals, dye extracts and polymers [304-309]. Heart-cut 2D-LC has been performed for the analysis of peptides, synthetic polymers, pharmaceuticals and environmental hydrocarbons [310-316], however the application of 2D-LC for the analysis of OGNs is currently limited to a few studies. The earliest paper demonstrating 2D-LC analysis of OGNs was in 2012 where unmodified homogeneous DNA OGNs were separated within an online comprehensive (HILIC)x(IP-RP) 2D-LC method [317] (see Figure 1.14). A peak capacity ( $n_T$ ) of 500 was achieved for analysis of 27 OGNs of varying size (2-10-mers), capitalising on OGN charge in the 1<sup>st</sup> dimension and hydrophobicity in the 2<sup>nd</sup> dimension (using 100 mM TEAA as the IPR). Within the 1<sup>st</sup> dimension, OGNs were retained by a polar interaction and separated on a polar, hydrophilic stationary phase with an aqueous mobile phase (5 mM ammonium formate pH 5) eluting the OGNs

based upon their net polarity from ribosyl and phosphoryl moieties. Orthogonality was observed between the modes of HILIC and IP-RP HPLC due to differential retention of OGNs containing thymine, adenine or cytosine bases. Reduced retention was observed in the 2<sup>nd</sup> dimension due to the eluent strength of the 1<sup>st</sup> dimension, so to overcome this challenge C18 trapping columns were used for solvent-aqueous substitution. Goyon and Zhang also used HILIC within 2D-LC methods for the analysis of antisense OGNs and their associated impurities [318]. As HILIC mobile phases are highly compatible with MS detection, the 2D-LC methods resolved OGNs using 25 mM ammonium acetate and acetonitrile in the 2<sup>nd</sup> dimension. IP-RP (using 16.3 mM TEA, 400 mM HFIP and methanol) and AEX (using 40 mM tris, acetonitrile and sodium bromide) was used for 1<sup>st</sup> dimension separations. Multiple FLP associated impurities were identified using the 2D-LC methods with high resolution MS detection.

In 2014, Álvarez Porebski and Lynen demonstrated offline comprehensive 2D separation of OGNs was achievable by interfacing IP-RP and SAX HPLC with capillary gel electrophoresis (CGE) [319]. Capillary gel electrophoresis is a size based gel electrophoretic separation technique, where analytes such as OGNs are separated in a capillary filled with a polymer based upon differences in charge. Increases in OGN charge as a result of increasing OGN length (in nucleotides) facilitate size based separation. Homogeneous OGNs consisting of either adenine, thymine, cytosine or uracil bases up to 35 nucleotides in length were analysed using offline comprehensive (IP-RP)x(CG) and (SAX)x(CG) 2D analysis. The 1<sup>st</sup> dimension HPLC separation was performed using 100 mM TEAA at pH 5.5 for IP-RP or sodium chloride eluting salt at pH 11.5 for SAX. The OGNs were separated orthogonally by sequence in the IP-RP and SAX 1<sup>st</sup> dimensions and then by size in a CGE 2<sup>nd</sup> dimension separation. Although sensitivity was an issue when coupling the two separation techniques, the results demonstrated improved resolution of complex samples, although not total resolution of all analytes.

Dual labelled OGNs with fluorophores were resolved by Anacleto *et al.*, using two orthogonal dimensions of IP-RP analysis [320]. In an offline 2D-LC purification method, 100 mM TEAA was used to separate the target OGN from highly retained impurities. Using an orthogonal 2<sup>nd</sup> dimension 100 mM TetBAB was employed to resolve OGNs by their length away from the target OGN. The more hydrophobic IPR TetBAB negated hydrophobicity differences between modified and unmodified analytes and was able to resolve a pure product from synthesis impurities. More recently, the application of 2D-LC for the analysis of OGNs was described by Koshel *et al.*, for the analysis of dye conjugated OGNs. 100 mM hexylammonium acetate demonstrated superior selectivity between shortmer OGNs and the FLP labelled OGN in comparison with a 15 mM TEA:400 mM mobile phase for IP-RP HPLC analysis. When analysed by MS, the TEA:HFIP mobile phase demonstrated >60 fold

reduction to the limit of detection. However, when conditions were coupled for heart-cut 2D-LC interfaced with MS analysis; the OGNs were resolved using the hexylammonium acetate mobile phase then heart cut peak fractions were introduced into the 2<sup>nd</sup> dimension (under TEA:HFIP conditions) with more sensitive MS analysis. The high organic solvent content of the first dimension (required to elute the OGN under strong IP-RP conditions) was diluted 3.5 fold with the co-introduction of 2<sup>nd</sup> dimension mobile phase alongside the 1<sup>st</sup> dimension fraction using a tee junction for an at column dilution approach. This enabled retention in the 2<sup>nd</sup> dimension by diluting the eluotropic conditions of the 1<sup>st</sup> dimension and demonstrates how solvent modulation can be employed to overcome the challenges of mobile phase in compatibility [321].

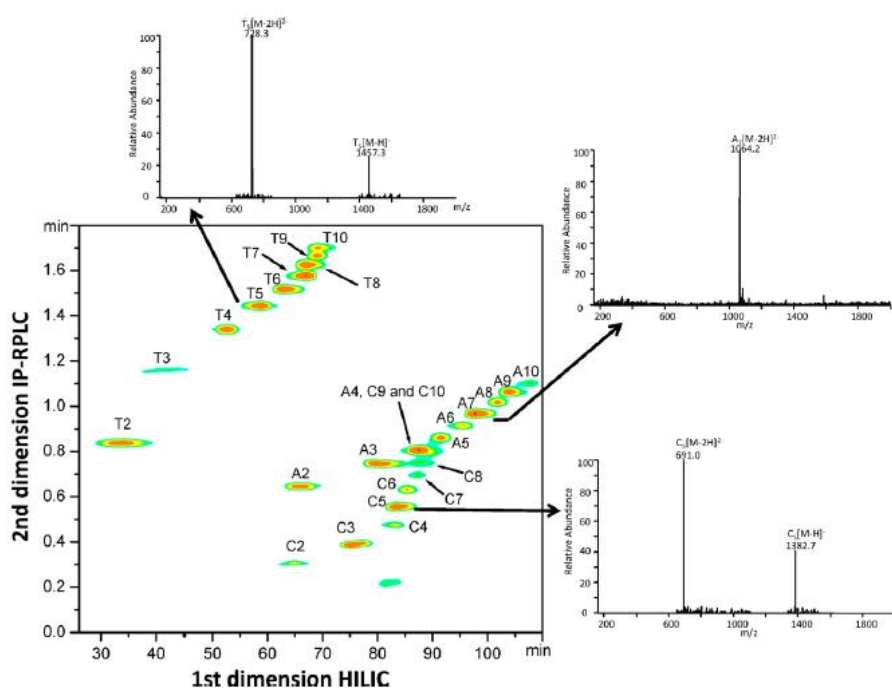


**Figure 1.14: Comprehensive (HILIC)x(IP-RP) analysis of 27 polymeric dA, dC, dT OGNs showing mass spectra of specific OGNs.** Re-printed by permission from Li *et al.* [317]. Elsevier: Journal of Chromatography A (2012). HILIC <sup>1</sup>D analysed on a Ascentis Silica column with a mobile phase gradient of 43-27 mM ammonium formate, pH 5 and 77-50% MeCN, with 15-45% gradient application of 5 mM ammonium formate pH 5 mobile phase at 35°C. IP-RP <sup>2</sup>D analysed on a Xbridge C18 column using 100 mM TEAA and a gradient of 6-12 % MeCN at 35°C.

The most diverse example of using 2D-LC methods for analysis of OGNs, with specific focus on synthesis impurities was published by Roussis *et al.*, in 2018 [322]. The study utilised 2D-LC HPLC equipment for both heart-cut and comprehensive method development for analysis of crude OGN

samples. The 2D-LC was coupled with a mass spectrometer for mass based detection of OGNs. In the first method of online heart-cut (SEC)-(IP-RP) 2D-LC, an OGN sample with lower molecular weight impurities was analysed. In heart cut mode, six fractions were collected for further analysis using 100 mM ammonium acetate in 1<sup>st</sup> SEC conditions and the 2<sup>nd</sup> dimension separation was performed using 5 mM TBuAA as IPR for IP-RP analysis. Although this demonstrated 2D-LC mobile phase compatibility, the method did not provide much benefit over 1D-LC for analysis of OGNs <30 nucleotides long in terms of peak capacity and orthogonal resolution. Another online heart-cut (RP)-(IP-RP) 2D-LC method was developed for the analysis of a crude OGN sample containing monomethoxytrityl (MMT) protected OGNs and their deprotected counterparts. A trap column was employed between the 1<sup>st</sup> and 2<sup>nd</sup> dimension to reduce 2<sup>D</sup> sample volume as broad peaks were observed in the first dimension analysis (utilising reversed phase conditions of 200 mM ammonium acetate and a methanol gradient). The resolved MMT-on and MMT-off OGNs were then further analysed in a second dimension of IP-RP using 5 mM TBuAA as the IPR. The reduction in sample processing using the method avoided further chemical conversion of the OGNs and allowed accurate characterisation of MMT status and impurity profile, which was beneficial for pH stability studies. The online heart-cut approach was further utilised for the (SAX)-(IP-RP) 2D-LC analysis of PS OGNs to identify isobaric impurities (the addition of an oxygen N [+O] or the removal of an oxygen and addition of a sulphur N [+S-O] to the OGN) that are difficult to resolve by MS alone or within a 1D separation. The results showed that dithioate impurities were resolved from a PS target OGN peak by SAX (utilising sodium bromide for elution) but addition of an oxygen atom to phosphodiester, N [+O] OGNs were not resolved, with differences in charge distributions between the two OGNs the proposed cause. The group also developed online comprehensive (RP)x(IP-RP) and (IP-RP)x(IP-RP) 2D-LC methods to analyse MMT-on OGNs and found that the (RP)x(IP-RP) was more orthogonal than (IP-RP)x(IP-RP) and could be qualitative or semi quantitative during analytical screening.

#### **1.4 Summary of findings and project aims.**

OGN therapeutics are emerging as an important class of therapeutic agents currently with a market value of >\$2 billion (which is estimated to grow in the coming years) [56, 57]. With limited regulatory governance, there remains the requirement to better understand the cohort of manufacturing impurities produced in solid phase synthesis. Analytical data feeds into understanding of the safety of different impurities, helps to optimise manufacturing processes and defines analytical strategies for applications for regulatory approval. Data generated in novel analytical approaches will help

further define levels of threshold reporting and identify new classes of OGN impurity as the chemical complexity continues to develop.

1D-LC is a powerful technique for the analysis of OGN therapeutics and has been widely used for separation of synthetic OGNs and their associated manufacturing impurities. Resolution of size variants (1-60-mers) has reached 1 nucleotide in both SAX and IP-RP modes of chromatography, which is likely to be the reason why both approaches are utilised within industry for analysis of OGNs and their associated manufacturing impurities. Size and sequence based separations are demonstrated in a range of conditions, however the closely related chemical nature of synthesis impurities with the target OGN results in co-elution and low resolution of some impurities with other impurities or with the FLP itself. Therefore, full characterisation of OGNs and their synthesis impurities is not possible under any 1D-LC approach with UV detection.

Although there are no specific regulatory policies on the reporting of OGN synthesis impurities, regulatory bodies and development scientists have published guidance on which impurities require characterisation. As the full subset of potential OGN impurities are not capable of being resolved using 1D approaches, there remains a need to further improve the chromatographic resolution of OGNs and their associated manufacturing impurities to facilitate better peak capacity and characterisation [98, 99]. For the analysis of OGN therapeutics, there are potentially 1000's of impurities present, however characterisation of these impurities can be reduced to the analysis of impurity subsets (according to their structure or chemistry). Coupling of MS to 1D-LC assists with characterisation of impurities, however this adds an additional step to the analytical method, requires expensive instrumentation and further technical ability of the analyst. Furthermore, given that MS cannot identify isobaric components, there is clearly a need to develop improved separation methods for the analysis of OGN therapeutics.

2D-LC has demonstrated improved peak capacity using multiple dimensions of analysis. 2D-LC has also shown utility in the analysis of many different types of analyte, however there are limited studies on the analysis of OGNs and their manufacturing impurities. Further development of 2D-LC methods would help to resolve closely or co-eluting OGNs with the application of higher peak capacities and dimensional orthogonality. Such methods could assist with characterisation of OGN impurities during synthesis optimisation, feed into safety and toxicology studies and simplify the separation space prior to using additional downstream detection methods.

### 1.4.1 Project aim and objectives.

**The aim of this thesis is to develop 2D-LC methods for the analysis of OGNs and their associated manufacturing impurities**

To achieve this aim, a number of objectives are required for the research. Initially, one-dimensional separations will be performed and optimised to facilitate orthogonal separations. OGN separations that are optimised to depend on either size or sequence demonstrate that orthogonal separations can be performed in a range of modes. The first objective of the research is to optimise such size or sequence dominated separation mechanisms in the modes of AEX, SEC and IP-RP HPLC. These optimisations will be performed on a set of model OGNs varying in size, sequence and level of chemical modification (specifically the PS modification). Focus will be placed upon the improvement of resolution and selectivity in order to improve chromatographic separations of OGNs and their associated manufacturing impurities.

The next objective of research will be to assess how orthogonal these optimised separations are, by using mathematical orthogonality approaches. In addition, the separations will be analysed to understand peak capacity and how a potential 2D-LC workflow increases resolution of OGN impurities. 2D-LC workflow designs will be created from orthogonality and peak capacity assessment.

After theoretical 2D-LC workflow design, the next objective of research will be to develop understanding of dimensional compatibility by undertaking feasibility experiments and optimising LC-based reference mapping strategies to identify OGN impurities within the analysis method. This approach will be confirmed by MS analysis of the 1<sup>st</sup> dimension fractions to confirm OGN impurities present within each heart-cut fraction of an offline 2D-LC method.

Following optimisation of an offline 2D-LC method, online heart-cut 2D-LC methods will be performed to demonstrate the approach in an automated strategy. Automation of analytical methods reduces preparation time and requirement for technical expertise of the analyst operator (which reduces analytical costs).

2D-LC methods will be optimised for unmodified OGNs to first demonstrate the process of method development. 2D-LC methods for unmodified OGNs will demonstrate utility of the method when applied to a range of unmodified OGN types, such as PCR primers. The chemical complexity of OGN analytes will be increased and 2D-LC analysis of model OGNs fully chemically modified with PS backbones will be developed. Incrementally increasing chemical complexity of analytes facilitates the understanding of retention behaviour and helps to develop strategies to overcome chromatographic challenges imposed by increased chemical complexity (such as reduced efficiency and lower selectivity). The final objective is to develop 2D-LC for the analysis of OGN therapeutics produced by GlaxoSmithKline, which are further chemically modified by PS, 2'-O-MOE and conjugate modifications.

## Chapter 2: Materials and Methods.

### 2.1 Materials.

#### 2.1.1 Equipment and HPLC columns.

Table 2.1: Equipment and HPLC columns.

Equipment and HPLC Columns	Manufacturer
Centrifuge	Haeraeus Biofuge Pico
Sonicator bath	Fisherbrand
Spectrophotometer 2000 Nanodrop	Thermo Fisher Scientific
pH Meter	Mettler Toledo
Analytical balance	Kern
Stirrer plate	Thermo Fisher Scientific
Vortex mixer	Waverly
Automatic pipettes	Gilson
Accucore 150Å C18 2.1*50 mm (Chapter 3)	Thermo Fisher Scientific
Accucore 150Å C18 2.1*100 mm (Chapter 6)	Thermo Fisher Scientific
DNAPac RP 2.1*100 mm	Thermo Fisher Scientific
DNAPac PA200 RS 4.6*15 mm	Thermo Fisher Scientific
Advance BioSEC 4.6*300 mm	Agilent
HPLC Ultimate 3000	Thermo Scientific
MaXis UHR ToF MS	Bruker
HPLC Viper MP35N tubing (0.1-0.18mm ID)	Thermo Fisher Scientific
20 µL viper sample loop	Thermo Fisher Scientific

#### 2.1.2 Chemicals and reagents.

Table 2.2: Chemical and reagents.

Chemicals and Reagents	Manufacturer
Acetonitrile (MeCN) HPLC grade	Fisher
Methanol (MeOH) HPLC grade	Fisher
Isopropanol (IPA) HPLC grade	Fisher
Triethylammonium acetate buffer 1 M pH7 (TEAA)	Sigma Aldrich
Tributylamine 99% (TBA)	Acros Organics
Tetrabutylammonium acetate 1 M (TetBAA)	Supelco
Tetrabutylammonium bromide 99% (TetBAB)	Sigma Aldrich
Sodium chloride 99% (NaCl)	Sigma Aldrich
Sodium perchlorate monohydrate (NaClO <sub>4</sub> H <sub>2</sub> O)	Alpha Aesar 97%

**Table 2.2 continued...: Chemical and reagents.**

<b>Chemicals and Reagents</b>	<b>Manufacturer</b>
Tris(hydroxymethyl)aminomethane 99.9% (Tris)	Sigma Aldrich
Monosodium phosphate 98% (NaH <sub>2</sub> PO <sub>4</sub> )	Sigma Aldrich
Potassium Chloride 99% (KCl)	Sigma Aldrich
1,1,1,3,3,3-Hexafluoro-2-propanol 99% (HFIP)	Sigma Aldrich
Tetrasodium ethylenediaminetetraacetate hydrate 99% (Na <sub>4</sub> EDTA)	Sigma Aldrich
Ammonium Phosphate 98% (H <sub>12</sub> N <sub>3</sub> O <sub>4</sub> P)	Sigma Aldrich
Water HPLC grade	Fisher
Sodium thiocyanate 98% (NaSCN)	ACS
Hydrochloric acid 37% (HCl)	Sigma Aldrich
Glacial Acetic Acid HPLC grade	J T Baker
Sodium hydroxide 98% (NaOH)	Sigma Aldrich
Oligonucleotides	Eurofins or GSK
ESI-L Low Concentration Tuning Mix (Part# G1969-85000)	Agilent Technologies

### **2.1.3 OGN sample preparation.**

OGNs were prepared from lyophilised form and solubilised (vortex mixing and centrifugation) in 100 µL of HPLC grade water. The stock concentration was calculated from the Eurofins sample QC sheet (mass of OGN and MW of OGN). For further validation, OGN samples were analysed using a Nanodrop spectrophotometer to analyse their absorbance at 260 nm wavelength. To prepare lower concentrations of OGN samples, OGN stocks were mixed (vortex and centrifugation) with HPLC grade water after dilution.

Various OGN sample sets were used within this research. Tables 2.3-2.6 summarise the OGNs used.

**Table 2.3: Model OGNs used for evaluation of size and sequence dependent separations in Chapter 3. OGNs are described by size in nucleotide length (nt), sequence and monoisotopic mass. A capital letter denotes a DNA nucleotide and a \* denotes a PS bond.**

OGN Model Set	OGN Description	Sequence 5' to 3'	Length (nt)	Monoisotopic Mass (Da)
19-24-mer size variant dT ladder	dT 19-mer	TTT TTT TTT TTT TTT TTT T	19	5714.912
	dT 20-mer	TTT TTT TTT TTT TTT TTT TT	20	6018.957
	dT 21-mer	TTT TTT TTT TTT TTT TTT TTT	21	6323.003
	dT 22-mer	TTT TTT TTT TTT TTT TTT TTT T	22	6627.049
	dT 23-mer	TTT TTT TTT TTT TTT TTT TTT TT	23	6931.095
	dT 24-mer	TTT TTT TTT TTT TTT TTT TTT TTT	24	7235.140
30-mer sequence variants	Sequence variant 1	TCC TTG ACC ATC TGC TCG TAC TCC TCG TCT	30	9006.485
	Sequence variant 2	ACA AAG GTG AGG TTT AAA AGA AGT TTT CTG	30	9328.595
16-mer PS variants	Unmodified variant	ACA AAA GTC CGT GAG A	16	4920.883
	Single PS on 5' terminal.	A*CA AAA GTC CGT GAG A	16	4936.860
	Single PS on 3' terminal.	ACA AAA GTC CGT GAG* A	16	4936.860
	Full PS.	A*C*A* A*A*A* G*T*C* C*G*T* G*A*G* A	16	5160.538

**Table 2.4: Unmodified OGNs utilised for 2D-LC method development in Chapter 4. Size/sequence variant OGNs and 1<sup>st</sup> generation model OGN therapeutic and its associated manufacturing impurities are described by impurity type, size in nucleotide length (nt), OGN sequence and monoisotopic mass. A capital letter denotes a DNA nucleotide.**

OGN Model set	OGN Description	Sequence	Length (nt)	Monoisotopic Mass (Da)
Size & Sequence isomer	19-mer i	CTA GTT ATT GCT CAG CGG T	19	5806.980
	19-mer ii	CGC CAT CCA CGC TGT TTT G	19	5727.963
	19-mer iii	ATT AGG ACA AGG CTG GTG G	19	5930.022
	19-mer iv	AGA GTT TGA TCA TGG CTC A	19	5840.003
	20-mer i	GGG ATG TTT AAT ACC ACT AC	20	6113.054
	20-mer ii	CCC TCA TAG TTA GCG TAA CG	20	6074.043
	20-mer iii	TTG CTG TTG CAC AGT GAT TC	20	6111.026
	20-mer iv	GGC AGC AGC CAC AGG TAA GA	20	6182.086
	21-mer i	GCC TGA ACA CCA TAT CCA TCC	21	6292.089
	21-mer ii	ACC GTA AGT AGC ATC ACC TTC	21	6347.094
	21-mer iii	GAC TGG TTC CAA TTG ACA AGC	21	6427.107
	21-mer iv	CGT TCG ACC CCG CCT CGA TCC	21	6276.056
	22-mer i	CTT TTC GGT TAG AGC GGA TGT G	22	6809.137
	22-mer ii	TAC GGT TAC CTT GTT ACG ACT T	22	6688.123
	22-mer iii	TGG TCT TGT TAG AAT TTG TTA C	22	6758.128
	22-mer iv	TCC GGA TTA TTC ATA CCG TCC C	22	6618.117

**Table 2.4 continued...: Unmodified OGNs utilised for 2D-LC method development in Chapter 4. Size/sequence variant OGNs and 1<sup>st</sup> generation model OGN therapeutic and its associated manufacturing impurities are described by impurity type, size in nucleotide length (nt), OGN sequence and monoisotopic mass. A capital letter denotes a DNA nucleotide.**

OGN Model set	OGN Description	Sequence 5' to 3'	Length (nt)	Monoisotopic Mass (Da)
1st generation unmodified OGN therapeutic model and impurities	Unmodified FLP	CTC AAA TAT ACT TAC GAT TA	20	6056.058
	5'-1 shortmer	TCA AAT ATA CTT ACG ATT A	19	5767.012
	5'-2 shortmer	CAA ATA TAC TTA CGA TTA	18	5462.966
	5'-3 shortmer	AAA TAT ACT TAC GAT TA	17	5173.920
	N+1 longmer	CTC AAA TAT ACT TTA CGA TTA	21	6360.104

**Table 2.5: Phosphorothioated OGNs utilised for 2D-LC method development in Chapter 5. Model A and B OGNs are two fully phosphorothioated OGN sequences and their associated manufacturing impurities are described by size in nucleotide length (nt), OGN sequence and monoisotopic mass. A capital letter denotes a DNA nucleotide and a \* denotes a PS bond.**

OGN Model Set	OGN Description	Sequence 5' to 3'	Length (nt)	Monoisotopic Mass (Da)
PS OGN Model A	FLP	C*T*C* A*A*A* T*A*T* A*C*T* T*A*C* G*A*T* T*A	20	6359.624
	5'-1 Shortmer	T*C*A* A*A*T* A*T*A* C*T*T* A*C*G* A*T*T* A	19	6054.601
	5'-2 Shortmer	C*A*A* A*T*A* T*A*C* T*T*A* C*G*A* T*T*A	18	5734.578
	5'-3 Shortmer	A*A*A* T*A*T* A*C*T* T*A*C* G*A*T* T*A	17	5429.555
	N+1 Longmer	C*T*C* A*A*A* T*A*T* A*C*T* T*T*A* C*G*A* T*T*A	21	6679.647
	P=O on 5' terminal	CT*C* A*A*A* T*A*T* A*C*T* T*A*C* G*A*T* T*A	20	6343.647
	P=O on 5'-1 shortmer 3' terminal	T*C*A* A*A*T* A*T*A* C*T*T* A*C*G* A*T*T*A	19	6038.624
PS OGN Model B	Target OGN	T*G*T* C*A*G* T*C*T* A*C*T* C*A*C* G*A*T* T*A	20	6367.603
	5'-1 Shortmer	G*T*C* A*G*T* C*T*A* C*T*C* A*C*G* A*T*T* A	19	6047.580
	5'-2 Shortmer	T*C*A* G*T*C* T*A*C* T*C*A* C*G*A* T*T*A	18	5702.551
	5'-3 Shortmer	C*A*G* T*C*T* A*C*T* C*A*C* G*A*T* T*A	17	5382.528
	N+1 Longmer	T*G*T* C*A*G* T*C*T* C*A*C* T*C*A* C*G*A* T*T*A	21	6672.626
	P=O on 5' terminal	TG*T* C*A*G* T*C*T* A*C*T* C*A*C* G*A*T* T*A	20	6351.626
	P=O on 5'-1 shortmer 5' terminal	GT*C*A*G*T*C*T*A*C*T*C*A*C*G*A*T*T*A	19	6031.603

**Table 2.6: Therapeutic OGNs utilised for 2D-LC method development in Chapter 6. Unconjugated and conjugated OGNs are two fully phosphorothioated OGN sequences (with additional 2'-O-MOE modifications) and their associated manufacturing impurities are described by size in nucleotide length (nt), OGN sequence and mass by manufacturing certificate of analysis specification.**

OGN Model Set	OGN Description	Sequence 5' to 3'	Specification Mass (Da)
PS, 2'-O-MOE therapeutic OGN	FLP	Confidential	7344.2
	N-1 Shortmer	Confidential	6924.8
	N-2 Shortmer	Confidential	6531.5
	N+1 Longmer	Confidential	7689.5
	P=O	Confidential	7328.1
PS, 2'-O-MOE therapeutic OGN conjugate	FLP	Confidential	8863.9
	N-1 Shortmer	Confidential	8518.6
	N-2 Shortmer	Confidential	8141.3
	N+1 Longmer	Confidential	9193.2
	P=O	Confidential	8847.8
	Abasic	Confidential	8730.8

#### 2.1.4 HPLC mobile phases.

A 0.2 M Na<sub>4</sub> EDTA stock solution was prepared by mixing 7.6 g Na<sub>4</sub> EDTA with water at a total volume of 100 mL in a glass bottle. This stock was used in IP-RP HPLC mobile phases.

The weak IP-RP, strong IP-RP (in conjunction with TetBAA) mobile phases were prepared within a 1000 mL volumetric flask by adding aqueous solutions together first (100 mL of 1 M TEAA stock solution, 0.5 mL of 0.2 M Na<sub>4</sub> EDTA stock solution and water to 1000 mL volume). In mobile phase B, the organic solvent (250mL MeCN) was added last. HFIP modified IP-RP mobile phases were also made using this approach (addition of 4.21-8.42 mL for 40 mM and 80 mM respectively). The HFIP and IPR were mixed thoroughly in the aqueous phase prior to slow addition of organic solvent to mix. Solutions were mixed by inversion of the volumetric flask.

A 100 mM stock solution of tributylammonium acetate (TBUAA) was prepared by adding 6 mL tributylamine to 225mL MeCN and 1.5 mL glacial acetic acid under inert gas and adding water to 250 mL volume. This stock was used when preparing mobile phases in volumetric flasks. Solutions were mixed by inversion of the volumetric flask.

1000 mL volume strong IP-RP mobile phases (in conjunction with TBuAA) were prepared by adding 50 mL of the 100 mM IPR stock solution to water with 10  $\mu$ L of 0.2M Na<sub>4</sub> EDTA stock solution. 50 mL of MeCN was added to mobile phase A and 750 mL was added to mobile phase B.

1000 mL volume strong IP-RP mobile phases (in conjunction with TetBAA) were prepared by adding 2.5 mL of the 1 M stock solution of TetBAA to water. 100 mL of MeCN was added to mobile phase A and 800 mL was added to mobile phase B.

1000 mL volume strong IP-RP mobile phases (in conjunction with TetBAB) were prepared by adding 0.8 g solid IPR powder to 100 mL water and mixing on a stirrer plate. Following solubilisation, organic solvents were added to the solutions. 100 mL of MeCN was added to mobile phase A and 800 mL was added to mobile phase B and the volume was increased to 1000 mL with water.

1000 mL volume SAX mobile phases (in conjunction with NaCl or NaClO<sub>4</sub>) were prepared by first weighing out solid salt powders (2.43 g tris for both mobile phases and 73.05 NaCl, 56.18 g NaClO<sub>4</sub> for mobile phase B) and adding to a flask with 600 mL water. Mobile phase pH was adjusted using either NaOH or HCl solutions. Water was added to total required volume, with addition of organic solvent (200 mL MeCN where required) last. The solutions were thoroughly mixed on a magnetic stirrer plate.

1000 mL volume SAX mobile phases (in conjunction with NaSCN) were prepared by first weighing out solid salt powders (5.75 g H<sub>12</sub>N<sub>3</sub>O<sub>4</sub>P for both mobile phases 81.07 g NaSCN for mobile phase B) and adding to a flask with 600 mL water. Mobile phase pH was adjusted using either NaOH solution. Water was added to total required volume, with addition of organic solvent (50 mL MeCN) last. The solutions were thoroughly mixed on a magnetic stirrer plate.

1000 mL SEC mobile phases were prepared by first weighing out solid salt powders (either 18 g NaH<sub>4</sub>PO or a mixture of 6 g NaH<sub>4</sub>PO with 7.45 KCl) and adding to a flask with 600 mL water. Mobile phase pH was adjusted using either NaOH or HCl solutions. Water was added to total required volume, with addition of organic solvent (up to 300 mL MeCN where required) last to prevent salt crystallisation in high organic conditions. The solutions were thoroughly mixed on a magnetic stirrer plate.

The HPLC phases were degassed using a sonicator bath for 30 mins where analytical equipment did not have a degassing module. HPLC mobile phases are stated in table 2.7.

**Table 2.7: HPLC mobile phases used for optimisation of HPLC analysis of OGNs.**

<b>HPLC Mode</b>	<b>Mobile Phase</b>
Weak IP-RP in conjunction with TEAA	<b>A:</b> 100 mM TEAA, 0.1 mM EDTA Na <sub>4</sub> , 0.1% v/v MeCN. <b>B:</b> 100 mM TEAA, 0.1 mM EDTA Na <sub>4</sub> , 25% v/v MeCN.
Strong IP-RP in conjunction with TBuAA	<b>A:</b> 5 mM TBuAA, 0.1 μM EDTA Na <sub>4</sub> , 10% v/v MeCN. <b>B:</b> 5 mM TBuAA, 0.1 μM EDTA Na <sub>4</sub> , 80% v/v MeCN.
Strong IP-RP in conjunction with TetBAA	<b>A:</b> 2.5 mM TetBAA, 10% v/v MeCN. <b>B:</b> 2.5 mM TetBAA, 80% v/v MeCN.
Strong IP-RP in conjunction with TetBAB	<b>A:</b> 2.5 mM TetBAB, 10% v/v MeCN. <b>B:</b> 2.5 mM TetBAB, 80% v/v MeCN.
HFIP modified IP-RP modified with 40 mM HFIP	<b>A:</b> 100 mM TEAA, 40 mM HFIP, 0.1 mM EDTA Na <sub>4</sub> , 0.1% v/v MeCN. <b>B:</b> 100 mM TEAA, 40 mM HFIP, 0.1 mM EDTA Na <sub>4</sub> , 25% v/v MeCN.
HFIP modified IP-RP modified with 80 mM HFIP	<b>A:</b> 100 mM TEAA, 80 mM HFIP, 0.1 mM EDTA Na <sub>4</sub> , 0.1% v/v MeCN. <b>B:</b> 100 mM TEAA, 80 mM HFIP, 0.1 mM EDTA Na <sub>4</sub> , 25% v/v MeCN.
SAX in conjunction with NaCl	<b>A:</b> 20 mM Tris, pH 6-5-12.5. <b>B:</b> 20 mM Tris, 1250 mM NaCl, pH 6-5-12.5
SAX in conjunction with NaCl and modified with MeCN	<b>A:</b> 20 mM Tris, pH 6-5-12.50, 20% v/v MeCN. <b>B:</b> 20 mM Tris, 1250 mM NaCl, pH 6-5-12.50, 20% v/v MeCN.
SAX in conjunction with NaClO <sub>4</sub>	<b>A:</b> 20 mM Tris, pH 6-5-12.5. <b>B:</b> 20 mM Tris, 1250 mM NaClO <sub>4</sub> , pH 6-5-12.5.
SAX in conjunction with NaClO <sub>4</sub> and modified with MeCN	<b>A:</b> 20 mM Tris, pH 6-5-12.50, 20% v/v MeCN. <b>B:</b> 20 mM Tris, 1250 mM NaClO <sub>4</sub> , pH 6-5-12.50, 20% v/v MeCN.
SAX in conjunction with NaSCN	<b>A:</b> 50 mM H <sub>12</sub> N <sub>3</sub> O <sub>4</sub> P, pH 8.5, 95:5% v/v MeCN. <b>B:</b> 50 mM H <sub>12</sub> N <sub>3</sub> O <sub>4</sub> P, pH 8.5, 95:5% v/v MeCN and 1000 mM NaSCN. <b>C:</b> MeCN.
SEC initial mobile phase	<b>ISOCRATIC:</b> 150 mM NaH <sub>4</sub> PO pH 7.5.
SEC optimised mobile phase	<b>ISOCRATIC:</b> 50 mM NaH <sub>4</sub> PO, 100 mM KCl pH 7.5.
SEC optimised mobile phase modified with MeCN	<b>ISOCRATIC:</b> 50 mM NaH <sub>4</sub> PO, 100 mM KCl pH 7.5, 30% v/v MeCN.

## 2.2 HPLC analytical equipment – configurations.

Configuration 1: Thermo Scientific (Dionex) U3000 HPLC with the following modules: SRD-3600 degasser, DGP-3600RS dual ternary pump system, WPS-3000TFC autosampler with fractionation valve, TCC-3000SD fan assisted column oven with 2\* multi switch valves and a VWD-3400RS UV-VIS multi wavelength detector.

Configuration 2: Thermo Scientific (Dionex) U3000 HPLC with the following modules: LPG-3400RS quaternary pump system, WPS-3000TBFC autosampler with fractionation valve, TCC-3000RS fan assisted column oven and a VWD-3400RS UV-VIS multi wavelength detector. All mobile phases used on this machine were degassed in a sonication bath for 30 minutes prior to analysis.

Configuration 3: Thermo Scientific (Dionex) U3000 HPLC with the following modules: SRD-3600 degasser, DGP-3600BM dual ternary pump system, WPS-3000TFC autosampler with fractionation valve, TCC-3000RS fan assisted column oven and a VWD-3400RS UV-VIS multi wavelength detector.

One dimensional HPLC was performed on all equipment configurations (configuration 1, 2, and 3), while 2D-LC was performed specifically on configuration 1. Analyses were performed with the analytical column held within a column oven set to between 30-80 °C or at ambient temperature with the column connected outside of the column oven. The mobile phase velocity is stated under each chromatogram and ranged between 0.2-1.2 mL/min. Thermo Fisher Viper MP35N biocompatible tubing was connected within the HPLC equipment (0.1-0.18 mm internal diameter - 0.1 mm for IP-RP/SEC and 0.18mm for SAX HPLC specifically). A 20 µL sample loop was used for all analyses. The analytical column was equilibrated with a minimum of 20 column volumes for SEC and SAX analysis and a minimum of 100 column volumes for IP-RP analysis. Coefficient of variation on retention time and peak area are stated in Appendix 1, Table A1.1. UV detection was performed at 260 nm for OGNs. Needle wash was composed of 10% v/v MeOH and the rear seal wash was 20% v/v IPA. The HPLC analytical methods were created using Chromeleon software (version 6.8, Thermo Scientific), which also was utilised for chromatographic data analysis. Analytical gradients are stated in figure legend of chromatograms.

Replicate analyses were performed for online and offline 2D-LC methods outlined in Chapters 3-6. Replicates are shown in Appendix 2.

### **2.2.1 HPLC equipment- fractionation.**

To perform fractionation, an extra valve was utilised. The fractionation valve allows samples to be introduced into the flow path via a bridge tube from the fractionation valve to the injection valve (see Figure 2.1a). The injection valve switches position to allow the sample to be introduced to the flow path and the fractionation valve allows unwanted effluent to divert to waste (see Figure 2.1b). At the required fractionation time-point, the fractionation valve switches position to divert effluent to an empty sample vial within the autosampler for fractionation (see Figure 2.1c). When fractionation is no longer required, the fractionation valve switches back to the analytical position (as shown in Figure 2.1b). The fractionated samples can then be further processed/analysed in an offline fashion.

The fractionation settings incorporated a 3 second delay time before diverting effluent to empty microvials within the autosampler (using a 0.1\*550 mm MP35N Viper tube of 4 µl volume). For 2D-LC methods, fractions were sampled between defined time points specific to the retention time window of the oligonucleotide sample (see Appendix 1, Table A1.2).

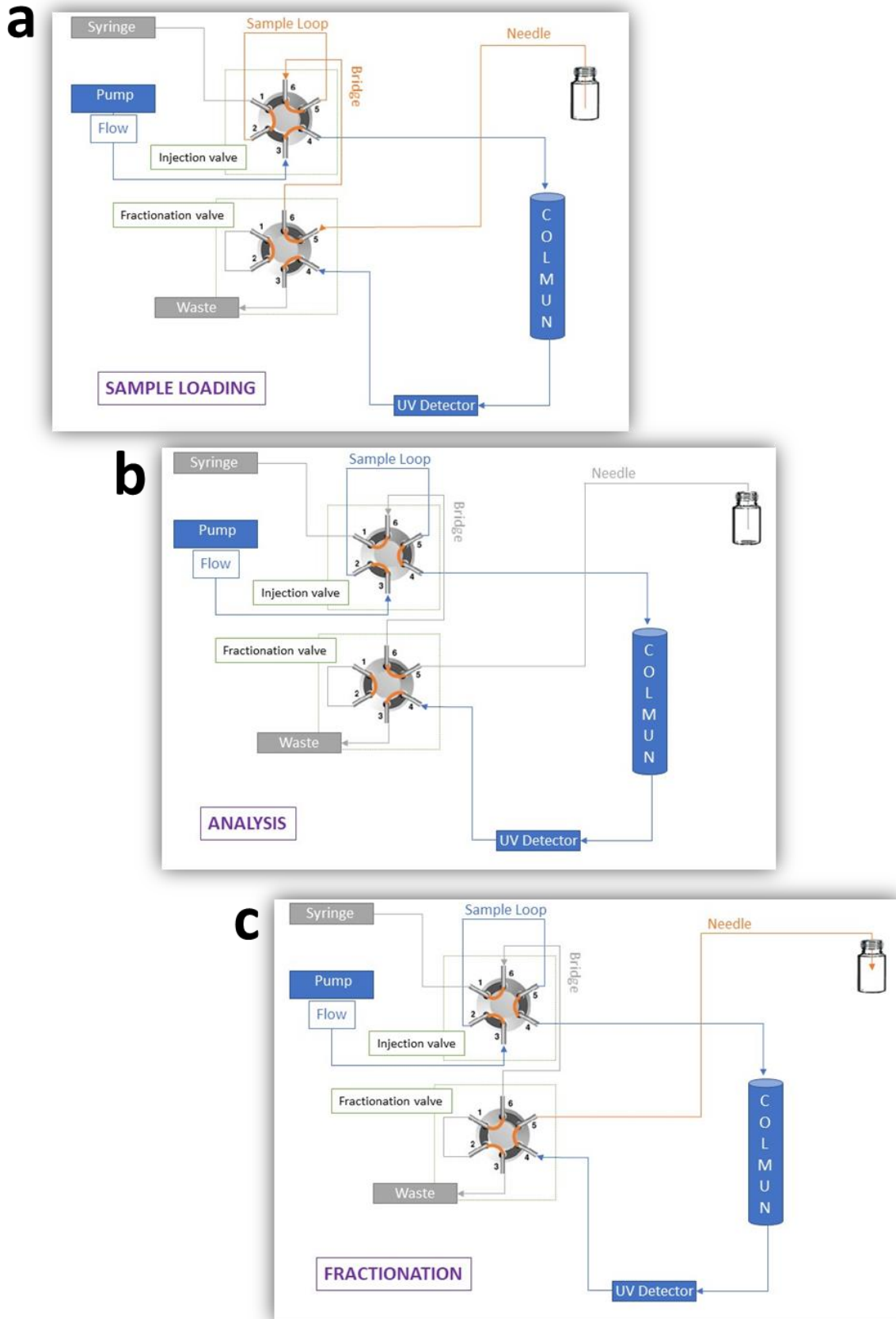


**Figure 2.1: Graphical representation of Thermo Scientific U3000 fractionation configuration. a: Sample loading. b: Analysis. c: Fractionation.**



## 2.2.3 HPLC data analysis.

### 2.2.3.1 Resolution.

Resolution ( $R_s$ ) was calculated by Chromeleon software using the European Pharmacopoeia standard formula (equation 2.1) for mixed samples. Where  $R_{tref.pk}$  is the retention time of the peak after the current peak,  $R_{tcur.pk}$  is the retention time of the current peak.  $PW_{HH}$  is peak width at half height.

Equation 2.1:

$$R_s = 1.18 * \frac{R_{tref.pk} - R_{tcur.pk}}{PW_{HHref.pk} + PW_{HHcur.pk}}$$

To manually calculate resolution between two peaks that were individually analysed, equation 2.2 was used where  $R_{t1}$  and  $R_{t2}$  are individual retention times of two peaks and  $W_1$  and  $W_2$  are the peak widths at the base of each peak.

Equation 2.2:

$$R_s = \left( \frac{R_{t2} - R_{t1}}{0.5(W_1 + W_2)} \right)$$

### 2.2.3.2 Efficiency.

Peak width at half height was generally used as a measure of efficiency of size based separations and chromatographic performance as the calculation of efficiency considers  $PW_{HH}$ ; however in Chapter 4, peak capacity was used to measure efficiency as close elution events led to a variation in  $PW_{HH}$ . To measure peak capacity in a second dimension of 2D-LC analysis, the mean peak width over the gradient was calculated and used in equation 2.3. Where  $T_g$  is the time of the elution gradient and  $W$  is average peak width.

Equation 2.3:

$$\text{Peak capacity} = \frac{Tg}{W}$$

### 2.2.3.3 Selectivity.

To calculate selectivity ( $\alpha$ ), equation 2.4 was used.  $Rt_0$  was derived from the solvent front (first identifiable peak within the separation).

Equation 2.4:

$$\alpha = \frac{Rt1 - Rt0}{Rt2 - Rt0}$$

### 2.2.3.4 Fractionation efficiency.

In strong IP-RP conditions, an OGN sample was analysed using 5 mM TBuAA, 0.1  $\mu$ M EDTA and 10-80% v/v MeCN, on a DNAPac RP column (2.1\*100 mm) as 1<sup>st</sup> dimension separation. Six 100  $\mu$ L fractions were collected between 8.5-11.5 minutes retention time to collect the OGN sample during separation. 5  $\mu$ L of each fraction was re-analysed under strong IP-RP HPLC conditions to analyse fractionation efficiency and <sup>1</sup>D dilution.

The chromatogram of Figure A2.3b shows that when fractions were reanalysed for quality control under identical conditions, the retention time window of the fractions decreases. This is a reflection of a reduction in column overloading. To calculate the fractionation efficiency the area of the total fraction was estimated using equation 2.5 (as only a portion of the fraction volume was reanalysed in a 2<sup>nd</sup> dimension). The total areas of each analysis in a second dimension were summed to obtain the 'Analysed fraction total area'. Using the calculated 'estimated total fraction area', fractionation efficiency is calculated using equation 2.6.

The 'area of fraction volume' was calculated by summing peak areas within the fraction window.

Equation 2.5:

$$\text{Estimated total fraction area} = \text{Analysed fraction total area} * \frac{\text{Original fraction volume}}{\text{Total analysed volume}}$$

Equation 2.6:

$$\text{Fractionation Efficiency (\%)} = \frac{\text{Estimated total fraction area}}{\text{Area of fraction volume}} * 100$$

Additionally, the amount of OGN within the analysed fraction was calculated using equation 2.7.

Equation 2.7:

$$\begin{aligned} & \text{Analysed Fraction total amount} \\ &= \frac{\text{Area of fraction volume}}{\text{Analysed fraction total area}} * \text{Amount of sample fractionated} \end{aligned}$$

#### 2.2.4 2D-LC Orthogonality.

The bin counting method is a geometrical approach to analysing orthogonality [302]. First, OGN retention times were normalised using equation 2.8 where  $Rt_{max}$  and  $Rt_{min}$  represent the last and first retention times of the analytes and  $Rt_i$  are the retention times of each analyte.  $Rt_i (norm)$  or normalised retention values result in integers between 0 and 1.

Equation 2.8

$$Rt_i (norm) = \frac{Rt_i - Rt_{min}}{Rt_{max} - Rt_{min}}$$

Normalised retention times of two chromatographic separations were coupled to accommodate a position on an x and y axis representing the 1<sup>st</sup> dimension on the x axis and 2<sup>nd</sup> dimension on the y axis. Data values were plotted onto a grid representing the separation space. The number of boxes that made the grid ('bins') were a reflection of maximal peak capacity ( $P_{max}$ ).  $P_{max}$  represented

the amount of analytes that were separated and the number of bins that contained data points was counted. Using this approach, orthogonality was therefore calculated using equation 2.9.

$$\text{Equation 2.9} \quad \text{Orthogonality \%} = \frac{\sum \text{bins} - \sqrt{P_{\text{max}}}}{0.63 * P_{\text{max}}} * 100$$

Orthogonality was also calculated using the minimum convex hull method [300] where the outermost data points on the scatter plot were joined and the area between them was calculated as a reflection of the amount of spread within the available separation space. The area of the polygon was calculated using a shoelace algorithm [323] on Python xy for scientists software (using Python version 2.7.10). The algorithm is stated in Appendix 1 Code A1.1.

### 2.3 LC-MS analysis.

Strong IP-RP HPLC in conjunction with TBuAA was used for the LC MS analysis of OGNs. Specifically a Thermo Fisher Scientific DNAPac RP column (2.1\*100 mm) was connected to HPLC configuration 1 (section 2.2.2). OGNs were separated by strong IP-RP at optimised conditions of 60 °C column temperature, 0.3 mL/min flow rate under a gradient of 5 mM TBuAA, 0.1 µM Na<sub>4</sub>EDTA, 34.5-59 % v/v MeCN. The HPLC was connected to the MS equipment via viper (0.1 mm ID) MP35N tubing into the ESI source.

Analysis was performed on a MaXis Q-TOF high resolution MS system (Bruker Daltonics) in negative ionisation mode. The MS settings were; capillary voltage of 3500 V with endplate offset of 500 V. Ionisation at 350 °C, nebuliser pressure at 35 psi and dry gas delivered at 10 l/min. Data was acquired over 19 minutes and analysed using Bruker Compass software (version 1.3, Bruker Daltonics). The MaXis Q-TOF was calibrated monthly using the ESI-L low concentration tuning mix standard and calibration settings on Bruker Compass software.

### 2.3.1 MS data analysis.

For all model OGNs; OGN monoisotopic mass and m/z values at different charge states was calculated with the assistance of Mongo Oligo mass calculator (version 2.08) [324]. For GSK supplied OGNs; OGN samples were supplied with a certificate of analysis mass specification and m/z values at different charge states were calculated using Microsoft Excel software. OGN mass was calculated to match the mass precision of the certificate of analysis (1 decimal place).

Data interrogation was performed using Bruker Compass Data Analysis software (version 4.1). Charge state deconvolution was performed using the peptides/small molecules algorithm of the software with an abundance cut-off set to 10%. Peaks were found using the Apex method with an absolute intensity threshold of intensity threshold of 80 counts to ensure low abundance monoisotopic peaks were found above the limit of detection of the noise (LOD=75). All deconvolution data was confirmed by interrogation of the mass spectrum and manual identification of the monoisotopic peak of the 3<sup>-</sup>, 4<sup>-</sup>, or 5<sup>-</sup> charge state OGN ion. To further confirm the OGN identity assignment based upon charge deconvolution, extracted ion chromatograms of the 4-charge state monoisotope OGN peaks were created to visualise OGN fraction occupancy. Monoisotopic masses of the 3<sup>-</sup>, 4<sup>-</sup> or 5<sup>-</sup> charge state was confirmed to be within 0.5 Da among replicate OGN analyses.

## Chapter 3: Optimisation of size and sequence dependent separations of OGNs using HPLC.

### Abstract.

Ion-pair reversed-phase (IP-RP), strong anion exchange (SAX) and size exclusion (SEC) chromatographic modes were optimised for both size and sequence based separations of oligonucleotides (OGNs). Optimisation of each mode of chromatography involved parameter manipulation, mobile phase chemistry optimisation and evaluation of stationary phases. Model OGNs varying in size, sequence and level of a common modification (phosphorothioation) were analysed within each mode. The aim was to develop orthogonal modes of separation prior to coupling within a two-dimensional workflow (2D-LC).

Using IP-RP high performance liquid chromatography (HPLC) in conjunction with the weak ion-pair reagent triethylammonium acetate (TEAA) resulted in OGN separations based on both size and sequence. Selectivity and resolution was most affected by changes to analysis temperature. Using a more hydrophobic ion-pair reagent, such as tributylammonium acetate (TBAAC) or adding hexafluoroisopropanol (HFIP) to the TEAA mobile phase resulted in a reduction in secondary interactions of the OGN with the stationary phase and more size dependent separation mechanisms. Furthermore, using these mobile phases improved the resolution of fully phosphorothioated OGNs. Using SAX HPLC, sequence based separations were demonstrated using sodium chloride in the mobile phase. By using a strong eluotropic salt (sodium perchlorate) in conjunction with alterations of the mobile phase pH and the addition of an organic modifier, this resulted in reduction in secondary interactions of the OGN with the stationary phase and more size dependent separation mechanism. Using SEC, size based separations of OGNs dominated in this lower resolution mode chromatography, optimisation of the mobile phase chemistry reduced secondary interactions. Results obtained in this chapter will be used for the development of two-dimensional workflows that couple the optimised modes of chromatography for size based separations in one dimension and sequence based separations in another dimension.

### 3.1 Introduction.

To investigate the feasibility of a 2D-LC workflow for the analysis of OGNs, separations in the 1<sup>st</sup> dimension were optimised prior to adoption of 2D-LC. The optimisation of a number of modes of chromatography was performed to demonstrate the capability (of each mode) to separate OGNs by size or sequence basis. Size and sequence based separations in alternate dimensions will be required to develop an orthogonal / pseudo-orthogonal 2D workflow. Another aim of single dimension separation optimisations was to investigate the relative degree of size or sequence dependence in each mode for a range of model OGNs. Further analysis of resolution, selectivity and efficiency, of each of the different chromatographic modes could be compared to assess their performance during size and sequence separations of OGN models. The modes of chromatography optimised in this study were IP-RP, SAX and SEC.

As described in Chapter 1 (see section 1.3.2), triethylammonium acetate, tributylammonium acetate, tetrabutylammonium acetate (TetBAA) and tetrabutylammonium bromide (TetBAB) are alkylamine ion-pair reagents (IPRs) with varying alkyl chain length. Assessment of various IPRs under IP-RP HPLC conditions elucidates the optimal IPR that facilitates either size or sequence dominant separations. IP-RP HPLC of OGNs is commonly performed using C18 stationary phases. With a multitude of C18 columns on the market, analysis of OGNs performed on different stationary phases demonstrates the ability to resolve closely eluting OGNs and facilitates more extreme analytical parameters to be utilised (such as higher analysis temperatures). Mobile phase chemistry optimisation with acidic modifier hexafluoroisopropanol (HFIP) can demonstrate the additives' ability to shift mechanisms of separation from OGN sequence to size.

Also described in Chapter 1 (see section 1.3.1), is the common use of salt gradients under SAX HPLC conditions for the analysis of OGNs. Various eluotropic salts can be utilised for SAX HPLC analysis and can demonstrate differential elution characteristics in respect to OGNs of varying modification. In addition, further manipulation of mobile phase chemistry can affect OGN base ionisation to facilitate sequence based separations or reduce secondary interactions between OGNs and the positively charged stationary phase (for more size dominant separation mechanisms). This concept (specifically organic solvent modification of the mobile phase) may also be applied within SEC HPLC to minimise secondary interactions between chemically modified OGNs and the SEC stationary phase.

Optimisations of single-dimension high performance liquid chromatography were performed using a range of OGN models, outlined in Table 3.2. A homopolymeric OGN mixture (dT19-24-mer) was used

to demonstrate size based separations. In this case, the OGN base composition only changes by a single dT with no significant differences in the structure of the different OGNs. Two 30-mer OGNs with different base composition, sequence and potential structures were utilised as models to study the effects of variable base sequence on the separation of the OGNs.

A major chemical modification employed within the design of antisense OGN therapeutics is the phosphorothioation of the phosphodiester backbone (see Chapter 1, section 1.2.2.1). This modification has been shown to improve chemical resilience to degradative enzymes and enhance the therapeutic efficacy of the drug [12]. In light of this commonly employed modification, a representative set of phosphorothioate (PS) models were used for single dimension separation optimisations. The 16-mer single stranded OGNs contained either a single PS bond at either the 3' or 5' end or a full PS OGN in which all the phosphodiester bonds were replaced with PS bonds. The introduction of a single PS bond introduces a chiral centre and results in the formation of two diastereoisomers [76]. The addition of the PS bond imparts an altered hydrophobicity on the OGN and therefore also serves as a model system to study the effect of altered chemistry (and potential structural differences) for OGNs of the same size under different modes of chromatography.

By building a knowledge database of the chromatographic behaviour of different model OGNs across a range of chromatographic modes, assessment and optimisation of separation mechanisms (size vs sequence) can be performed. Modes (or conditions within a chromatographic mode) can be coupled to facilitate orthogonal separations utilising sized based separations in one dimension and sequence in another – once optimisations of separation mechanisms have been demonstrated (as shown in Figure 3.1).

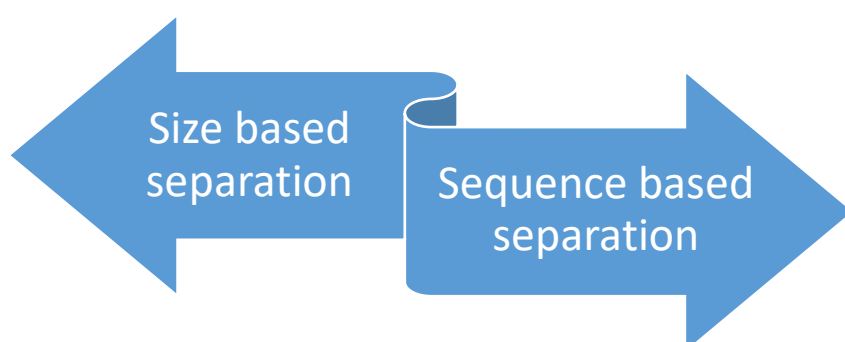


**Figure 3.1: Orthogonal OGN separations within a 2D-LC workflow aim to separate on a size basis or a sequence basis.** Therefore the aim of single dimension optimisations is to facilitate size and sequence based separations for coupling within a 2D-LC workflow.

## Results and Discussion

### **3.2 Optimisation of size and sequence based separations of OGNs using ion-pair reversed-phase HPLC.**

#### **3.2.1 Optimisation of weak ion-pair reversed-phase chromatography for analysis of OGNs.**

As described in Chapter 1 (section 1.3.2), under IP-RP HPLC conditions, an IPR with relatively short alkyl chains and/or a low abundance of them is termed as a 'weak' IPR. It facilitates secondary interactions between the bases of OGNs and the stationary phase due to insufficient stationary phase IPR saturation.

These secondary hydrophobic interactions increase in strength from cytosine > guanine > adenine > thymine [189]. The IPR triethylammonium acetate (TEAA) is known as a weak IPR. Using TEAA in IP-RP HPLC results in OGN separations dependent on both the size and sequence of the OGN as its short alkyl chains do not impede interactions between the stationary phase and the OGN bases [189, 214]. Weak IP-RP HPLC was performed using a mobile phase of 100 mM TEAA, 0.1 mM tetrasodium ethylenediaminetetraacetic acid (Na<sub>4</sub> EDTA) and 0.1-25% v/v acetonitrile (MeCN). OGN separations were optimised by alteration to analytical parameters (such as flow rate, elution gradient or analysis temperature) to demonstrate size and sequence dependent separations. Chromatographic performance was assessed by analysis of resolution (Rs), efficiency (determined by the peak width at half height –PWHH) and selectivity by retention time and order.

In this study, two stationary phases were utilised in conjunction with weak IP-RP optimisation: a macroporous polymeric PS-DVB C18 phase (DNAPac RP) and a solid core silica C18 phase (Accucore C18). The polymeric DNAPac RP stationary phase is resistant to extremes of pH or temperature, whereas the solid core Accucore C18 stationary phase exhibits high resolution and resistance to higher pressures. The characteristics of both stationary phases is highlighted in more detail below in Table 3.1.

**Table 3.1: Characteristics of DNAPac RP and Accucore C18 columns.**

<b>Characteristic</b>	<b>DNAPac RP</b>	<b>Accucore C18</b>
<b>Pressure Limit</b>	276 Bar	1000 Bar
<b>pH range</b>	0-14	1-11
<b>Temperature Limit</b>	100 °C	70 °C
<b>Phase Chemistry</b>	Polymeric	Carbon loaded silica (9%), spherical solid core
<b>Particle Size</b>	4 µm	2.6 µm
<b>Pore Size</b>	Macroporous	150 Å
<b>Loading capacity</b>	Medium	Low

### **3.2.1.1 Size dependent separations of OGNs using weak IP-RP HPLC.**

The first analytical aim was to optimise size dependent separation of OGNs within weak IP-RP HPLC. This would be performed via manipulation of the parameters of flow rate and gradient for the analysis of OGNs under weak IP-RP HPLC conditions. To optimise flow rate using weak IP-RP HPLC, unmodified dT size variants were analysed (see Table 3.2). An equimolar mixture of the dT 19-24-mer size variants (dT-ladder) was separated under different flow rates (0.2, 0.4 and 0.6 mL/min) covering the optimum flow rate for a 2.1\*50 mm Accucore C18 column of 0.4 mL/min. The results for the analysis on the Accucore C18 column are shown in Figure 3.2a.

**Table 3.2: Model OGNs used for evaluation of size and sequence dependent separations. OGNs are described by size in nucleotide length (nt), sequence and monoisotopic mass. A capital letter denotes a DNA nucleotide and a \* denotes a PS bond.**

OGN Model Set	OGN Description	Sequence 5' to 3'	Length (nt)	Monoisotopic mass (Da)
19-24-mer size variant dT ladder	dT 19mer	TTT TTT TTT TTT TTT TTT T	19	5714.912
	dT 20mer	TTT TTT TTT TTT TTT TTT TT	20	6018.957
	dT 21mer	TTT TTT TTT TTT TTT TTT TTT	21	6323.003
	dT 22mer	TTT TTT TTT TTT TTT TTT TTT T	22	6627.049
	dT 23mer	TTT TTT TTT TTT TTT TTT TTT TT	23	6931.095
	dT 24mer	TTT TTT TTT TTT TTT TTT TTT TTT	24	7235.140
30-mer sequence variants	Sequence variant 1	TCC TTG ACC ATC TGC TCG TAC TCC TCG TCT	30	9046.485
	Sequence variant 2	ACA AAG GTG AGG TTT AAA AGA AGT TTT CTG	30	9328.595
16-mer PS variants	Unmodified variant	ACA AAA GTC CGT GAG A	16	4920.883
	Single PS on 5' terminal.	A*CA AAA GTC CGT GAG A	16	4936.860
	Single PS on 3' terminal.	ACA AAA GTC CGT GAG* A	16	4936.860
	Full PS.	A*C*A* A*A*A* G*T*C* C*G*T* G*A*G* A	16	5160.538

The results show that resolution is lowest at 0.6 mL/min flow rate; this is consistent with previous observations, where optimal resolution for OGN separations was observed typically at lower flow rate [214] as this is a result of reduced mass transfer at higher flow rate. Resolution at 0.4 mL/min and 0.2 mL/min was not significantly different between analyses, however a marked increase in signal intensity is observed at 0.2 mL/min. mAU with a decrease in flow rate from 0.4 to 0.2 mL/min.

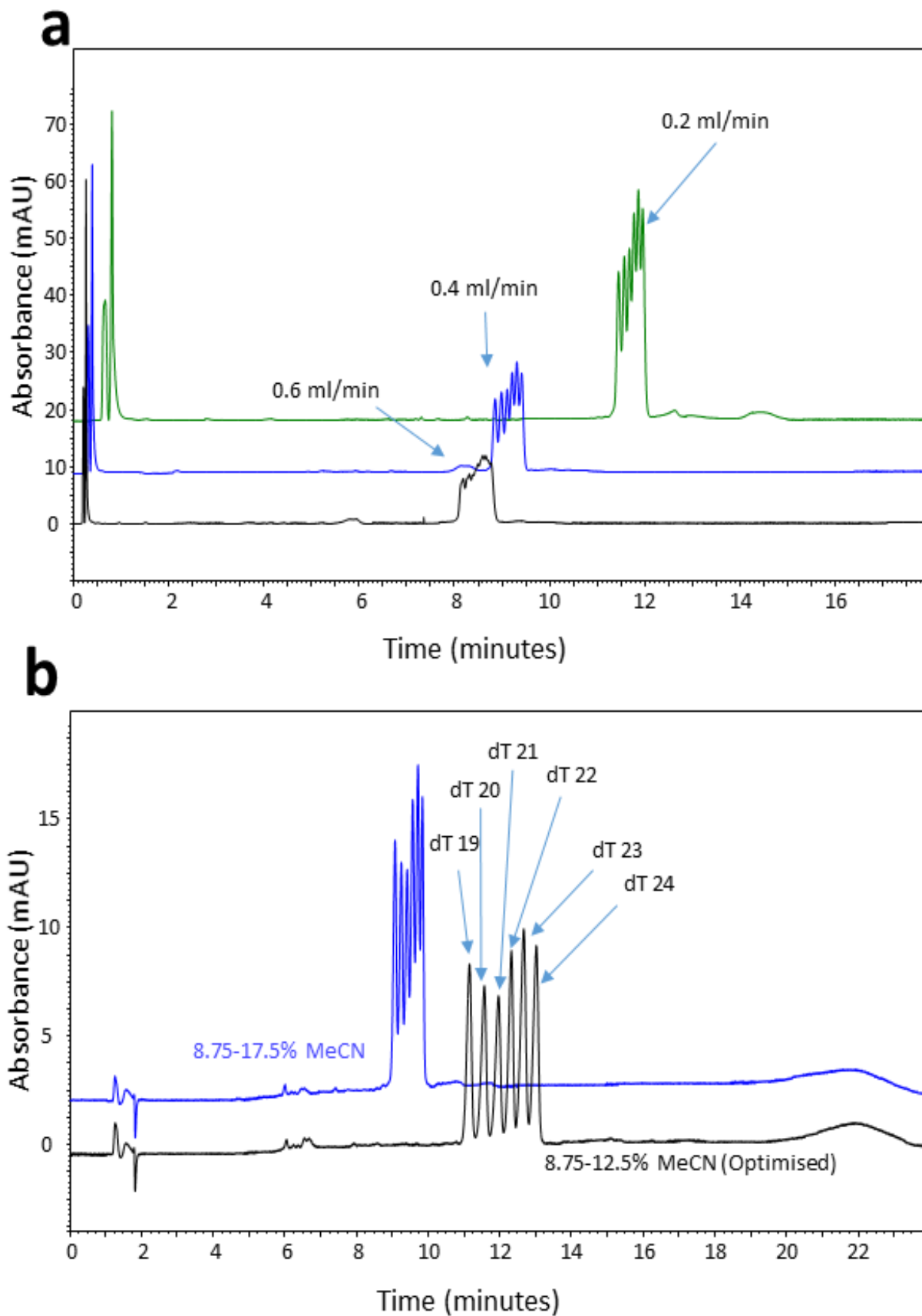


**Figure 3.2: Optimisation of flow rate and elution gradient using weak IP-RP HPLC.** 100 mM TEAA, 0.1 mM Na<sub>4</sub> EDTA, 0-25% v/v MeCN. **a:** 30 picomole dT-ladder analysed at 30 °C, 8.75-17.5% v/v MeCN gradient between 1-15 min on Accucore C18 column. 0.6 - 0.2 ml/min flow rate. **b:** 32 picomole samples of dT-ladder analysed at 40 °C. Gradients of 8.75-12.5/17.5% v/v MeCN between 1-15 min were applied at 0.2 ml/min on a DNAPac RP column.

Average peak signal height increased from 15.5 to 32.3. This effect is possibly a result of increased analyte residence time within the flow cell of the UV detector at lower linear velocity and thus increased sensitivity. Performing analyses at a reduced flow rate could potentially improve the limits of detection of low concentration species, such as OGN manufacturing impurities.

Aiming to investigate the effect of gradient upon resolution of the size variants, the dT-ladder was analysed using a range of gradients. A reduction in the slope of gradient, and thus percentage of organic modifier added per unit time, facilitated improved resolution of the size variants. The smaller (and least hydrophobic) OGNs were first to elute within the gradient with their reduced hydrophobicity requiring less organic modifier (than longer OGNs) within the mobile phase for elution. A comparison of two gradients is shown in Figure 3.2b, and demonstrates an increase in average OGN resolution when a shallower gradient is applied. Average resolution increased from 0.9 to 1.4 when the flow rate was reduced from 0.63% MeCN min<sup>-1</sup> to 0.27% MeCN min<sup>-1</sup>. The results of Figure 3.2 show that size based separation of homogeneous OGNs is obtained by optimising the flow rate and elution gradient within IP-RP HPLC analysis.

### **3.2.1.2 Sequence dependent separations of OGNs using weak IP-RP HPLC.**

The second analytical aim was to optimise sequence dependent separations under weak IP-RP HPLC conditions. This would be performed via the optimisation of analysis temperature in addition to use of optimised elution gradient and mobile phase flow rate (optimised for size based separations of section 3.2.1.1 but applicable for further work to maintain high resolution and chromatographic efficiency).

Studies by Huber *et al.* and Baek *et al.* demonstrate that an increase in column temperature increases analyte mass transfer and thus improves resolution of OGNs [195, 325]. In addition, increased analysis temperature affects OGN base stacking, self-hybridization and linearizes its 3D conformation. OGN base sequence contributes to the OGN 3D conformation, which also sterically affects OGN interaction with the stationary phase [189]. Linearization of the OGN as a result of increased analysis temperature, changes its interactional behaviour with the stationary phase as more structural moieties are made available. As a result, retention of OGNs of differing sequence changes with increases in temperature.

Sequence dependent separation was analysed with two unmodified 30-mer OGNs of different sequence (see Table 3.2). Analysis parameters were kept constant except for an increase in column

temperature for comparative analyses. The column temperature was increased from 30 °C to 70 °C and OGN peaks were tracked with reference OGN analyses to track changes in sequence based retention. The OGN with the highest AT content theoretically should elute last, as these bases are more hydrophobic in nature and contribute to OGN partitioning within the IP-RP HPLC separation [189]. At 30 °C, within the black trace of Figure 3.3a, an opposite retention order to what is expected of these OGNs was observed with the more hydrophobic sequence- where sequence variant 2 elutes before sequence variant 1. The aberrant elution order may be due to the 3D conformation of the analytes at lower separation temperature, where OGN interactions are influenced/inhibited by self-association and base stacking. As the analysis temperature was increased to 50 °C and 70 °C, the OGN elution order started to exhibit more predictable patterns based upon the hydrophobicity of the OGN sequences. Interestingly, at 50 °C the OGNs co-elute, making the separation for those specific sequences size based rather than sequence based. OGN resolution is highest at a lower separation temperature, although chromatographic efficiency is higher at increased temperature, as average PWHH decreases from 0.13 minutes at 30 °C to 0.10 minutes at 70 °C.

Following analysis of the sequence variants using weak IP-RP HPLC, further analysis was performed using 16-mer PS model OGNs. As described in section 3.1, the addition of a PS bond introduces a chiral centre to the molecule and the formation of diastereoisomers ('Rp' vs 'Sp'). The resulting diastereoisomers have different base stacking characteristics and hydrophobic interactions with the stationary phase and can therefore be resolved [113, 326]. Given the identical molecular weight of the diastereoisomers, their separation requires a HPLC mechanism based predominantly on sequence dependency. To examine resolution of diastereoisomers, PS OGNs were analysed at 30 °C, 50 °C and 70 °C. The results in Figure 3.3 b-c show that resolution of diastereoisomers was dependent on the position of the PS bond within the single PS OGN. Figure 3.3b shows that when the diastereoisomer is positioned towards the 3' end, separation was achieved at 30 °C. However, at elevated separation temperatures (more size dependent separations) co-elution of the diastereoisomers was observed. This is due to the linearization of the OGN to such an effect that the diastereoisomers partition towards the stationary phase equally- causing co-elution. When the PS bond is on the 5' terminal, diastereoisomer resolution is observed at all separation temperatures (see Figure 3.3c). These results suggest that although size based separation of a single PS OGN was demonstrated at temperatures above 50 °C, size based separation performance may not be ubiquitous across a range of OGNs in these conditions due to minute structural differences.

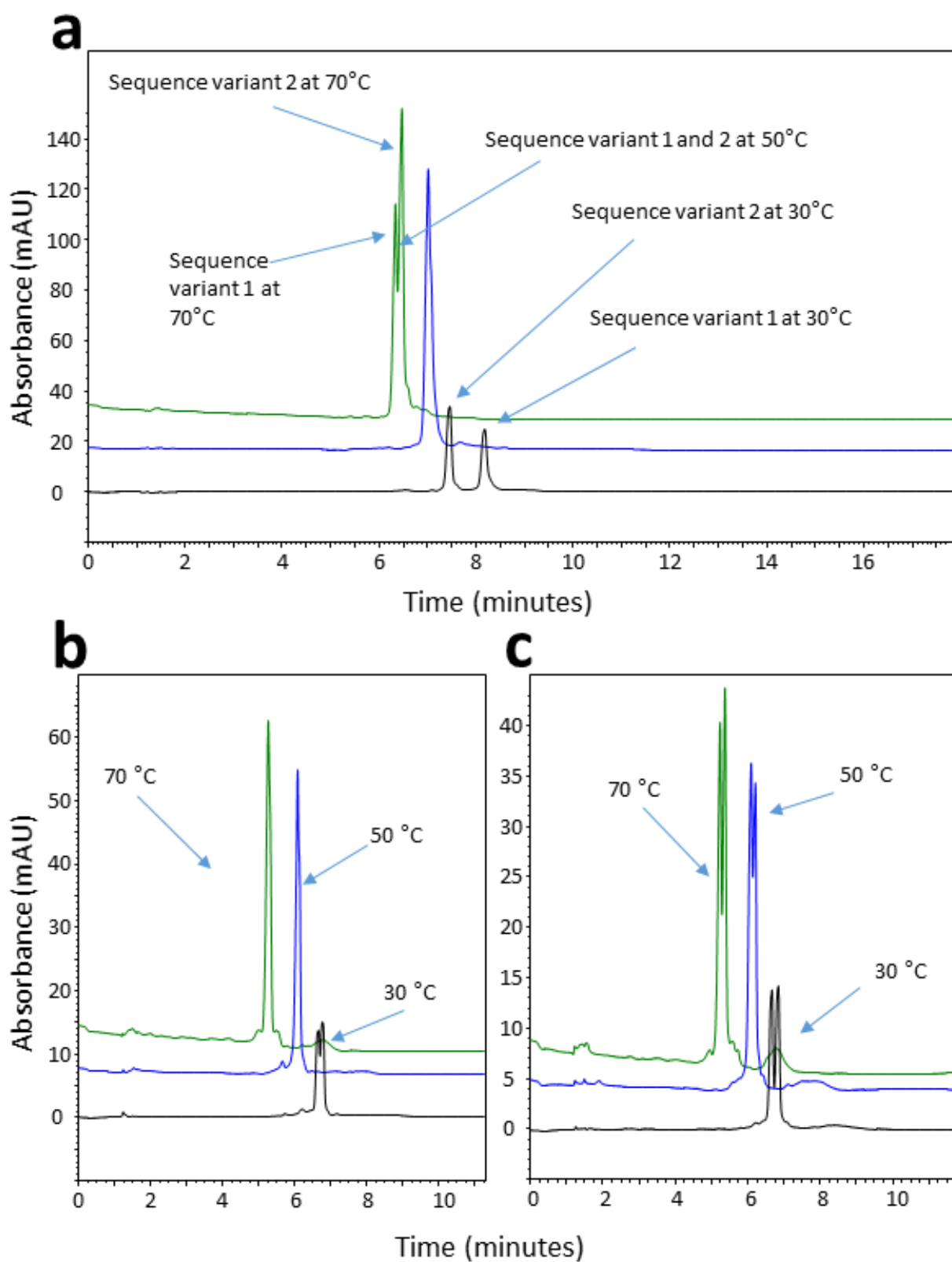


**Figure 3.3: Optimisation of analysis temperature using weak IP-RP HPLC.** 30 picomole samples analysed at 0.2 ml/min at 30-70°C using a gradient of 100 mM TEAA, 0.1 mM Na<sub>4</sub> EDTA 8.75-17.5% v/v MeCN gradient between 1-15 min on a DNAPac RP column. **a:** 30-mer sequence variants. **b:** 16-mer Ps OGN (at 3' terminal). **c:** 16-mer PS OGN (at 5' terminal).

The results show that size and sequence based separations can be manipulated by column temperature. A caveat of this separation optimisation strategy is that peaks must be tracked during analysis, and in this case peaks were tracked with reference standard co-analyses. Tracking identifies shifting elution order behaviours as OGN 3D conformations and interaction behaviours change with temperature. Further optimisations aimed to use optimised chromatographic parameters such as gradient slope, separation temperature and flow rate to enhance resolution, efficiency and sensitivity respectively.

An equimolar mixture of unmodified, single modified and full PS OGN models was separated in low flow, low analysis temperature conditions (see Figure 3.4). Size based separation does not dominate here as all the OGNs analysed are of equal length. The OGNs separate due to incremental phosphorothioation imparting incremental hydrophobicity with each chemical modification. This leads to the full PS OGN eluting last from the column. A noticeable difference in peak width is observed between unmodified/single PS models (0.05/0.07 minutes) and the full PS OGN (0.84 minutes). This is due to the 1000's of diastereoisomers of the full PS OGN slightly resolving from each other, but not enough to be identified as individual peaks. The full PS peak of Figure 3.4 is in fact 1000's of closely resolving peaks- demonstrating sequence dependent separation. Resolution of full PS diastereoisomers is minimally reduced at elevated analysis temperature (see Appendix 2, Figure A2.1).

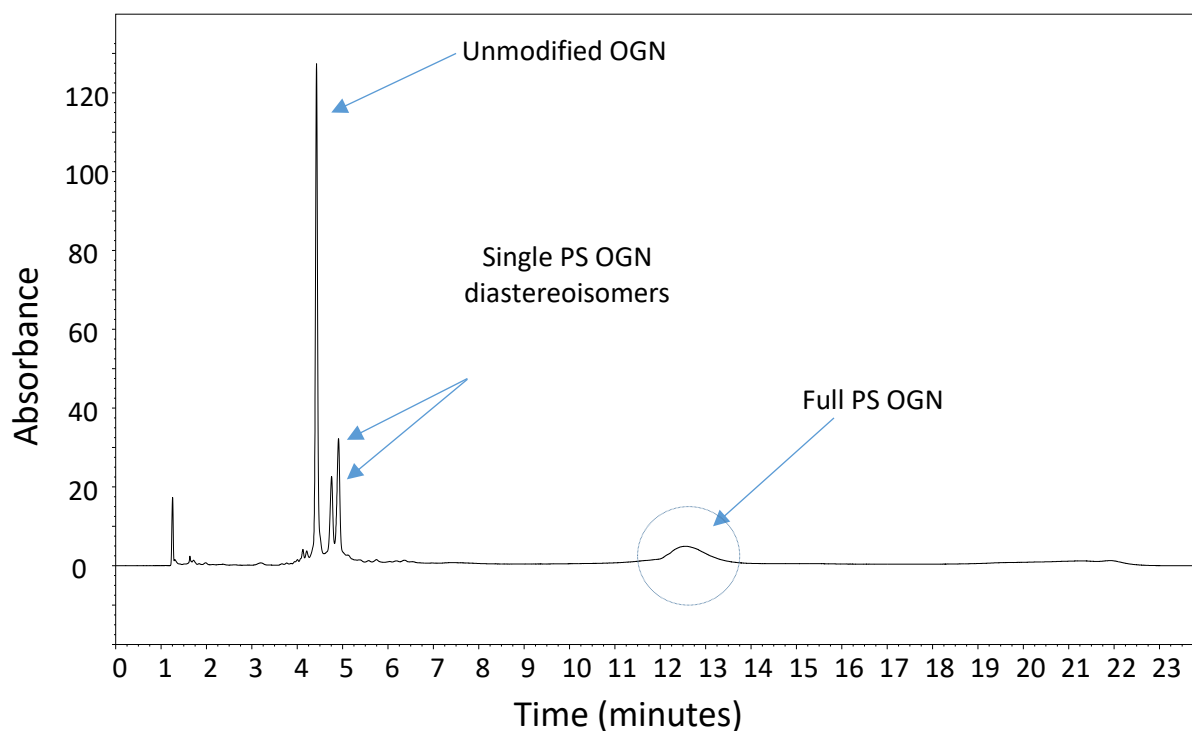


**Figure 3.4: Separation of PS variant OGNs using weak IP-RP HPLC.** 50 picomole sample of 16-mer PS variants analysed at 0.2 ml/min, on a DNAPac RP column at 30 °C, 100 mM TEAA, 0.1 mM Na<sub>4</sub>EDTA, 8.75-17.5%  $v/v$  MeCN gradient between 1-15 min.

### **3.2.2 Optimisation of strong ion-pair reversed-phase chromatography for the analysis of OGNs.**

As described in Chapter 1 (section 1.3.2), an increase in the hydrophobicity of the IPR by using longer alkyl chains drives the ion-pair reagent to partition more towards the stationary phase surface [230]. Using more hydrophobic (stronger) IPRs leads facilitates more prominent dynamic ion exchange retention mechanisms between the OGN by the stationary phase during separations. In comparison to triethylamine, tributylamine or tetrabutylamine alkyl chains contain two extra carbons and these longer hydrocarbons partition more strongly toward the stationary phase- saturating its surface more than triethylamine. More pronounced phase saturation results in reduced secondary interactions between OGN bases and the stationary phase due to steric inhibition of secondary interactions.

#### **3.2.2.1 Size dependent separations of OGNs using strong IP-RP HPLC.**

To study the effect of different IPRs on OGN chromatography, a comparative analysis of a variety of strong IPRs for size based separations of the model OGNs was performed. Optimised analysis parameters, such as column temperature and elution gradient were used for size based separations of the dT ladder within a mobile phase containing up to 80% v/v MeCN as eluting organic modifier. Initial IPR optimisation was performed using TBUAA, TetBAA and TetBAB for the analysis of the dT ladder, see Figure 3.5a.

To investigate the effect of a 'stronger' IPR on the analysis of PS OGNs, the 16-mer full PS OGN model was analysed using TBUAA. A comparison between analysis performed with TBUAA and TEAA is shown in Figure 3.5b. Using TEAA, the OGN PWHH corresponding to a 50 picomole sample (shown in Figure 3.5b) was 0.87 minutes. Analysis using TBUAA as ion-pair reagent reduced PWHH to 0.24 minutes, demonstrating an increase in size based separations and improvement in overall peak shape for the fully PS OGN. Due to the predominant size based separation, this results in co-elution of 1000's of diastereoisomers under strong IP-RP HPLC conditions and a significant reduction in PWHH for the full PS OGN. The results show that signal intensity and chromatographic efficiency are improved with use of TBUAA.

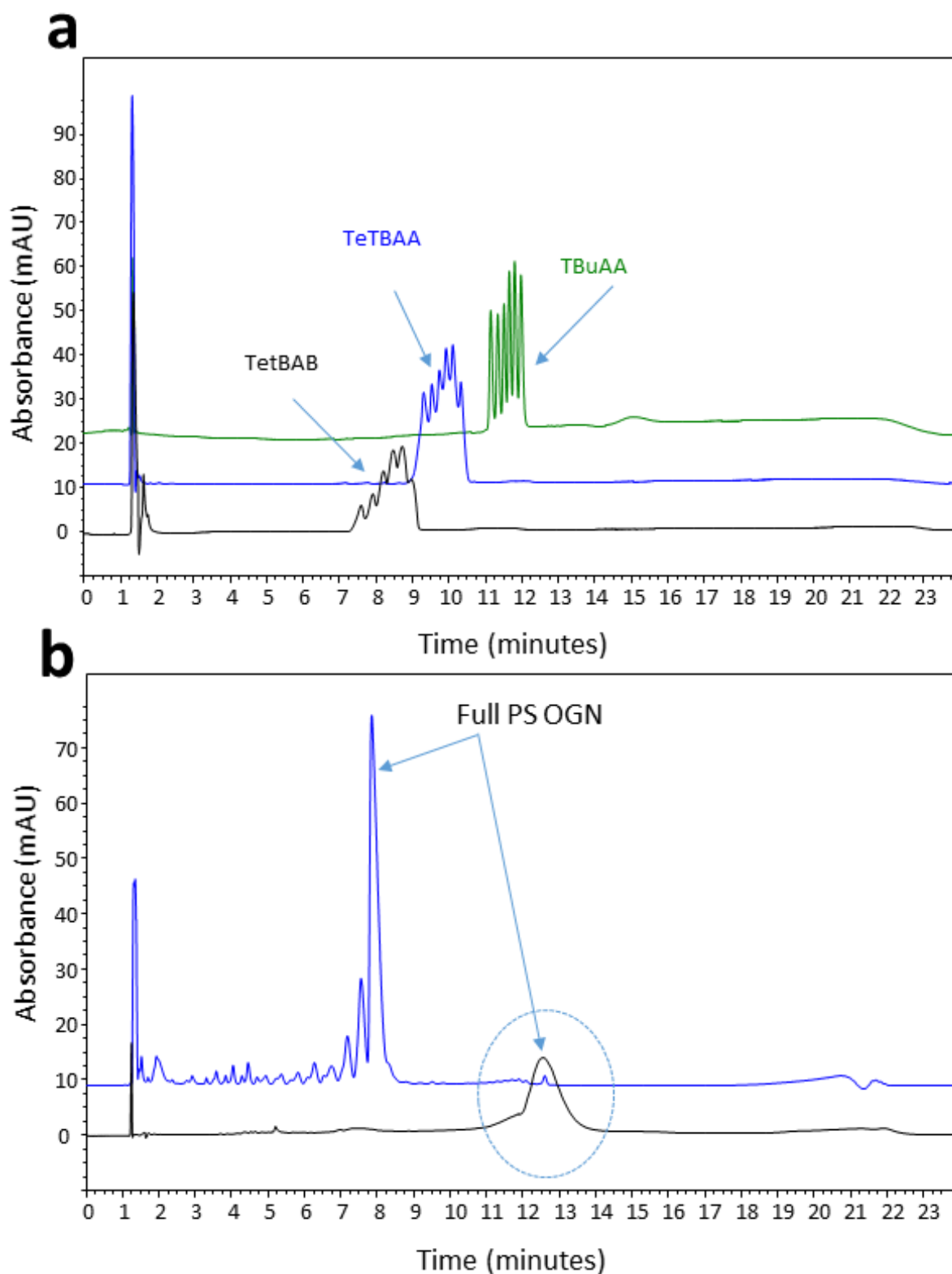


**Figure 3.5: Strong IPR comparisons and improved chromatographic effect on full PS OGN using strong IP-RP HPLC.** 50 picomole samples were analysed at 30 °C, 0.2 ml/min on a DNAPac RP column. **a:** Comparison of TBuAA (5 mM TBuAA, 0.1  $\mu$ M Na<sub>4</sub> EDTA, 27.5-73% v/v MeCN between 1-15 min), TetBAA (2.5 mM TetBAA, 45-80% v/v MeCN between 1-15 min) and TetBAB (2.5 mM TetBAB, 52-73% v/v MeCN between 1-15 min) to analyse the dT ladder. **b:** 16-mer full PS OGN- comparison of weak and strong ion-pair reagents. Analysis under a gradient of 100 mM TEAA, 0.1 mM EDTA, 8.75-17.5% v/v MeCN from 1-15 min (black trace) and 5 mM TBuAA, 0.1  $\mu$ M Na<sub>4</sub> EDTA, 34.5- 45% v/v MeCN from 1-15 min (blue trace).

The results show that at the concentrations used, TBuAA performs best for OGN separations, where resolution and efficiency was highest when utilising TBuAA within the mobile phase. Based on these results, TBuAA was utilised for strong ion-pair size based separation optimisations.

Continuing with the aim of optimising analytical parameters for size based separations, the dT ladder was analysed on a DNAPac RP column under two gradients – 42.5-52% v/v MeCN and 34.5-45% v/v MeCN shown in Figure 3.6a at 50 °C (blue and green traces of Figure 3.6a). Comparison of resolution under these conditions shows that a shallower gradient enables higher resolution. Specifically resolution increases from 1.22-1.36 to 1.39-1.70 respectively. The results demonstrate that size based separation is improved by a low rate of eluting modifier during the separation, which is consistent with results from section 3.2.1.1. To further optimise size dependent separation of the dT ladder, the analysis temperature was increased from 50-70 °C under a gradient of 34.5-45% v/v MeCN (green and brown traces of Figure 3.6a). Aiming to confirm that resolution increases with an increase in temperature, separations were compared between analyses at the two analysis temperatures, shown in Figure 3.6a on a DNAPac RP column. Resolution increases from 1.39-1.70 to 1.56-1.92 when the analysis temperature rises 20 °C, which demonstrates an increase in mass transfer, reduction of secondary structure formation, linearization of the OGN structure and improved size based separation.

Resolution under identical conditions can vary between stationary phases. Within this work, two reversed phase stationary phases were used for analytical work. A macroporous PS-DVB C18 polymeric phase (DNAPac RP column - 2.1\*100 mm) and a solid core silica C18 phase (Accucore C18 column – 2.1\*50 mm). To assess the degree of variance between the two stationary phases, the dT ladder was analysed using identical strong IP-RP HPLC conditions. The results from Figure 3.6a show that under identical gradients, using a flow rate of 0.2 mL/min at 50 °C, the Accucore (black trace) produced a higher resolution of the dT ladder. This is partly due to the increased hydrophobicity of the Accucore stationary phase and partly as a result of the lower pore volume of the stationary phase particles. Resolution could be matched using the DNAPac RP stationary phase and a shallower gradient (34.5-45% v/v MeCN), however PWHH was increased by 82% to that obtained using the Accucore C18 stationary phase. A comparison between analytical temperature, elution gradient and stationary phase (reflecting Figure 3.6a) is shown in Table 3.3. The table identifies changes in signal height, PWHH and resolution as a function of analytical parameter or stationary phase change.

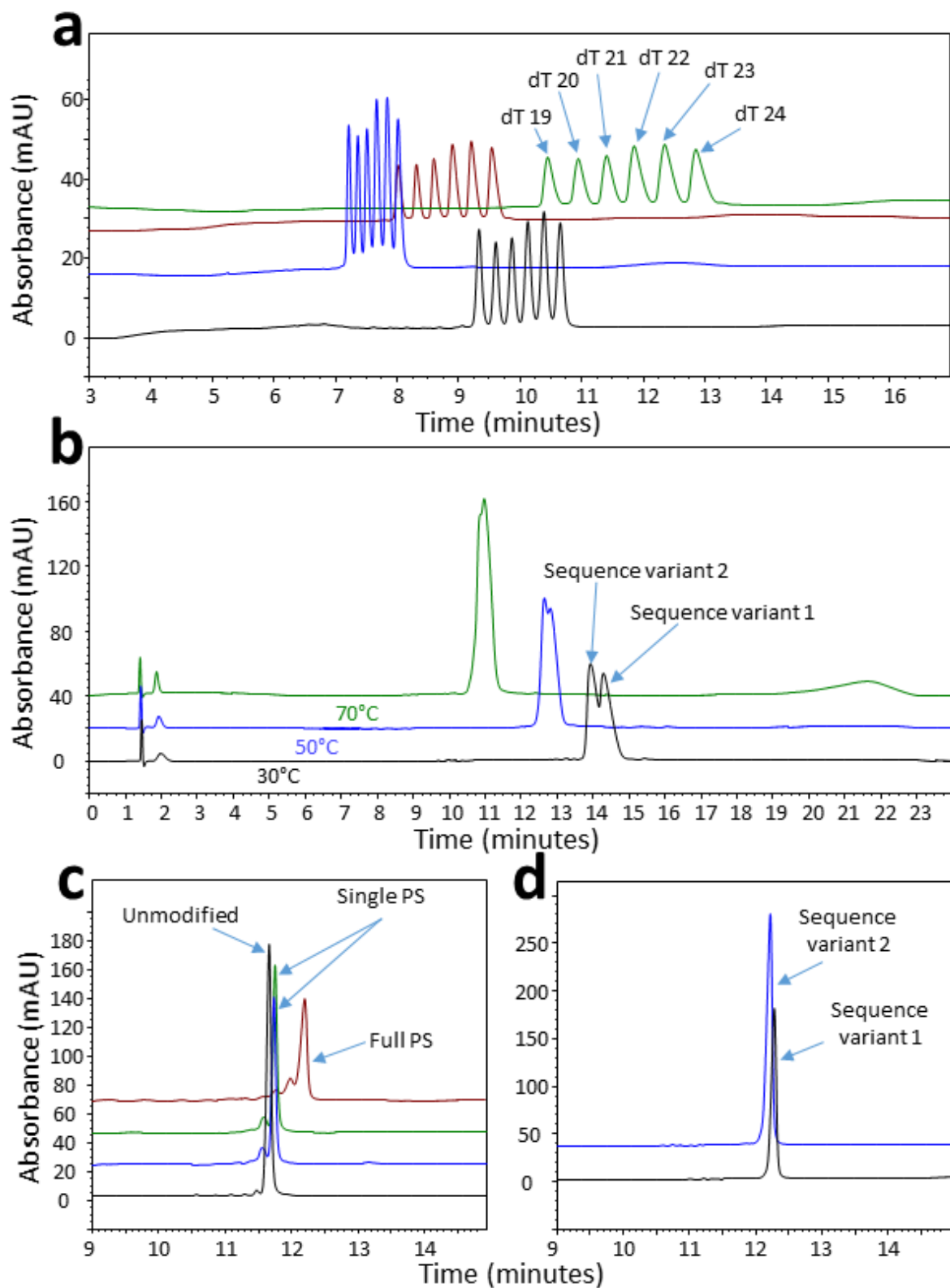


**Figure 3.6: Optimisation of analysis temperature, elution gradient and stationary phase for analysis of OGNs using strong IP-RP HPLC.** Analyses at 0.2 ml/min within a mobile phase of 5 mM TBuAA, 0.1  $\mu$ M Na<sub>4</sub>EDTA, 10-80% v/v MeCN. **a:** 30 picomole samples of a dT ladder. Black trace – Accucore C18 column at 50 °C, under 42.5- 52% v/v MeCN gradient from 1-15 min. Blue trace – DNAPac RP column at 50 °C, under 42.5- 52% v/v MeCN gradient from 1-15 min. Green trace - DNAPac RP column at 50 °C, under 34.5- 45% v/v MeCN gradient from 1-15 min. Brown trace – DNAPac RP column at 70 °C, under 34.5- 45% v/v MeCN gradient from 1-15 min. **b:** 50 picomole samples of 30-mer sequence variants. DNAPac RP column at 30-50 °C, 34.5-59% v/v MeCN gradient between 1-15 min. **c:** 30 picomole samples of 16-mer PS variants at 30 °C. Accucore C18 column, under a gradient of 27.5-73 % v/v MeCN from 1-15 min. **d:** 30 picomole samples of 30-mer sequence variants at 50 °C. Accucore C18 column under a gradient of 27.5-73% v/v MeCN from 1-15 min.

**Table 3.3: Comparison of stationary phases DNAPac and Accucore C18 under two gradients and two analysis temperatures.** Chromatographic performance indicated by signal height, resolution and peak width at half height.

Column	Analysis temperature (°C)	Gradient of MeCN (% v/v from 1-15 minutes)	Resolution (Rs)	Signal height (mAU)	PWHH (minutes)
Accucore C18	50	42.5- 52	1.39-1.71	25.12	0.11
DNAPac RP	50	42.5- 52	1.22-1.36	37.75	0.08
DNAPac RP	50	34.5- 45	1.39-1.70	13.39	0.20
DNAPac RP	70	34.5- 45	1.56-1.92	16.57	0.11

### 3.2.2.2 Sequence dependent separations of OGNs using strong IP-RP HPLC.

Utilisation of TEAA for weak IP-RP HPLC facilitated secondary interactions to occur between OGN bases and the stationary phase, which resulted in both sequence and size based separation mechanisms. More hydrophobic OGNs (those with higher amounts of adenine or thymine bases) should adsorb more strongly towards the stationary phase and elute last. However at a low separation temperature, the OGN with highest AT content eluted first- demonstrating aberrant retention patterns due to potential secondary structure conformation. At higher separation temperatures, linearization of the OGN structure reduced aberrant retention patterns between sequence isomers to more predictive retention patterns. To analyse the effects of strong IPRs on sequence based separation, the 30-mer sequence variant OGN models were analysed using TBuAA at different temperatures (see Figure 3.6b). The results show that under strong IP-RP HPLC conditions, the sequence variant OGNs do not co-elute, demonstrating that the mechanism of separation is not completely size dependent under these conditions. In comparison to analysis using weak IP-RP HPLC conditions and TEAA as IPR, where baseline resolution of the sequence variants was achieved at 30 °C, it is clear that at the same temperature under strong IP-RP HPLC conditions, the two sequence variants elute with similar retention times. This demonstrates a higher dependence on size based separation than sequence within strong IP-RP HPLC.

To further compare strong IP-RP to weak IP-RP, the range of 16-mer PS variants (see Table 3.2) was analysed (see Figure 3.6c). The results show that the two diastereoisomers of a single PS OGN co-elute at a similar retention time to the unmodified OGN, which demonstrates increased size dependency in comparison to weak IP-RP conditions. However, the full PS OGN elutes at an increased retention time compared to the singly modified and unmodified OGN, demonstrating how incremental phosphorothioation imparts additional hydrophobicity to the OGN. As the full PS OGN and single PS OGNs do not co-elute with the unmodified OGN, this demonstrated that a completely size based separation is not achieved with the use of the IPR TBUAA and dual separation mechanisms occur within OGN separations. However, comparison with the results obtained using TEAA (see Figure 3.3a) shows that size based separation is increased with the use of a stronger IPR. Consistent with the analysis above, these results demonstrate that by altering the IPR (from weak to strong) and the temperature, it is possible to alter the mechanism of separation from both size and sequence dependent to predominantly size dependent. Although it should be noted that it was not possible to achieve fully size dependent separations as shown the analysis of the PS and 30-mer sequence variant OGNs.

Individual 30-mer sequence variants were analysed at optimised conditions of 50 °C on an Accucore C18 column (see Figure 3.6d). The results show that total size based separation of the 30-mer sequence variants is also not obtained using this alternative stationary phase. These results confirm those obtained within PS OGN separations under strong IP-RP HPLC conditions on a DNAPac RP column.

### **3.2.3 Optimisation of hexafluoroisopropanol modified ion-pair reversed-phase liquid chromatography for the analysis of OGNs.**

#### **3.2.3.1 Size dependent separation of OGNs using HFIP modified IP-RP HPLC.**

Previous results had shown that using a strong IPR enabled predominantly size based separations of OGNs. An alternative approach was also studied to optimise size based separations by using weak IP-RP HPLC combined with hexafluoroisopropanol (HFIP). As discussed in Chapter 1 (section 1.3.2) HFIP is an acidic alcohol that is commonly paired with triethylamine (TEA) for the analysis of OGNs by HPLC-mass spectrometry (LC-MS) [260]. TEA:HFIP mobile phase systems have been shown to

improve the efficiency of separation of full PS OGNs in IP-RP HPLC [249]. It has been proposed that HFIP has a desolubilising effect on the IPR - forcing its adsorption further towards the stationary phase [189, 238]. Thereby, secondary interactions are reduced due to increased stationary phase saturation (with the IPR), and more dynamic ion-exchange separation occurring. The majority of LC-MS studies previously used 400 mM HFIP with 16.3 mM TEA (see Chapter 1, section 1.3.2). In this research, it was proposed to use alternative mobile phases using lower concentrations of HFIP as this is both expensive and hazardous. Gong and McCullagh have demonstrated the use of lower concentrations of HFIP in combination with a range of ion-pair reagents [254]. Therefore, final concentrations of 40 and 80 mM HFIP were used in combination with 100 mM TEAA for HFIP modified IP-RP HPLC analysis of OGNs. Here the HFIP is employed as an additive to increase stationary phase IPR saturation and not as the IPR counterion.

The first aim of HFIP modified IP-RP HPLC analysis was to compare HFIP modified conditions to non-HFIP conditions. Using a ratio of 100 mM TEAA to 80 mM HFIP, size based separation of the dT ladder was performed. A comparison between IP-RP HPLC analysis in the presence and absence of HFIP is shown in Figure 3.7a. The results demonstrate that under identical conditions of temperature, gradient and flow rate, resolution of the dT ladder is increased when 80 mM HFIP is present within the mobile phase (specifically  $R_s$  increases from 0.98-1.11 to 1.86-2.21) with baseline separation observed. Improvements in resolution were also achieved by further optimisation of the elution gradient resulting in baseline resolution of the dT ladder (see Figure 3.7a). Further analysis of the 30-mer sequence variants using the HFIP:TEAA mobile phase is shown in Figure 3.7b. The results show that at 50 °C there is a small difference in retention time, demonstrating some sequence based separation of the two 30-mers.

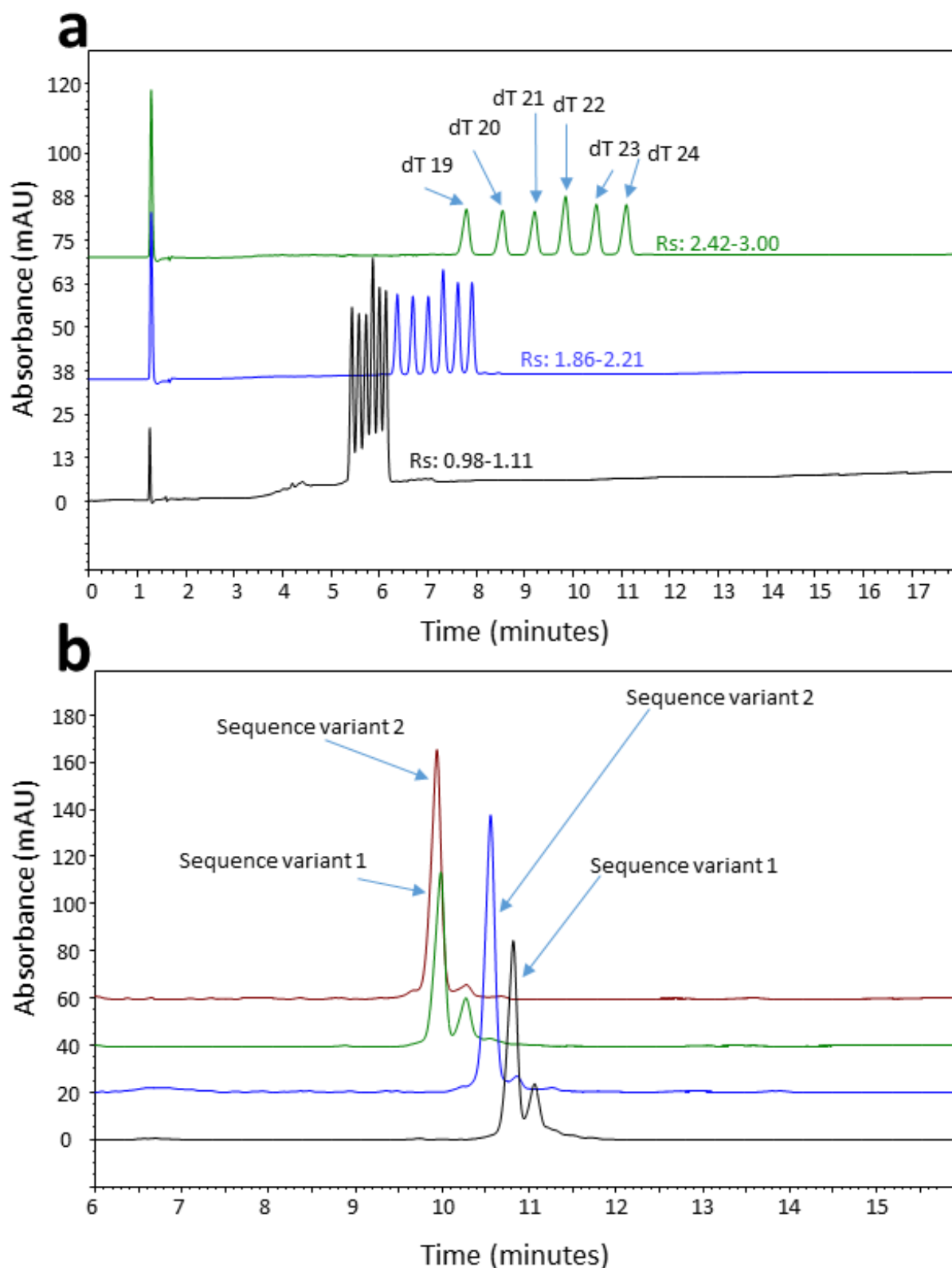


**Figure 3.7: Optimisation of elution gradient and analysis temperature under HFIP modified IP-RP HPLC conditions.** Analysis performed at 0.2 ml/min using a DNAPac RP column with 100 mM TEAA, 80 mM HFIP, 0.1 mM  $\text{Na}_4\text{EDTA}$ , 0-25%  $\text{v/v}$  MeCN. **a:** 50 picomole samples of dT ladder analysed at  $70^\circ\text{C}$ . Black trace – comparison with weak IP-RP HPLC conditions under a gradient of 100 mM TEAA, 0.1 mM  $\text{Na}_4\text{EDTA}$ , 8.75-17.5%  $\text{v/v}$  MeCN from 1-15 min. Blue trace – HFIP modified IP-RP HPLC under gradient of 8.75-17.5%  $\text{v/v}$  MeCN from 1-15 min. Green trace- HFIP modified IP-RP HPLC under gradient of 8.75-12.5%  $\text{v/v}$  MeCN from 1-15 min. **b:** 30 picomole samples of 30-mer sequence variants. Gradient of 8.75-17.5%  $\text{v/v}$  MeCN applied from 1-15 min. Black and Blue traces  $-50^\circ\text{C}$ . Green and brown traces-  $70^\circ\text{C}$ .

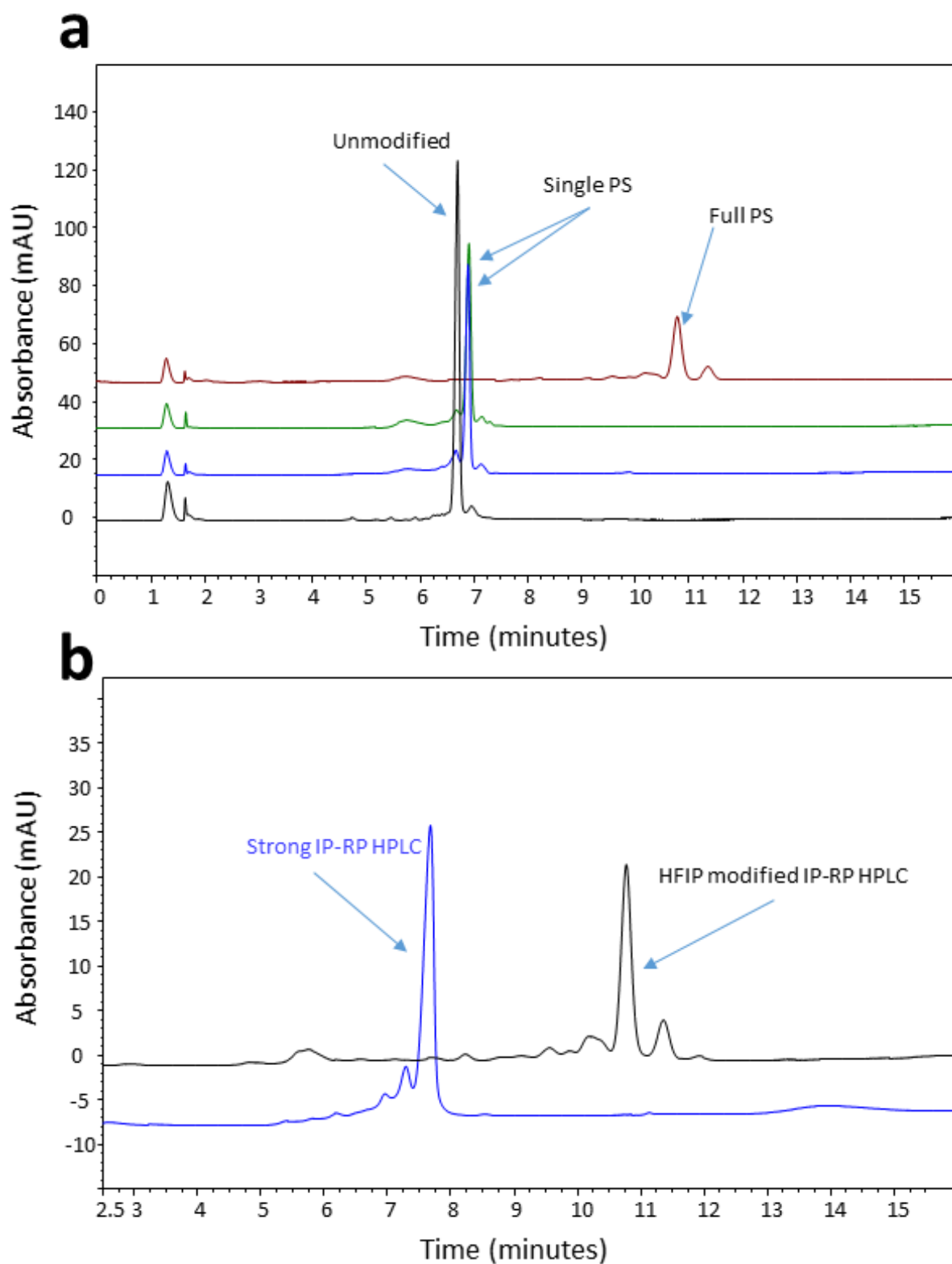


**Figure 3.8: Optimised analysis of PS OGNs using HFIP modified IP-RP HPLC.** HFIP modified IP-RP HPLC performed at 0.2 ml/min, at 70°C using a DNAPac RP column on 30 picomole samples. A mobile phase consisting of 100 mM TEAA, 80 mM HFIP, 0.1 mM Na<sub>4</sub> EDTA and 0-25% v/v MeCN was used. **a:** Optimised separation of 16-mer PS variants under 8.75-17.5% v/v MeCN gradient applied from 1-15 min. **b:** Comparison of optimised analysis of 16-mer full PS OGN under strong IP-RP HPLC and HFIP modified IP-RP HPLC conditions. Black trace –HFIP modified IP-RP: 100 mM TEAA, 80 mM HFIP, 0.1 mM Na<sub>4</sub> EDTA and 8.75-17.5% v/v MeCN gradient applied from 1-15 min. Selectivity changes lead to resolution of an extra peak at around 11.5 min retention time. Blue trace – Strong IP-RP: 5 mM TBuAA, 0.1 μM Na<sub>4</sub> EDTA, 34.5-45% v/v MeCN gradient applied from 1-15 min.

However, at 70 °C the two 30-mers co-elute, demonstrating the move towards size dominant separation of these OGNs under these conditions. It is proposed that at higher temperatures effective denaturing of the OGNs occurs, therefore minimising potential conformational differences of the two OGNs. Thus, this combination of OGN linearization and reduction of secondary interactions leads to more dynamic ion exchange separation mechanisms and increased size dominant separations between the two 30-mer sequence isomers.

### **3.2.3.2 Sequence dependent separation of OGNs using HFIP modified IP-RP HPLC.**

Having previously demonstrated size based separation with the analysis of the two 30-mer sequence variants using a TEAA:HFIP mobile phase. Further investigation of OGN retention behaviour was performed to study the extent of sequence based separation of the 16-mer PS variants. The results are shown in Figure 3.8a and demonstrate that at 70 °C, the two diastereoisomers of the single PS modified OGNs co-elute, achieving size based separation. However, the 16-mer PS variants have different retention times, demonstrating that sequence based separation occurs under these conditions. In comparison with separations using TEAA without the addition of HFIP in the mobile phase (see Figure 3.4), the PWHH of the full PS OGN was improved by 67% - 0.55 to 0.18 min for a 30 picomole sample. Further comparison with the data using the strong ion-pair reagent is shown in Figure 3.8b and shows a similar PWHH for the full PS (0.17 minutes) for a 30 picomole sample. Differences in the chromatographic profile of the main and closely eluting peaks demonstrate that there are potential changes in selectivity between the different mobile phases. The addition of HFIP to a weak IPR not only improves peak shape of the full PS OGN in comparison to using TEAA alone, but also induces the resolution of species that co-elute under other conditions (such as strong ion-pair conditions).

Further optimisation of the mobile phase was performed in effort to maintain resolution of OGNs but at a lower concentration of HFIP of 40 mM. Comparisons of size based separations of the dT ladder using 40 mM and 80 mM HFIP in the mobile phase are shown in Figure 3.9a. Resolution of the dT ladder remained constant when HFIP concentration was halved within the mobile phase ( $R_s=1.4-1.7$ ), which in enables separations at reduced cost, lower toxicity and higher environmental sustainability.

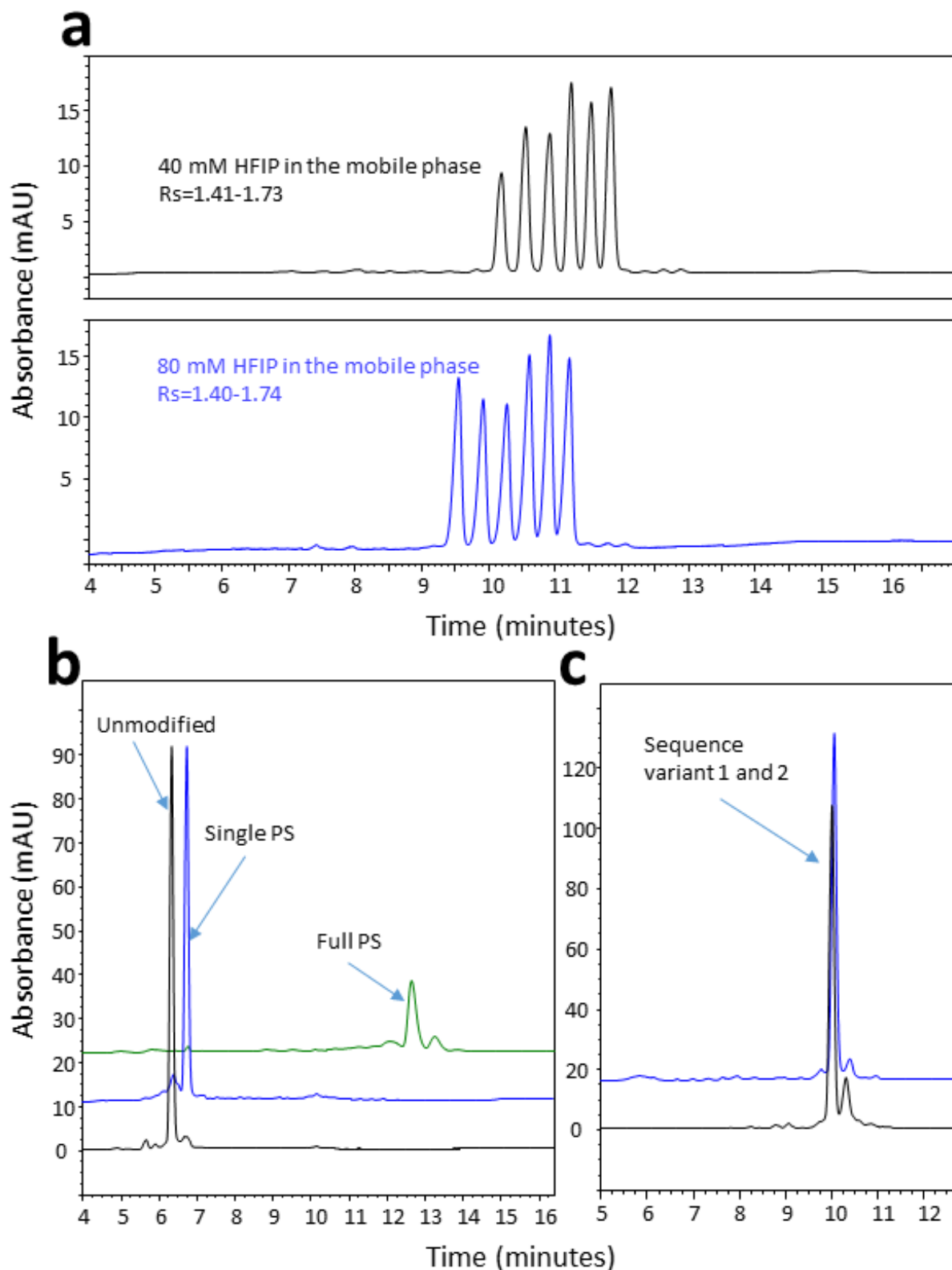


**Figure 3.9: Optimisation of HFIP modified IP-RP mobile phase for analysis of OGNs.** Analyses performed on a DNAPac RP column at 0.2 ml/min at 70°C to 30 picomole samples. HFIP modified IP-RP HPLC using a mobile phase of 100 mM TEAA, 40 mM HFIP, 0.1 mM Na<sub>4</sub>EDTA and 0-25% v/v MeCN was used to compare to one with 80 mM HFIP concentration. **a:** Comparative analyses of the dT under 8-75-17.5% v/v MeCN between 1-15 min. **b:** Optimised analysis of 16-mer PS variants using a gradient of 8.75-17.5% MeCN (40mM HFIP) applied from 1-15 min. **c:** Optimised analysis of 30-mer sequence variants using a gradient of 8.75-17.5% v/v MeCN (40mM HFIP) applied from 1-15 min.

To further assess whether this effect could be translated for mixed base or chemically modified OGNs, analysis of the OGNs models (30-mer sequence variants and 16-mer PS models) was performed. The results are shown in Figure 3.9 b-c and demonstrate that using 40 mM HFIP within the mobile phase in conjunction with separation at 70 °C, the 30-mer sequence variants and 16-mer diastereoisomers co-elute, as was achieved using 80 mM HFIP in the mobile phase. Analysis of the full PS OGN using 40 mM HFIP in the mobile phase led to an increased peak width from 0.18 min to 0.23 min in comparison to using 80 mM HFIP in the mobile phase. This shows a slight reduction in size dependent separation of full PS OGNs.

### **3.2.4 Summary of work using IP-RP HPLC for OGN analysis.**

In summary, IP-RP HPLC was performed in an approach to optimise size and sequence based separations. Analysis of a range of different model OGNs were analysed to assess both the chromatographic performance and degree of size and sequence dependent separation under different conditions. Optimisation of chromatographic parameters such as flow rate, column temperature and elution gradient was performed to enhance either size or sequence based separation of the analytes. Optimisation of the IPR in conjunction with the addition of an acidic alcohol was also performed in an approach to enhance size based separations.

The results show that using a weak IPR, such as TEAA, results in both size and sequence dependent separations. The sequence, structure and chemical composition of the OGN strongly influences the chromatography under these conditions, as demonstrated by the separation of the 30-mer sequence variants and diastereoisomers of the PS OGNs. Manipulation of the analysis temperature can be used to change the selectivity of the 30-mer sequence variants and 16-mer PS diastereoisomers where an increase in temperature (denaturing) reduces the secondary structure of the OGNs, thereby shifting the separation mechanism towards OGN size, as demonstrated by co-elution of diastereoisomers and smaller PWHH.

Changing to a strong IPR such as TBuAA or addition of HFIP (40/80 mM) to the weak IPR TEAA, combined with analysis at 70 °C resulted in more size dependent separations. This was exemplified with the co-elution of the 30-mer sequence variants and diastereoisomers of the PS OGN. However, under these conditions, completely size dependent separations of the PS OGNs was not achieved- as demonstrated by the different retention times of the phosphodiester, single PS and full PS variants. Furthermore, a significant improvement in peak shape of the full PS OGN was observed, which

would improve the size dependent separations of a fully PS OGN and its fully PS manufacturing impurities.

### **3.3 Optimisation of size and sequence separations of OGNs using strong anion exchange HPLC.**

#### **3.3.1 Optimisation of strong anion exchange chromatography for the analysis of OGNs - using sodium chloride as eluotropic salt.**

As discussed in Chapter 1 (section 1.3.1), SAX chromatography employs a positively charged stationary phase to electrochemically adsorb negatively charged OGNs for retention. OGNs are eluted from the stationary phase by the incremental gradient of a competitive counter-ion concentration, such as chloride, provided by eluotropic salt sodium chloride (NaCl). OGN retention increases with the amount of negatively charged phosphate groups of the backbone, and thus separation mechanisms are strongly associated with the size of the OGN [162]. There are also secondary interactions that occur between the bases of the OGN and the stationary phase due to their differing polarity, which imparts a sequence effect on separations [157]. Higher mobile phase pH further ionises tautomeric bases guanine and thymine, which influences selectivity in reflection of the base sequence of an OGN. Those OGNs with more tautomeric bases are strongly ionised in mobile phases with higher pH [169].

A mobile phase of 20 mM Tris, 0-1250 mM NaCl pH 8 was initially prepared for SAX HPLC optimisations. The stationary phase utilised for strong anion exchange in this study was a DNAPac PA200 Rs polymeric stationary phase. The polymeric stationary phase has some resistance to high pH at low temperature and resistance to high temperature at a lower pH, and has demonstrated high resolution separations in previous studies (see Chapter 1, section 1.3.1) . Functionalised nanobeads bonded to a non-porous substrate enable improved mass transfer processes, which leads to higher OGN resolution and chromatographic efficiency. The phase has an added benefit of high loading capacity, so could potentially be used for semi preparative separations, see Table 3.4 for column characteristics.

**Table 3.4: Characteristics of the DNAPac PA200 Rs column.**

<b>Characteristic</b>	<b>DNAPac PA200 Rs</b>
<b>Pressure Limit</b>	689 Bar
<b>pH range</b>	2.5-12.5
<b>Temperature Limit</b>	85 °C
<b>Phase Chemistry</b>	Polymeric- non porous, quaternary ammonium ion
<b>Particle Size</b>	4 µm
<b>Loading Capacity</b>	High

### **3.3.1.1 Size dependent separations of OGNs using SAX HPLC in conjunction with NaCl.**

The first aim was to optimise SAX HPLC analytical parameters such as temperature, elution gradient and mobile phase chemistry, and assess the degree of size and sequence based separation when analysing OGNs. Starting with a mobile phase of 20 mM Tris, 0-1250 mM NaCl, pH 8, model OGNs (see Table 3.2) were analysed.

Analysis temperature has proved to have a strong effect on the manipulation of either size or sequence based separations within IP-RP HPLC. To assess if temperature has as much influence within the mode of SAX HPLC, column temperature was optimised for size based separations using the dT ladder (see Figure 3.10a). The results show the high resolution separation of the dT 19-24-mers, which is near to baseline at 30 °C ( $R_s=1.46-1.91$ ), was further improved by increasing the analysis temperature. However, an increase to 50 °C showed optimum resolution for this sample as this began to decrease at a higher analysis temperature of 70 °C ( $R_s$  at 50°C = 1.63-2.29 and  $R_s$  at 70 °C = 1.53-2.27). The retention times of the OGN ladder increases with increasing separation temperature, this is a result of the OGN structures linearizing and making more negative charges available for interaction with the stationary phase at higher temperatures [162].

Next, the salt elution gradient was optimised for size based separations of the dT ladder by decreasing the slope of the gradient was decreased (as was done within work using IP-RP HPLC), and increasing the starting concentration of counter ion, without altering the slope of the gradient (see Figure 3.10b). The results show that resolution can be increased by both strategies with resolution values increasing from 1.46-1.91 to 1.90-2.45 with a 38% reduction in elution gradient slope, 1.96-2.23 with an increase of starting counter ion concentration of 34%.

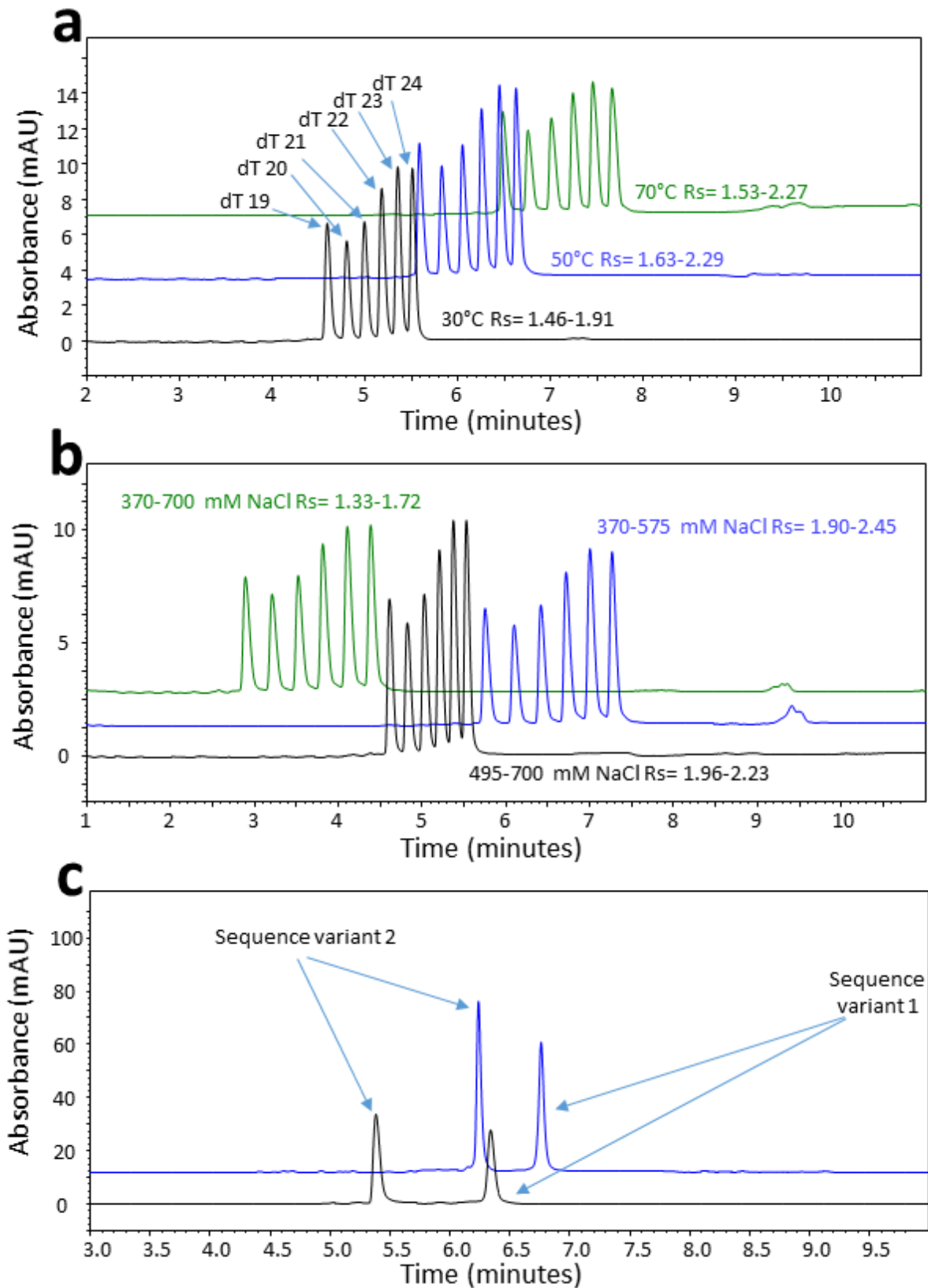


**Figure 3.10: Optimisation of temperature, elution gradient and mobile phase for analysis of OGNs by SAX HPLC.** 50 picomole samples analysed on a DNAPac PA200 Rs, mobile phase of 20 mM Tris, 0-1.25 M NaCl pH 8 at 1.2 ml/min. **a:** dT ladder under 20 mM Tris, 370-700 mM NaCl gradient from 0-7.7 min increasing to 700-1000 mM NaCl between 7.7-10.1 min at 30-70 °C. **b:** dT ladder analysed at 30 °C. Black trace- 370-700 mM NaCl gradient from 0-7.7 min increasing to 700-1000 mM between 7.7-10.1 min. Blue trace – 370-575 mM NaCl gradient from 0-7.7 min increasing to 575-1000 mM between 7.7-10.1 minutes. Green trace - 495-700 mM NaCl gradient from 0-7.7 min increasing to 700-1000 mM NaCl between 7.7-10.1 min. **c:** 30-mer sequence variants analysed at 30 °C, 370-700 mM NaCl gradient from 0-7.7 min increasing to 700-1000 mM between 7.7-10.1 min. Black trace – Mobile phase pH 8 with 0% v/v MeCN. Blue trace – Mobile phase pH 8 with 20% v/v MeCN.

### 3.3.1.2 Sequence dependent separations of OGNs using SAX HPLC in conjunction with NaCl.

Following optimisation of SAX HPLC parameters for the size dependent separation of the dT ladder, further analysis of the model OGN cohort was performed. Analyses of the two 30-mer sequence variants in different mobile phase conditions is shown in Figure 3.10 c. Using 20 mM Tris, 0-1250 mM NaCl, pH 8, the resolution of the 30-mer sequence variants was 8.91. To investigate how sequence based separations can be reduced via minimising secondary base interactions, further analysis was performed by adding an organic solvent to the mobile phase. This has been shown to affect OGN retention as organic solvents reduce secondary interactions between OGN bases and the stationary phase [157]. Addition of 20% v/v MeCN to the mobile phase prior to SAX HPLC analysis of the 30-mer sequence variants results in a 13% decrease in resolution to 7.14, due to reduced secondary interactions between the bases and the stationary phase. These results are consistent with previous observations [157, 169] demonstrating that mobile phase chemistry can be optimised to improve or reduce sequence based separations by effecting secondary interactions of OGN bases and the stationary phase. However, even with the addition of 20% v/v MeCN to the mobile phase, strong sequence dependent OGN separations were observed using SAX HPLC. The impact of this is that SAX parameters can't be easily manipulated to change retention mechanisms, and so as a 1D method, is biased in relation to separation mechanism.

Further analysis of the PS variants using SAX HPLC is shown in Figure 3.11. Consistent with previous observations in literature, the results show the separation of the two diastereoisomers of the 16-mer PS OGN with different retention times to the phosphodiester OGN, highlighting the strong sequence dependent effects, similar to those observed using weak IP-RP HPLC (see Figure 3.4). Retention time increases with the increase in phosphorothioation as incremental sulfurization of the anion results in higher binding affinity for the stationary phase by lipophilic secondary interactions [135, 156]. Within this analysis, the full PS OGN did not elute within the gradient. A blank analysis is shown in Figure 3.11 to clarify that the peak at 12.5 minutes is not the full PS OGN but a reflection of the high salt in the wash step. It is proposed that the full PS OGN will elute as a broad peak, resulting in difficult detection and is not suited for analysis in these chromatographic conditions.

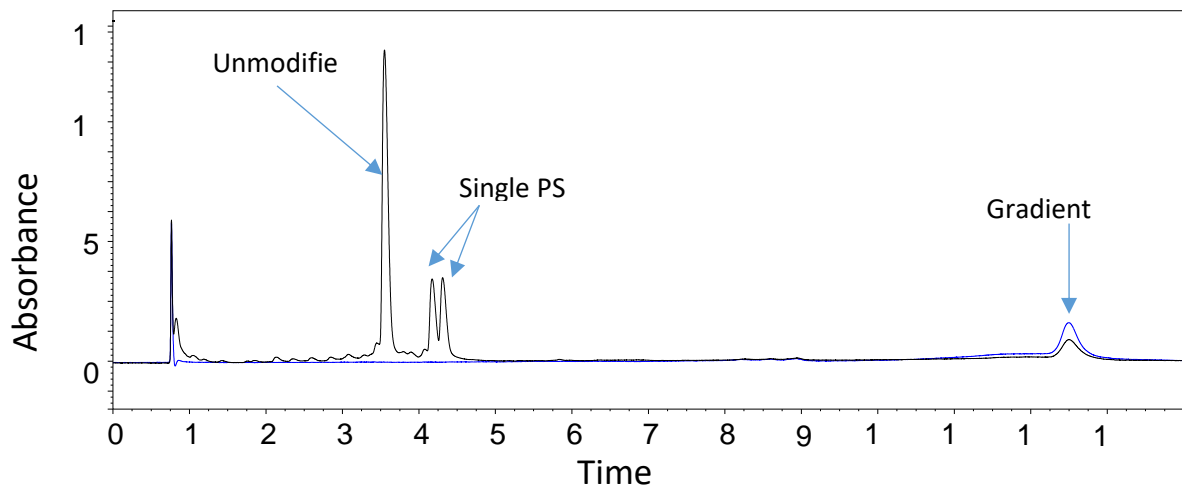


**Figure 3.11: Analysis of 50 picomole sample of 16-mer PS variants using SAX HPLC in conjunction with NaCl.** 30 °C at 1.2 mL/min using a DNAPac PA200 Rs column. Gradient of 20 mM tris, 370-700 mM NaCl, pH 8 applied from 0-7.7 min increasing to 700-1000 mM between 7.7-10.1 min. Blue trace- Blank analysis.

### 3.3.2 Optimisation of strong anion exchange for the analysis of OGNs- using sodium perchlorate as elutropic salt.

#### 3.3.2.1 Size dependent separations of OGNs using SAX HPLC in conjunction with NaClO<sub>4</sub>.

Previous results had shown that using the elutropic salt NaCl for SAX HPLC analysis of OGNs resulted in a strong sequence dependent separations unsuitable for the analysis of full PS OGNs. Therefore, in an approach to enhance size dependent separations of OGNs using SAX-LC, alternative salts of stronger elutropic strength including sodium thiocyanate (NaSCN) and sodium perchlorate (NaClO<sub>4</sub>) were assessed. NaSCN is known to dissociate into a 'soft' base thiocyanide [135, 327]. NaClO<sub>4</sub> is an alternative salt, which has previously been employed for OGN analysis by SAX HPLC [157].

Initial work focussed on using mobile phases containing NaSCN to analyse the dT ladder (see Appendix 2, Figure A2.2). The results show that the NaSCN absorbs UV light at 260-280 nm wavelength. This results in high absorbance during a gradient elution. In addition, the resolution of dT OGNs were lower compared to using NaCl. Therefore, further analysis using an alternative (UV non-absorbing) salt (NaClO<sub>4</sub>) was performed for continued optimisation of SAX HPLC.

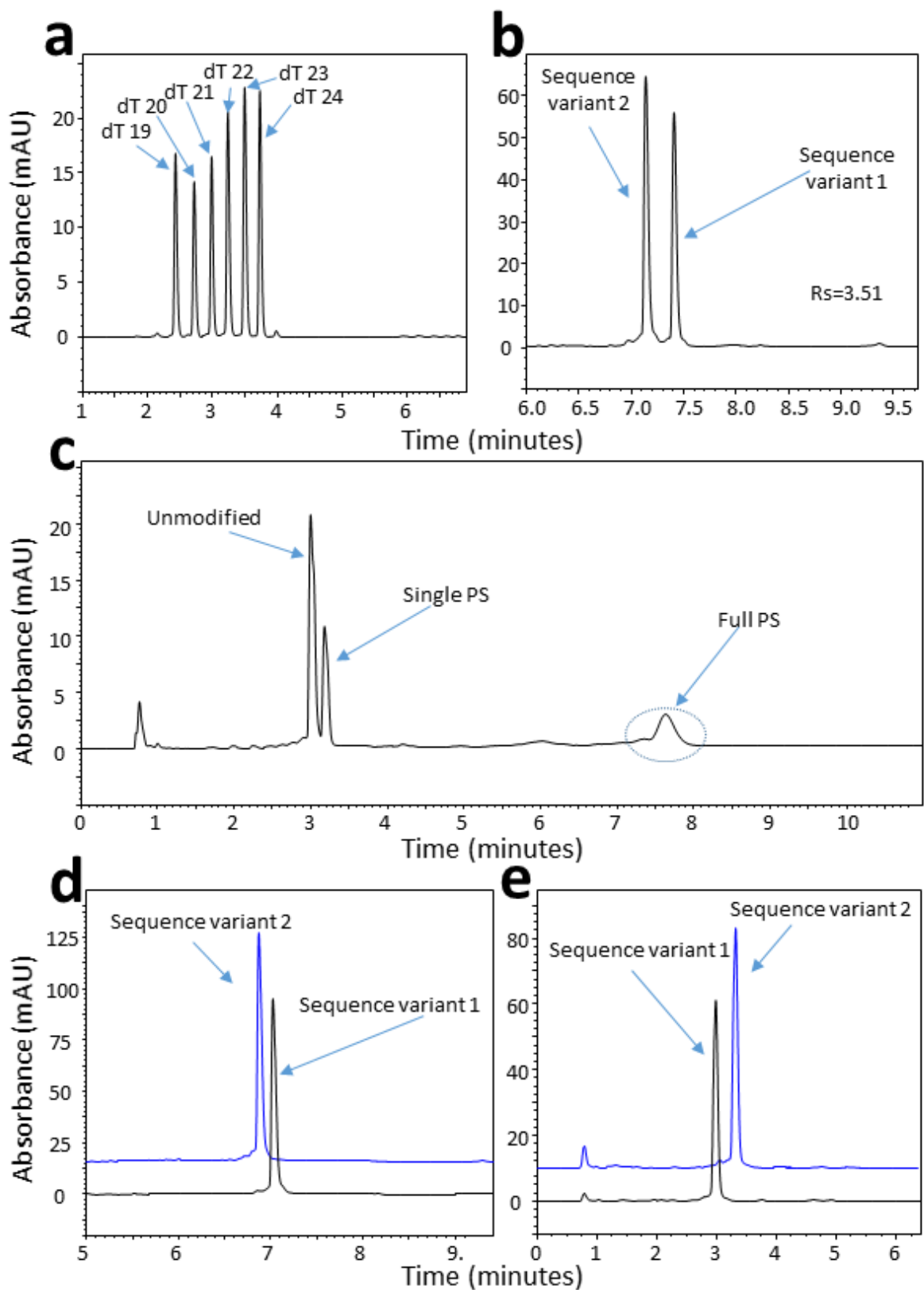


**Figure 3.12: Optimisation of SAX HPLC using  $\text{NaClO}_4$  as eluting salt for OGN analysis.** 50 picomole samples analysed at 1.2 ml/min on a DNAPac PA200 Rs column, at 30°C. 20 mM Tris, 0-400 mM  $\text{NaClO}_4$  and 20%  $v/v$  MeCN, pH 6.5/8/12.5. **a:** dT ladder analysed under 98.4-144 mM  $\text{NaClO}_4$  gradient applied from 0-7.7 min increasing to 144-320 mM between 7.7-10.1 min. pH 8. **b:** 30-mer sequence variants analysed under 38.4-144 mM  $\text{NaClO}_4$  gradient applied from 0-7.7 min increasing to 144-320 mM between 7.7-10.1 min. pH 8. **c:** 16-mer PS variants analysed under 98.4-304 mM  $\text{NaClO}_4$  gradient applied from 0-7.7 min increasing to 304-320 mM between 7.7-10.1 min. pH 8. **d:** 30-mer sequence variants analysed under 38.4-144 mM  $\text{NaClO}_4$  gradient applied from 0-7.7 min increasing to 144-320 mM between 7.7-10.1 min. pH 6.5. **e:** 30-mer sequence variants analysed under 122.4-184 mM  $\text{NaClO}_4$  gradient applied from 0-7.7 min increasing to 184-320 mM between 7.7-10.1 min. pH 12.5.

A mobile phase of 20 mM Tris, 0-400 mM NaClO<sub>4</sub>, pH 8, 20% v/v MeCN was utilised for initial analysis of the dT ladder (see Figure 3.12a). The results show that NaClO<sub>4</sub> was an efficient eluotropic salt for anion exchange where baseline resolution of the dT ladder was obtained (Rs= 3.01-3.56). There was a vast difference in the required concentration of eluting salt when comparing NaCl to NaClO<sub>4</sub> mobile phases, where a much lower concentration of NaClO<sub>4</sub> was required for elution. This can be of benefit, as avoiding high salt concentrations for chromatographic separations reduces corrosive effects upon the LC system and supports the lifetime of the equipment.

### **3.3.2.2 Sequence dependent separations of OGNs using SAX HPLC in conjunction with NaClO<sub>4</sub>.**

The 30-mer sequence and 16-mer PS OGN variants were separated using NaClO<sub>4</sub> gradient elution; this resulted in less sequence dependent separations compared to NaCl, as demonstrated by the co-elution of the PS diastereoisomers and loss of resolution of the sequence variants (see Figure 3.12 b-c). Using NaClO<sub>4</sub>, the full PS OGN was eluted within the gradient, however PWHH was larger than the unmodified or singly modified OGN (0.21 vs 0.08 minutes respectively). The optimised separation shows that the incremental addition of phosphorothioation results in increased retention of the OGN due to increased secondary hydrophobic interactions between the OGN backbone and stationary phase. In addition, using NaClO<sub>4</sub> for SAX HPLC analysis of OGNs sequence dependent effects are still observed from the resolution of the 30-mer sequence variants in Figure 3.12 b, d and e.

Continuing to optimise the mobile phase to further promote sequence based separations, analysis was performed at pH 6.5 and 12.5 to compare high and low mobile phase pH. Sequence based separations were manipulated to demonstrate pH effect on selectivity as a reflection of increased ionisation of tautomeric bases guanine and thymine (see Figure 3.12 d-e). At pH 6.5, with the addition of 20% v/v MeCN to the mobile phase, the retention order of the sequence variants reflects the stronger interactions between the cytosine and thymine bases (being of higher abundance within the sequence) of sequence variant 1. Retention order changes at pH 12.5 where sequence variant 2 demonstrates higher affinity for the stationary phase. This is likely a reflection of increased ionization of the tautomeric guanine and thymine bases at elevated pH. Both mobile phase pH conditions show that sequence based separations occur. However, size based separations can be improved by interrupting secondary interactions and self-association at low and high mobile phase pH respectively. Therefore, both size and sequence dependent separations occur under SAX HPLC

conditions, leading to the conclusion that this is more of a mixed mode separation mechanism of chromatography in respect to OGNs [328].

### **3.3.3 Summary of work using SAX HPLC for OGN analysis.**

In summary, SAX HPLC was performed in an approach to optimise size and sequence base OGN separations. Analysis of a range of different model OGNs were analysed to assess both the resolution and degree of size and sequence based separation under different conditions.

The results show that using mobile phases containing NaCl, high resolution separations of the dT ladder was achieved. Further analysis of the sequence variants and PS variants demonstrated that the mechanism is dependent on both size and sequence, similar to weak IP-RP HPLC. A number of strategies were employed to enhance size based separations using SAX HPLC including the use of NaClO<sub>4</sub> as an alternative to NaCl in the mobile phase and the addition of an organic modifier (20% v/v MeCN) which reducing secondary interactions. However, SAX is clearly strongly sequence dependent in relation to OGN separations, which can be further increased by changing the mobile phase pH.

## **3.4 Optimisation of size dominant separations of OGNs using size exclusion HPLC.**

### **3.4.1 Optimisation of size dependent separations using SEC HPLC for the analysis of OGNs.**

SEC differs from other modes of chromatography in that the analyst's prerogative is to reduce all interactions between the analyte and the stationary phase and is an entropic separation mode. Therefore the stationary phase serves to physically separate analytes rather than by chemical adsorption or partitioning and the mobile phase serves solely to carry the analyte through the column without a change in chemistry to effect analyte interaction [153]. A stationary phase with 130 Å pore size was chosen for separations of OGNs according to the recommended pore size for molecules less than 10,000 Daltons in mass, see Table 3.5 for column characteristics.

**Table 3.5: Characteristics of Advance BioSEC column.**

<b>Characteristic</b>	<b>Advance BioSEC</b>
<b>Pressure Limit</b>	400 Bar
<b>pH range</b>	2-8.5
<b>Temperature Limit</b>	80 °C
<b>Phase Chemistry</b>	Silica particles with hydrophilic bonded layer
<b>Particle Size</b>	2.7 µm
<b>Loading Capacity</b>	High

Initial work focused on using an Advance BioSec column with 150 mM sodium phosphate ( $\text{NaH}_2\text{PO}_4$ ) mobile phase at pH 7.5 for OGN separations. The first aim of optimisation of SEC was to assess the level of resolution obtained and determine the levels of secondary interaction between analytes and the stationary phase. The analysis of the 19-24-mer size mixture, as well as each individual OGN is shown in Figure 3.13a. The results show that resolution is low under these conditions, leading to a wide single peak – no resolution of the individual OGNs in the dT ladder were observed. Single OGN analyses validate this, as shown in Figure 3.13b, with only partial resolution of dT20 and dT24 observed under these conditions, see Figure 3.13c.

Further analysis of the two 30-mer sequence variants were also analysed to elucidate if there were any secondary interactions occurring between unmodified OGNs and the stationary phase (see Figure 3.13d). The results show that the two 30-mers co-elute, indicating that the base composition does not affect retention volume within this mode of chromatography and that this mode of chromatography is size dependent as anticipated.

To further assess the size based separation of OGNs using SEC, the 16-mer PS variants were analysed. The results are shown in Figure 3.14a and demonstrate that the two diastereoisomers and the phosphodiester OGN co-elute. The full PS OGN eluted later than its counterparts, demonstrating that additional secondary interactions are occurring – potentially due to the level of phosphorothioation. This is also demonstrated by the PWHH increasing for the full PS model in comparison to the unmodified or single PS models; specifically 0.27 to 0.40 minutes. These results further demonstrate that predominantly size based OGN separations are achieved using SEC. However, complete size dominant separation is still not achieved due to late elution of the 16-mer full PS OGN.

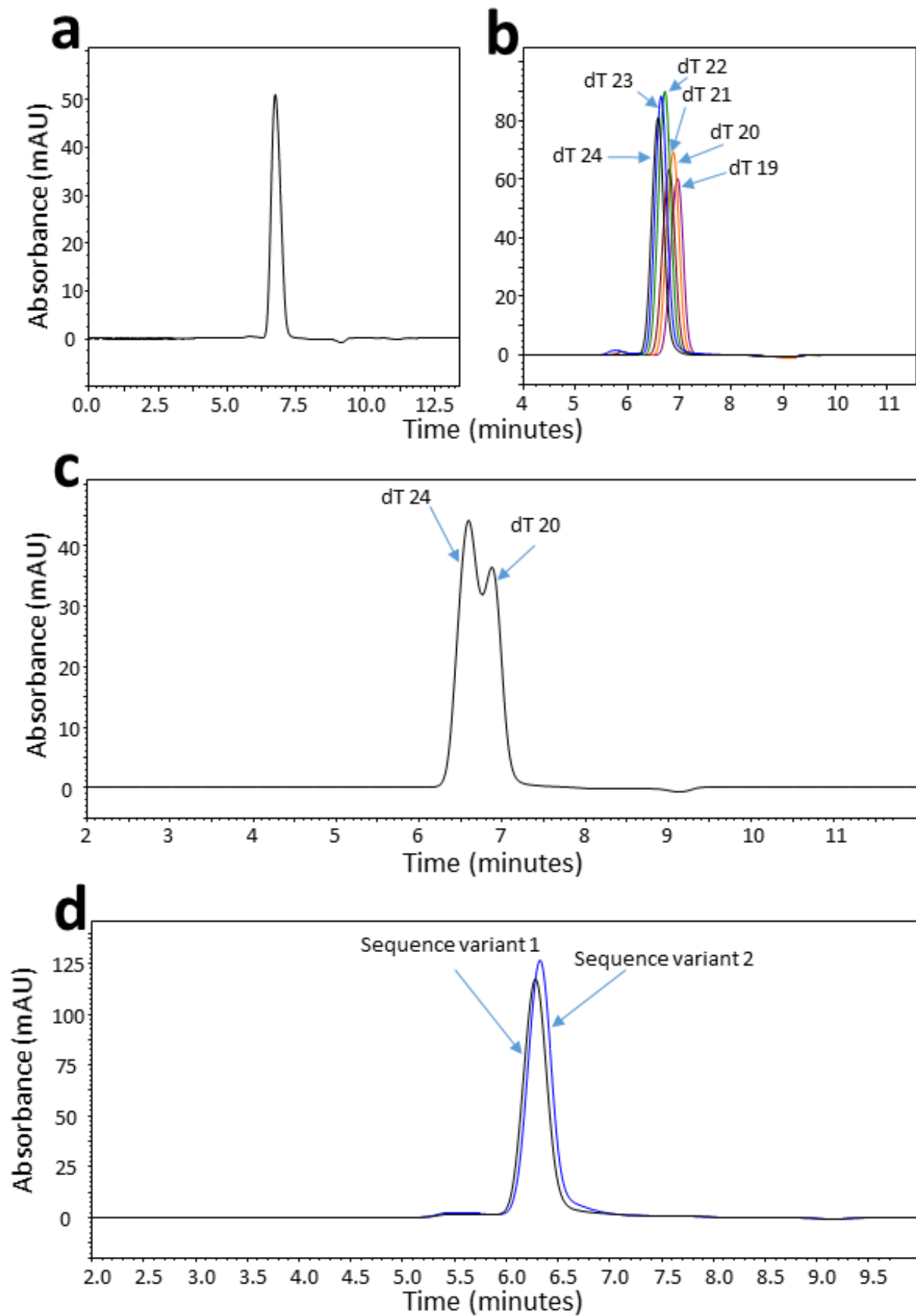


**Figure 3.13: Optimisation of SEC HPLC for the analysis of OGNs.** 50 picomole samples analysed isocratically on an Advance BioSEC column at 30 °C and 0.35 ml/min. Mobile phase of 150 mM  $\text{NaH}_2\text{PO}_4$ , pH 7.5. **a:** dT ladder analysis. **b:** dT 19-24-mer size variants analysis. **c:** dT 20-mer and dT 24-mer size variant mixture analysis. **d:** 30-mer sequence variants analysis.

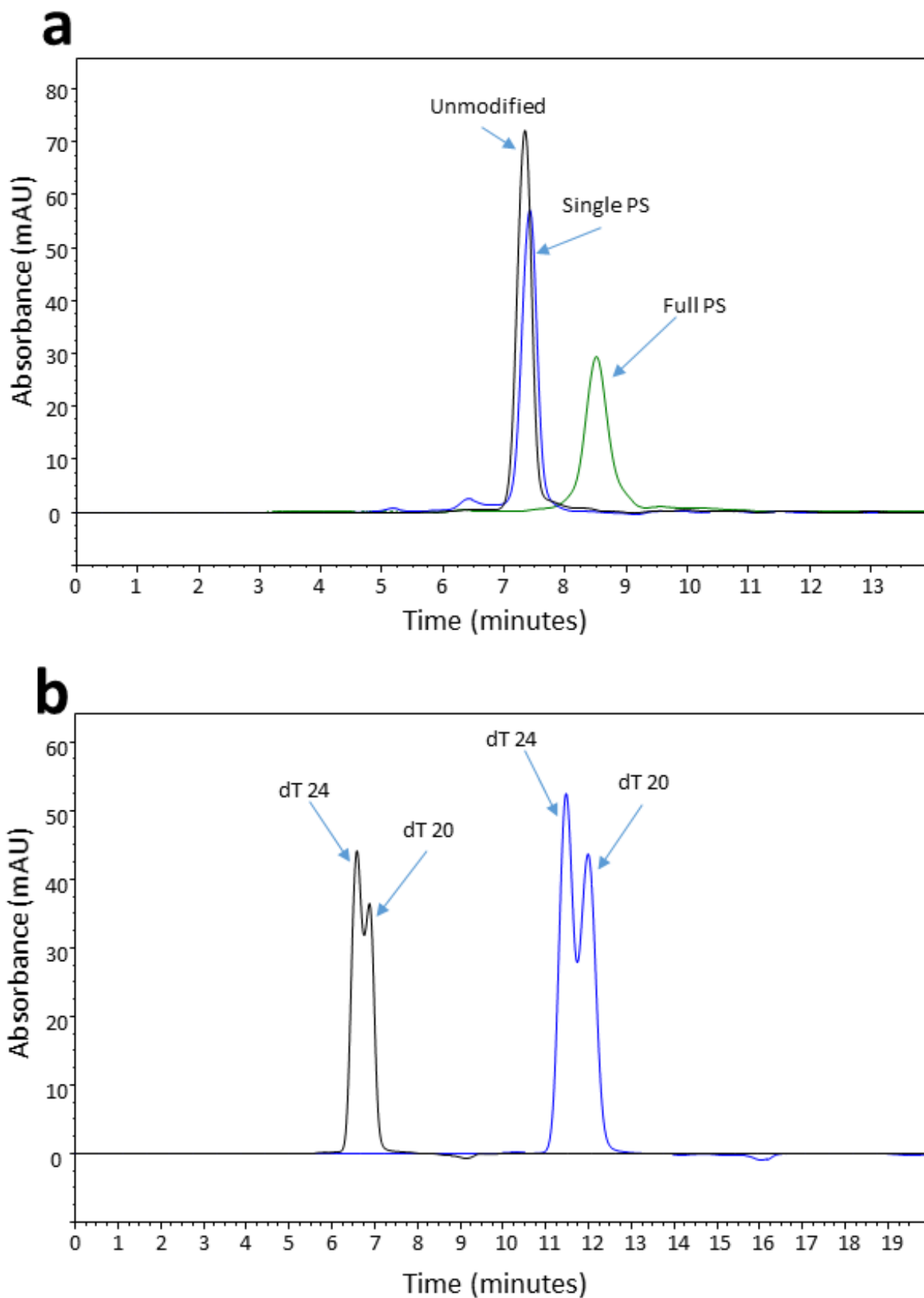


**Figure 3.14: Optimisation of flow rate for analysis of oligonucleotides using SEC HPLC.** 50 picomole samples analysed at 30 °C, using an Advance BioSEC column. Analysis performed isocratically with 150 mM  $\text{NaH}_2\text{PO}_4$ , pH 7 mobile phase. **a:** 16-mer PS variants analysed at 0.35 ml/min. **b:** dT 20-mer and 24-mer size variant mixture analysed at 0.2-0.35 ml/min.

To increase the resolution of OGNs in these conditions, the mobile phase velocity was also explored as a lower flow rate has been previously shown to increase resolution [329]. The linear velocity was decreased from 0.35 mL/min to 0.2 mL/min to maximise the diffusion of analytes in and out of the stationary phase pores during separation. The analysis of a poly dT 20-mer and poly dT 24-mer showed an increase in resolution at a lower mobile phase velocity, however this was not enough to baseline resolve OGNs differing by 5 nucleotides in length (Figure 3.13b).

Although the Advance BioSec has a hydrophilic layer bonded to its silica particles to prevent secondary hydrophobic interactions between analytes and the stationary phase, the results of the analysis of the 16-mer PS variants clearly show evidence of secondary hydrophobic interactions (see Figure 3.14a). This has been noted elsewhere in the literature where Shimoyama *et al.*, added an organic modifier to a mobile phase containing 50 mM NaH<sub>2</sub>PO<sub>4</sub> and 100 mM potassium chloride (KCl) to reduce secondary interactions of OGNs during SEC analysis [269]. Therefore, further optimisation of the mobile phases was performed using alternative salts and organic modifier in an attempt to increase resolution and reduce secondary hydrophobic interactions.

The first alternative mobile phase for comparative analysis was 50 mM NaH<sub>2</sub>PO<sub>4</sub>, 100 mM KCl at pH 7.5 for a separation of the dT 19-24-mer size variants. The retention data was compared to previous analyses and is shown in Figure 3.15a. The comparison showed that OGNs generally eluted in a smaller elution volume in the optimised mobile phase, indicating a reduction in secondary interactions. This is likely a result of the KCl encouraging native state conformation more than that of NaH<sub>2</sub>PO<sub>4</sub> alone, reducing secondary interactions with the stationary phase by conformation induced steric inhibition [330].

To further optimise the mobile phase, 30% v/v MeCN was added in an attempt to further reduce secondary hydrophobic interactions. 30% was the highest volume that could be added before pressure fluctuations caused by adverse changes in salt solubility were observed within the chromatographic system. The addition of organic solvent helps to reduce hydrophobic secondary interactions between bases of the OGNs and the stationary phase [269].

The dT ladder and 16-mer PS variants were analysed using a mobile phase of 50 mM NaH<sub>2</sub>PO<sub>4</sub>, 100 mM KCl, pH 7.5 with 30% MeCN. The separations were performed at 30 °C, isocratically, under a flow rate of 0.2 mL/min to facilitate best resolution. The results are shown in Figure 3.15 b-c and demonstrate that the resolution of the dT ladder was not significantly improved under these conditions.

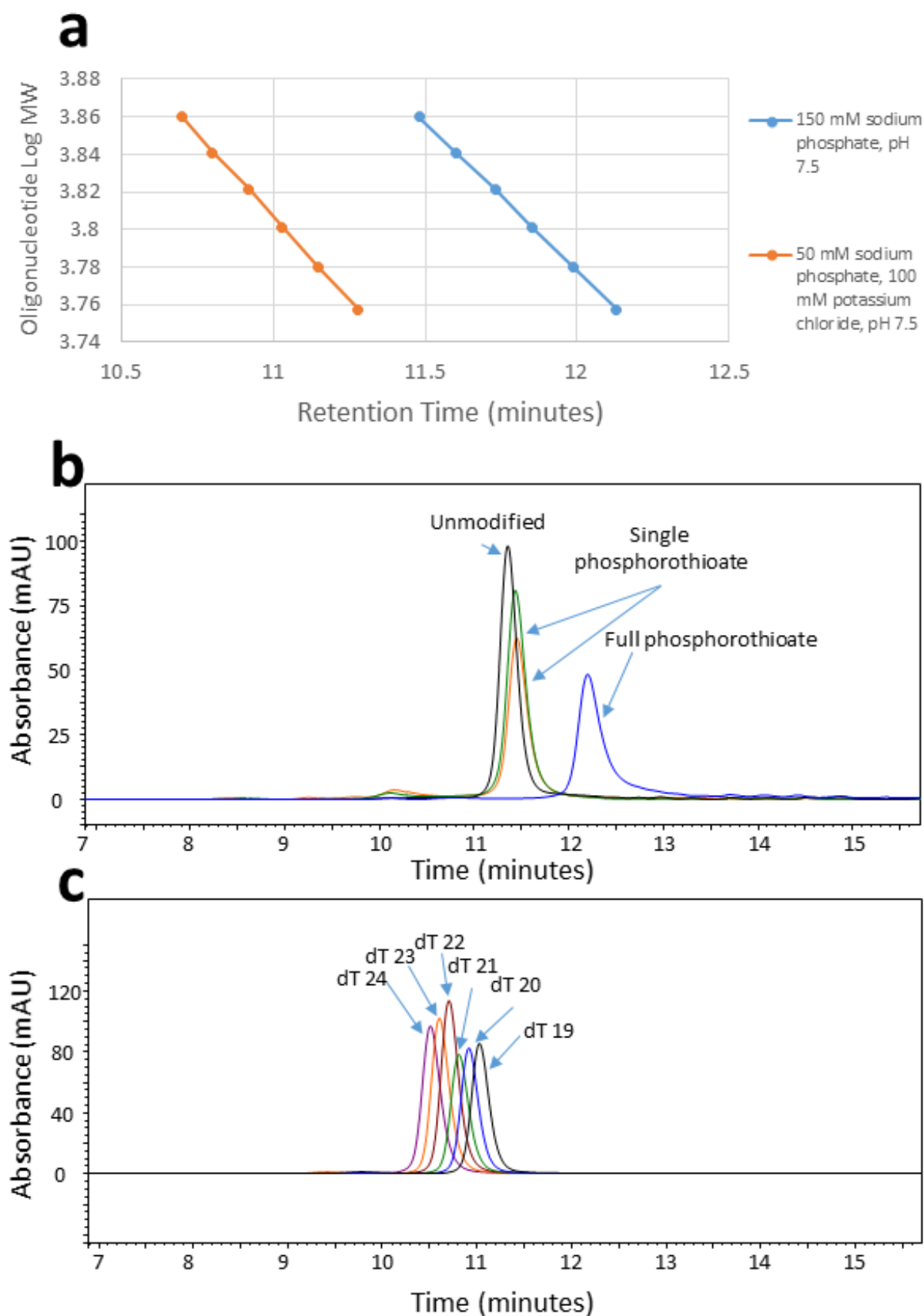


**Figure 3.15: Optimisation of SEC HPLC mobile phase for analysis of OGNs.** 50 picomole samples analysed isocratically on an Advance BioSEC column at 30 °C, 0.2 ml/min. Optimised mobile phase of 50 mM  $\text{NaH}_2\text{PO}_4$ , 100 mM KCl, pH 7.5 with 30%  $v/v$  MeCN. **a:** Scatter plot of oligonucleotide log MW vs retention time for mobile phase comparison. Analyses of dT 19-24-mer size variants were compared between two mobile phase conditions. Orange data series – Mobile phase of 50 mM  $\text{NaH}_2\text{PO}_4$ , 100 mM KCl, pH 7.5. Blue data series – 150 mM  $\text{NaH}_2\text{PO}_4$ , pH 7.5. **b:** 16-mer PS variant analysis. **c:** dT 19-24-mer size variant analysis.

Analysis of the 16-mer PS variants shows that under these mobile phase conditions, later retention of the full PS OGN was still observed (see Figure 3.15b). Comparisons of PWHH of the OGNs in both the absence and presence of MeCN in the mobile phase demonstrated a decrease by 25% with the addition of the organic modifier. In addition, PWHH for the full PS OGN decreased by 33% under these conditions. These results show that secondary interactions can be reduced with optimisation of the mobile phase organic content and salt composition. Resolution between OGN size or PS variants was not significantly increased with a reduction in secondary interactions, as Figure 3.15 b-c demonstrates, this is likely due to suboptimal stationary phase pore size and not the chemical composition of the mobile phase.

### **3.4.2 Summary of work using SEC HPLC for OGN analysis.**

In summary, SEC was performed as an approach to optimise size based OGN separations. Analysis of a range of different model OGNs were analysed to assess both the resolution achieved and degree of size based separation under different conditions. Optimisation of mobile phase composition, organic modifier and flow rate were performed to enhance the efficiency of chromatography by reducing secondary interactions between the OGNs and the stationary phase. The results showed that typically the resolution of OGN separations using SEC is lower compared to other modes of chromatography previously assessed. As expected, size dependent separations dominate in this mode of chromatography. However, the full PS OGN elutes at a different retention volume in comparison to the single PS and unmodified OGNs of the same size, indicating that completely size based separations (independent of chemistry and structure) were not achieved using SEC analysis and some modifications to the mobile phase are necessary to reduce secondary interactions.

### **3.5 Conclusions.**

A wide range of different modes of chromatography were developed and optimised for the analysis of OGNs, including IP-RP, SAX and SEC. Size and sequence based separations were optimised in each mode using a variety of different OGN models, including dT 19-24-mers, 30-mer sequence variants and 16-mer PS variants. The results showed that using IP-RP-LC, sequence based separations were more facile at low temperatures, using the weaker ion-pair reagent (TEAA). Size based separations

were optimised by manipulation of analysis temperature, addition of HFIP as mobile phase additive and the utilisation of a more hydrophobic ion-pair reagent (TBuAA). Within the SAX mode of chromatography, sequence based separations dominated, as demonstrated by the significant difference in retention time between the two 30-mer OGN sequences. However, size based separations were achievable by reducing mobile phase pH, adding organic modifier to the mobile phase and utilisation of a strong eluotropic salt (NaClO<sub>4</sub>). For SEC- based separations, lower resolution separations of the OGNs were observed. Baseline separation of the dT ladder was not achieved using SEC in contrast to IP-RP and SAX HPLC, but size based separations were optimised by reducing the flow rate and changing the mobile phase salt composition. For example, the addition of an organic modifier to the mobile phase helped reduce secondary interactions between the full PS OGN and the stationary phase. However, a difference in retention time between the unmodified and full PS OGN was still observed, demonstrating that SEC separations are not fully size dependent and the influence of the PS chemistry still exists under these conditions (see Figure 3.16 for a graphical conclusion).

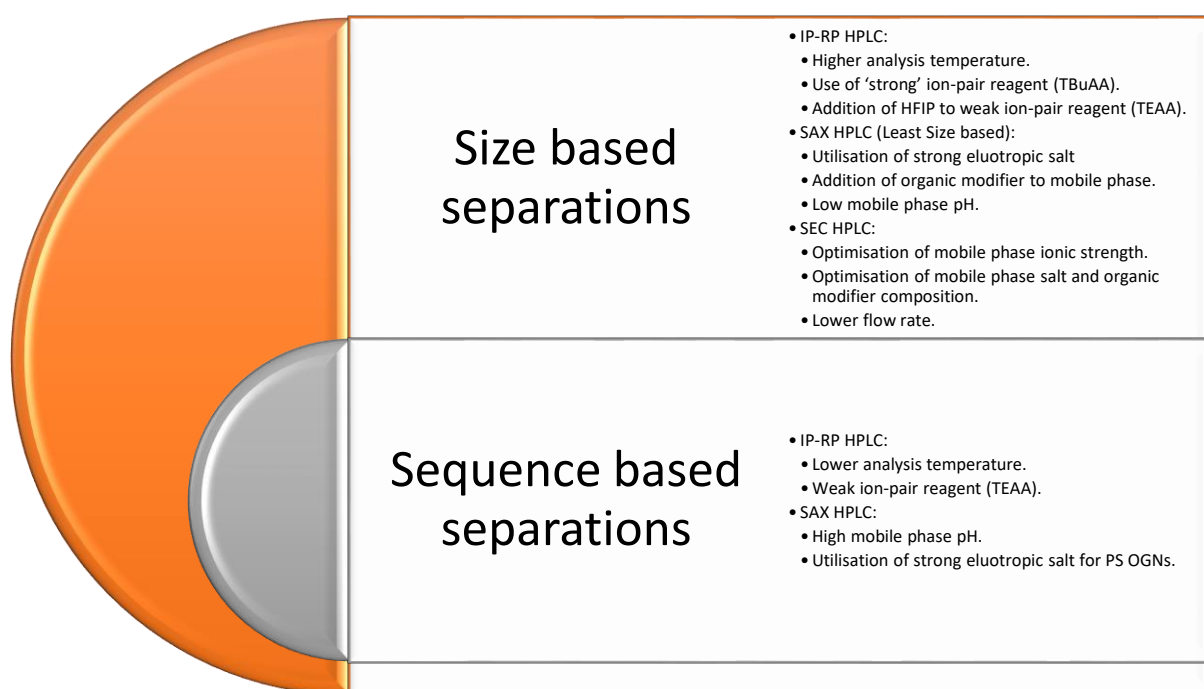


Figure 3.16: Conclusions for size and/or sequence based separations of OGNs using IP-RP, SAX and SEC HPLC.

1D chromatographic optimisations performed in this Chapter (size and sequence dependent separations) will be utilised for future development of two-dimensional workflows. Orthogonal separations aim to separate by size in one dimension and sequence in the second dimension. Analysis of OGNs using the IP-RP, SAX and SEC modes has demonstrated biases in separation mechanisms. However, size and sequence dependence is present in all modes (especially for OGNs with complex chemistry, such as PS OGNs) and 2D-LC for the analysis of OGNs would never be truly orthogonal but in fact pseudo-orthogonal. Therefore, based on the results and optimisations performed, the following potential couplings of modes are proposed (see Table 3.6) and will be investigated in subsequent chapters.

**Table 3.6: Estimations of orthogonal modes of chromatography for analysis of OGNs.**

<b>Size based separation</b>	<b>Sequence based separation</b>
Strong IP-RP HPLC	Weak IP-RP HPLC
Strong IP-RP HPLC	High pH SAX HPLC
Strong IP-RP HPLC	HFIP modified IP-RP HPLC
SEC HPLC	Weak IP-RP HPLC
SEC HPLC	High pH SAX HPLC
SEC HPLC	HFIP modified IP-RP-LC
HFIP modified IP-RP HPLC	Weak IP-RP HPLC
HFIP modified IP-RP HPLC	High pH SAX HPLC

## Chapter 4: Optimisation of two-dimensional Liquid-Chromatography for the analysis of unmodified OGNs.

### Abstract.

The aim of this Chapter was to develop a 2D-LC analytical method for the analysis of unmodified oligonucleotides (OGNs). Initial work focussed on optimising size and sequence dominant separations of size and sequence variant OGNs by using 1D HPLC prior to the optimisation of 2D-LC workflows.

Unmodified OGNs were analysed using previously optimised size and sequence dependent modes of IP-RP and SAX HPLC. Analysis by 1D HPLC aimed to elucidate the retention behaviour of size and sequence variant OGNs. The retention data was used for the analysis of orthogonality of three workflows: (strong IP-RP)-(SAX), (strong IP-RP)-(HFIP modified IP-RP) and (HFIP modified IP-RP)-(SAX) 2D-LC. Two orthogonality metrics were used to understand workflow orthogonality, specifically the bin counting and minimum convex hull methods. Feasibility testing highlighted that the workflow of (strong IP-RP)-(SAX) 2D-LC demonstrated high orthogonality and good chromatographic efficiency. In addition, the mobile phases of each dimension were compatible and maintained retention in the 2<sup>nd</sup> dimension. Further development of the method involved developing a reference mapping strategy to track OGN retention within the 2<sup>nd</sup> dimension of analysis based upon UV detection. This was developed in conjunction with LC-MS to qualitatively validate its robustness.

The 2D-LC method was further developed to enable online 2D-LC analysis of each sample set. Development of an online 2D-LC method for analysis of unmodified OGNs demonstrates the utility of this approach for OGNs and builds a platform for development of 2D-LC methods for the analysis of more complex OGNs, such as phosphorothioates and OGN therapeutics.

## 4.1 Introduction.

In Chapter 3, it was demonstrated that 1D HPLC analysis could be optimised for size and sequence dependent separations of OGNs. IP-RP (using TEAA, TBuAA and TEAA:HFIP), SEC (modified with MeCN) and SAX (using NaClO<sub>4</sub> and NaCl, modified where appropriate with MeCN) chromatographic modes could be used to analyse a range of OGNs, such as size, sequence and chemical modification variants. Analysis temperature, flow rate, elution gradient and mobile phase chemistry were optimised to facilitate increased resolution and efficiency during analysis.

2D-LC orthogonally separates complex mixtures and simplifies the separation space by reducing co-elution events. As all chromatographic conditions optimised for sequence dominance also showed some influence of size basis for the separation, 2D-LC analysis of OGNs would be more pseudo-orthogonal rather than fully orthogonal. Nevertheless, workflows that dominantly separate OGNs by size in one dimension and sequence in the other dimension were designed using knowledge of the separation mechanisms occurring among the different modes of HPLC. Development of 2D-LC for unmodified OGNs can provide a basis of method development strategy for subsequent optimisation of 2D-LC analysis methods for OGN therapeutics (where separation will be further challenged by chemical modification of these analytes). Most new generation OGN therapeutics are chemically modified, therefore formulating a strong understanding of more simplistic molecule behaviour builds a repertoire of knowledge that would contribute to OGN therapeutic 2D-LC workflow optimisation. In addition, a 2D-LC analytical method for unmodified OGNs can be utilised for alternative OGN analytes, such as the analysis of PCR primers, OGN probes or in OGN mapping experiments. As described in Chapter 1, the orthogonality of a 2D-LC method can be evaluated using a range of metrics and can provide a theoretical understanding of which workflow coupling is of best utility (most orthogonal) for further testing via 2D-LC analysis.

It is hypothesized that the evaluation of OGN size or sequence dependent separations in a range of modes will enable the design of a 2D-LC workflow. An online heart-cut 2D-LC method can be experimentally tested after orthogonal separations are evaluated. This Chapter is divided into three parts to describe the approach to method development. Part A introduces the focus on orthogonality analysis, Part B describes how offline 2D-LC can provide information on workflow feasibility and give more control over method development by reference mapping and Part C demonstrates how online 2D-LC is performed as an optimised method.

## Results and Discussion

### Part A

#### 4.2 Analysis of OGN retention behaviour in 1D HPLC.

1D-LC optimisation was performed using model OGNs to understand size and sequence dependent separations in a range of chromatographic modes (Table 4.1 outlines previously optimised conditions from Chapter 3). However, the diversity of size and sequence in model OGNs used in Chapter 3 was generally low. To further demonstrate orthogonal separations based upon size and sequence, more diverse sample sets of unmodified size and sequence OGN variants were utilised for 2D-LC method development. In addition, a 1<sup>st</sup> generation unmodified OGN therapeutic model, and its associated manufacturing impurities, were analysed by 2D-LC to demonstrate the utility of the multidimensional approach for OGN therapeutics and their failure sequences. OGNs used within this study are described in Table 4.2. Initial work focused on analysing the retention behaviour of OGN sample sets under optimised conditions and Figure 4.1 a-d shows the 1D HPLC retention behaviour of the sample sets. The retention data of size and sequence OGN variants were sequentially utilised for orthogonality assessment for three potential 2D-LC workflows.

**Table 4.1: Optimised chromatographic conditions employed for 1D HPLC analysis and sequential retention behaviour assessment of size and sequence variant OGNs.**

<b>Chromatographic Mode</b>	<b>Mobile Phase</b>	<b>Stationary Phase</b>
Weak IP-RP HPLC	100 mM TEAA, 0.1 mM Na <sub>4</sub> EDTA, 0-25% v/v MECN	DNAPac RP
Strong IP-RP HPLC	5 mM TBUAA, 0.1 μM Na <sub>4</sub> EDTA, 10-80% v/v MECN	DNAPac RP
HFIP modified IP-RP HPLC	100 mM TEAA, 40 mM HFIP 0.1 mM Na <sub>4</sub> EDTA, 0-25% v/v MECN	DNAPac RP
SAX-LC	20 mM Tris, 0-400 mM NaClO <sub>4</sub> , pH 11.5, 20% v/v MECN.	DNAPac Pa200 Rs

**Table 4.2: Unmodified OGNs utilised for 2D-LC method development. Size/sequence variant OGNs and 1<sup>st</sup> generation model OGN therapeutic and its associated manufacturing impurities are described by impurity type, size in nucleotide length (nt), OGN sequence and monoisotopic mass. A capital letter denotes a DNA nucleotide.**

Model OGN	Model Type	Sequence	Monoisotopic Mass (Da)
19-mer i	Size & Sequence isomer	CTA GTT ATT GCT CAG CGG T	5806.980
19-mer ii	Size & Sequence isomer	CGC CAT CCA CGC TGT TTT G	5727.963
19-mer iii	Size & Sequence isomer	ATT AGG ACA AGG CTG GTG G	5930.022
19-mer iv	Size & Sequence isomer	AGA GTT TGA TCA TGG CTC A	5840.003
20-mer i	Size & Sequence isomer	GGG ATG TTT AAT ACC ACT AC	6113.054
20-mer ii	Size & Sequence isomer	CCC TCA TAG TTA GCG TAA CG	6074.043
20-mer iii	Size & Sequence isomer	TTG CTG TTG CAC AGT GAT TC	6111.026
20-mer iv	Size & Sequence isomer	GGC AGC AGC CAC AGG TAA GA	6182.086
21-mer i	Size & Sequence isomer	GCC TGA ACA CCA TAT CCA TCC	6292.089
21-mer ii	Size & Sequence isomer	ACC GTA AGT AGC ATC ACC TTC	6347.094
21-mer iii	Size & Sequence isomer	GAC TGG TTC CAA TTG ACA AGC	6427.107
21-mer iv	Size & Sequence isomer	CGT TCG ACC CCG CCT CGA TCC	6276.056
22-mer i	Size & Sequence isomer	CTT TTC GGT TAG AGC GGA TGT G	6809.137
22-mer ii	Size & Sequence isomer	TAC GGT TAC CTT GTT ACG ACT T	6688.123
22-mer iii	Size & Sequence isomer	TGG TCT TGT TAG AAT TTG TTA C	6758.128
22-mer iv	Size & Sequence isomer	TCC GGA TTA TTC ATA CCG TCC C	6618.117
Unmodified FLP (20-mer)	Full length product (1 <sup>st</sup> generation unmodified OGN therapeutic model)	CTC AAA TAT ACT TAC GAT TA	6056.058
Unmodified 5'-1 (19-mer)	Shortmer (associated manufacturing impurity)	TCA AAT ATA CTT ACG ATT A	5767.012
Unmodified 5'-2 (18-mer)	Shortmer (associated manufacturing impurity)	CAA ATA TAC TTA CGA TTA	5462.966
Unmodified 5'-3 (17-mer)	Shortmer (associated manufacturing impurity)	AAA TAT ACT TAC GAT TA	5173.920
Unmodified N+1 (21-mer)	Longmer (associated manufacturing impurity)	CTC AAA TAT ACT TTA CGA TTA	6360.104

In Chapter 3, model OGNs demonstrated both size and sequence dependent separations in a range of modes, with SAX-LC achieving highly sequence dominant separations and strong IP-RP-LC achieving highly size dominant separations. Although, under IP-RP conditions, sized based OGN separation could be manipulated with the use of a more hydrophobic (strong) IPR or the addition of HFIP to the mobile phase to encourage dynamic ion exchange processes.

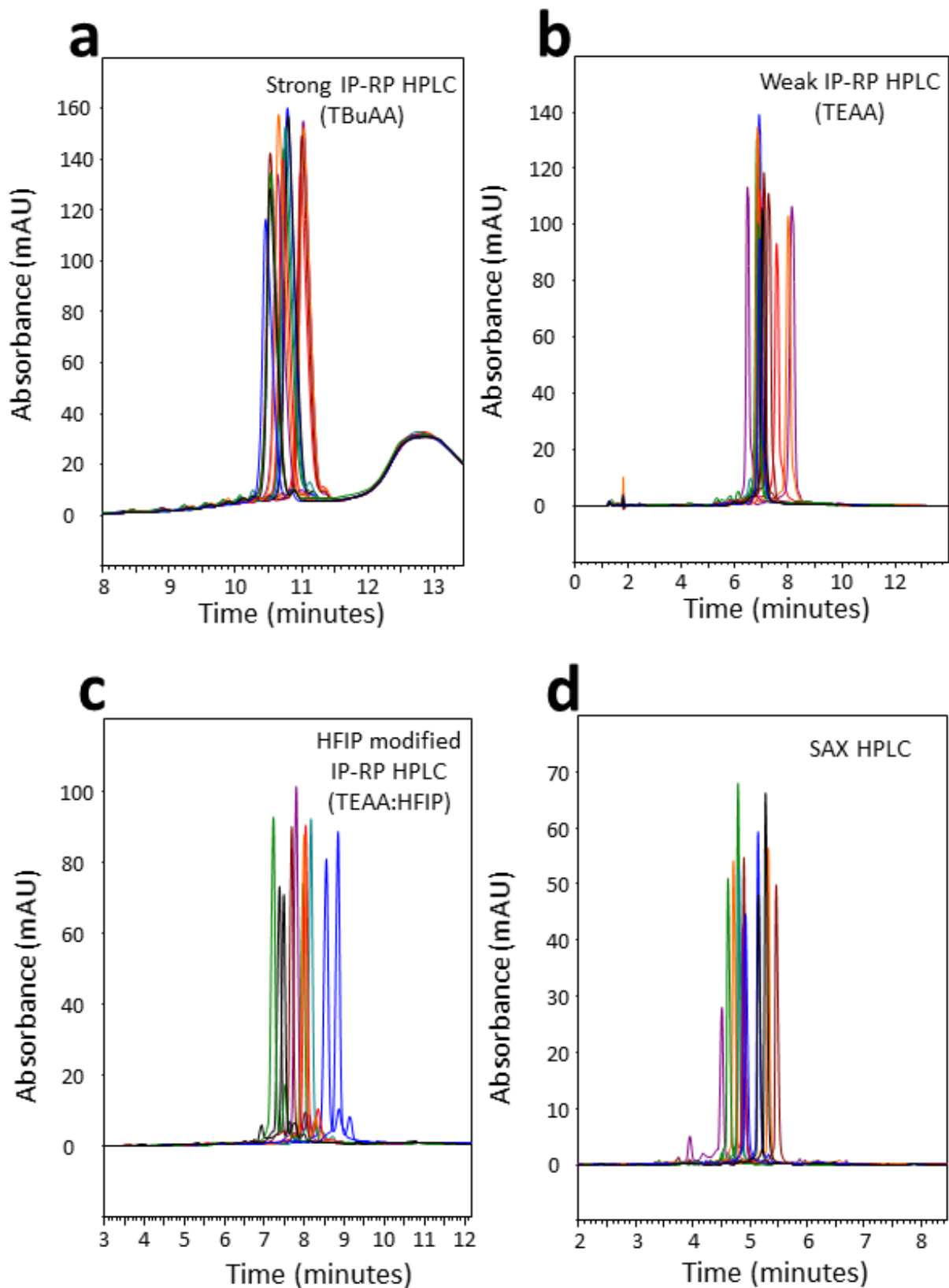


**Figure 4.1: Analysis of retention behaviour of 19-22-mer size and sequence variants analysed using SAX and IP-RP HPLC.**  
**a:** Strong IP-RP HPLC using 5 mM TBUAA, 0.1  $\mu$ M  $\text{Na}_4$  EDTA and 27.5-73%  $\text{v/v}$  MeCN gradient from 1-15 min. 50 picomole samples analysed at 0.2 ml/min at 60  $^\circ\text{C}$  using a DNAPac RP column. **b:** Weak IP-RP HPLC using 100 mM TEAA, 0.1 mM  $\text{Na}_4$  EDTA and 8.75-12.5%  $\text{v/v}$  MeCN gradient from 1-15 min. 50 picomole samples analysed at 0.2 ml/min at 30  $^\circ\text{C}$  using a DNAPac RP column. **c:** HFIP modified IP-RP HPLC using 100 mM TEAA, 40 mM HFIP, 0.1 mM  $\text{Na}_4$  EDTA and 8.75-17.5%  $\text{v/v}$  MeCN gradient from 1-15 min. 30 picomole samples analysed at 0.2 ml/min at 70  $^\circ\text{C}$  using a DNAPac RP column. **d:** SAX HPLC using 20 mM Tris, 80-160 mM  $\text{NaClO}_4$  from 0-7.7 minutes. 50 picomole samples analysed at 0.8 ml/min at 30  $^\circ\text{C}$  using a DNAPac Pa200 Rs column.

The results of Figure 4.1 show that separation of unmodified OGNs across the range of optimised chromatographic conditions resulted in retention behaviours consistent with data obtained in Chapter 3. Generally, smaller OGNs eluted first among the range of analytical conditions of Figure 4.1 a-d, reflecting that there is a size basis to all separations. Sequence based separations were enabled by enhanced secondary interactions between the OGN bases and the stationary phases used [169, 189].

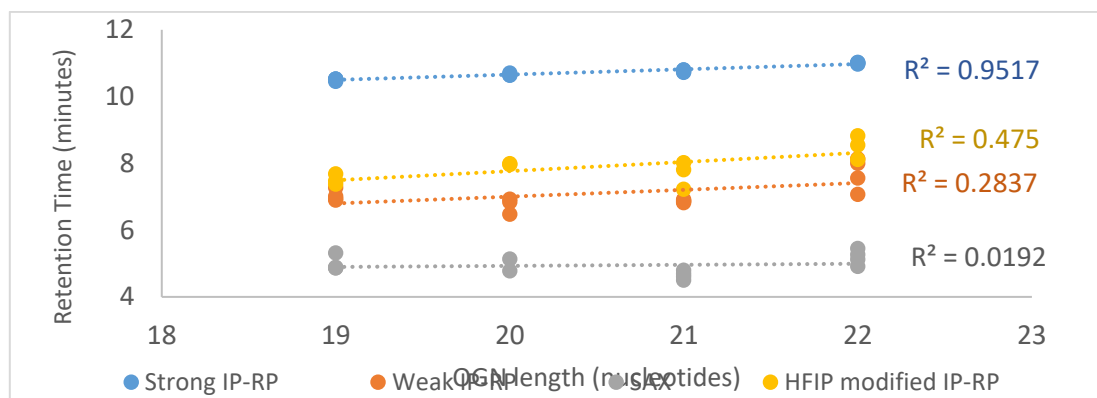


**Figure 4.2: Comparison of OGN size versus retention time using strong IP-RP (TBuAA), weak IP-RP (TEAA), SAX ( $\text{NaClO}_4/\text{MeCN}$  and HFIP modified IP-RP (TEAA:HFIP) HPLC conditions.**

To further understand size or sequence dependence under the range of chromatographic conditions, the correlation between OGN retention (in minutes) and size (in nucleotides) was compared (see Figure 4.2). The results show that size-based separation is dominant in strong IP-RP mode (in conjunction with TBuAA) at 60°C, consistent with high linear regression between OGN size of the OGNs and retention time ( $R^2 = 0.952$ ). Under these conditions, secondary interactions are reduced to minimise sequence based separations, however this is not completely ablated (as there would be 4 peaks where OGNs co-elute by size in Figure 4.1a). The correlation decreases when analysing weak IP-RP (using TEAA) data ( $R^2 = 0.284$ ), indicating that a size based separation was not as predominant for IP-RP HPLC employing TEAA (see Figure 4.1b and Figure 4.2). However, this may be adjusted by adding HFIP to the mobile phase, which as the data shows, results in a shift in separation back towards size dominance and a slightly higher linear regression of 0.475 (see Figure 4.2). The separation under HFIP modified IP-RP conditions also showed that the addition of HFIP to the mobile phase improved the peak shape (and potentially resolution of closely eluting analytes) of the OGNs as peak shouldering was visibly reduced under these conditions (Figure 4.1c). Analysis of OGNs using

SAX HPLC (shown in Figure 4.1d) demonstrated the highest dependency on sequence based separations as can be determined from a linear regression value of 0.019 (see Figure 4.2).

Using peak width at half height (PWHH) as a general measure of efficiency (as smaller PWHH leads to higher efficiency), weak IP-RP HPLC demonstrated sequence based separation, but with the highest PWHH of 0.16 minutes and therefore the poorest efficiency. In comparison, Figure 4.1d shows that SAX HPLC analysis improves PWHH by 267% to (0.06 minutes). Comparatively, for IP-RP HPLC, addition of a low concentration of HFIP to the weak IP-RP mobile phase, as shown in Figure 4.1c, reduced PWHH to 0.11 minutes.

### 4.3 Orthogonality assessments of 2D-LC workflows for analysis of OGNs.

As described in Chapter 1, many attempts have been made to statistically and geometrically analyse orthogonality within 2D-LC separations [297]. An orthogonality measurement must be a defined metric between 0-1 or 0-100 % to convey a property of coverage of the separation space.

Orthogonal separations of unmodified size and sequence variants highlight the applicability of 2D-LC analysis to other types of nucleic acid of similar chemistry, such as PCR primer separations, DNA/RNA probe analysis or RNase mapping experiments where complex mixtures of OGNs are present and will benefit from 2D-LC analysis. The bin counting method outlined by Gilar *et al.*, [302] was utilised for OGN 2D-LC orthogonality assessments as normalisation of the retention data negated the void separation space of heart-cut 2D-LC. Retention times of the size and sequence variant OGN 1D separations were normalised to facilitate comparison between modes in a 2D separation space bin scatter plot. Gilar *et al.*, demonstrated the methodology of negating unused separation space by retention time normalisation, see equation 2.8.

Equation 2.8

$$Rt_i (norm) = \frac{Rt_i - Rt_{min}}{Rt_{max} - Rt_{min}} \quad [302]$$

Where  $Rt_{max}$  and  $Rt_{min}$  represent the retention times of the first and last eluting OGNs respectively. The retention time of OGNs ( $Rt_i$ ) are converted to normalised retention values ( $Rt_{norm}$ ) in the range of 0-1. See Table 4.3 for normalised retention values of the OGN variants across the 4 modalities of chromatography.

**Table 4.3: Normalised retention values for 1D HPLC analyses of size and sequence variants in a range of chromatographic modes.**

Size/sequence variant	Chromatographic mode			
	Strong IP-RP HPLC	Weak IP-RP HPLC	SAX HPLC	HFIP modified IP-RP HPLC
	<i>Normalised Retention</i>			
19-mer i	0.13	0.33	0.40	0.16
19-mer ii	0.00	0.28	0.39	-
19-mer iii	0.13	0.25	0.41	0.09
19-mer iv	0.13	0.48	0.86	0.29
20-mer i	0.34	0.22	0.29	0.46
20-mer ii	0.32	0.00	-	-
20-mer iii	0.45	0.27	0.67	0.48
21-mer i	0.52	0.24	0.00	-
21-mer ii	0.61	0.23	0.12	0.50
21-mer iii	0.59	0.27	0.32	0.36
21-mer iv	0.48	0.21	0.21	0.00
22-mer i	0.96	0.36	1.00	0.56
22-mer ii	1.00	0.92	0.66	-
22-mer iii	1.00	1.00	0.81	1.00
22-mer iv	0.93	0.65	0.44	0.83

To assess orthogonality using the bin counting method, the number of analytes acts as peak capacity maximum within a normalised 2D-LC retention space ( $P_{max}$ ). The separation space is equally divided into bins that span the chromatographic separation equal in number to the amount of separated components. Within elution order analyses, the amount of separated variants ranged from 11 to 15. For an equally spaced separation space, the assumption of maximal peak capacity was made to be 16 for a 4 x 4 geometric separation space. This was done under the assumption that 1-5 more analytes within the range would be chemically similar and occupy a retention time within the 4\*4 separation space. The first, size based dimension of strong IP-RP HPLC represented the y axis, with the second, sequence based separation representing the x axis.

Once plotted, the bins with occupant data points of retention values across the separation space were counted. Using simulations of an unbound space, 63% of area coverage represents orthogonal separations while 10% coverage indicates no orthogonality [289]. Using this information, Gilar *et al.*, proposed an orthogonality assessment equation outlined in equation 2.9.

Equation 2.9

$$\text{Orthogonality (\%)} = \frac{\sum \text{bins} - \sqrt{P_{\text{max}}}}{0.63 * P_{\text{max}}} * 100$$

Where  $\sum \text{bins}$  is the amount of bins occupied by a data points and  $P_{\text{max}}$  is the peak capacity as a reflection of number of analytes. Using this equation, the orthogonality of the three workflows were calculated, as shown in Table 4.4. The results from orthogonality assessments show larger dispersion across the chromatographic space within the workflow (strong IP-RP)-(SAX 2D-LC) compared to (strong IP-RP)-(weak IP-RP) or (strong IP-RP)-(HFIP modified IP-RP) workflows. As assumptions were made for maximal peak capacity, a second metric of orthogonality was calculated. To further evaluate orthogonality, the x and y values of retention values were used to calculate the Rutan method of minimum convex hull area [300]. This method analyses the degree of spread within the separation space by the area of separation space coverage. This was done with a shoelace algorithm in Python software and gave a result between 0 and 1, which was converted to % (shown in Table 4.4). Figures 4.3 a-c show plots of normalised separation spaces for (strong IP-RP)-(weak IP-RP), (strong IP-RP)-(SAX) and (strong IP-RP)-(HFIP modified IP-RP) 2D-LC workflows. The counted bins with occupant data points (used for the bin counting method) are highlighted and the minimum convex hull is also outlined.

In summary, the results from the orthogonality assessment of 1D HPLC data (see Figure 4.3) demonstrated that two workflows are potential analytical strategies for the 2D-LC analysis of OGNs: (strong IP-RP)-(weak IP-RP) and (strong IP-RP)-(SAX). Mathematically, their orthogonality within a 2D-LC workflow was determined as 40-60% and 51-66% using the geometric bin counting method [302] and the minimum convex hull method [300] respectively. As described in Chapter 1, orthogonality values would, in theory, remain constant if analytical dimensions were reversed. However, for retention order predictability, size based separation was targeted for the first dimension separation of 2D-LC. Therefore, OGNs of the same size that co-elute in the 1<sup>st</sup> dimension could be orthogonally separated by sequence in the 2<sup>nd</sup> dimension of analysis.

**Table 4.4: Orthogonality of each 2D-LC workflow analysed using the bin counting method and the minimum convex hull method.**

2D-LC workflow	$\sum \text{bins occupied}$	Orthogonality (bin counting method) (%)	Orthogonality (minimum convex hull method) (%)
(strong IP-RP)-(weak IP-RP)	8	40	51
(strong IP-RP)-(SAX)	10	60	66
(strong IP-RP)-(HFIP modified IP-RP)	7	30	38

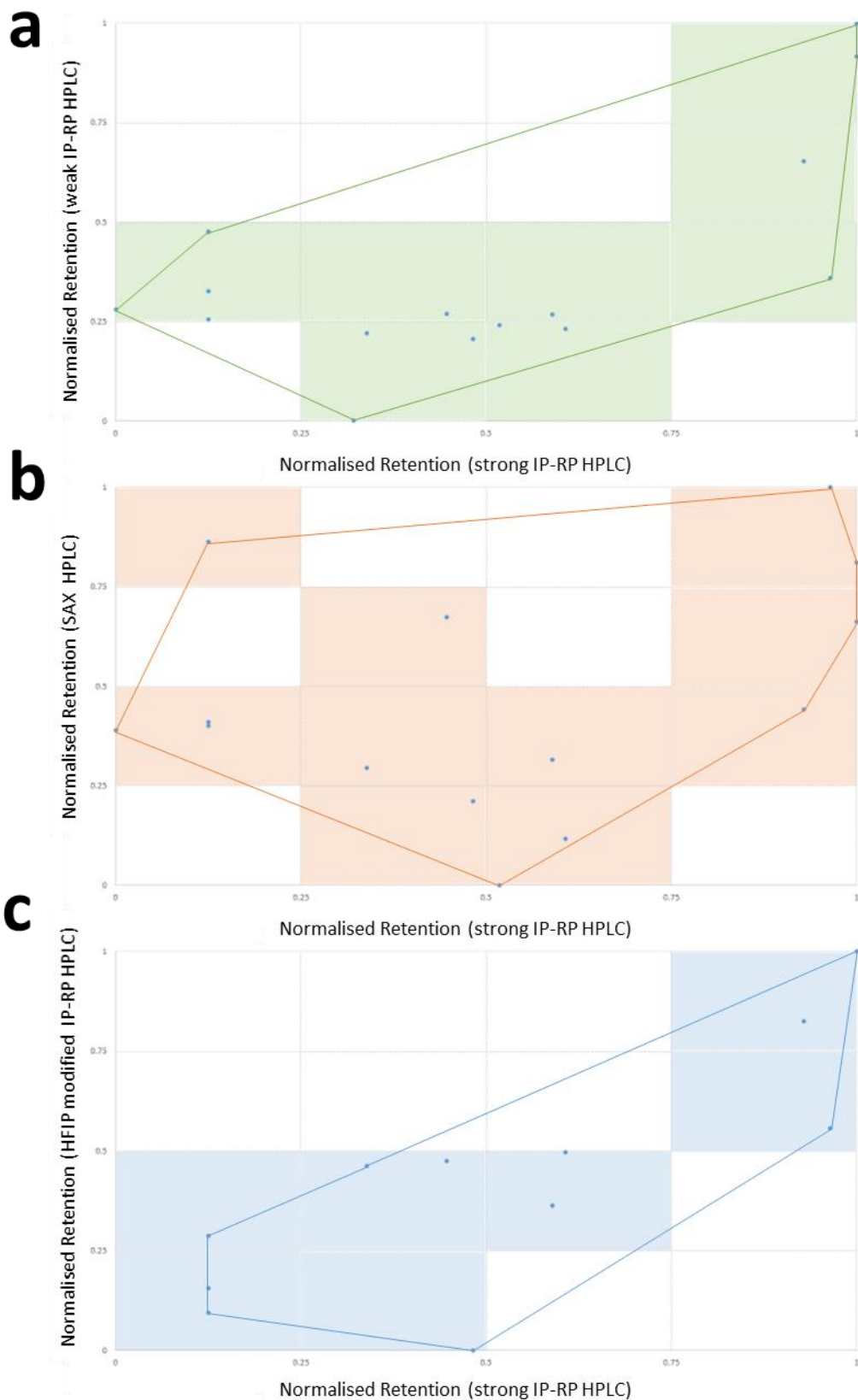


**Figure 4.3: 2D-LC scatter plots of normalised retention times for 2D-LC workflows.** Shaded bins are those occupied by OGN retention values and red lines indicate borders of the minimum convex hull area. **a:** (strong IP-RP)-(weak IP-RP) 2D-LC workflow. <sup>1</sup>D- HPLC conditions outlined in Figure 4.1a. <sup>2</sup>D- HPLC conditions outlined in Figure 4.1b. **b:** (strong IP-RP)-(SAX) 2D-LC workflow. <sup>1</sup>D- HPLC conditions outlined in Figure 4.1a <sup>2</sup>D- HPLC conditions outlined in Figure 4.1d. **c:** (strong IP-RP)-(HFIP modified IP-RP) 2D-LC workflow. <sup>1</sup>D- HPLC conditions outlined in Figure 4.1a. <sup>2</sup>D- HPLC conditions outlined in Figure 4.1c.

## **Part B**

### **4.4 Mobile phase compatibility using 2D-LC for the analysis of OGNs.**

Orthogonality assessment of 1D HPLC data resulted in the identification of two workflows as potential analytical strategies for the 2D-LC analysis of unmodified OGNs: (strong IP-RP)-(weak IP-RP) and (strong IP-RP)-(SAX). Further studies were performed to ensure that the mobile phases were compatible and maintained retention between the 1<sup>st</sup> and 2<sup>nd</sup> dimensions of a 2D-LC method.

Within the strong IP-RP HPLC 1<sup>st</sup> dimension analysis, OGNs elute within a mobile phase organic modifier content of 45-52% v/v MeCN. This could potentially hinder retention in further dimensions also using organic modifier as eluting reagent (making the mode non-retentive), such as weak or HFIP modified IP-RP. In addition, the organic modifier eluent may not be miscible with the 2<sup>nd</sup> dimension mobile phase. Solvent incompatibilities are a significant problem in 2D-LC due to miscibility issues and analyte non-retention caused by strong eluting power of the 1<sup>st</sup> dimension eluent [291]. Therefore, to experimentally validate the orthogonality in two workflows of 2D-LC, the first aim was to analyse the mobile phase compatibility of the proposed 2D-LC workflows to ensure there was minimal/no effect on retention or mobile phase compatibility in the 2<sup>nd</sup> dimension.

#### **4.4.1 Analysis of OGNs using (strong IP-RP)-(weak IP-RP) 2D-LC.**

To perform offline 2D-LC analysis, a Thermo Scientific U3000 HPLC with fractionation valve was utilised (see Chapter 2, section 2.2.1). To analyse the compatibility of (strong IP-RP)-(weak IP-RP) 2D-LC, a 1650 picomole sample of an equimolar mixture of the size and sequence variant OGNs (see Table 4.2) was analysed. Offline Strong IP-RP HPLC was performed using 5 mM TBuAA, 0.1 μM Na<sub>4</sub> EDTA and 10-80% v/v MeCN, on a DNAPac RP column (2.1\*100 mm) as 1<sup>st</sup> dimension separation. The 1<sup>st</sup> dimension column was overloaded to avoid sample loss through dilution in the 2<sup>nd</sup> dimension [292] although this was to the detriment of resolution in the 1<sup>st</sup> dimension. Six 100 μL fractions were collected between 8.5-11.5 minutes retention time to capture the size and sequence variant OGNs during strong IP-RP HPLC 1<sup>st</sup> dimension. Fractions were re-analysed in the 1<sup>st</sup> dimension to

experimentally test fractionation efficiency (See Chapter 2 and Appendix 2, Figure A2.3 and Table A2.1), which was determined to be approximately 80%.

The 1<sup>st</sup> dimension fractions were re-analysed offline using weak IP-RP HPLC as the 2<sup>nd</sup> dimension. Weak IP-RP HPLC was performed with 100 mM TEAA, 0.1 mM Na<sub>4</sub> EDTA and 0-25% v/v MeCN on a DNAPac RP column (2.1\*100 mm). Figure 4.4a shows the offline 2D-LC analysis of the 19-22-mer size and sequence variant mixture from strong IP-RP HPLC to weak IP-RP HPLC. OGNs were retained on the stationary phase of the 2<sup>nd</sup> dimension of analysis, despite eluting at approximately 50% v/v MeCN within the mobile phase of the 1<sup>st</sup> dimension. The low organic starting conditions of the 2<sup>nd</sup> dimension may have a dispersive effect upon the MeCN in the sample plug due to the creation of a concentration gradient, which facilitated analyte retention.

#### **4.4.2 Analysis of OGNs using (strong IP-RP)-(SAX) 2D-LC.**

Similar to the study in section 4.4.1, offline 2D-LC using a workflow of (strong IP-RP)-(SAX) was also performed to analyse mobile phase compatibility. A 500 picomole sample of 19-24-mer size and sequence variants, at equimolar concentration was analysed using strong IP-RP HPLC conditions. Six 100 µL fractions were collected between 14.5-17.5 minutes retention time to capture the size and sequence variants during separation and then the fraction were re-analysed in a 2<sup>nd</sup> dimension of SAX HPLC (see Figure 4.4b). Fractions collected within the 1<sup>st</sup> dimension analysis of Figure 4.4b were re-analysed offline using SAX HPLC as the 2<sup>nd</sup> dimension. SAX HPLC was performed with 20 mM Tris, 0-400 mM NaClO<sub>4</sub>, pH 11.5 with 20% v/v MeCN, on a DNAPac PA200 Rs column. The results show that the organic modifier within the 1<sup>st</sup> dimension eluent does not affect retention in the 2<sup>nd</sup> dimension as retained peaks were observed in 2<sup>nd</sup> dimension analysis. In addition, the injection peak area does not vary between blank and fraction sample showing that OGNs were retained.

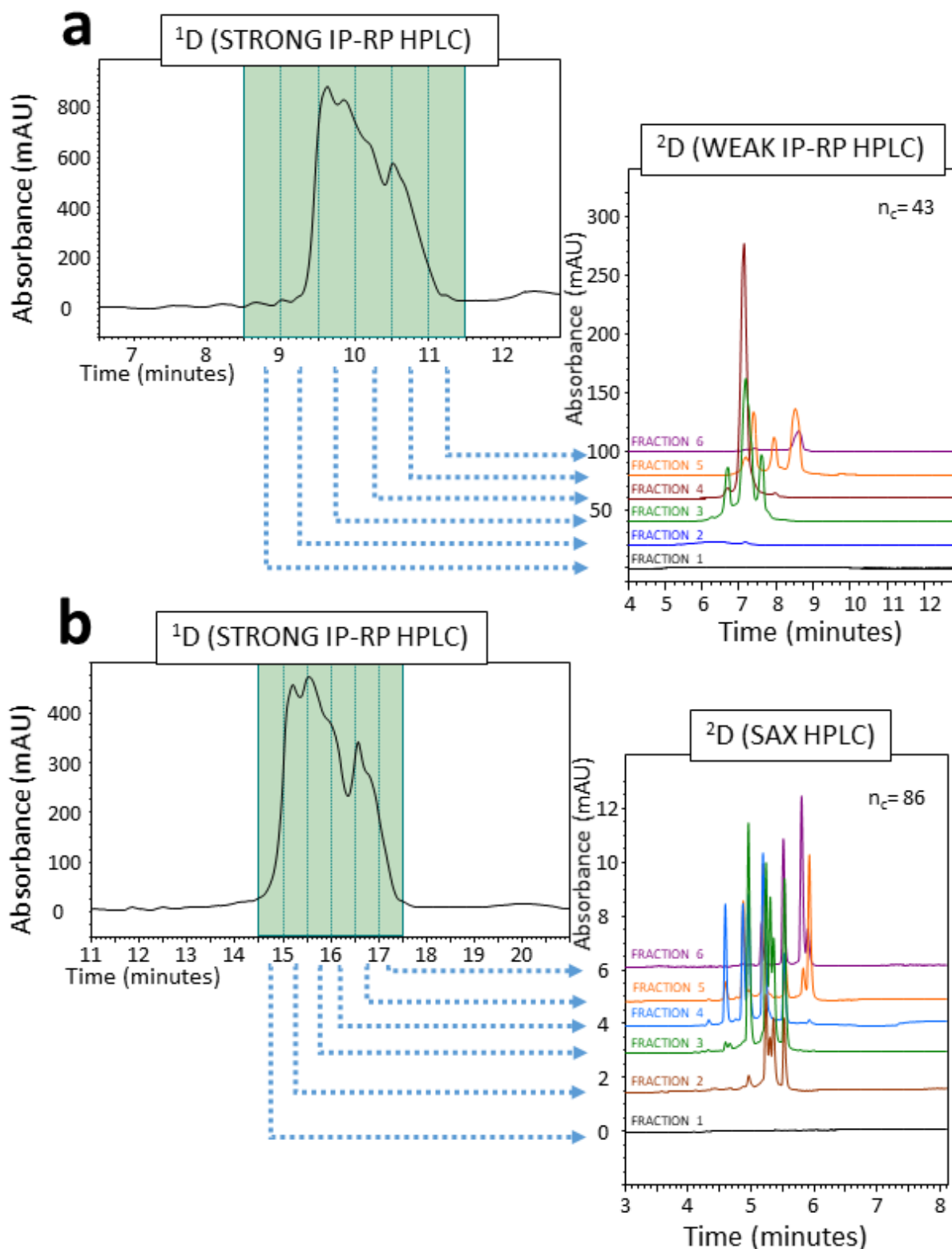


**Figure 4.4: Offline 2D-LC feasibility analysis of OGNs using strong IP-RP HPLC to weak IP-RP or SAX HPLC.** Peak capacity ( $n_c$ ) was calculated for the 2D. **a:** 1650 picomole sample of 19-22-mer size and sequence variant OGN mixture. Separated using strong IP-RP HPLC under a gradient of 5 mM TBuAA, 0.1  $\mu$ M Na<sub>4</sub> EDTA and 27.5-73% v/v MeCN from 1-15 min. Analysis at 0.2 ml/min, 60 °C using a DNAPac RP column. 10 $\mu$ l of each fraction was reanalysed in weak IP-RP 2<sup>nd</sup> dimension using 100 mM TEAA, 0.1 mM Na<sub>4</sub> EDTA and 8.75-12.5% v/v MeCN gradient from 1-15 min. Analysis at 0.2 ml/min, 30 °C on a DNAPac RP column. **b:** 500 picomole sample of 19-22 mer size and sequence variant OGN mixture. First dimension separation using strong IP-RP HPLC using 5 mM TBuAA, 0.1  $\mu$ M Na<sub>4</sub> EDTA and 34.5-59% v/v MeCN from 1-15 min. Analysis at 0.2 ml/min, 50 °C using a DNAPac RP column. 10 $\mu$ l of each fraction reanalysed using SAX HPLC- 20 mM Tris, 80-160 mM NaClO<sub>4</sub> between 0-7.7 minutes and 160-320 mM NaClO<sub>4</sub> between 7.8-10.1 minutes pH 11.5 and 20% v/v MeCN. Analysis at 0.8 ml/min, 30 °C using a DNAPac PA200 Rs column.

#### **4.4.3 Analysis of peak capacity in 2D-LC analysis of OGNs.**

Normalised retention time values were calculated from 1D HPLC retention data in a range of chromatographic conditions (Part A). From these values, orthogonality was analysed by two methods, which suggested that a (strong IP-RP)-(SAX) 2D-LC workflow was most orthogonal for OGNs. High orthogonality is a good predictor for 2D-LC workflow design, however does not take into account chromatographic performance. One measure of analysing performance is the calculation of peak capacity to demonstrate the ability to resolve closely related structures, such as the size and sequence variant OGNs described in Table 4.2.

Under weak IP-RP conditions for 2<sup>nd</sup> dimension analysis, peak capacity was 43. In comparison to this value, utilisation of a SAX 2<sup>nd</sup> dimension increased peak capacity to 86. Although peak identities within this separation could not be characterised to demonstrate changes in OGN selectivity over the workflow, higher peak capacity demonstrates a higher ability to resolve OGNs separating within the 2<sup>nd</sup> dimension (and thus enable their characterisation using retention time alignment with references or mass spectrometry analysis).

#### **4.5 Optimisation of offline 2D-LC and a reference mapping strategy for 2D-LC method development.**

The results of 2D-LC orthogonality assessment and feasibility analysis indicated that (strong IP-RP)-(SAX) 2D-LC is the most appropriate workflow for the separation of OGNs due to its high orthogonality score and 2<sup>nd</sup> dimension peak capacity, see section 4.2-4.4. The offline 2D-LC workflow was used to separate mixtures of OGNs in conjunction with the development of a mapping strategy to identify OGN retention in the 2<sup>nd</sup> dimension. Mass spectrometry analysis was utilised to validate the reference mapping of OGNs within the workflow, this was performed with analytes of the 1<sup>st</sup> dimension of separation, because this mode (strong IP-RP HPLC in conjunction with TBuAA) was compatible with mass spectrometry. The salt utilised for the 2<sup>nd</sup> dimension SAX HPLC analysis is not suitable for LC-MS analysis due to high levels of adductation with the analytes [181].

Three OGN model sets were analysed within this work: two sample sets of equimolar size and sequence variants and a 1<sup>st</sup> generation OGN therapeutic model with its associated manufacturing impurities added at 1.5% total concentration were analysed (see Tables 4.5-4.7). The manufacturing

impurities of the 1<sup>st</sup> generation OGN therapeutic model set were added to a 1.5% total concentration to mimic low impurity levels seen after purification of the full length product of solid phase synthesis and ensure all impurities were present in the representative sample.

**Table 4.5: OGNs used for Test set 1 (size and sequence variant OGNs).**

Size/Sequence variant	Sequence	Monoisotopic Mass (Da)
<b>Test Set 1</b>		
19-mer i	CTAGTTATTGCTCAGCGGT	5806.980
19-mer iii	ATTAGGACAAGGCTGGTGG	5930.022
20-mer i	GGGATGTTTAATACCACTAC	6113.054
21-mer iv	CGTTCGACCCCGCTCGATCC	6276.056
22-mer ii	TACGGTTACCTTGTACGACTT	6688.123
22-mer iv	TCCGGATTATTCATACCGTCCC	6618.117

**Table 4.6: OGNs used for Test set 2 (size and sequence variant OGNs).**

Size/Sequence variant	Sequence	Monoisotopic Mass (Da)
<b>Test Set 2</b>		
19-mer iv	AGAGTTTGATCATGGCTCA	5840.003
20-mer iii	TTGCTGTTGCACAGTGATTC	6111.026
20-mer iv	GGCAGCAGCCACAGGTAAGA	6182.086
21-mer ii	ACCGTAAGTAGCATCACCTTC	6347.094
21-mer iii	GACTGGTTCCAATTGACAAGC	6427.107
22-mer i	CTTTTCGGTTAGAGCGGATGTG	6809.137

**Table 4.7: OGNs used for first generation OGN therapeutic model set (with manufacturing N-x/N+1 impurities).**

Size/Sequence variant	Sequence	Monoisotopic Mass (Da)
<b>1<sup>st</sup> generation OGN therapeutic model set</b>		
20-mer FLP	CTCAAATATACTTACGATTA	6056.058
19-mer 5'-1	TCAAATATACTTACGATTA	5767.012
18-mer 5'-2	CAAATATACTTACGATTA	5462.966
17-mer 5'-3	AAATATACTTACGATTA	5173.920
21-mer N+1	CTCAAATATACTTTACGATTA	6360.104

#### 4.5.1 Offline 2D-LC of OGN test sets in conjunction with reference mapping and mass spectrometry validation.

Offline 2D-LC analysis was performed using 1000 picomole OGN samples. Within the 1<sup>st</sup> dimension using strong IP-RP HPLC (5 mM TBuAA, 0.1  $\mu$ M Na<sub>4</sub> EDTA and 10-80% v/v MeCN) replicate OGN analyses were collected into six or seven 100  $\mu$ L fractions. 20  $\mu$ L of each fraction was analysed in a 2<sup>nd</sup> dimension using a SAX mobile phase of 20 mM Tris, 0-400 mM NaClO<sub>4</sub>, pH 11.5 with 20% v/v MeCN. Alongside analysis of the 1<sup>st</sup> dimension fractions, concurrent reference OGN analyses were performed, aiming to identify and map OGN retention in the 2<sup>nd</sup> dimension. Reference standards were prepared in a diluent of 5 mM TBuAA, 0.1  $\mu$ M Na<sub>4</sub> EDTA and 45% v/v MeCN to avoid discrepancies in diluent between fractions and references (10-80 picomole reference OGN samples were analysed).

Offline 2D-LC analysis of test set 1 and 2 and the 1<sup>st</sup> generation OGN therapeutic model sets are shown in Figures 4.5, 4.7 and 4.8. Superimposing the reference standards onto the 2<sup>nd</sup> dimension chromatogram enables alignment of retention times for mapping. Mapping analytes within fractions highlights that size dependent separation mechanisms occur within the 1<sup>st</sup> dimension, with smallest analytes occupying the initial fractions and largest occupying the latter fractions. Retention is sequence selective in the 2<sup>nd</sup> dimension as larger OGNs are shown to elute before smaller OGNs within the SAX separation.

Analysis of the size and sequence variant test sets by 2D-LC is shown in Figure 4.5 and 4.7a. The results show that resolution is low in the 1<sup>st</sup> dimension due to oversaturation of the stationary phase. However, this enables sensitivity in the 2<sup>nd</sup> dimension for reference mapping. Analysis of the 1<sup>st</sup> dimension fractions within the SAX 2<sup>nd</sup> dimension shows that the OGNs map to reference standards, with the exception of reference standard 20-mer i of test set 1. A proposed reason for the retention time discrepancy between 20-mer i reference standard and the OGN within test set 1, (eluting within fractions 2 and 3) is insufficient temperature equilibration of the stationary phase, despite duplicate blank pre-analyses being performed. Reference standard OGNs and test set OGNs were successfully mapped to each other based on their retention times.

The 1<sup>st</sup> generation OGN therapeutic and associated manufacturing impurities was also analysed by offline (strong IP-RP)-(SAX) 2D-LC (shown in Figure 4.8a). The results show that in the 1<sup>st</sup> dimension of separation, the N-x impurities co-elute under the main peak of the FLP OGN. However, using SAX separation in the 2<sup>nd</sup> dimension the impurities were shown to begin to resolve within fraction 3.

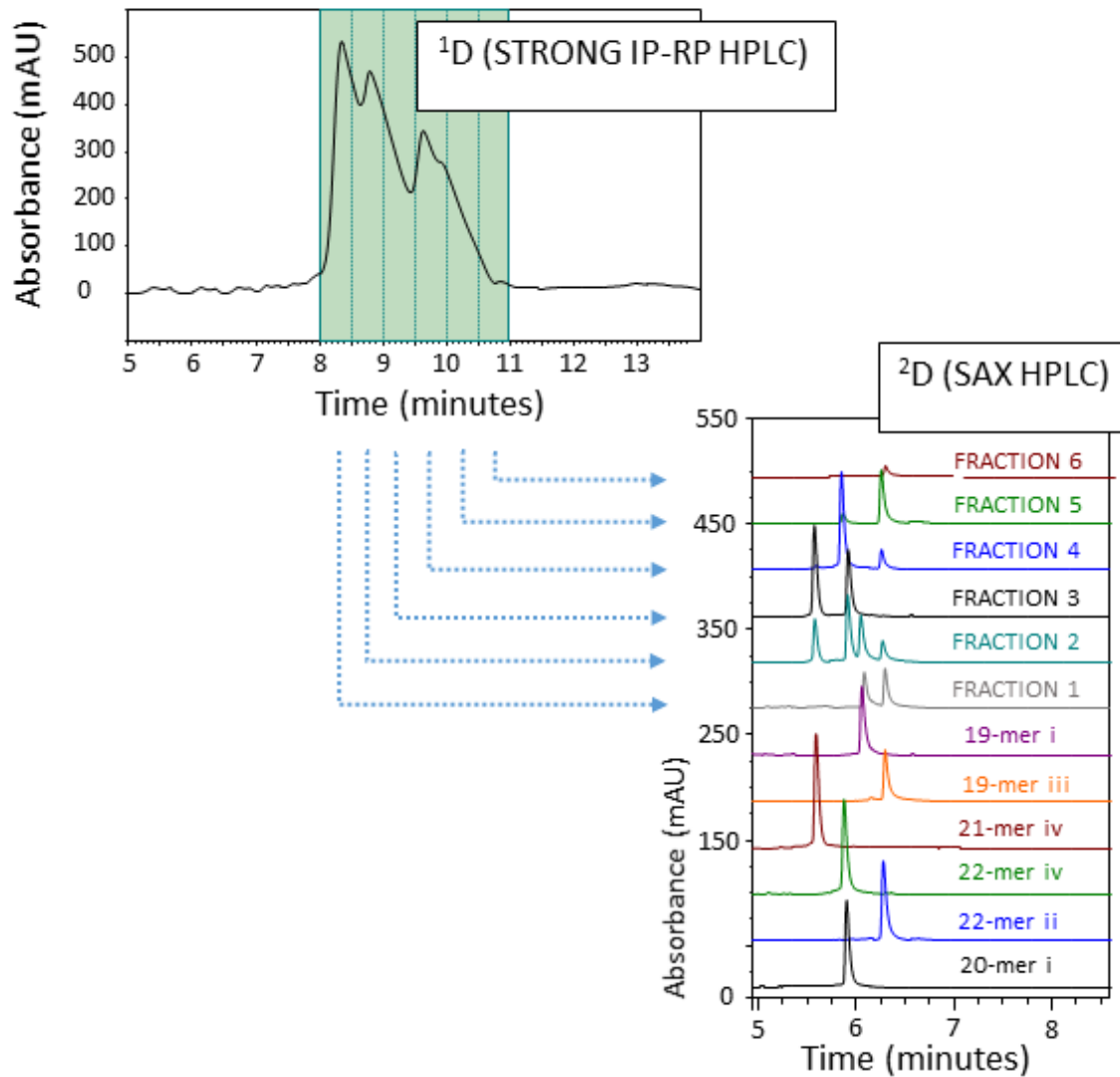


**Figure 4.5: Offline 2D-LC using strong IP-RP to SAX HPLC to analyse test set 1.** 1000 picomole sample of 19-22-mer size and sequence variant OGN mixture a: 1<sup>st</sup> dimension strong IP-RP under 5 mM TBuAA, 0.1  $\mu$ M Na<sub>4</sub>EDTA and 34.5-59% v/v MeCN gradient from 1-15 min. Analysis at 0.2 ml/min, 50 °C using a DNAPac RP column. 20  $\mu$ l of each fraction was reanalysed in a 2<sup>nd</sup> dimension using SAX under 20 mM Tris, 80-160 mM NaClO<sub>4</sub> between 0-7.7 min and 160-320 mM NaClO<sub>4</sub> between 7.7-10.1 min pH 11.5 and 20% v/v MeCN. Analysis at 0.8 ml/min, 30 °C using a DNAPac PA200 Rs column. Reference OGNs analysed concurrently at 30 picomole sample amount

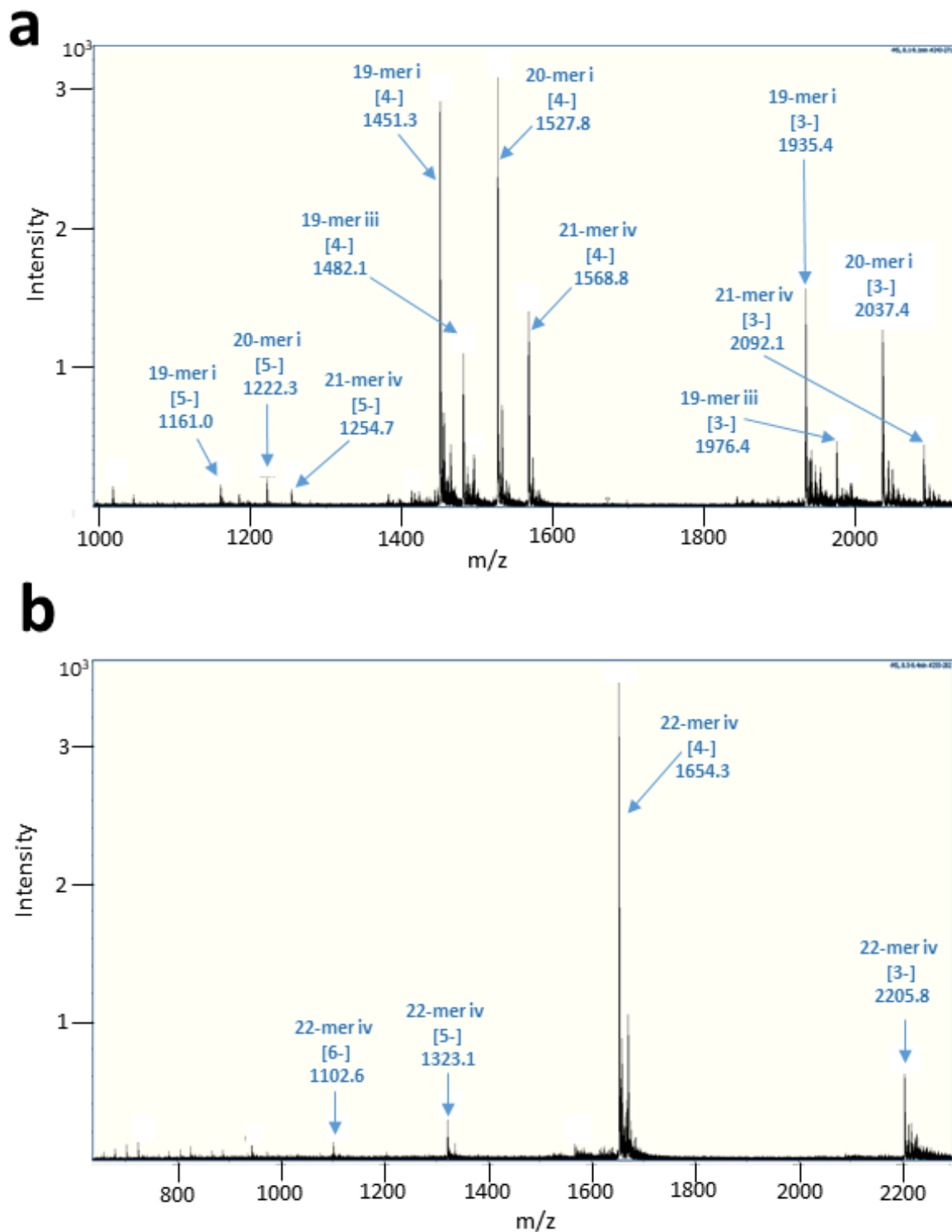


**Figure 4.6: Offline 2D-LC using strong IP-RP to SAX HPLC to analyse test set 1. a:** OGN identification by LC-MS (see Chapter 2 methods). Mass spectrum of fraction 2 of the 1<sup>st</sup> dimension. **b:** OGN identification by LC-MS (see Chapter 2 methods). Mass spectrum of fraction 4 of the 1<sup>st</sup> dimension.

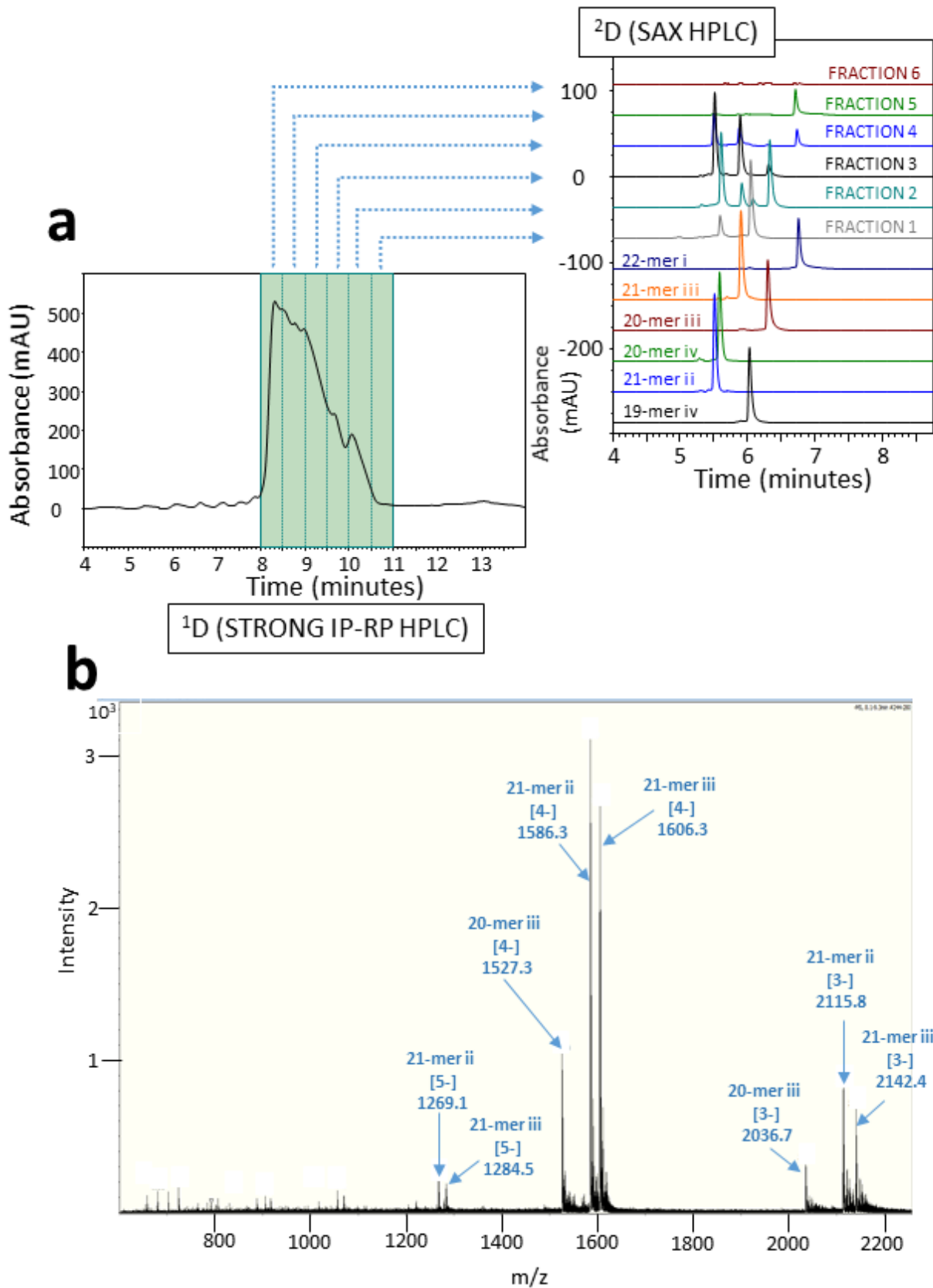


**Figure 4.7: Offline 2D-LC using strong IP-RP to SAX HPLC to analyse Test set 2.** 1000 picomole sample of 19-22-mer size and sequence variant OGN mixture. **a:** 1<sup>st</sup> dimension strong IP-RP HPLC under 5 mM TBuAA, 0.1  $\mu$ M Na<sub>4</sub> EDTA and 34.5-59% v/v MeCN gradient from 1-15 min. Analysis at 0.2 ml/min, 50 °C using a DNAPac RP column. 20  $\mu$ l of each fraction was reanalysed in the 2<sup>nd</sup> dimension using SAX HPLC. Analysis using 20 mM Tris, 80-160 mM NaClO<sub>4</sub> between 0-7.7 min and 160-320 mM NaClO<sub>4</sub> between 7.7-10.1 min pH 11.5 and 20% v/v MeCN. Analysis at 0.8 ml/min, 30 °C using a DNAPac PA200

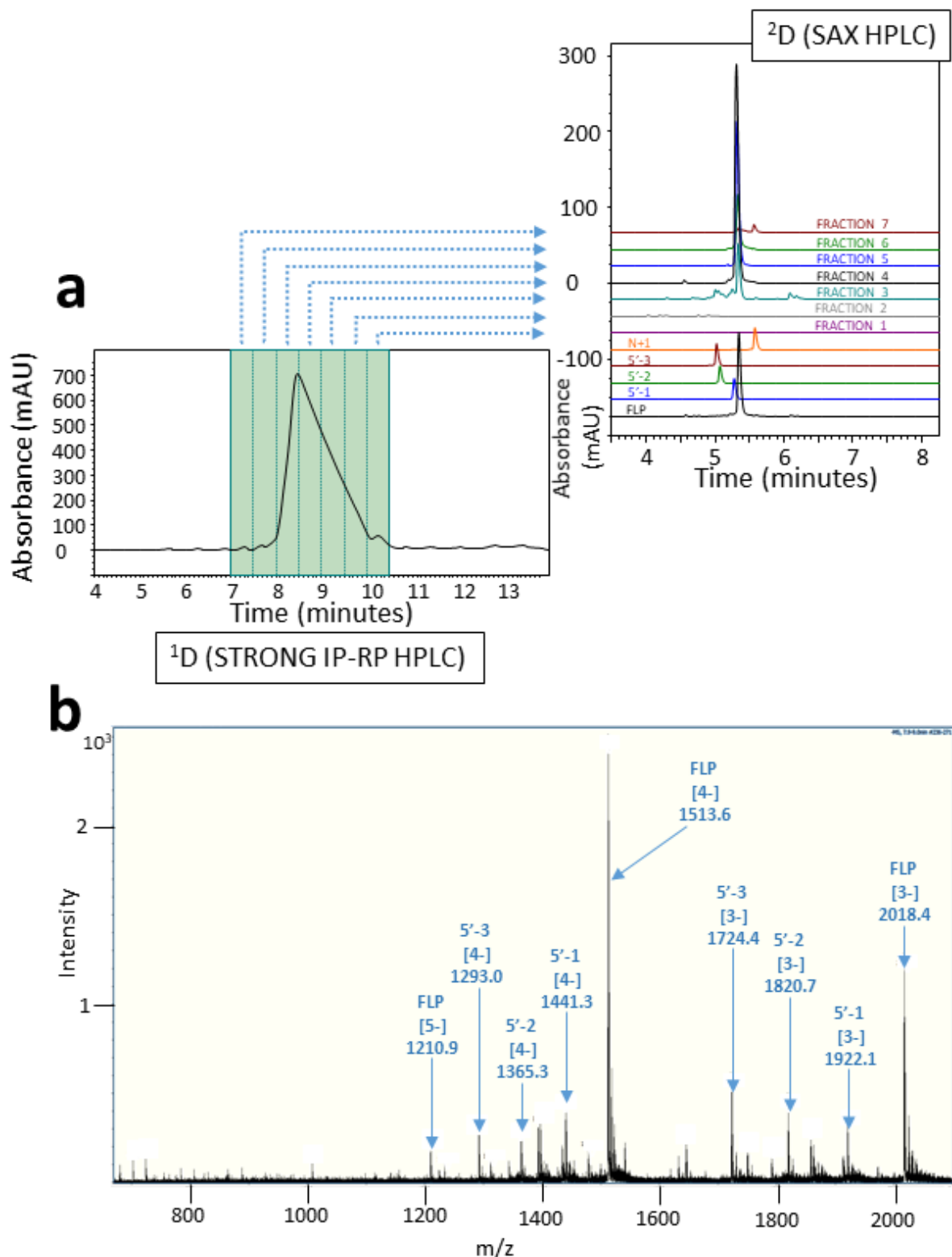


**Figure 4.8: Offline 2D-LC using strong IP-RP to SAX HPLC to analyse 1000 picomole sample of a 20-mer unmodified oligonucleotide therapeutic and its 17-21-mer associated manufacturing impurities added at 1.5% concentration. a:** 1<sup>st</sup> dimension analysis using strong IP-RP under a gradient of 5 mM TBuAA, 0.1  $\mu$ M Na<sub>4</sub> EDTA and 34.5-59% v/v MeCN from 1-15 min. Analysis at 0.2 ml/min, 50 °C using a DNAPac RP column. 20  $\mu$ l of each fraction was reanalysed in the 2<sup>nd</sup> dimension using SAX HPLC under a gradient of 20 mM Tris, 80-160 mM NaClO<sub>4</sub> between 0-7.7 min and 160-320 mM NaClO<sub>4</sub> between 7.7-10.1 min pH 11.5 and 20% v/v MeCN. Analysis at 0.8 ml/min, 30 °C using a DNAPac PA200 Rs column. Reference OGNs analysed concurrently at 10 and 80 picomole sample amount for impurities and FLP reference OGN respectively. **b:** OGN identification by LC-MS (see Chapter 2 methods). Mass spectrum of fraction 3 of the 1<sup>st</sup> dimension.

Co-elution is possibly an effect of overloading of the stationary phase or as a result of high FLP concentration in respect to impurity concentration. Interestingly, there are other manufacturing impurities that are shown within the 2<sup>nd</sup> dimension that potentially would not be observed in one dimensional analysis. For example, peaks in fraction 3 and fraction 7 both align with the N+1 reference standard, the peak in fraction 3 has the same retention time as the N+1 impurity but is of differing size due to its elution time within the initial fractions of a size based separation (see Figure 4.8a). Although this impurity was not identified by the mapping strategy, the identification of its presence by 2D-LC is useful for giving the manufacturing/development scientist an indication of the level of impurities within a manufacturing or purified batch. Further analysis by LC-MS could be used to identify this peak and others like it, however was not deemed necessary for the optimisation of the 2D-LC workflow of this Chapter.

#### **4.5.1.1 Mass spectrometry analysis of first dimension fractions of OGNs.**

Aiming to validate that the reference mapping strategy was accurate, LC-MS analysis was utilised to track OGN species within the 2D-LC workflow. Replicate fractions of the 1<sup>st</sup> dimension separation were analysed by LC-MS to identify OGNs in each fraction. LC-MS analysis using strong IP-RP was performed in conjunction with a MaXis UHR Q-TOF instrument (see Chapter 2). Example mass spectra are shown in Figures 4.6-4.8. Following LC-MS analysis, deconvolution was used to determine the OGN masses and subsequent identifications, which are summarised in Tables 4.8-4.10. LC-MS data was compared to the reference mapping data to correctly align reference OGNs to peaks within a sample. Fractions of the 1<sup>st</sup> dimension analysis of test set 1 were analysed by LC-MS and OGNs within each fraction were identified (see Table 4.8). Example mass spectra for fraction 2 and 4 is shown in Figure 4.6a and 4.6b respectively. The corresponding OGN identifications based on mass is highlighted. Table 4.8 shows which OGNs were identified within fractions 1-6 of the 1<sup>st</sup> dimension fractionation analysis by strong IP-RP HPLC.

2<sup>nd</sup> dimension reference mapping analysis by HPLC highlighted an aberrant retention time for OGN '20-mer i' reference standard, as the reference OGN eluted earlier than its corresponding OGN in the test set sample- within fractions 2 and 3. In the mapping analysis '20-mer i' co-eluted with '22-mer iv'. However, mass spectrometry data confirms that '20-mer i' was present in fractions 2 and 3 while

'22-mer iv' was present in fraction 4. It is likely that the temperature of the column was not stable during reference mapping analysis of reference OGN '20-mer i' in SAX-LC.

Within the reference mapping analysis, '21-mer iv' and '22-mer ii' were present in low concentration in fraction 4. This was not identified and confirmed by mass spectrometry analysis, potentially due to ion suppression '22-mer iv', which was present in high abundance within the sample. High analyte concentration within the droplets of the electrospray can inhibit ionisation of analytes in low concentration within that droplet [273].

**Table 4.8: LC-MS identification of OGN masses in each fraction of the 1<sup>st</sup> dimension analysis of test set 1.**

<b>Fraction</b>	<b>OGN Observed Monoisotopic Mass (Da)</b>	<b>OGN Theoretical Monoisotopic Mass (Da)</b>	<b>Observed Monoisotopic m/z of [M-4H] 4<sup>-</sup></b>	<b>Theoretical Monoisotopic m/z of [M-4H] 4<sup>-</sup></b>	<b>Identity Assignment</b>
1	5807.204	5806.980	1450.793	1450.737	19-mer i
	5930.248	5930.022	1481.554	1481.497	19-mer iii
2	6113.284	6113.054	1527.313	1527.255	20-mer i
	5807.204	5806.980	1450.793	1450.737	19-mer i
	6276.288	6276.056	1568.064	1568.006	21-mer iv
	5930.252	5930.022	1481.555	1481.497	19-mer iii
3	6113.288	6113.054	1527.314	1527.255	20-mer i
	6276.284	6276.056	1568.063	1568.006	21-mer iv
4	6618.372	6618.117	1653.585	1653.521	22-mer iv
	6688.360	6688.123	1671.082	1671.023	22-mer ii
5	6688.372	6688.123	1671.085	1671.023	22-mer ii
	6618.372	6618.117	1653.585	1653.521	22-mer iv
6	6688.368	6688.123	1671.084	1671.023	22-mer ii

OGNs of test set 2 were fractionated by 1<sup>st</sup> dimension strong IP-RP HPLC analysis and then analysed by LC-MS to identify OGNs within each fraction. Table 4.9 shows which OGNs were identified within fractions 1-6 of the 1<sup>st</sup> dimension fractionation analysis by strong IP-RP HPLC. An example mass spectrum is shown in Figure 4.7b. The results of the LC-MS analysis complement the data obtained from reference mapping analysis in Figure 4.7.

Table 4.9: LC-MS identification of OGN masses in each fraction of the 1<sup>st</sup> dimension analysis of test set 2.

Fraction	OGN Observed Monoisotopic Mass (Da)	OGN Theoretical Monoisotopic Mass (Da)	Observed Monoisotopic m/z of [M-4H] 4 <sup>-</sup>	Theoretical Monoisotopic m/z of [M-4H] 4 <sup>-</sup>	Identity Assignment
1	5840.220	5840.003	1459.047	1458.993	19-mer iv
	6182.368	6182.086	1544.584	1544.513	20-mer iv
2	6111.264	6111.026	1526.808	1526.748	20-mer iii
	5840.224	5840.003	1459.048	1458.993	19-mer iv
	6182.316	6182.086	1544.571	1544.513	20-mer iv
	6427.332	6427.107	1605.825	1605.769	21-mer iii
3	6347.344	6347.094	1585.828	1585.765	21-mer ii
	6427.356	6427.107	1605.831	1605.769	21-mer iii
	6111.260	6111.026	1526.807	1526.748	20-mer iii
4	6809.392	6809.137	1701.340	1701.276	22-mer i
	6347.344	6347.094	1585.828	1585.765	21-mer ii
	6427.348	6427.107	1605.829	1605.769	21-mer iii
5	6809.392	6809.137	1701.340	1701.276	22-mer i
6	6810.384	6809.137	1701.588	1701.276	22-mer i

Manufacturing impurities added at 1.5% total sample concentration and the FLP of a therapeutic OGN model were fractionated within a 1<sup>st</sup> dimension strong IP-RP HPLC analysis and each fraction was analysed further by LC-MS. The OGNs within each fraction were identified (see Table 4.10). The results show that some peaks that were identified by UV detection were not identified by mass spectrometry detection, a likely result of being present in concentration below the limit of detection or competitive inhibition of ionisation by the full length product OGN. No OGNs were identified within fractions 1 and 2, however fraction 3 contains the N-x manufacturing impurities. The N+1 manufacturing impurity is identified within fraction 7 and the FLP is identified within fractions 3-7. An example mass spectrum is shown in Figure 4.8b.

**Table 4.10: LC-MS identification of OGN masses within each fraction of the 1<sup>st</sup> dimension analysis. Sample of the 1<sup>st</sup> generation (unmodified) OGN and manufacturing N-x/N+1 impurities at 94% and added 1.5% total sample concentration respectively.**

<b>Fraction</b>	<b>OGN Observed Monoisotopic Mass (Da)</b>	<b>OGN Theoretical Monoisotopic Mass (Da)</b>	<b>Observed Monoisotopic m/z of [M-4H] 4<sup>-</sup></b>	<b>Theoretical Monoisotopic m/z of [M-4H] 4<sup>-</sup></b>	<b>Identity Assignment</b>
1	-	-	-	-	-
2	-	-	-	-	-
3	6056.276	6056.058	1513.061	1513.006	FLP
	5768.220	5767.012	1441.047	1440.745	5 <sup>1</sup> -1
	5463.108	5462.966	1364.769	1364.733	5 <sup>1</sup> -2
	5174.064	5173.920	1292.508	1292.472	5 <sup>1</sup> -3
4	6056.280	6056.058	1513.062	1513.006	FLP
5	6056.276	6056.058	1513.061	1513.006	FLP
6	6056.280	6056.058	1513.062	1513.006	FLP
7	6360.340	6360.104	1589.077	1589.018	N+1
	6056.264	6056.058	1513.058	1513.006	FLP

In summary, equimolar size and sequence variants within two test sets were analysed by offline (strong IP-RP)-(SAX) 2D-LC. A 1<sup>st</sup> generation unmodified OGN therapeutic model and its N-x/N+1 manufacturing impurities added at 1.5% total sample concentration were also analysed by the offline 2D-LC workflow. Samples were heart-cut fractionated during the 1<sup>st</sup> dimension separation and re-analysed within the 2<sup>nd</sup> dimension of SAX-LC. Alongside analyses of the fractions within the 2<sup>nd</sup> dimension, reference OGNs were separated to map OGNs in each fraction via retention time alignment. In addition, fractions of the 1<sup>st</sup> dimension were analysed by LC-MS to identify OGNs in each fraction of the 1<sup>st</sup> dimension and validate the reference mapping strategy within the 2<sup>nd</sup> dimension. There were no compatibility issues observed between mobile phases of each dimension, showing that this workflow is appropriate for an online approach.

Following offline 2D LC analysis of the OGN mixtures, OGNs of each sample set were identified in each fraction using the reference mapping strategy. Further validation of the OGN identifications was performed using mass spectrometry. HPLC-UV detection was a more sensitive detection method

within this workflow (in comparison with mass spectrometry detection) due to potential suppression of ionisation by the ion pair reagent used in this study.

## **Part C**

### **4.6 Optimisation of an online heart-cut 2D-LC workflow for analysis of OGNs.**

To further optimise the (strong IP-RP)-(SAX) 2D-LC method for analysis of unmodified OGNs, an online workflow was developed (see Chapter 2, section 2.2.3). The 1<sup>st</sup> dimension mobile phase was delivered through the left pump and the 2<sup>nd</sup> dimension mobile phase through the right pump. A multi-switch valve directed the mobile phase through the injection valve to another multi-switch valve. The second multi-switch valve (working in conjunction with the 1<sup>st</sup>) would deliver mobile phase to the correct dimension stationary phase. The 1<sup>st</sup> dimension stationary phase column was contained within a temperature controlled column oven, while the 2<sup>nd</sup> dimension stationary phase column was situated outside the column oven. This was due to incompatibility of the 2<sup>nd</sup> dimension conditions with elevated analysis temperature (high pH of the mobile phase would degrade the stationary phase above 30 °C). Once the sample had been separated in the 1<sup>st</sup> dimension column, it would travel through the UV detector and toward a fractionation valve. The fractionation valve directed the 1<sup>st</sup> dimension separation back through the needle to be delivered into empty microvials within the auto-sampler. These vials were then used as sample vials for the 2<sup>nd</sup> dimension analysis. In this equipment set-up, heart-cut online 2D-LC was enabled.

OGN samples analysed in offline 2D-LC mode (see section 4.5) were analysed by online heart-cut 2D-LC. The online workflow was performed with the aim of reproducing data obtained during offline 2D-LC analysis. Specifically, 1000 picomole samples of equimolar 19-22-mer size and sequence OGN variant test set 1 and 2 were separated and fractionated into six or seven 100 µL fractions within strong IP-RP conditions (5 mM TBuAA, 0.1 µM Na<sub>4</sub> EDTA and 10-80% v/v MeCN). 20 µL of each of these fractions were analysed in a SAX HPLC 2<sup>nd</sup> dimension (20 mM Tris, 0-400 mM NaClO<sub>4</sub>, pH 11.5 with 20% v/v MeCN) alongside 30 picomoles of each reference OGN for reference mapping analysis (see Figure 4.9 a-b). 2D-LC was performed on two replicate samples of each test set, as well as replicates of the 1<sup>st</sup> generation unmodified OGN mixed with impurities added at 1.5% concentration (see Figure 4.9c). The 1<sup>st</sup> generation OGN therapeutic 1000 picomole sample was fractionated into

seven 100  $\mu$ L fractions within the 1<sup>st</sup> dimension. 20  $\mu$ L of each fraction was analysed in a SAX HPLC 2<sup>nd</sup> dimension alongside reference standards at 10 picomole and 80 picomole sample amount (for manufacturing impurities and the FLP respectively). Reference standards were diluted to concentration within 5 mM TBuAA, 0.1  $\mu$ M Na<sub>4</sub>EDTA and 45% v/v MeCN to avoid discrepancies in diluent between fractions and references. The diluent was developed via analysis of eluting conditions from the 1<sup>st</sup> dimension separation.

Test set 1 of 19-22-mer size and sequence variants was analysed by the online 2D-LC workflow (see Figure 4.9a). The results are consistent with the previous offline 2D-LC analysis shown in Figure 4.5 of section 4.6. OGNs within each fraction were identified by reference mapping and knowledge of the size based separation mechanism dominating the 1<sup>st</sup> dimension of the workflow. Test set 2 of 19-22-mer size and sequence variants were also analysed by the online workflow and the results are consistent with previous offline 2D-LC analysis (see Figure 4.7a of section 4.5). The 1<sup>st</sup> generation, unmodified OGN therapeutic test set (with N-x/N+1 manufacturing impurities at 1.5% total concentration) was analysed within the online heart-cut 2D-LC workflow (see Figure 4.9c). The results were comparable to offline 2D-LC data (as shown in Figure 4.8a of section 4.5). Reference OGNs were co-analysed within the 2<sup>nd</sup> dimension and enable identification of 5'-1, 5'-2, 5'-3 (N-x) and N+1 impurities alongside the full length product.

The key findings are that once offline 2D-LC is optimised with a reference mapping strategy, it is relatively facile to automate the method to be performed online. The benefits of moving towards an online 2D-LC method include the ability to automate the analysis and the overall time to complete the HPLC analysis. In theory the HPLC system could be set up and used without the need for repetitive system equilibration (such as what is needed each time a chromatographic mobile phase is changed), which reduces analysis time. Keeping hardware connected in place also can increase the lifetime of tubing and the equipment, such as the column.

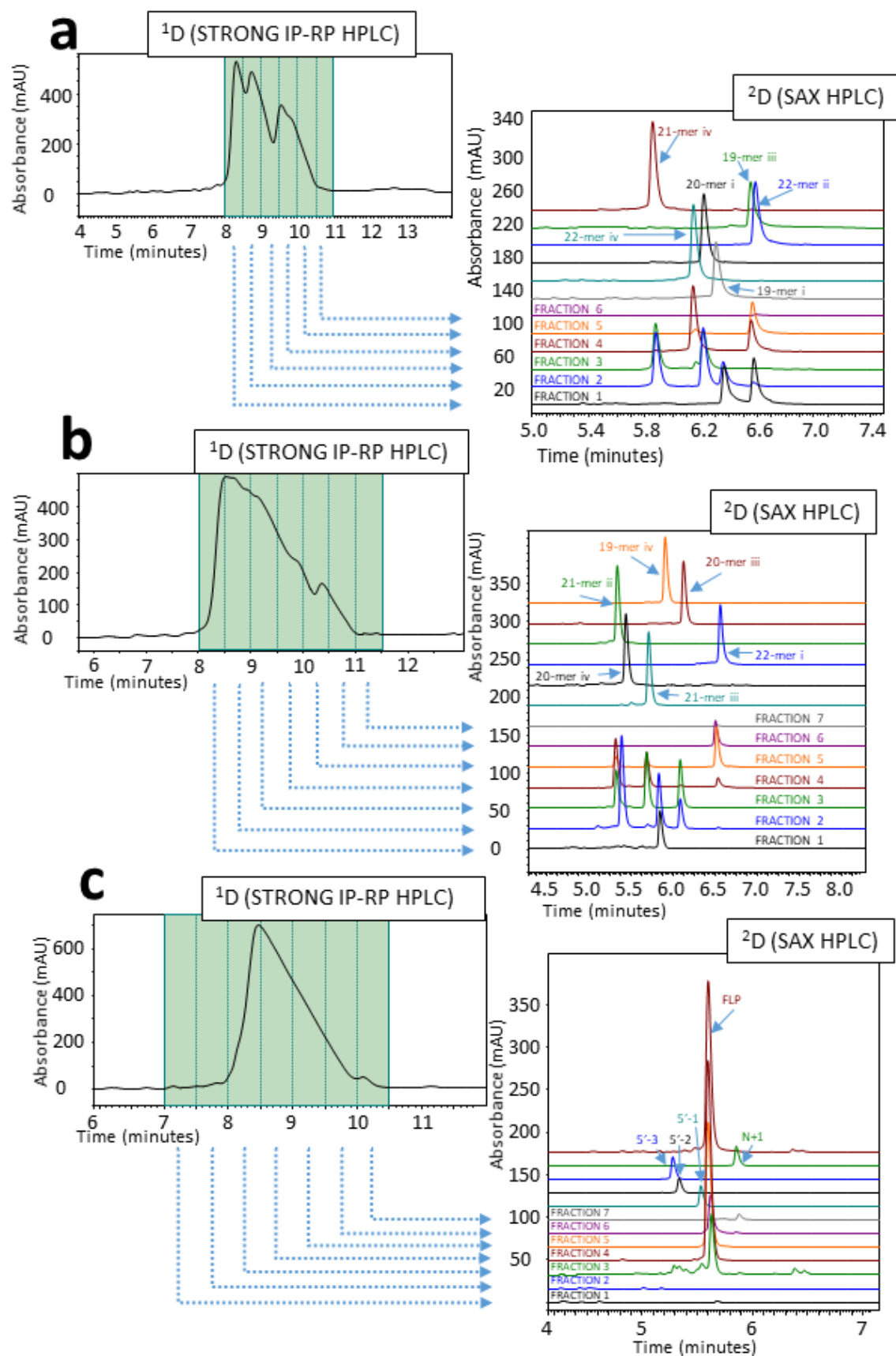


**Figure 4.9: Online 2D-LC analysis of OGNs using strong IP-RP to SAX HPLC.** <sup>1</sup>D separation under 5 mM TBuAA, 0.1 μM Na<sub>4</sub> EDTA and 34.5-59% v/v MeCN gradient from 1-15 min. Analysis at 0.2 ml/min, 50 °C using a DNAPac RP column. 100 μl Fractions were collected and then 20 μl of each was separated in a 2<sup>nd</sup> dimension under a gradient of 20 mM Tris, 80-160 mM NaClO<sub>4</sub> between 0-7.7 min and 160-320 mM NaClO<sub>4</sub> between 7.7-10.1 min pH 11.5 and 20% v/v MeCN. Analysis at 0.8 ml/min, ambient temperature using a DNAPac PA200 Rs column. **a:** Analysis of a 1000 picomole sample of 19-22 mer size and sequence variant OGN mixture (TEST SET 1). **b:** 1000 picomole sample of 19-22 mer size and sequence variant OGN mixture (TEST SET 2). **c:** 1000 picomole sample of 17-21 mer mixture of unmodified OGN and manufacturing impurities added at 1.5% of total concentration.

## 4.7 Conclusions.

The analysis of complex mixtures of OGNs and OGN therapeutics and their related impurities (which are chemically complex) leads to low selectivity in 1D HPLC separations. Co-elution and close elution events are minimised by optimising workflows that are able to orthogonally separate OGNs between two dimensions of analysis. While there have been a number of studies focussing on optimisation of 1D HPLC analysis of OGNs (see Chapter 1, section 1.3), there has been modest focus on the development of 2D-LC methods for the analysis of OGNs (especially methods that focus on resolving shortmers as little as N-1 from a FLP).

An optimised 2D-LC workflow for the analysis of OGNs was performed by first studying the 1D HPLC OGN retention behaviour within previously optimised weak IP-RP (using TEAA), strong IP-RP (using TBA), HFIP modified IP-RP (using TEAA:HFIP) and SAX (using NaClO<sub>4</sub> and 20% v/v MeCN) HPLC. Retention data was analysed using orthogonality metrics to determine orthogonal couplings of the different modes within a 2D-LC workflow. The orthogonality of two 2D-LC workflows was assessed using the Gilar 'bin counting' and 'minimum convex hull' methods [300, 302] and then experimentally tested for feasibility. After comparing workflows of (strong IP-RP)-(weak IP-RP) 2D-LC and (strong IP-RP)-(SAX) 2D-LC, the latter workflow demonstrated higher orthogonality and higher chromatographic performance (as measured by 2<sup>nd</sup> dimension peak capacity). In addition, further studies demonstrated that there were no problems associated with mobile phase compatibility in the two different offline 2D-LC workflows.

The offline (strong IP-RP)-(SAX) 2D-LC workflow was developed further using a reference mapping strategy to identify the peaks in the 2<sup>nd</sup> dimension of the method. Furthermore, OGN identifications were also confirmed by LC-MS analysis of the 1<sup>st</sup> dimension fractions. Using offline 2D-LC methods in conjunction with a reference mapping strategy enabled the identification of all OGNs from the model OGN test samples within the online 2D-LC workflow. Finally, an online heart-cut 2D-LC method was developed using strong IP-RP HPLC in the 1<sup>st</sup> dimension and SAX HPLC in the 2<sup>nd</sup> dimension. After designing and setting up a 2D-LC flow path on a Thermo Scientific U3000 HPLC, equimolar size and sequence variants within two test sets were analysed using online heart-cut 2D-LC using strong IP-RP HPLC in the 1<sup>st</sup> dimension and SAX HPLC in the 2<sup>nd</sup> dimension. A first generation unmodified OGN therapeutic model and its N-x/N+1 manufacturing impurities added at 1.5% total sample concentration were also analysed by the online 2D-LC workflow.

This approach is the first development of online heart-cut 2D-LC workflow for orthogonal separations of OGNs using (5 mM TBUAA, 0.1  $\mu$ M Na<sub>4</sub> EDTA, 10-80% v/v MeCN)-(20 mM Tris, 0-400 mM NaClO<sub>4</sub> pH 11.5, 20% v/v MeCN) conditions. The results demonstrated that 2D-LC can overcome the challenges posed by co-elution or low resolution in one dimensional separations.

The equipment was functionalised from a dual pump 1D HPLC system to a 2D-LC system with the use of multi-switch valves and utilisation of a fractionation valve. Although there are 2D-LC machines available to purchase, many laboratories do not have the funding for extra equipment. By designing the 2D-LC flow path in this way, the utility of modestly priced kit extras (multi-switch valves) in the analytical laboratory is demonstrated. Moving toward automated online 2D-LC analysis methods reduces preparation and equilibration time and can increase the lifetime of equipment. Orthogonal 2D-LC separations of unmodified size and sequence variants, such as those in test sets 1 and 2, highlight how an optimised 2D-LC analysis method developed in this study could be used in a wide range of applications where complex mixtures of OGNs are present. For example: analysis of OGNs and their manufacturing impurities, the analysis of complex mixtures of DNA/RNA, probe analysis or the analysis of OGNs generated from RNase/DNase mapping experiments.

## Chapter 5: Optimisation of 2D-LC for the analysis of phosphorothioated oligonucleotides.

### Abstract.

The aim of this Chapter was to develop a 2D-LC analytical method for the analysis of phosphorothioated oligonucleotides (PS OGNs). Initial work focussed on understanding the retention behaviour of the associated manufacturing impurities of PS OGNs using 1D HPLC methods prior to the development of 2D-LC workflows. PS OGNs were analysed using previously optimised conditions for size and/or sequence dependent separations. Specifically, analysis using IP-RP (either in conjunction with TBuAA or a TEAA:HFIP combination) and SAX chromatographic conditions elucidated the retention behaviour of PS OGNs and their associated manufacturing impurities, such as shortmers, longmers and P=O. Retention data was analysed by both the bin counting and minimum convex hull methods to analyse orthogonality of a range of 2D-LC workflows. Low resolution of impurities from the FLP was observed during SAX HPLC analysis of these OGNs and did not facilitate workflows containing SAX in either dimension. The P=O impurity co-eluted with the FLP under strong IP-RP conditions. Separation of the P=O is achieved using HFIP modified IP-RP HPLC. However, feasibility analysis demonstrated that eluting conditions of strong IP-RP are incompatible with HFIP modified IP-RP conditions in a 2<sup>nd</sup> dimension.

Optimisation of a 2D-LC method was achieved using HFIP modified IP-RP in the 1<sup>st</sup> dimension and a 2<sup>nd</sup> dimension of strong IP-RP HPLC. This method design demonstrated compatibility between eluting conditions of a strong IP-RP 1<sup>st</sup> dimension and the 2<sup>nd</sup> dimension analysis of PS OGNs (HFIP modified IP-RP). The 2D-LC method was developed further by optimisation of offline analysis along with a reference OGN mapping strategy (confirmed by LC-MS analysis of fractions from the 1<sup>st</sup> dimension). Using this method, the P=O impurities were resolved from the FLP in the 1<sup>st</sup> dimension and the 2<sup>nd</sup> dimension analysis was successfully used to separate shortmer impurities from the FLP. However, the reference mapping strategy was not beneficial for tracking impurity retention in the 2<sup>nd</sup> dimension due to co and close elution events in strong IP-RP HPLC analysis of PS OGNs. The method was further developed for online 2D-LC analysis and was shown to reproduce the data from the offline 2D-LC approach. 2D-LC using the (HFIP modified IP-RP)-(strong IP-RP) method was therefore not fully able to separate all the associated manufacturing impurities of PS OGNs. Analysis was challenged by co and close elution of impurities and the FLP.

## 5.1 Introduction.

Phosphorothioated (PS) OGN therapeutics, such as antisense OGNs (ASOs), contain chemically modified bonds between their nucleotides. As described in Chapter 1 (section 1.2.2), one of the oxygens of the bond is substituted for a sulphur atom during synthesis (see Figure 5.1).

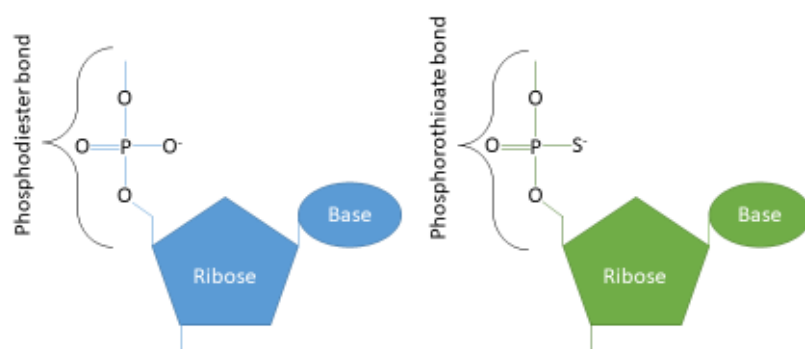


**Figure 5.1: PS OGN structure. Comparison of phosphodiester bond with a phosphorothioate bond.**

Previous work (see Chapter 3) showed that using modes of chromatography where sequence dependent OGN separations dominate, such as weak IP-RP HPLC and SAX HPLC, the analysis of full PS OGNs results in broad peaks. This was due to the partial resolution of the large number of diastereoisomers present. This effect was most noticeable using weak IP-RP HPLC (in conjunction with TEAA) and could not be ablated with parameter optimisation. Optimisation of the IPR to a more hydrophobic IPR (TBuAA) or modification of the mobile phase with the addition of HFIP improved PWHH, demonstrating more dynamic ion-exchange retention mechanisms and thus size dependent separations. In addition, optimisation of the TEAA mobile phase with the addition of HFIP also showed an alternative peak cohort within the separation (see Chapter 3, Figure 3.10b), reflecting an alternate selectivity between strong IP-RP HPLC and HFIP modified IP-RP HPLC for full PS OGNs. SAX and SEC analyses of full PS OGNs were improved by addition of MeCN to the mobile phase. This reduced secondary interactions between the bases of the OGN and the stationary phase, demonstrated by decreased PWHH or co-elution of PS OGN variants.

The aim of this work was to develop an online heart-cut 2D-LC method for the analysis of PS OGNs and low level OGN impurities. As phosphorothioate modification results in diastereoisomer formation and increased secondary interactions in a number of chromatographic modes, the 2D-LC

method needs to be developed to reduce broadened peaks and secondary interactions. Phosphorothioation to the OGN also introduces more impurity types; in addition to shortmers and longmers, the phosphorothioate bond may oxidize to form a phosphodiester bond. The transformation to a phosphodiester bond introduces potential P=O impurities into the OGN mixture- where the phosphorothioated OGN may have one or more P=S>P=O bonds. The resolution of P=O impurities from the FLP can be challenging, as in most chromatographic modes, these impurities will closely elute or co-elute with the PS OGN of equal length. The research hypothesis for this chapter is that 2D-LC can improve the resolution of shortmer, longmer and P=O impurities from PS OGNs through orthogonal separations. In addition, the use of optimised chromatographic conditions for PS OGNs can facilitate improved resolution across a 2D-LC separation.

The process of 2D-LC development was similar to that outlined in Chapter 4. First, the retention behaviour of OGNs within sample sets were analysed under a range of chromatographic modes (SAX, strong IP-RP and HFIP modified IP-RP). 1D separations were assessed for chromatographic performance by identifying changes in OGN elution order, PWHH and resolution of impurities from the FLP. 2D-LC workflows were proposed using the results from orthogonality and chromatographic performance analysis. A targeted approach was adopted for the analysis of P=O impurities, which are challenging to separate by 1D HPLC. The 2D-LC workflow was experimentally tested by evaluating mobile phase compatibility between dimensions and ensuring OGNs retained within the second dimension. Offline 2D-LC was optimised with an OGN reference mapping strategy (which was confirmed by LC-MS). Finally, an online heart-cut 2D-LC workflow was performed.

Results of this Chapter are presented similarly to data in Chapter 4, where the stepwise development of method optimisation is segregated into 3 parts. Part A focuses on 1D HPLC analysis of PS OGNs. Part B presents the optimisation of offline 2D-LC and Part C demonstrated an online 2D-LC analytical method.

## Results and Discussion

### Part A

#### 5.2 Analysis of PS OGN retention behaviour in 1D HPLC.

Previously, a number of modes of chromatography were optimised that were suitable for the analysis of PS OGNs by enhancing size dependent separations (Chapter 3). The chromatographic conditions optimised for analysis of PS OGNs are highlighted in Table 5.1.

**Table 5.1: Optimised chromatographic conditions employed for 1D HPLC analysis and sequential retention behaviour assessment of PS OGNs.**

<b>Chromatographic Mode</b>	<b>Mobile Phase</b>	<b>Stationary Phase</b>
Strong IP-RP HPLC	5 mM TBUAA, 0.1 $\mu$ M Na <sub>4</sub> EDTA, 10-80% v/v MeCN	DNAPac RP
HFIP modified IP-RP HPLC	100 mM TEAA, 40 mM HFIP 0.1 mM Na <sub>4</sub> EDTA, 0-25% v/v MeCN	DNAPac RP
SAX HPLC	20 mM Tris, 0-400 mM NaClO <sub>4</sub> , pH 11.5, 20% v/v MeCN	DNAPac Pa200 Rs

During optimisation of 1D HPLC (Chapter 3), single and fully PS OGN models were analysed to help understand their chromatographic behaviour under different conditions. In this study, two fully phosphorothioated model OGNs were used for analysis within a 2D-LC workflow, along with their associated manufacturing impurities at low concentration (see Tables 5.2 and 5.3). OGN impurities are often present at low concentration post manufacturing purification of the FLP [136, 322]. Although the majority of newer generation OGN therapeutics have additional chemical modifications (such as 2'-MOE, 2'-O-Me or 2'-F), analysis of model OGNs containing just the PS chemical modification enables better understanding of the effect of phosphorothioation on chromatographic behaviour of OGN therapeutics containing PS bonds [12]. Initial work focussed on the analysis of retention behaviour of the PS OGNs that represent typical full PS OGNs and their related impurities.

**Table 5.2: Fully phosphorothioated model A OGN and its associated manufacturing impurities described by size in nucleotide length (nt), OGN sequence and monoisotopic mass.** A capital letter denotes a DNA nucleotide and a \* denotes a PS bond.

OGN Name	OGN Type	Sequence	Monoisotopic Mass (Da)
<b>PS OGN Model A</b>			
Full length Product (FLP)	Target OGN	C*T*C* A*A*A* T*A*T* A*C*T* T*A*C* G*A*T* T*A	6359.624
5'-1	Shortmer	T*C*A* A*A*T* A*T*A* C*T*T* A*C*G* A*T*T* A	6054.601
5'-2	Shortmer	C*A*A* A*T*A* T*A*C* T*T*A* C*G*A* T*T*A	5734.578
5'-3	Shortmer	A*A*A* T*A*T* A*C*T* T*A*C* G*A*T* T*A	5429.555
N+1	Longmer	C*T*C* A*A*A* T*A*T* A*C*T* T*T*A* C*G*A* T*T*A	6679.647
P=O	Oxidation on FLP 5' terminal	CT*C* A*A*A* T*A*T* A*C*T* T*A*C* G*A*T* T*A	6343.647
5'-1, P=O	Oxidation on 5'-1 3' terminal	T*C*A* A*A*T* A*T*A* C*T*T* A*C*G* A*T*T* A	6038.624

**Table 5.3: Fully phosphorothioated model B OGN and its associated manufacturing impurities described by size in nucleotide length (nt), OGN sequence and monoisotopic mass.** A capital letter denotes a DNA nucleotide and a \* denotes a PS bond.

OGN Name	OGN Type	Sequence	Monoisotopic Mass (Da)
<b>PS OGN Model B</b>			
Full length Product (FLP)	Target OGN	T*G*T* C*A*G* T*C*T* A*C*T* C*A*C* G*A*T* T*A	6367.603
5'-1	Shortmer	G*T*C* A*G*T* C*T*A* C*T*C* A*C*G* A*T*T* A	6047.580
5'-2	Shortmer	T*C*A* G*T*C* T*A*C* T*C*A* C*G*A* T*T*A	5702.551
5'-3	Shortmer	C*A*G* T*C*T* A*C*T* C*A*C* G*A*T* T*A	5382.528
N+1	Longmer	T*G*T* C*A*G* T*C*T* C*A*C* T*C*A* C*G*A* T*T*A	6672.626
P=O	Oxidation on FLP 5' terminal	TG*T* C*A*G* T*C*T* A*C*T* C*A*C* G*A*T* T*A	6351.626
5'-1, P=O	Oxidation on 5'-1 5' terminal	GT*C* A*G*T* C*T*A* C*T*C* A*C*G* A*T*T* A	6031.603

Equimolar OGN samples were analysed by strong IP-RP, HFIP modified IP-RP and SAX HPLC (see Figure 5.2 for model A PS OGN data). The resolution between each impurity and the FLP was calculated for analysis under SAX HPLC conditions. Resolution averaged at 0.62 between impurities and the FLP using SAX HPLC. Peak fronting was observed for all OGNs due to low resolution of closely eluting shortmers. Co-elution of many of the related impurities was also observed under SAX HPLC conditions, for example, the 5'-2 and P=O impurities elute at the same retention time.

Resolution increased to 1.27 under strong IP-RP HPLC conditions (using TBUAA as ion-pair reagent), enabling better separation of shortmers from the FLP (see Figure 5.2b). P=O impurities eluted close to the full PS OGN under strong IP-RP HPLC conditions. Analysis of samples under HFIP modified IP-RP HPLC conditions (see Figure 5.2c) facilitated separation of the P=O impurities away from their fully PS sequence counterparts (5'-1 and the FLP) and better resolution of impurities from the FLP (1.51 average). Figure 5.2c shows that the FLP and 5'-1 co-elute, the P=O and 5'-1 P=O co-elute and the 5'-2 and 5'-3 co-elute. At the time of analysis, the N+1 OGN in this sample was not available, and therefore is not within 1D HPLC analysis (but is used for 2D-LC method development). As all modes of chromatography used a predominantly size based separation, the N+1 impurity is estimated to be last eluting OGN within the set. Table 5.4 summarises key parameters measured, including selectivity ( $\alpha$ ), resolution and PWHH. Average  $\alpha$  and PWHH are similar for all three separations, showing that the impurities have close retention times to the FLP under optimised conditions. However, there is a significant increase in resolution in HFIP modified IP-RP HPLC conditions as a result of increased selectivity of some of the impurities from the FLP.

The analysis was repeated using a different OGN sequence and related impurities (PS model set B - see Table 5.3). The HPLC results are shown in Figure 5.3 a-c. Figure 5.3a shows retention behaviour under SAX HPLC conditions. Consistent with the analysis of the model A set, resolution under these conditions is low at 0.59 between the impurities and the FLP. The 5'-1 impurity peak is considerably lower in signal height and area in comparison with other OGN analyses. This is potentially due to error in stock preparation from the lyophilised product. For this work, the retention order was qualitatively assessed and a low signal would not impact on conclusions drawn from retention order studies. Additionally, the N+1 peak appears to be larger than expected, likely due to stock preparation errors. The 5'-3 shortmer eluted first followed by a co-elution of the 5'-1 P=O and 5'-2 impurities.

The next OGNs to elute were the P=O, 5'-1 impurities, followed by the FLP and N+1 OGN that closely elute within the separation. Compared to SAX, the resolution of OGNs and the FLP within the sample set increases to 0.86 under strong IP-RP HPLC conditions, as can be seen in Figure 5.2b.

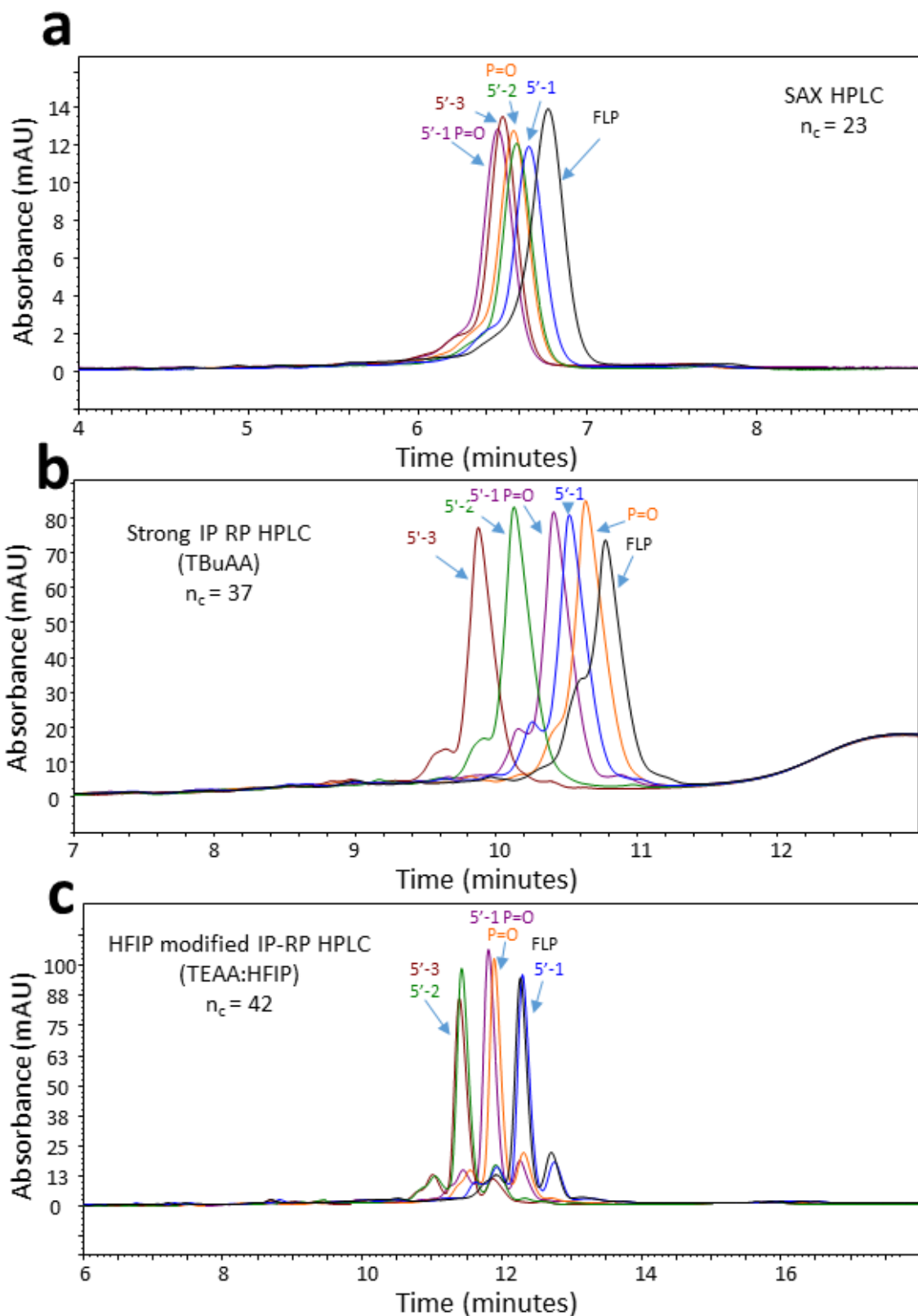


**Figure 5.2: Elution order assessment of Model A PS OGN and associated impurities using SAX, strong IP-RP and HFIP modified IP-RP HPLC conditions ( $n_c$  is peak capacity).** **a:** SAX HPLC using 20 mM Tris, 80-264 mM NaClO<sub>4</sub> 20% v/v MeCN gradient from 0-7.7 min. 30 picomole samples analysed at 0.8 ml/min and 30 °C using a DNAPac Pa200 Rs column. **b:** Strong IP-RP HPLC using 5 mM TBuAA, 0.1 μM Na<sub>4</sub> EDTA and 34.5-59% v/v MeCN gradient from 1-15 min. 50 picomole samples analysed at 0.2 ml/min and 50 °C using a DNAPac RP column. **c:** HFIP modified IP-RP HPLC using 100 mM TEAA, 40 mM HFIP, 0.1 mM Na<sub>4</sub> EDTA and 8.75-17.5% v/v MeCN gradient from 1-15 min. 30 picomole samples analysed at 0.2 ml/min at 75 °C using a DNAPac RP column.

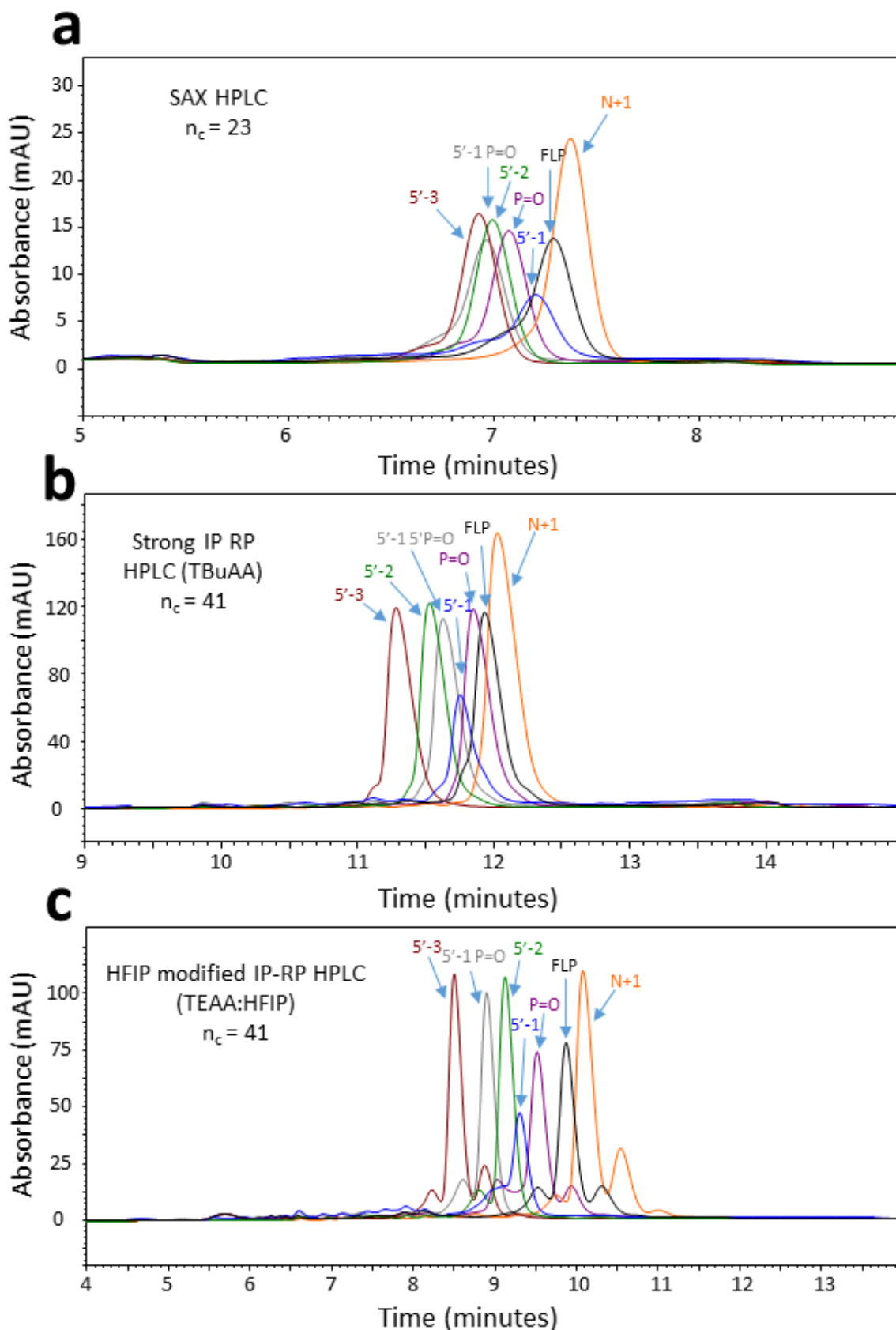


**Figure 5.3: Elution order assessment of Model B PS OGN and associated impurities using SAX, strong IP-RP and HFIP modified IP-RP HPLC conditions.** **a:** SAX HPLC using 20 mM Tris, 80–264 mM NaClO<sub>4</sub> 20% v/v MeCN gradient from 0–7.7 min. 30 picomole samples analysed at 0.8 ml/min and 30 °C using a DNAPac Pa200 Rs column. **b:** Strong IP-RP HPLC using 5 mM TBuAA, 0.1 μM Na<sub>4</sub> EDTA and 34.5–59% v/v MeCN gradient from 1–15 min. 50 picomole samples analysed at 0.2 ml/min and 50 °C using a DNAPac RP column. **c:** HFIP modified IP-RP HPLC using 100 mM TEAA, 40 mM HFIP, 0.1 mM Na<sub>4</sub> EDTA and 8.75–17.5% v/v MeCN gradient from 1–15 min. 30 picomole samples analysed at 0.2 ml/min at 75 °C using a DNAPac RP column.

Elution order also varies compared to SAX HPLC in reflection of a larger dependence on size based separation within strong IP-RP HPLC with the P=O impurities eluting slightly earlier than their length counterparts. The highest resolution was observed under HFIP modified IP-RP HPLC conditions at 2.05, consistent with the results of model A analysis. Analysis of the model B OGN impurities in HFIP modified conditions showed increased resolution compared to model A, (see Figure 5.2c and Figure 5.3c) where no co-elution of any of the OGNs was observed for model B. These results highlight that the difference in OGN sequences also effect separation from their related impurities.

The P=O impurities eluted before their length counterparts but the elution order was not as size dependent as under strong IP-RP conditions due to the 5'-2 impurity eluting after then 5'-1 P=O impurity in HFIP modified IP-RP conditions. Table 5.4 shows that PWHH remained the same for all separations, however there is a clear pattern of higher selectivity and resolution between OGNs in both sample sets from the data observed in HFIP modified IP-RP HPLC separations. In addition, peak capacity was generally higher under HFIP modified conditions.

**Table 5.4: Analysis of PWHH,  $n_c$ , resolution and selectivity for separations of model A and B sample sets under SAX, strong IP-RP and HFIP modified IP-RP HPLC.** Green highlighted boxes show baseline resolution of impurities from FLP.

<b>Model A</b>	<b>SAX-LC</b>	<b>Strong IP-RP-LC</b>	<b>HFIP IP-RP-LC</b>
<b>Mean PWHH (min)</b>	0.20	0.22	0.19
<b>Mean Resolution from FLP</b>	0.61	1.27	1.51
<b>Mean <math>\alpha</math> from FLP</b>	1.04	1.05	1.05
<b>Peak Capacity (<math>N_c</math>)</b>	23	37	42
<b>Model B</b>	<b>SAX-LC</b>	<b>Strong IP-RP-LC</b>	<b>HFIP IP-RP-LC</b>
<b>Mean PWHH (min)</b>	0.20	0.20	0.20
<b>Mean Resolution from FLP</b>	0.59	0.86	2.05
<b>Mean <math>\alpha</math> from FLP</b>	1.03	1.03	1.08
<b>Peak Capacity (<math>n_c</math>)</b>	23	41	41

In respect to elution order for both sample sets, strong IP-RP HPLC analysis demonstrated that shorter OGNs eluted first and longer OGNs eluted last with only a small retention time difference of the P=O impurities compared to their PS length counterparts. A similar retention order was observed under HFIP modified IP-RP HPLC conditions, which was able to separate upon a size basis. However, there was additional separation of the P=O impurities (resolution of the P=O impurities increased by approximately 350% under HFIP modified conditions), demonstrating a reduction in size dependent

separations compared to strong IP-RP HPLC. SAX HPLC analysis demonstrated the lowest dependence on size out of the three modes assessed. This is also demonstrated by the observation that P=O impurities did not elute with or near their PS length counterparts. These results are consistent with the results obtained in Chapter 3 that demonstrated that SAX HPLC exhibits the most sequence dependent and strong IP-RP HPLC is most size dependent for the analysis of OGNs.

### **5.2.1 Orthogonality assessments of 2D-LC workflows for analysis of PS OGNs.**

The second aim was to construct potential couplings of the HPLC modes to facilitate improved separations of PS OGNs in 2D-LC by assessing orthogonality. Normalised retention data of analytes within the cohort can be utilised for orthogonality assessment of two analytical conditions for 2D-LC [302], as well as indicate utility of mode couplings for separation of target impurities. The results of retention order experiments of section 5.2 highlight the difficulty and complexity of 1D separations of PS OGNs and their associated synthesis impurities. The increased complexity of chemistry within the sample sets, for example the presence of diastereoisomers and phosphodiester impurities, leads to difficulty when aiming to resolve all related impurities in a single dimension separation in comparison to separation of size variant unmodified OGNs (Chapter 4).

Orthogonality assessments were useful in designing 2D-LC workflows for the analysis of unmodified OGN size and sequence isomers (Chapter 4). Differences in selectivity between unmodified OGNs facilitated orthogonality metrics to be utilised in the design process of a 2D-LC analytical method. Selectivity differences were a reflection of differences in sequence chemistries of OGNs analysed. The sequences of OGN impurities and their corresponding FLP within the PS model sample sets are very similar in contrast to those in unmodified test sets. The base sequence has been maintained among the impurities (to better reflect the cohort of OGN sequences observed as impurities during solid phase synthesis). Overall hydrophobicity can be affected by structural differences (loss of nucleotides), differences in base composition (as a result of nucleotide loss or gain) and chemistry (OGNs containing phosphodiester bonds). Therefore the aim of orthogonality assessment is to calculate the independence of separation mechanisms between two dimensions of analysis. This was performed using the bin counting and minimum convex hull method as performed in Chapter 4 [300, 302]. Scatter plots are shown in Appendix 2, Figures A2.6-A2.7 and orthogonality values are displayed in Table 5.5.

**Table 5.5: Orthogonality measurements for OGNs of Model Set A and B using the bin counting and minimum convex hull methods.**

<b>Model A PS OGN sample Set</b>			
<b>Workflow</b>	<b><math>\Sigma</math> bins occupied</b>	<b>Orthogonality (bin counting method) (%)</b>	<b>Orthogonality (minimum convex hull method) (%)</b>
(strong IP-RP)-(SAX)	4	41.01	40
(SAX)-(HFIP modified IP-RP)	4	41.01	50
(strong IP-RP)-(HFIP modified IP-RP)	3	14.55	36
<b>Model B PS OGN sample Set</b>			
<b>Workflow</b>	<b><math>\Sigma</math> bins occupied</b>	<b>Orthogonality (bin counting method) (%)</b>	<b>Orthogonality (minimum convex hull method) (%)</b>
(strong IP-RP)-(SAX)	4	41.01	30
(SAX)-(HFIP modified IP-RP)	3	14.55	30
(strong IP-RP)-(HFIP modified IP-RP)	3	14.55	15

Due to a low number of analytes within the range, the amount of bins, and  $P_{max}$  value was 6 for the bin counting method (Equation 2.9). This led to vast differences in orthogonality value between numbers of bins occupied. Table 5.5 shows that the difference between occupation of 3 and 4 bins was 26.46%, which potentially skewed the visualisation of separation space coverage by this method. The application of the minimum convex hull method derived separation space coverage by the geometric location of periphery retention values within the space, and thus is potentially unbiased by number-of bins available to count.

For both methods, higher orthogonality measurements were observed with workflows incorporating SAX HPLC. This is expected as SAX HPLC demonstrated increased sequence based OGN separations in comparison to the other modes (Chapter 3). The caveat of incorporating SAX HPLC into a 2D-LC workflow for PS OGNs is that resolution is lower in comparison to that obtained during analysis of unmodified OGNs in test set 1 and 2 (Table 5.4 and Chapter 4, section 4.2). The key outcomes of this analysis are that all workflows are above the 10% threshold of non-orthogonality [289] with orthogonality ranging between 15-50% (depending on metric analysis method). Lower values of orthogonality reflect the pseudo-orthogonality occurring within separations due to the requirement of predominantly size dependent separations required in both dimensions when analysing PS OGNs – in order to prevent broad peaks.

Orthogonality metrics consider normalised retention times but ignore resolution between analytes. As a result, workflows that statistically appear more orthogonal may not be able to resolve analytes

experimentally. From analysis of PS OGN retention order data of these model sample sets, it became clear that a directed analytical approach was needed for target impurity analysis, due to the observations of these challenges.

Current 1D HPLC methods typically use strong IP-RP HPLC (in conjunction with TBuAA) [232, 237] to analyse PS OGNs. However, when using such approaches it is difficult to separate the P=O impurity as it often closely/co-elutes near or under the main peak of the FLP. This is demonstrated by analysis of model A and B sample sets where the resolution of P=O impurities from their fully PS counterparts is 0.34 (see Figure 5.1b and 5.2b). In this study, optimisation of an alternative mobile phase (using HFIP modified IP-RP) has enabled the P=O impurity to be resolved from the main peak. However it closely/co-elutes with other impurities in 1D HPLC- suggesting a 2D-LC workflow would assist in its characterisation. A targeted approach to utilising 2D-LC for the separation and analysis of this type of impurity would be to heart cut the FLP peak and resolve its P=O impurity in a 2<sup>nd</sup> dimension. Incorporating the need for orthogonal separations to resolve OGN impurities from the FLP, a targeted 2D-LC workflow was designed using (strong IP-RP)-(HFIP modified IP-RP) HPLC, aiming to characterise P=O impurities that co-elute in the 1<sup>st</sup> dimension by resolving and identifying them in a 2<sup>nd</sup> dimension. Optimisation of this proposed workflow would simplify the separation space in order to characterise target molecules- in this case, the P=O type impurity.

In summary, SAX HPLC, strong IP-RP HPLC and HFIP modified IP-RP HPLC were used to analyse two different PS OGN sequences and their associated manufacturing impurities. Chromatographic performance was analysed by assessing the resolution, selectivity and PWHH of the OGNs under the different chromatographic conditions. In addition, the orthogonality of the three combinations of the different chromatographic modes was also assessed using orthogonality metrics. The orthogonality metrics suggested that the optimal 2D-LC workflows include SAX HPLC in one of the two dimensions. However, low resolution was observed under SAX HPLC compared to other modes. Therefore, orthogonality metrics are only useful as indicators for the design of 2D-LC workflows and must be used alongside other performance data. In addition, the results showed that under strong IP-RP HPLC conditions, co-elution of the P=O impurity and the FLP was observed. The results of 1D-LC separations are consistent with previous studies using this IP-RP in conjunction with TuBAA [232, 237] and demonstrate a current analytical challenge experienced within industry. In this study, using HFIP modified IP-RP HPLC conditions, the P=O impurity was resolved from the FLP -highlighting particular advantages of this method to separate the P=O impurity from the FLP in a 1D HPLC analysis. To overcome the challenge of the P=O impurity closely/co-eluting with other impurities (such as the 5'-1 P=O or 5'-1) in HFIP modified IP—RP HPLC, use of 2D-LC analysis could further

simplify the separation space for characterisation. A (strong IP-RP)-(HFIP modified IP-RP) 2D-LC workflow was proposed for further optimisation and feasibility analysis.

## **Part B**

### **5.3 Mobile phase compatibility using 2D-LC for the analysis of PS OGNs.**

#### **5.3.1 Analysis of PS OGNs using (strong IP-RP)-(HFIP modified IP-RP) 2D-LC.**

The first aim was to analyse the feasibility of a 2D-LC workflow using strong IP-RP in the 1<sup>st</sup> dimension and HFIP modified IP-RP in the 2<sup>nd</sup> dimension. Feasibility was assessed by analysing the mobile phase compatibility between the two dimensions and the ability to retain analytes within the 2<sup>nd</sup> dimension. A 100 picomole sample of model B FLP was analysed in strong IP-RP HPLC conditions (5 mM TBuAA, 0.1  $\mu$ M Na<sub>4</sub> EDTA, 10-80% v/v MeCN) and was collected within a 200  $\mu$ L fraction (see Figure 5.4a). The area of the FLP peak was 48.17 mAU\*min at 87% relative area. Assuming a fractionation efficiency of approximately 80% (see Chapter 2, section 2.2.4.4) this would result in a total of 38.54 mAU\*min area in a 2<sup>nd</sup> dimension analysis. 20  $\mu$ L of the fraction was re-analysed in a 2<sup>nd</sup> dimension under HFIP modified IP-RP HPLC (100 mM TEAA, 40 mM HFIP 0.1 mM Na<sub>4</sub> EDTA, 0-25% v/v MeCN) conditions. The results are shown in Figure 5.4b and show that there is a large injection peak followed by the analyte peak (peak area of 1.14 mAU\*min), which is less than the expected 38.54 mAU\*min for a 20  $\mu$ L sample. These results demonstrate a reduction of retention of the analyte within the 2<sup>nd</sup> dimension. Under strong IP-RP HPLC conditions, model B FLP elutes at approximately 50% v/v MeCN within the mobile phase, this high concentration of MeCN as diluent for the 2<sup>nd</sup> dimension prevents OGNs retaining to the stationary phase.

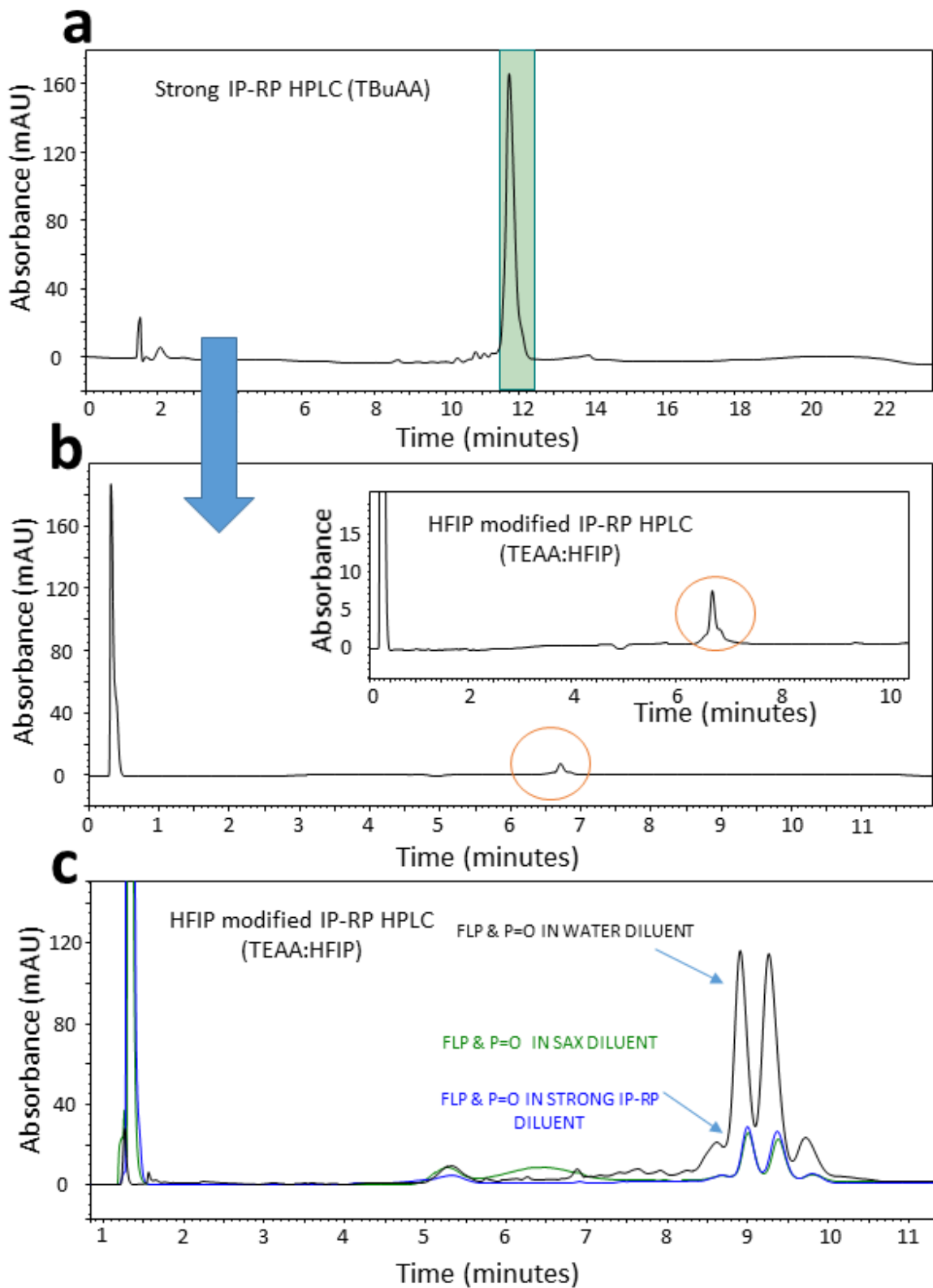


**Figure 5.4: Feasibility assessment for (strong IP-RP)-(HFIP modified IP-RP) 2D-LC of PS OGNs.** **a:** PS OGN Model B FLP analysis under strong IP-RP using 5 mM TBuAA, 0.1  $\mu\text{M}$   $\text{Na}_4\text{EDTA}$  and 27.5-73%  $\text{v/v}$  MeCN gradient from 1-15 min. 50 picomole samples analysed at 0.2 ml/min and 30  $^\circ\text{C}$  using a DNAPac RP column. Whole peak fractionation for reanalysis in a 2<sup>nd</sup> dimension. **b:** 2<sup>nd</sup> dimension feasibility analysis of Ps OGN Model B FLP in HFIP modified IP-RP HPLC using 100 mM TEAA, 40 mM HFIP, 0.1 mM  $\text{Na}_4\text{EDTA}$  and 11.25-22.5%  $\text{v/v}$  MeCN gradient from 1-15 min. 30 picomole samples analysed at 0.4 ml/min and 70  $^\circ\text{C}$  using an Accucore C18 column. Inset-zoomed view. **c:** PS OGN Model A FLP and P=O analysed under HFIP modified IP-RP HPLC using 100 mM TEAA, 40 mM HFIP, 0.1 mM  $\text{Na}_4\text{EDTA}$  and 11.25-17.5%  $\text{v/v}$  MeCN gradient from 1-15 min. 100 picomole samples analysed at 0.2 ml/min and 75  $^\circ\text{C}$  using a DNAPac RP column. OGNs diluted in  $\text{H}_2\text{O}$ , strong IP-RP and SAX eluents.

Aiming to analyse OGN retention further, PS OGNs in a range of diluents/eluents were analysed in HFIP modified IP-RP HPLC. Model A and B FLP and P=O impurities were prepared in water, strong IP-RP diluent (5 mM TBuAA, 0.1  $\mu$ M Na<sub>4</sub> EDTA and 50% v/v MeCN) and SAX diluent (20 mM tris with 200 mM NaClO<sub>4</sub> pH 11.5) and OGN peak areas were compared (see Figure 5.4c). The results show that 100 picomoles of sample in water results in a net OGN peak area of 63.877 mAU\*min. OGNs in strong IP-RP and SAX diluents (eluting conditions of 1<sup>st</sup> dimension) demonstrated a net peak area of 12.67 mAU\*min and 11.05 mAU\*min respectively. This highlights that retention is reduced by approximately 80% for both eluting conditions and aligns with results shown in Figure 5.4b. In addition, this suggests that a workflow using SAX HPLC in the 1<sup>st</sup> dimension would not be feasible under these conditions due to the acetonitrile within the mobile phase (a constituent used to reduce secondary interactions and improve peak shape). These results suggest that employing a 2D-LC method using (strong IP-RP in conjunction with TBuAA)-(HFIP modified IP-RP) or (SAX with MeCN)-(HFIP modified IP-RP) HPLC for analysis of PS OGNs is not feasible as the 1<sup>st</sup> dimension is not compatible with the 2<sup>nd</sup> dimension creating a need for a redesign of the workflow. Continuing with the idea that simplification of the separation space and resolution of the P=O impurity is possible when coupling strong IP-RP HPLC and HFIP modified IP-RP HPLC, it was proposed that the workflow could be rearranged to (HFIP modified IP-RP HPLC 1<sup>st</sup> dimension)-(strong IP-RP HPLC 2<sup>nd</sup> dimension). This has been proposed as the eluting conditions of HFIP modified IP-RP are at approximately 14% v/v MeCN and would therefore allow retention in a 2<sup>nd</sup> dimension.

### **5.3.2 Analysis of PS OGNs using (HFIP modified IP-RP)-(strong IP-RP) 2D-LC.**

To test if eluting conditions of the 1<sup>st</sup> dimension (using HFIP modified IP-RP) would affect retention in the 2<sup>nd</sup> dimension (using strong IP-RP), PS OGNs provided by GlaxoSmithKline were analysed in diluents mimicking different elution conditions. OGNs were prepared in water, HFIP modified IP-RP (100 mM TEAA, 40 mM HFIP 0.1 mM Na<sub>4</sub> EDTA, 0-25% v/v MeCN) and SAX HPLC (20 mM Tris, 0-400 mM NaClO<sub>4</sub>, pH 11.5 with 20% v/v MeCN) and peak areas were compared (see Figure 5.5). The results show that the net peak area of analytes in water diluent is 23.49 mAU\*min compared to 3.11 mAU\*min in SAX eluent and 26.28 mAU\*min in HFIP IP-RP eluent. These results indicate that SAX diluent results in significant loss of signal intensity (87%). In contrast, using HFIP modified IP-RP diluent does not result in any signal loss in the 2<sup>nd</sup> dimension and OGN retention is not affected using (HFIP modified IP-RP)-(strong IP-RP) 2D-LC.

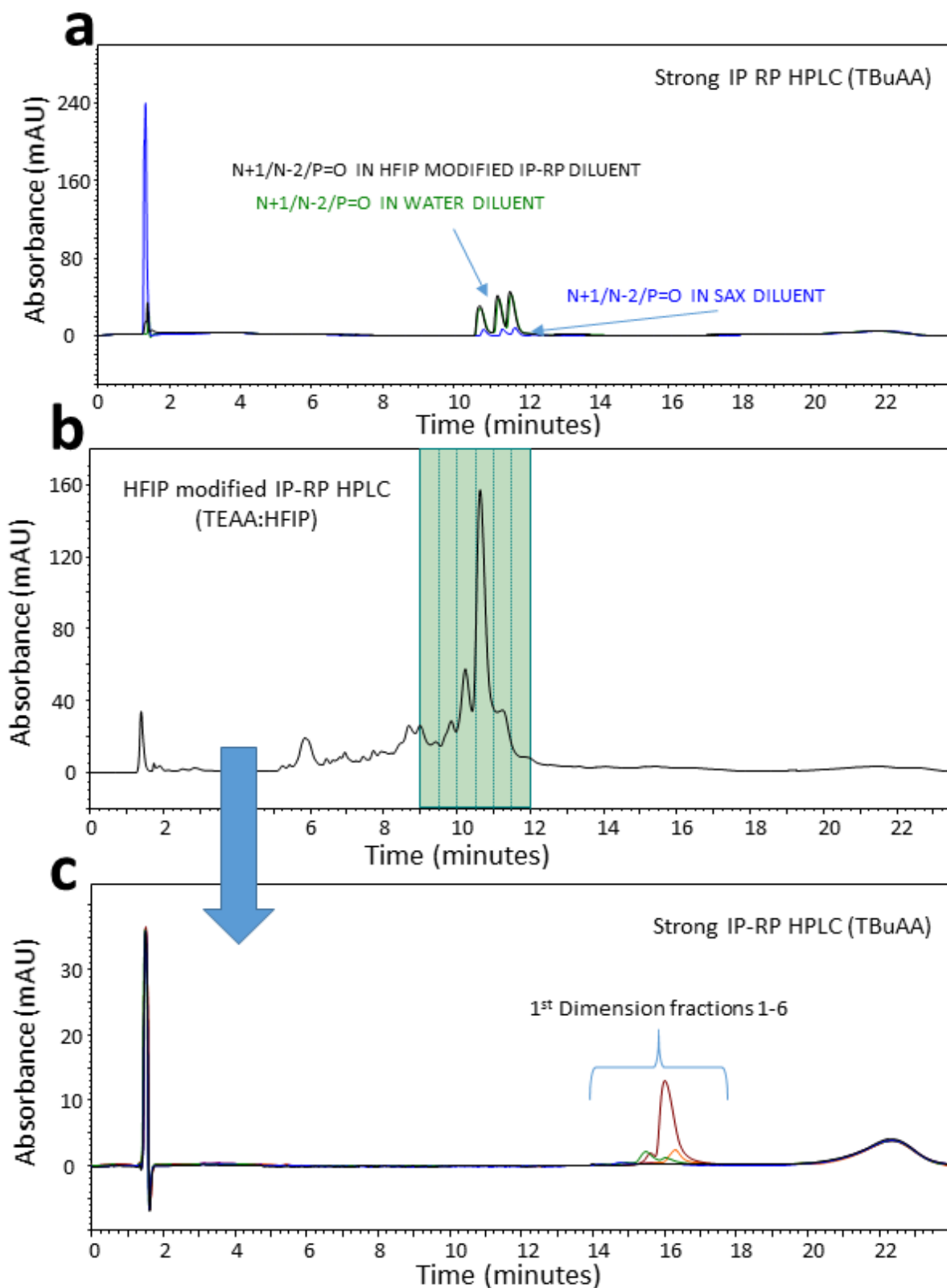


**Figure 5.5: Feasibility assessment for (HFIP modified IP-RP)-(strong IP-RP) 2D-LC of PS OGNs.** **a:** GSK PS OGN impurities N+1, N-2 and P=O analysed in strong IP-RP using 5 mM TBuAA, 0.1  $\mu\text{M}$   $\text{Na}_4$  EDTA and 34.5-59%  $\text{v/v}$  MeCN gradient from 1-15 min. Analysis at 0.2 ml/min and 50  $^\circ\text{C}$  using a DNAPac RP column. 50 picomole samples were diluted in  $\text{H}_2\text{O}$ , HFIP modified IP-RP and SAX eluents. **b:** 1<sup>st</sup> dimension feasibility analysis of PS OGN Model A FLP in HFIP modified IP-RP using 100 mM TEAA, 40 mM HFIP, 0.1 mM  $\text{Na}_4$  EDTA and 11.25-17.5%  $\text{v/v}$  MeCN gradient from 1-15 min. 100 picomole sample analysed at 0.2 ml/min, 75  $^\circ\text{C}$  and fractionated using a DNAPac RP column. **c:** Analysis of fraction 1-6 in a 2<sup>nd</sup> dimension using strong IP-RP under 5 mM TBuAA, 0.1  $\mu\text{M}$   $\text{Na}_4$  EDTA and 34.5-45%  $\text{v/v}$  MeCN gradient from 1-15 min. Fractions analysed at 0.2 ml/min and 50  $^\circ\text{C}$  using a DNAPac RP column.

The next aim was to test feasibility of a 2D-LC workflow for the analysis of PS OGNs. Using the rearranged workflow of (HFIP modified IP-RP)-(Strong IP-RP), a 100 picomole sample of Model A FLP mixed with each manufacturing impurity at 1.5% concentration was analysed in the offline 2D-LC workflow. The analysis of model A is shown in Figure 5.5b. Consistent with the previous analysis (Figure 5.5a), no significant loss in signal intensity or problems of OGN retention was observed, highlighting the suitability of a 2D-LC method using (HFIP modified IP-RP)-(strong IP-RP) HPLC from the analysis of PS OGNs.

#### **5.4 Optimisation of offline 2D-LC and a reference mapping strategy for 2D-LC method development.**

##### **5.4.1 Offline 2D-LC of PS OGN test sets in conjunction with reference mapping.**

Following confirmation of mobile phase compatibility of a (HFIP-modified IP-RP)-(strong IP-RP) 2D-LC method for the separation of PS OGNs, the workflow required further optimisation to include a reference OGN mapping strategy (as described in Chapter 4) and demonstrate the benefit of using 2D-LC to resolve closely co-eluting impurities from the FLP. The experimental aims of the development of an offline 2D-LC workflow for the analysis of PS OGN models were to confirm elution order and identify OGNs from each fraction from the 1<sup>st</sup> dimension separation (HFIP modified IP-RP HPLC) using reference standards in the 2<sup>nd</sup> dimension analysis (strong IP-RP HPLC). The reference mapping strategy would be confirmed with LC-MS analysis of the 1<sup>st</sup> dimension fractions.

The first aim was to analyse the FLP combined with low levels of manufacturing impurities to confirm the elution order and assess any further co-elution due to concentration differences in the 1<sup>st</sup> dimension analysis (HFIP modified IP-RP HPLC). 1000 picomole samples of Model A and B PS OGNs at 91% FLP concentration with an addition of 1.5% concentration of each impurity OGN in sample were analysed under HFIP modified IP-RP HPLC conditions (100 mM TEAA, 40 mM HFIP 0.1 mM Na<sub>4</sub> EDTA, 90-25% v/v MeCN). 15 picomole reference OGN samples of impurities were concurrently analysed to confirm elution order within the separation and matched to data obtained during equimolar separations. The results for Model A OGN and its associated impurities are shown in Figure 5.6a within the 1<sup>st</sup> dimension separation chromatogram. The data shows that the shortmers 5'-3 and 5'-2 are earliest co-eluters. The phosphodiester impurities co-elute next to the

main FLP peak, while the 5'-1 shortmer impurity co-elutes under it. The N+1 impurity is last to elute, shouldering the FLP main peak. These results are consistent with previous studies (see section 5.2). Due to co-elution, there is potential for a 2D-LC separation to resolve co-eluting OGNs using strong IP-RP HPLC. The results for Model B and its associated impurities is shown in Figure 5.6b within the 1<sup>st</sup> dimension separation chromatogram. The elution order of the OGNs demonstrates a slightly different selectivity within this sample set. The 5'-1 P=O elutes first, in between the 5'-3 and 5'-2 impurities. The 5'-1 and P=O closely elute within the separation and the FLP and N+1 OGNs are last to elute. There is increased selectivity and thus resolution of the impurities from each other within the separation. In both 1<sup>st</sup> dimension chromatograms, the retention time of the 15 picomole reference OGNs varies from the 1000 picomole sample, this could be an effect of oversaturating the column with 1000 picomoles of sample, thereby shifting retention time [214]. To better identify peak occupancies, spiking experiments were performed for both Model A and B and are shown in Appendix 2, Figure A2.8. The close eluting peak to the left of the main peak is confirmed to be the P=O and 5'-1 P=O for model A and the P=O and 5'-1 impurities for model B.

Another aim of optimising the offline 2D-LC workflow was to map and identify OGN peaks in the 2<sup>nd</sup> dimension using the reference mapping strategy outlined in Chapter 4. This strategy utilises concurrent single reference OGN analyses to map peaks of the 2<sup>nd</sup> dimension in the 2D-LC workflow. Reference samples of the FLP and manufacturing impurities of Model A FLP were prepared using a diluent of 100 mM TEAA, 40 mM HFIP and 14.4% v/v MeCN. These were analysed at 15 picomole and 80 picomole sample amounts for the manufacturing impurities and FLP respectively. Concurrently, 20 µL of each fraction from the 1<sup>st</sup> dimension analysis was analysed in the 2<sup>nd</sup> dimension of strong IP-RP HPLC (5 mM TBuAA, 0.1 µM Na<sub>4</sub> EDTA and 10-80% v/v MeCN).

The results for model A PS OGN 2D-LC analysis is shown in Figure 5.6a. The results show that the 5'-3 and 5'-2 reference OGNs aligned to peaks within earlier fractions and demonstrate increased peak capacity within 2D-LC (for these impurities) as they co-elute under HFIP modified IP-RP conditions. As the P=O/FLP and 5'-1 P=O/5'-1 OGNs co elute under strong IP-RP conditions, there is retention time alignment among multiple reference OGNs. Fraction 3 in the 1<sup>st</sup> dimension, may sample a small amount of the main peak, potentially sampling some of the FLP OGN within the fraction. A more accurate fractionation approach (such as use of fraction loops and sample docking valve) would avoid sampling the FLP, however, due to a lack of baseline resolution, FLP sampling is almost unavoidable. The later eluting peak of fraction 4 aligns with the N+1 reference OGN. Model B separation by offline 2D-LC was also performed (see Figure 5.6b).

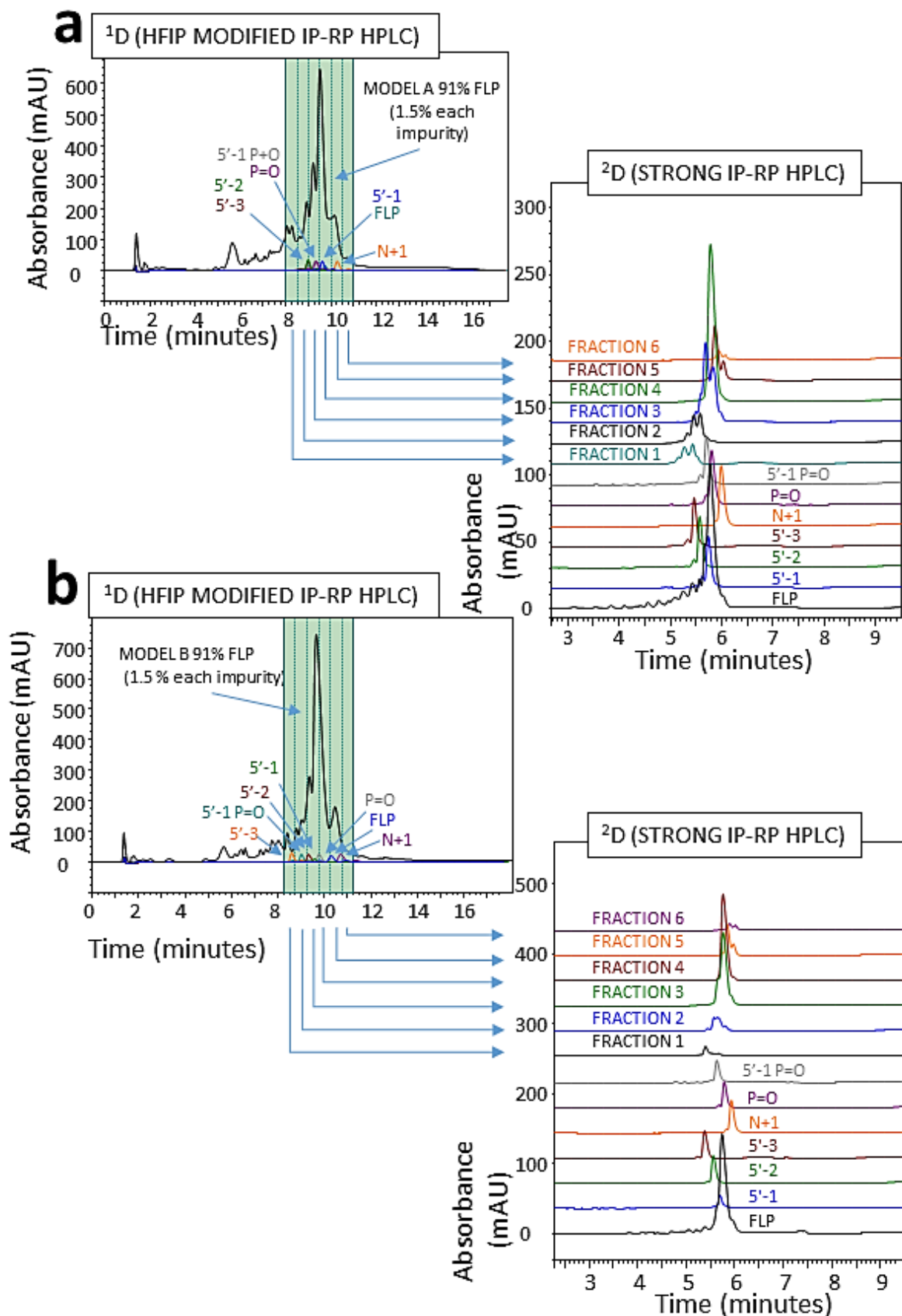


**Figure 5.6: Offline HFIP modified IP-RP to strong IP-RP 2D-LC analysis of Model A and B PS OGNs.** 1<sup>st</sup> dimension using 100 mM TEAA, 40 mM HFIP, 0.1 mM Na<sub>4</sub> EDTA and 11.25-17.5% v/v MeCN gradient from 1-15 min. 1000 picomole sample analysed at 0.2 ml/min and 75 °C and fractionated, using a DNAPac RP column. 2<sup>nd</sup> dimension using 5 mM TBuAA, 0.1 μM Na<sub>4</sub> EDTA and 34.5-59% v/v MeCN gradient from 1-15 min. Analysis at 0.2 ml/min and 50 °C using a DNAPac RP column. 15 picomole samples of reference OGNs were analysed in the 1<sup>st</sup> dimension to track elution order. **a:** Offline 2D-LC analysis of Model A PS OGN sample set with FLP at 91% sample amount and impurities at 1.5 % sample amount. **b:** Offline 2D-LC analysis of Model B PS OGN set with FLP at 91% sample amount and impurities at 1.5 % sample amount.

The results show lower resolution of analytes within the 2<sup>nd</sup> dimension (in comparison to model A analysis) due to close elution of the 5'-2 and 5'-1 P=O impurities creating a broad peak in fraction 2. The results from analysis of fraction 3 show multiple alignment of reference OGNs, which made peak assignment difficult.

An increase in peak capacity was observed during 2D-LC analysis of model A PS OGN where co-eluting peaks of the 1<sup>st</sup> dimension resolved within the 2<sup>nd</sup> dimension analysis. However, demonstration of an increase in peak capacity using the 2D-LC workflow for model B PS OGN and its manufacturing impurities was difficult to determine. Some fraction peaks were difficult to align to reference standards due to the co-eluting nature of some impurities within strong IP-RP HPLC, for example, the P=O and FLP OGN references showed similar retention times. The results show that the reference mapping needed to be further interrogated and analysed by LC-MS to further understand which OGN impurities were in each fraction of the 1<sup>st</sup> dimension.

#### **5.4.2 Mass spectrometry analysis of first dimension fractionation of PS OGNs.**

Due to the difficulties in characterising the components in the 2<sup>nd</sup> dimension analysis using reference standards of the PS OGNs, LC-MS analysis of the 1<sup>st</sup> dimension fractions was performed. Samples were prepared at 91% concentration FLP and an additional 1.5% of each impurity with a total sample amount of 1000 picomoles. The 1<sup>st</sup> dimension HPLC separations are shown in Figure 5.7 a-b.

Fractions 1-6 of the model A fractionation were analysed by strong IP-RP LC-MS. The identification of OGNs within each fraction by charge deconvolution was confirmed by identifying monoisotopic m/z values for the 3<sup>-</sup> and 4<sup>-</sup> charge states of each OGN. To further confirm the presence of OGNs within each fraction, identity confirmation was performed by interrogating each mass spectrum obtained during data acquisition, this would combat loss of signal via the integration of mass spectra over a given time period (in this case- across a chromatographic peak). Figure 5.7c shows the isotopic envelope for the 3<sup>-</sup> charge state of the 5'-1 impurity identified in fraction 3. The green arrow indicates the monoisotopic m/z peak at 2017.241, which corresponds to a mass of 6054.747 Da.

Fractions 1-6 of Model B were also analysed using this approach and the isotopic envelope of the 3-charge state of the P=O impurity identified in fraction 3 (Figure 5.7d). Table 5.6 shows the identified OGNs based on the LC-MS analysis of each fraction of two replicate analyses of model A.

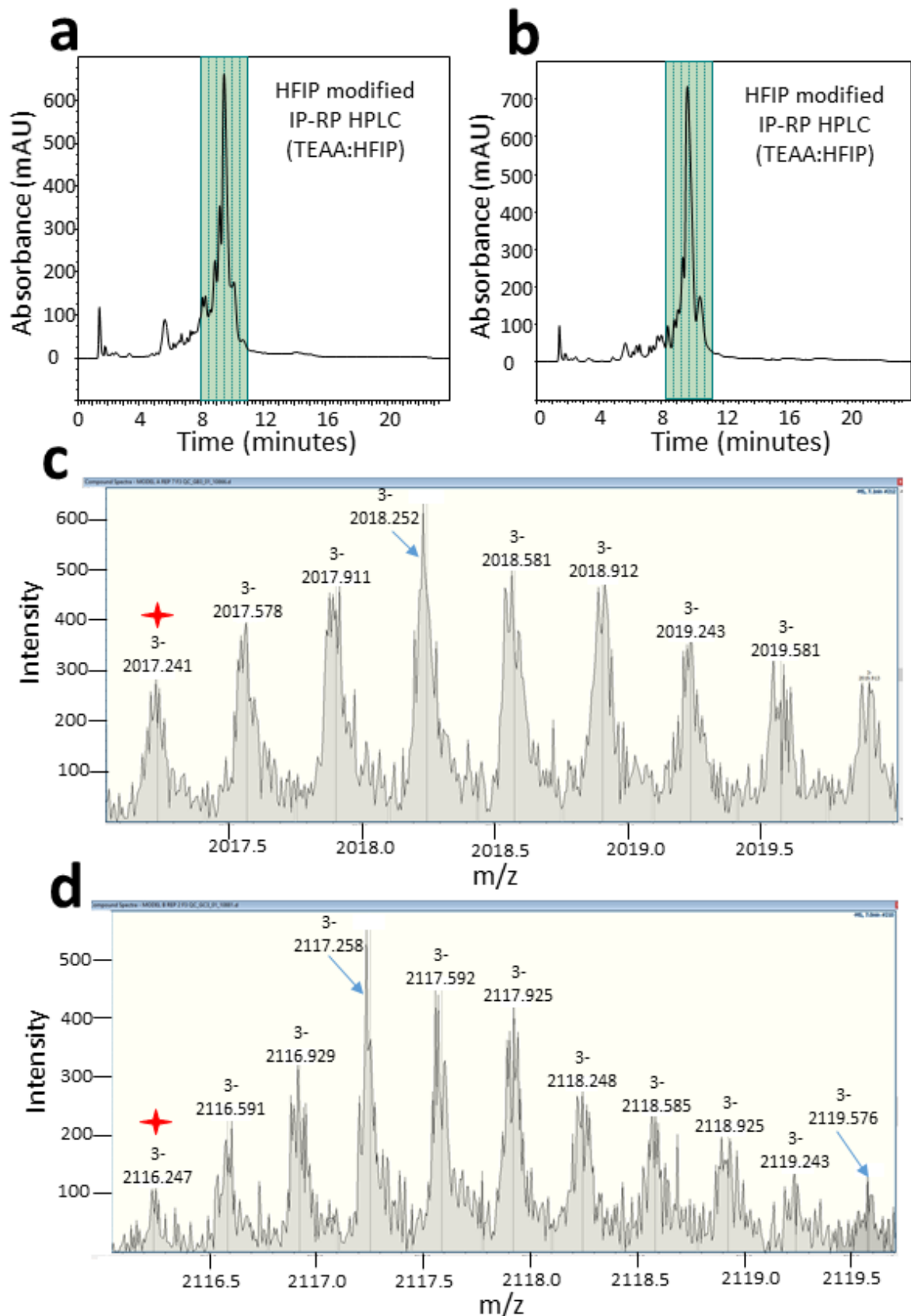


**Figure 5.7: LC-MS analysis of model A and B PS OGN 1<sup>st</sup> dimension fractions.** PS OGNs sample sets of 91% FLP and additional 1.5% each imp were fractionated (HFIP modified IP-RP using 100 mM TEAA, 40mM HFIP, 0.1 mM Na<sub>4</sub>EDTA and 11.25-17.5% v/v MeCN gradient from 1-15 min. 1000 picomole samples analysed at 0.2 ml/min and 75 °C using a DNAPac RP column) and re-analysed by strong IP-RP LC-MS (method explained in chapter 2). **a:** Model A fractionation using HFIP modified IP-RP HPLC **b:** Model B fractionation using HFIP modified IP-RP HPLC **c:** Mass spectrum isotopic envelope of Model A 5'-1 impurity 3- charge state within fraction 3 (monoisotopic ion noted by red star). **d:** Mass spectrum isotopic envelope of Model B P=O impurity 3- charge state within fraction 3 (monoisotopic ion noted by red star).

Although chromatographic peaks are observed in fraction 1 and 6 using LC-UV detection, no identification was possible from the MS analysis. This is likely due to low efficiency of ionisation observed using IP-RP LC-MS, where the ion pair reagent suppresses ionisation of analytes. Low levels of OGN ions were not detected as a result of being below the limits of detection on this instrument. The MS analysis of fraction 2 complements the 2D-LC analysis and reference mapping (see figure 5.6a which identified the 5'-3 and 5'-2 impurities).

The LC-MS analysis of fraction 3 identified a number of OGN masses, which are shown in Table 5.6 in increasing retention time order. A  $m/z$  of 2123.609 was the peak of highest intensity in fraction 5 corresponding to a mass of 6373.851 Da (mass difference of 14.227 Da), which is proposed to be an adducted form of the FLP. This is possibly a result of photo-oxidation during the 1<sup>st</sup> dimension analysis [322], where oxygen is adducted to the OGN. The proposition of photooxidation to the FLP is consistent with previous LC-MS data of the FLP OGN where the N [+adduct] is in low abundance (without the prior UV analysis the fractionated OGNs had been subject to). Photo-oxidation could be avoided with a robust fractionation process in the 1<sup>st</sup> dimension without UV detection. The N+1 impurity is identified in fraction 5, however the 4<sup>-</sup> charge state ion dominated within the mass spectra, which is likely as a result of the mass range limitations of the analysis. The LC-MS data provides more insight than the OGN reference mapping strategy using HPLC alone and confirms that the approach is unable to map impurities eluting within the 2<sup>nd</sup> dimension due to co-elution of OGNs in strong IP-RP HPLC.

The model B PS OGN and associated manufacturing impurities were also fractionated in HFIP modified IP-RP conditions and then analysed by LC-MS. Table 5.7 shows the identified OGNs based on the LC-MS analysis of two replicate samples. The LC-MS analysis identified shortmer impurities within earlier fractions, and the N+1 impurity was observed in fraction 5. Consistent with the data from analysis of the model A PS OGN, the most abundant peaks related to a mass larger than the FLP. The observed 3<sup>-</sup> charge state of which was  $m/z$  of 2126.589 within fraction 5, relating to an OGN mass of 6382.791 Da (mass adduction of 15.188 Da). The P=O and 5'-1 P=O impurities were identified in fractions 2 and 3, demonstrating increased selectivity for these impurities within the 1<sup>st</sup> dimension separation under HFIP modified IP-RP HPLC conditions.

Table 5.6: LC-MS identification OGN masses within each fraction of the 1<sup>st</sup> dimension analysis of PS OGN Model A and its associated manufacturing impurities added at 1.5% total sample concentration.

Fraction	OGN Observed Monoisotopic Mass (Da)	OGN Theoretical Monoisotopic Mass (Da)	Observed Monoisotopic m/z of [M-3H] 3 <sup>-</sup>	Theoretical Monoisotopic m/z of [M-3H] 3 <sup>-</sup>	Identity Assignment
1	n/a	n/a	n/a	n/a	n/a
2	5429.691	5429.555	1808.889	1808.844	5 <sup>-</sup> -3
	5734.65	5734.578	1910.542	1910.518	5 <sup>-</sup> -2
3	5429.709	5429.555	1808.895	1808.844	5 <sup>-</sup> -3
	5734.689	5734.578	1910.555	1910.518	5 <sup>-</sup> -2
	6038.727	6038.624	2011.901	2011.867	5 <sup>-</sup> -1 P=O
	6054.747	6054.601	2017.241	2017.192	5 <sup>-</sup> -1
	6344.85	6343.647	2113.942	2113.541	P=O
	6359.808	6359.624	2118.928	2118.867	FLP
4	6054.777	6054.601	2017.251	2017.192	5 <sup>-</sup> -1
	6359.811	6359.624	2118.929	2118.867	FLP
5	6373.851	Unknown	2123.609	Unknown	FLP[+adduct]
	6679.736	6679.647	1668.926	1668.904	N+1 (4 <sup>-</sup> )
6	n/a	n/a	n/a	n/a	n/a

Table 5.7: LC-MS identification of OGN masses within each fraction of the 1<sup>st</sup> dimension analysis of PS OGN Model B and its associated manufacturing impurities added at 1.5% total sample concentration.

Fraction	OGN Observed Monoisotopic Mass (Da)	OGN Theoretical Monoisotopic Mass (Da)	Observed Monoisotopic m/z of [M-3H] 3 <sup>-</sup>	Theoretical Monoisotopic m/z of [M-3H] 3 <sup>-</sup>	Identity Assignment
1	5382.642	5382.528	1793.206	1793.168	5 <sup>-</sup> -3
2	5702.610	5702.551	1899.862	1899.842	5 <sup>-</sup> -2
	6031.668	6031.603	2009.548	2009.526	5 <sup>-</sup> -1 P=O
3	6351.738	6351.626	2116.238	2116.201	P=O
	6367.824	6367.603	2121.600	2121.527	FLP
4	6367.785	6367.603	2121.587	2121.527	FLP
5	6382.791	Unknown	2126.589	Unknown	FLP[+adduct]
	6673.854	6672.626	2223.610	2223.201	N+1
6	n/a	n/a	n/a	n/a	n/a

In summary, evaluation of a 2D-LC workflow of strong IP-RP to HFIP modified IP-RP 2D-LC resulted in incompatibility between the eluting conditions of the 1<sup>st</sup> dimension and analysis in the 2<sup>nd</sup> dimension. The method was reversed and tested again to investigate if a simple reversal would circumnavigate mobile phase incompatibility issues. Retention in the second dimension of strong IP-RP was maintained within a workflow of HFIP modified IP-RP to strong IP-RP 2D-LC. The low level (added at 1.5% concentration) impurities were observed in both the first and second dimension, however, co-elution events occurred. Transitioning from 1D to 2D HPLC analysis increased peak capacity and the 5'-3 and 5'-2 shortmers were identified by the reference mapping strategy. However, due to the co-elution of other impurities under strong IP-RP HPLC conditions, it was difficult to identify other impurities.

## **Part C**

### **5.5 Optimisation of an online heart-cut 2D-LC workflow for analysis of PS OGNs.**

To develop an online heart-cut 2D-LC method for the analysis of PS OGNs, the HPLC equipment was set up according to Chapter 2, Figure 2.2. Online 2D-LC using HFIP modified IP-RP HPLC to strong IP-RP HPLC was performed to analyse model A and B PS sample sets. The online workflow aimed to reproduce data obtained during offline 2D-LC of the analytes (see section 5.4) in an automated online process. Specifically, 1000 picomole samples of Model A and B were separated and fractionated into six 100  $\mu$ L fractions within the 1<sup>st</sup> dimension (100 mM TEAA, 40 mM HFIP, 0.1 mM Na<sub>4</sub> EDTA, 0-25% v/v MeCN), collected into micro vials stored within the auto-sampler via the fractionation valve. Within the method, the mobile phase was switched to the 2<sup>nd</sup> dimension automatically. 20  $\mu$ L of each fraction was analysed in the 2<sup>nd</sup> dimension of strong IP-RP-LC (5 mM TBuAA, 0.1  $\mu$ M Na<sub>4</sub> EDTA, 10-80% v/v MeCN) alongside 15 picomole reference samples of associated manufacturing impurities and a FLP reference standard of 100 picomoles. Reference OGNs were prepared in a diluent of 80 mM TEAA, 40 mM HFIP, 0.1 Na<sub>4</sub> EDTA and 14.4% v/v MeCN to mimic eluting conditions of the 1<sup>st</sup> dimension. For each model OGN set, two replicate analyses were performed using online heart-cut 2D-LC.

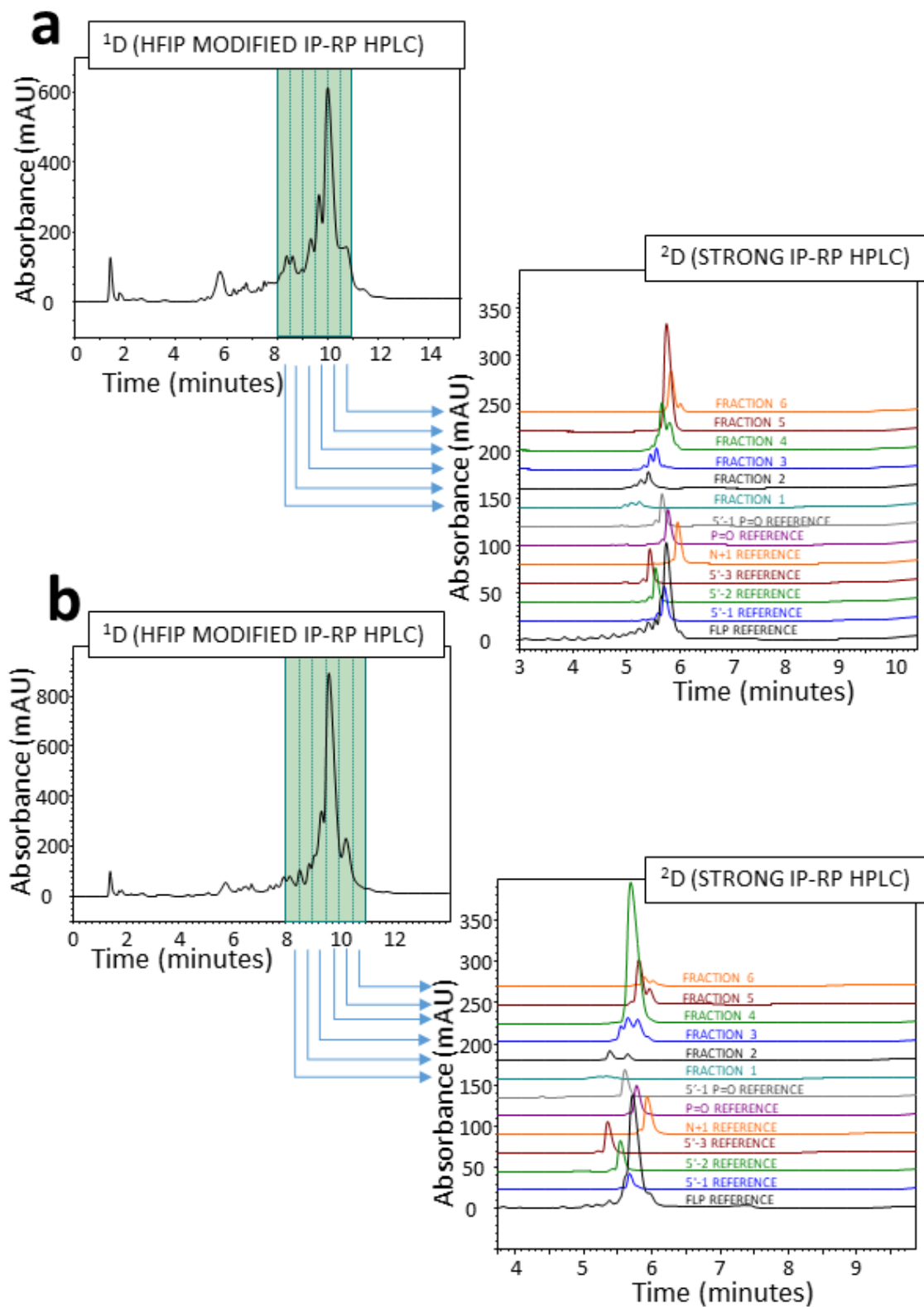


**Figure 5.8:** Online heart-cut HFIP modified IP-RP to strong IP-RP 2D-LC analysis of PS OGN Model A and B samples. 1<sup>st</sup> dimension HFIP modified IP-RP HPLC using 100 mM TEAA, 40 mM HFIP, 0.1 mM Na<sub>4</sub> EDTA and 11.25-17.5% v/v MeCN gradient from 1-15 min. 1000 picomole sample analysed at 0.2 ml/min, 75 °C and fractionated, using a DNAPac RP column. 2<sup>nd</sup> dimension strong IP-RP using 5 mM TBuAA, 0.1 μM Na<sub>4</sub> EDTA and 34.5-59% v/v MeCN gradient from 1-15 min. Analysis at 0.2 ml/min and 50 °C using a DNAPac RP column. 15 picomole samples of reference OGNs were analysed in the 1<sup>st</sup> dimension to track elution order. **a:** Online 2D-LC performed on Model A PS OGN sample set with FLP at 91% sample amount and impurities at 1.5 % sample amount. **b:** Online 2D-LC performed on Model B PS OGN sample set with FLP at 91% sample amount and impurities at 1.5 % sample amount.

The online 2D-LC of PS model A sample set is shown in Figure 5.8a. The results complement data obtained during offline 2D-LC analysis of the sample set (section 5.4) demonstrating that an automated 2D-LC method can be set-up using this chromatographic equipment design. The 5'-3 reference standard aligns in retention time with peaks in fraction 2 and 3. The 5'-2 reference standard aligns with peaks in fractions 3 and 4. The N+1 reference OGN aligns with the late eluting peak in fraction 6, and this shows that the reference mapping strategy was able to identify OGN impurities 5'-3, 5'-2 and N+1 within the 2D-LC method. Close and co-elution of the remaining reference standards (demonstrating  $R_s < 1.2$ ) in the sample set prevented the identification of all peaks within the 2D-LC workflow by reference standard mapping. This demonstrates that for these analytes, the reference mapping strategy was not sufficiently able to identify impurities without the assistance of MS detection. The online 2D-LC analysis of the PS model B sample is shown in Figure 5.8b, and as with the online analysis of the model A sample set, the model B sample set online 2D-LC results are consistent with the data obtained in offline 2D-LC. The 5'-1 P=O reference OGN is identifiable in fraction 2, as is the 5'-3 reference standard. Allocation of peak identities in fraction 3 is difficult to due to co-elution in the 2<sup>nd</sup> dimension analysis. The N+1 impurity was identified in later fractions of the 1<sup>st</sup> dimension (fractions 5 and 6), and these results also confirm that for the impurities of the model B OGN, the reference mapping strategy could not identify the full cohort of impurities without MS detection and a simplification of the analytical complexity was not met by relying on reference mapping using 2D-LC UV detection.

In summary, an online heart-cut 2D-LC workflow was optimised and performed for the analysis of PS OGNs and their associated manufacturing impurities. The results demonstrate that the mapping strategy used in the second dimension is not comprehensive in identifying the FLP, 5'-1, P=O and 5'-1 P=O OGNs due to co and close elution in strong IP-RP HPLC. In reference to the Model A 5'-2 and 5'-3 impurities, an increase of peak capacity was observed in 2D-LC (in comparison to 1D HPLC) as they co-elute in HFIP modified IP-RP HPLC conditions.

## 5.6 Conclusions.

A range of chromatographic modes were used for 1D HPLC analysis of PS OGNs and their associated manufacturing impurities. Analysis of PWHH, selectivity and resolution of the OGNs were used to compare separations between different modes. A key outcome from this work is the observation that HFIP modified IP-RP HPLC was able to resolve the P=O impurity from the FLP, which is useful as

this impurity co-elutes under other IP-RP conditions (for example IP-RP in conjunction with TBuAA). Although SAX demonstrates more sequence dependency during OGN separation, poor peak shape and low resolution was observed when analysing these PS OGNs. Use of SAX within 2D-LC of oligonucleotides may be better utilised for OGNs exhibiting narrower peaks, such as those with lower levels of phosphorothioation.

The orthogonality of (strong IP-RP)-(SAX), (SAX)-(HFIP modified IP-RP) and (strong IP-RP)-(HFIP modified IP-RP) 2D-LC workflows was analysed. Although methods with a SAX dimension showed higher orthogonality, chromatographic resolution was lowest in this mode. Therefore, a focus was placed on the ability to separate and characterise the P=O impurity using the (strong IP-RP)-(HFIP modified IP-RP) 2D-LC method was chosen for development. A (strong IP-RP)-(HFIP modified IP-RP) 2D-LC workflow was initially assessed, however the modes were not compatible and resulted in a lack of retention of the OGN in the 2<sup>nd</sup> dimension. This challenge could have been overcome with sample processing prior to analysis in the 2<sup>nd</sup> dimension. However, this would detract from the aim of developing an online automated 2D-LC method. Therefore the modes were swapped to test a (HFIP modified IP-RP)-(strong IP-RP) workflow for feasibility. The OGNs retained in the 2<sup>nd</sup> dimension, which indicated compatibility between mobile phases and so the method was developed further in offline 2D-LC mode.

A series of different PS OGNs and their manufacturing impurities (model A and B) were separated by an offline 2D-LC method alongside reference OGNs to develop a mapping strategy for online 2D-LC. The first dimension fractions were also analysed by LC-MS to identify OGNs within each 2<sup>nd</sup> dimension. The mapping strategy demonstrated capability to map shortmer and longmer impurities within the 2<sup>nd</sup> dimension. However, due to co-elution and close elution in the strong IP-RP 2<sup>nd</sup> dimension, this approach was not able to identify the P=O impurities, 5'-1 shortmer and FLP as separate peaks. Data from LC-MS analysis confirmed these findings.

The 2D-LC analytical method was developed further for online analysis of PS OGNs. The results were in agreement with offline 2D-LC data and highlighted the ambiguity in the reference mapping strategy. A way of optimising the method further would be to analyse reference OGNs within the 1<sup>st</sup> dimension separation (at higher concentration), as well as the second. This could improve the number of impurities that a reference mapping strategy could identify. In addition, this work was performed on one type of stationary phase (DNAPac RP) to enable separation at elevated temperatures. Alternative stationary phases may provide alternative selectivity to resolve more impurities within each dimension, for example the 5'-1 impurity from the FLP. Further options are discussed in Chapter 7.

## Chapter 6: Optimisation of two-dimensional liquid chromatography for the analysis of OGN therapeutics.

### Abstract.

As new OGN therapeutics continue to be developed, increasing amounts of chemical modifications are used, which increases OGN chemical complexity and reduces chromatographic efficiency. The aim of this Chapter was to develop and utilise 2D-LC methods for the analysis of an unconjugated and conjugated OGN therapeutics from GSK. These OGNs contained a mixture of PS, 2'-O-MOE and GalNac conjugation modifications. 2D-LC workflows that rely on mapping strategies rather than MS for the analysis of OGN manufacturing impurities have not been previously attempted.

Initial work focussed on 1D HPLC analysis to study retention order and selectivity differences using strong IP-RP, SAX and HFIP modified IP-RP. The orthogonality of potential couplings of different modes was determined using the retention data. Pseudo-orthogonal 2D-LC modes were predicted using strong IP-RP or HFIP modified IP-RP in the 1<sup>st</sup> dimension prior to SAX 2<sup>nd</sup> dimension analysis. Offline and online 2D-LC workflows were developed to analyse OGN therapeutics and their impurities.

Due to the increased chemical complexity of these OGN therapeutics (compared to fully phosphorothioated OGN models in Chapter 5), in particular the chemical conjugation to the OGN therapeutic, low resolution of the impurities was observed. Offline and online (HFIP modified IP-RP)- (SAX) 2D-LC methods were performed that separated N-1 and N-2 impurities in the 1<sup>st</sup> dimension for the therapeutic OGN. However, this reduced to resolution of the N-2 impurity only for the conjugated OGN. In the 2<sup>nd</sup> dimension the separation space was therefore simplified and enabled identification of the P=O impurity for the unmodified OGN. The P=O and N-1 impurities co-eluted in a peak away from the FLP when analysing the conjugated OGN under identical conditions. Separation of the N+1 or abasic impurities was not achieved within this work.

Due to the reduction in resolution of OGN impurities under these conditions, the reference mapping strategy was not able to characterise all of the impurities. However, these results provide further insight for the future development of 2D-LC methods that could potentially achieve this with further optimisation including higher selectivity. This method could serve as a qualitative approach to tracking impurities during manufacturing optimisation, provided that the separations are optimised to the specific OGN sequence and chemical modification.

## 6.1 Introduction.

OGN therapeutics are commonly chemically modified to increase efficacy, reduce renal clearance and improve resistance to degradative enzymes (see Chapter 1, section 1.2.2). Chemical modification is OGN therapeutic type specific, however typical modifications to approved OGN therapeutics include full phosphorothioation of the backbone (ASOs), combinations of 2' ribose modifications: 2'-O-MOE, 2'-O-Me and 2'-F (siRNA, ASOs), use of morpholino OGNs (SSOs) and conjugation or capsulation (for cell delivery) [12, 20, 28]. As OGN therapeutic approvals become more successful, pharmaceutical companies seek analytical methods for improved characterisation of drug product and drug substance. Further detail on the impurities caused during manufacturing can be shared with regulatory bodies to assist with developing regulatory guidance and standardisation.

The current challenges observed during 1D HPLC separations of OGN therapeutics are the co-elution of closely related species and LC mode incompatibility with MS. Often the co-eluting impurity species must be extracted from a MS total ion count, which poses questions as to the degree of ionisation suppression by the FLP at much higher concentration within the sample. Although LC-MS analysis is the common approach for characterising OGN impurities, utilisation of MS technology adds complexity and expense to experimental and data analysis. Simpler analytical methods that do not rely on MS detection could provide utility within OGN manufacturing to reduce the costs of manufacturing.

Previously, a 2D-LC workflow was developed and utilised using (HFIP modified IP-RP)-(strong IP-RP) HPLC to analyse PS model OGNs (Chapter 5). Although the workflow demonstrated selectivity changes between dimensions, increases in peak capacity were difficult to determine using a reference mapping strategy alone. Co-elution of OGNs in a strong IP-RP 2<sup>nd</sup> dimension did not facilitate characterisation of the P=O impurity from the FLP, which was an objective of the proposed methods however, optimisation of 1D HPLC provided useful information on retention behaviour and indicated where the 2D-LC method could be further optimised. Therefore, the aim of this Chapter was to develop and utilise 2D-LC workflows for the analysis of an unconjugated and conjugated therapeutic OGN from GSK. The therapeutic OGN contained a mixture of PS and 2'-O-MOE modified nucleotides, with and without conjugation to a GalNac cell delivery molecule (similar to the structure shown in Chapter 1, section 1.2.3, Figure 1.5), and is more complex compared to model OGNs analysed using 2D-LC in previous Chapters.

The OGNs used for this work are fully phosphorothioated, thus it is expected that chromatographic peak shapes are likely to be broad, similarly to OGNs analysed in Chapter 5. The increased chemical complexity of the therapeutic OGN and OGN-conjugate is likely to further negatively impact upon chromatographic resolution and peak shape due to increased secondary interactions with the stationary phase and more diverse range of OGN manufacturing impurities present. Chapters 4 and 5 demonstrated that an initial analysis using a range of 1D-LC conditions provides a good overview of retention behaviour of the OGN and so this approach was adopted. 1D HPLC analysis and orthogonality assessments provided information on the dominance of size or sequence based separation mechanisms and which conditions would be suitable within a 2D-LC workflow for therapeutic OGNs (Part A). Offline and online 2D-LC workflows were then developed to analyse the GSK antisense OGN alongside associated manufacturing impurities (Part B and Part C).

## **Results and Discussion**

### **Part A**

#### **6.2 Analysis of OGN therapeutic retention behaviour in 1D HPLC.**

The range of chromatographic conditions outlined in Table 6.1 was used to investigate the selectivity and resolution of therapeutic OGNs and OGN-conjugates via 1D HPLC. These conditions promote size dependent separations and are designed to reduce secondary interactions that negatively impact chromatographic efficiency. Experiments were performed to analyse elution order and retention behaviour of equimolar mixtures of both sample sets (see Table 6.2 and 6.3) to analyse changes in selectivity across the range of conditions.

**Table 6.1: Optimised chromatographic conditions employed for 1D HPLC analysis and sequential retention behaviour assessment of OGN therapeutics.**

<b>Chromatographic Mode</b>	<b>Mobile Phase</b>	<b>Stationary Phase</b>
Strong IP-RP-LC	5 mM TBuAA, 0.1 $\mu$ M Na <sub>4</sub> EDTA, 10-80% ACN	DNAPac RP
HFIP modified IP-RP-LC	100 mM TEAA, 80 mM HFIP 0.1 mM Na <sub>4</sub> EDTA, 0-25% ACN	Accucore C18 150 Å
SAX-LC	20 mM tris, 0-400 mM NaClO <sub>4</sub> , pH 11.5, 20% v/v ACN.	DNAPac Pa200 Rs

**Table 6.2: Unconjugated therapeutic OGN and its associated manufacturing impurities are fully phosphorothioated OGN sequences (with additional 2'-O-MOE modifications) -described by OGN/impurity type and mass by manufacturing certificate of analysis specification.**

<b>OGN Name</b>	<b>OGN Type</b>	<b>Sequences</b>	<b>Monoisotopic Mass (Da)</b>
Full length Product (FLP)	Target OGN	Confidential	7344.2
5'-1	Shortmer	Confidential	6924.8
5'-2	Shortmer	Confidential	6531.5
N+1	Longmer	Confidential	7689.5
P=O	Oxidation to FLP	Confidential	7328.1

**Table 6.3: GalNac conjugated therapeutic OGN and its associated manufacturing impurities are fully phosphorothioated OGN sequences (with additional 2'-O-MOE modifications) -described by OGN/impurity type and mass by manufacturing certificate of analysis specification.**

<b>OGN Name</b>	<b>OGN Type</b>	<b>Sequence</b>	<b>Monoisotopic Mass (Da)</b>
Full length Product (FLP)	Target OGN	Confidential	8863.9
5'-1	Shortmer	Confidential	8518.6
5'-2	Shortmer	Confidential	8141.3
N+1	Longmer	Confidential	9193.2
P=O	Oxidation to FLP	Confidential	8847.8
Abasic	Loss of a base	Confidential	8730.8

The therapeutic OGN and therapeutic OGN conjugate and their associated manufacturing impurities were analysed using a range of chromatographic conditions (strong IP-RP, HFIP modified IP-RP and SAX HPLC). The 1D HPLC analysis of the therapeutic OGN and the therapeutic OGN-conjugate and associated manufacturing impurities are shown in Figures 6.1 and 6.2 respectively. The results from separation of the therapeutic OGN and its associated manufacturing impurities using SAX HPLC (see Figure 6.1a) show that the P=O and N+1 impurities are more resolved from the FLP ( $R_s = 1.16$  and  $0.54$  respectively) than the shortmer impurities ( $R_s = 0.29$  for N-1 and  $0.41$  for N-2). PWHH was an average of 0.30 minutes, which is similar to that observed for fully PS OGNs in Chapter 5 at 0.33 minutes. This demonstrates that the increased chemical complexity of the therapeutic OGN does not broaden the peak further using SAX conditions. Further analysis of the therapeutic OGN and its associated manufacturing impurities in an alternate chromatographic mode (using HFIP modified IP-RP conditions) is shown in Figure 6.1b. The results show that baseline resolution of the two shortmer impurities (N-1 and N-2) from the FLP was achieved. The FLP and P=O/ N+1 impurity peaks have larger PWHH compared to the N-1/N-2 OGNs (increasing from 0.26 to 0.53 minutes respectively). Although the N-1 shortmer is not baseline resolved from the next OGN in the sample set (N-1 to P=O  $R_s = 0.94$ ) there is enough selectivity to observe the shortmer eluting as an individual peak.

The results from the analysis using strong IP-RP-LC conditions are shown in Figure 6.1c and demonstrate a strong size dependent separation, with the smaller shortmer OGN eluting first and longer impurity eluting last. Resolution is low between the N+1, N-1, P=O and FLP OGN, however PWHH is smallest among the three chromatographic conditions averaging at 0.27 minutes. Table 6.4 summarises resolution between the therapeutic OGN and its associated manufacturing impurities under the range of chromatographic conditions. There is a significant reduction in peak capacity across the range of conditions analysed. This is due to increased chemical complexity of the OGN therapeutics.

**Table 6.4: Resolution between the FLP of the therapeutic OGN and its associated manufacturing impurities in SAX, strong IP-RP (using TBUAA) and HFIP modified IP-RP (using TEAA:HFIP) HPLC.**

Impurity	SAX HPLC	HFIP modified HPLC	Strong IP-RP HPLC
N-1	0.30	1.47	0.63
N-2	0.42	2.34	1.30
N+1	0.54	0.20	0.47
P=O	1.16	0.38	0.27

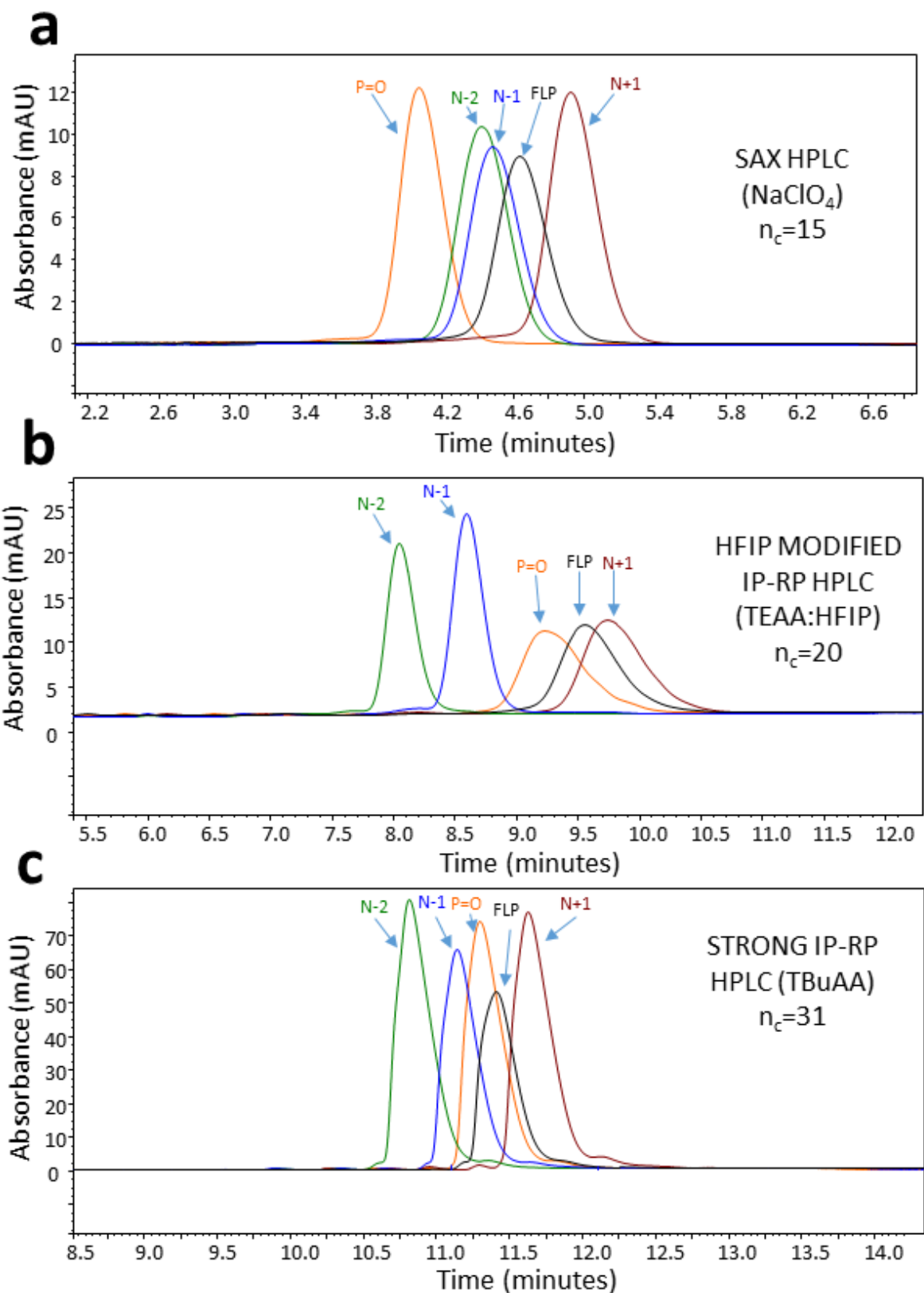


**Figure 6.1: Elution order assessment of the therapeutic OGN and associated impurities analysed using SAX, HFIP modified IP-RP and strong IP-RP HPLC conditions.** **a:** SAX HPLC using 20 mM Tris, 160-264 mM NaClO<sub>4</sub> pH 11.5 with 20% v/v MeCN. Gradient from 0-7.7 minutes. 30 picomole samples analysed at 0.8 ml/min and 30 °C using a DNAPac Pa200 Rs column. **b:** HFIP modified IP-RP HPLC using 100 mM TEAA, 80 mM HFIP, 0.1 mM Na<sub>4</sub> EDTA and 16.25-21.25% v/v MeCN gradient from 1-15 minutes. 30 picomole samples analysed at 0.3 ml/min and 30 °C using an Accucore C18 column. **c:** Strong IP-RP HPLC using 5 mM TBuAA, 0.1 μM Na<sub>4</sub> EDTA and 34.5-59% v/v MeCN from 1-15 minutes. 50 picomole samples analysed at 0.2 ml/min and 50 °C using a DNAPac RP column.

Analysis of the conjugated OGN and its associated conjugated manufacturing impurities under the range of HPLC conditions are shown in Figure 6.2 a-c. Using SAX HPLC conditions (Figure 6.2 a), the results show changes in selectivity are observed between the N-1 and N-2 shortmers compared to the unconjugated OGN sample set (see Figure 6.1a). The retention order is reversed in respect to these impurities. This change in selectivity is possibly a result of steric hindrance effects of the conjugate molecule as the OGN base sequence and nucleotide chemical modification is identical between the therapeutic OGN and the therapeutic OGN-conjugate. Resolution of the P=O impurity remained at 1.16, but the N+1 impurity resolution reduced to 0.32. PWHH was unaffected by conjugation and remained at 0.3 minutes. An additional impurity analysed within this sample set is an abasic impurity, which represents a depurinated OGN impurity. Under SAX conditions the abasic impurity co-eluted with the N+1 OGN.

Analysis in HFIP modified IP-RP conditions is shown in Figure 6.2b. When compared with data obtained from the analysis of the unconjugated sample set, selectivity changes are also observed within the separation. The N-1 shortmer increased in retention time so that its resolution from the FLP was reduced. The N-2 impurity was the only impurity baseline resolved from the FLP peak ( $R_s = 2.18$ ).

The conjugated sample set was also analysed under strong IP-RP HPLC conditions and the results are shown in Figure 6.2c. The results show selectivity of the N-1 impurity and FLP increased in comparison to analysis of the unconjugated OGN using these conditions, but not enough to baseline resolve the impurity from the FLP. There is a strong dependency on size based separation using strong IP-RP HPLC for the therapeutic OGN conjugate and its associated manufacturing impurities. This is demonstrated by the low PWHH, which is lowest among all chromatographic conditions and mirrors the unconjugated sample set at an average of 0.27 minutes. Low PWHH under these conditions demonstrate that diastereoisomer resolution is reduced due to the reduction in secondary interactions between the OGN and the stationary phase, and thus improvement in size based separation. Table 6.5 summarises resolution between the therapeutic OGN-conjugate and its associated manufacturing impurities under the range of chromatographic conditions.

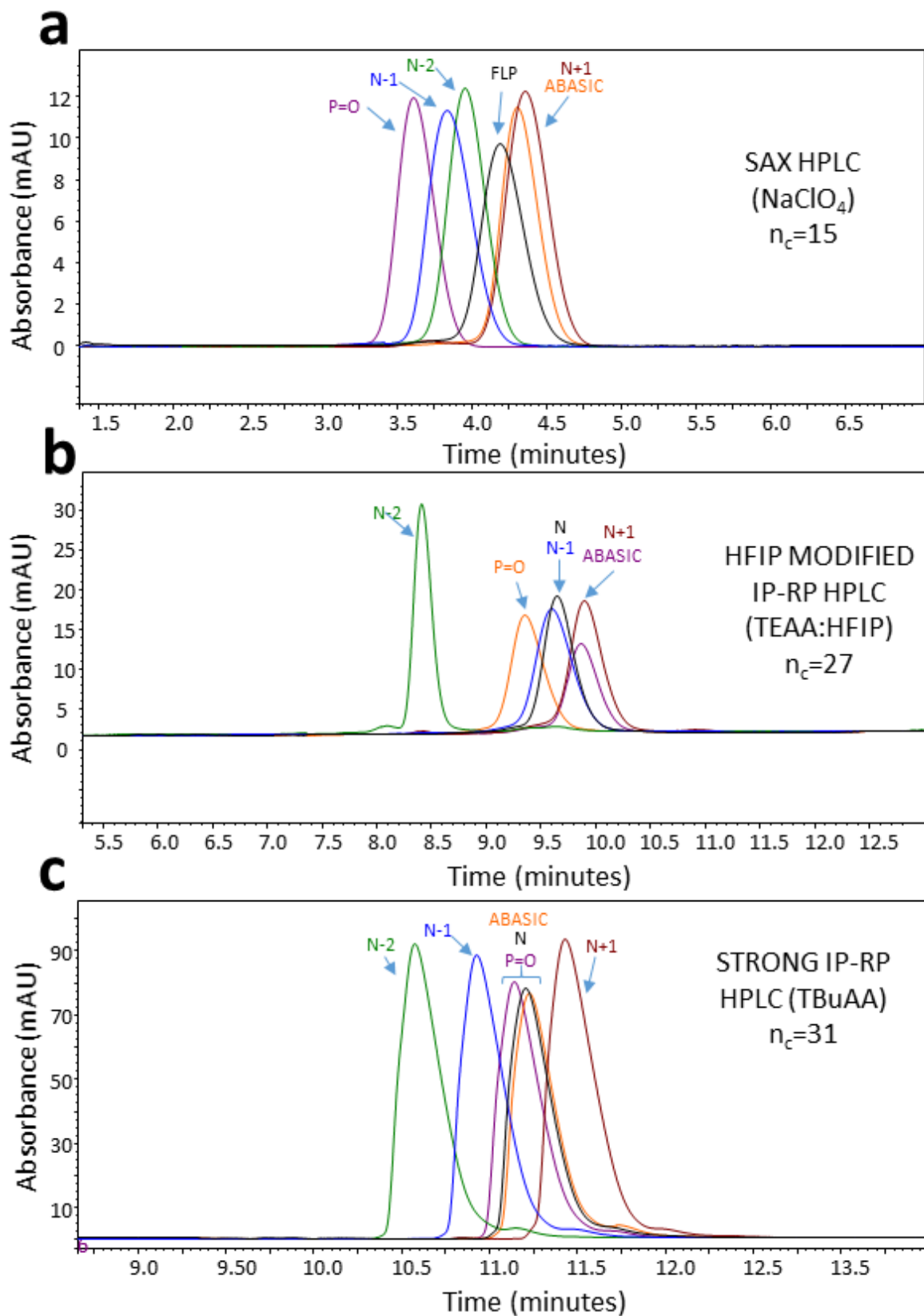


**Figure 6.2: Elution order assessment of the conjugated therapeutic OGN and associated impurities analysed using SAX, HFIP modified IP-RP and strong IP-RP HPLC conditions.** **a:** SAX HPLC using 20 mM Tris, 160-264 mM NaClO<sub>4</sub> pH 11.5 with 20% v/v MeCN, gradient from 0-7.7 minutes. 30 picomole samples analysed at 0.8 ml/min and 30 °C using a DNAPac Pa200 Rs column. **b:** HFIP modified IP-RP HPLC using 100 mM TEAA, 80 mM HFIP, 0.1 mM Na<sub>4</sub> EDTA and 16.25-21.25% v/v MeCN gradient from 1-15 minutes. 30 picomole samples analysed at 0.3 ml/min and 30 °C using an Accucore C18 column. **c:** Strong IP-RP HPLC using 5 mM TBuAA, 0.1 μM Na<sub>4</sub> EDTA and 34.5-59% v/v MeCN gradient from 1-15 minutes. 50 picomole samples analysed at 0.2 ml/min and 50 °C using a DNAPac RP column.

**Table 6.5: Resolution between the FLP of the therapeutic OGN-conjugate and its associated manufacturing impurities in SAX, strong IP-RP (using TBuAA) and HFIP modified IP-RP (using TEAA:HFIP) HPLC.**

Impurity	SAX HPLC	HFIP modified HPLC	Strong IP-RP HPLC
N-1	0.67	0.09	0.64
N-2	0.48	3.02	1.34
N+1	0.32	0.46	0.47
P=O	1.16	0.53	0.15
ABASIC	0.24	0.42	0.05

### 6.2.1 Orthogonality assessments of 2D-LC workflows.

As described in Chapter 5, the bin counting method of analysing orthogonality [302] is limited by small sample sets and does not fully describe the amount of spread within the separation space when low numbers of analytes (and therefore bins) are used within the analysis. To analyse orthogonality, the minimum convex hull method [300] was used to analyse normalised retention values of three couplings: (Strong IP-RP)-(SAX), (Strong IP-RP)-(HFIP modified IP-RP) and (HFIP modified IP-RP)-(SAX). The orthogonality data is presented in Table 6.6 and the scatter plots shown in Appendix 2, Figures A2.11-A2.12.

**Table 6.6: Orthogonality analysis of potential mode couplings in 2D-LC by minimum convex hull method: OGN therapeutic sample sets.**

Sample Set	2D-LC mode coupling	Minimum convex hull value (%)
Therapeutic OGN and associated impurities	(strong IP-RP)-(SAX)	38
	(strong IP-RP)-(HFIP modified IP-RP)	12
	(HFIP modified IP-RP)-(SAX)	41
Therapeutic OGN-conjugate and associated impurities	(strong IP-RP)-(SAX)	44
	(strong IP-RP)-(HFIP modified IP-RP)	23
	(HFIP modified IP-RP)-(SAX)	43

The results from the orthogonality analysis shows that a combination of either strong IP-RP (using TBuAA) or HFIP modified IP-RP (using a TEAA:HFIP combination) with SAX HPLC results in highest orthogonality for OGN separation. The 1<sup>st</sup> dimension separation should facilitate the highest resolution between the FLP and its associated manufacturing impurities, prior to the orthogonal, sequence dependent separation by SAX HPLC. Although both strong and HFIP modified IP-RP are both size dependent modes, analysis of Tables 6.4 and 6.5 show that the highest resolution of impurities is achieved under HFIP modified IP-RP conditions for both OGN sample sets. On this basis, the HFIP modified IP-RP HPLC conditions are most appropriate as a 1<sup>st</sup> dimension, however orthogonality metric and 1D-LC retention data alone may be insufficient to determine the best workflow for OGNS with this level of chemical complexity. Experimental confirmation must be achieved via the investigation of both (strong IP-RP)-(SAX) and (HFIP modified IP-RP)-(SAX) 2D-LC methods.

In summary, the 1D-LC analysis of the therapeutic OGN and the therapeutic OGN-conjugate and their associated manufacturing impurities was performed using strong IP-RP, HFIP modified IP-RP and SAX conditions. The results showed predominantly size dependent separations in the strong IP-RP and HFIP modified IP-RP HPLC conditions. Additional sequence dependent effects were observed in SAX HPLC conditions, in particular where the P=O impurity eluted prior to the N-1 and N-2 impurities. Further analysis of the therapeutic OGN-conjugate showed that the impurity selectivity changed in comparison to the unconjugated therapeutic OGN. This demonstrated that the conjugation effects the interactions between the OGN and the stationary phase through steric effects and potential reduction in net differences in hydrophobicity as a result of conjugation.

In addition, orthogonality metrics were analysed to indicate potential couplings of chromatographic conditions within a 2D-LC workflow. The minimum convex hull metric was utilised for orthogonality analysis as the number of analytes within the sample sets was low. The results indicated that (HFIP modified IP-RP)-(SAX) and (strong IP-RP)-(SAX) were the most orthogonal workflows. For the directed analysis of the P=O impurity, the former workflow showed optimal potential for the unconjugated OGN therapeutic sample set.

## **Part B**

### **6.3 Mobile phase compatibility using 2D-LC analysis of OGN therapeutics.**

Analysis of 1D-LC retention behaviour and 2D-LC workflow orthogonality demonstrated that two 2D-LC workflows may be appropriate for the analysis of the therapeutic OGN and therapeutic OGN conjugate and their associated manufacturing impurities, but this must be confirmed by further experimental evaluation via feasibility testing using an offline 2D-LC approach. Feasibility analysis of both 2D-LC workflows evaluates retention and mobile phase compatibility between the two dimensions of the proposed 2D-LC methods outlined in Part A.

From experimental work in Chapter 5, it became evident that analysing samples in diluents matching the eluting conditions of the 1<sup>st</sup> dimension (which could be estimated from the elution conditions of experiments performed in section 6.2) was important in estimating any sensitivity loss and mobile phase incompatibility. Using this approach, OGN impurities N-2, P=O and N+1 of the conjugated OGN therapeutic sample set were mixed equimolarly in eluting conditions of strong IP-RP HPLC and HFIP modified IP-RP HPLC (with 40 mM HFIP), as well as water diluent. Analysis of the OGNs in strong IP-RP, HFIP modified IP-RP and water diluents was performed using SAX HPLC conditions, and the results are shown in Figure 6.3a. The results show no loss in peak heights in comparison to OGNs in water diluent, demonstrating that retention would be maintained when employing SAX-LC as a 2<sup>nd</sup> dimension in a 2D-LC workflow.

To ensure this effect is consistent at higher concentrations of HFIP using HFIP modified IP-RP HPLC, the FLP and P=O impurity was analysed in a water diluent and diluent of HFIP modified IP-RP HPLC conditions using 80 mM HFIP. The analysis within SAX HPLC conditions is shown in Figure 6.3b and the data mirrors that in Figure 6.3a. This demonstrates that either (strong IP-RP)-(SAX) or (HFIP modified IP-RP)-(SAX) 2D-LC methodologies would be appropriate for analysis of OGN therapeutics.

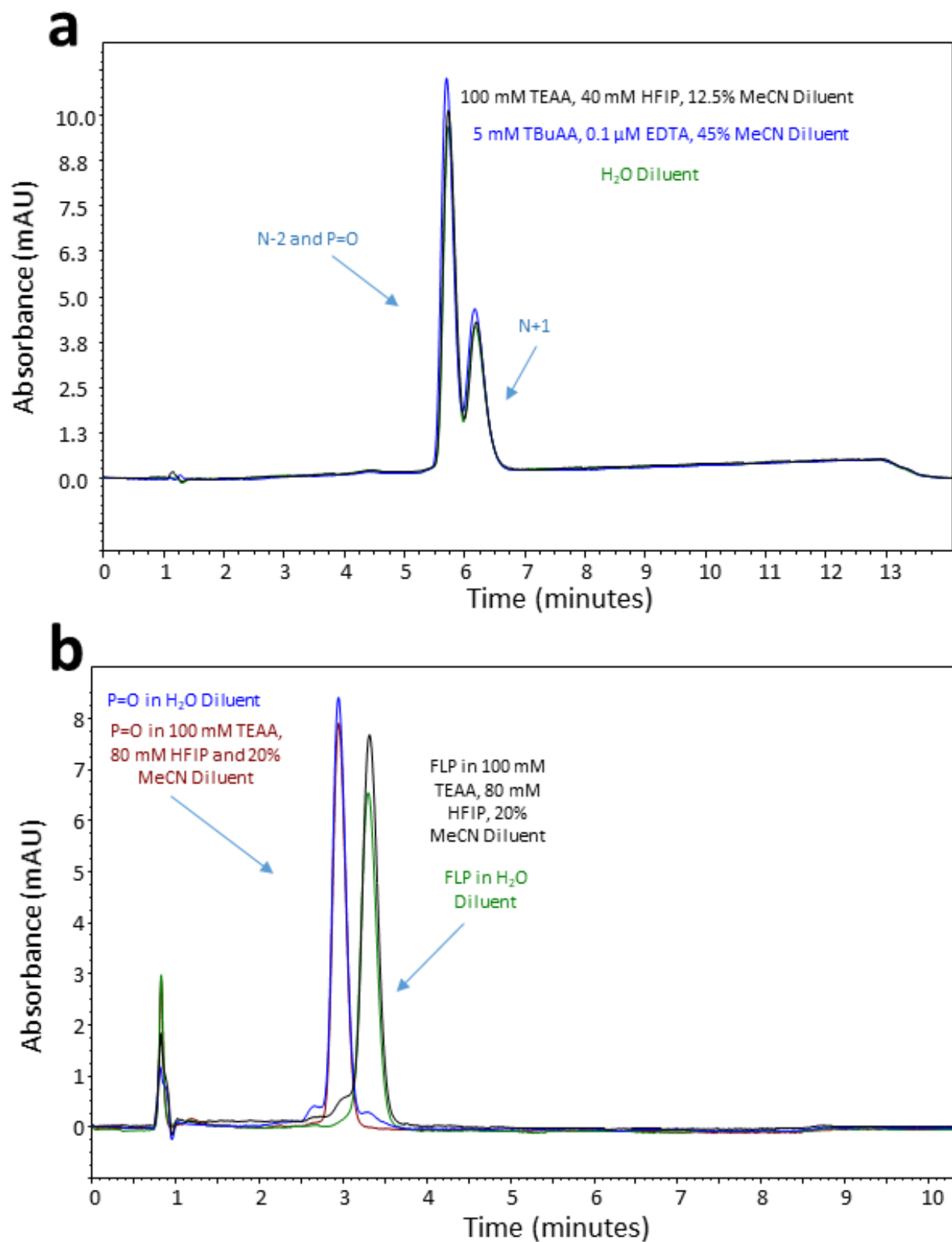


**Figure 6.3: Feasibility analysis- testing therapeutic OGN retention in a range of diluents using SAX HPLC conditions.** SAX-HPLC performed using a gradient of 20 mM Tris, 160-264 mM NaClO<sub>4</sub> pH 11.5 with 20% v/v MeCN at 30 °C using a DNAPac Pa200 Rs column. **a:** 30 picomole samples of an equimolar mixture of the N-2, P=O and N+1 impurities of the conjugated OGN therapeutic, analysed at 0.8 ml/min. Comparison of water, strong IP-RP HPLC and HFIP modified IP-RP HPLC (using 40 mM HFIP) diluents. Gradient applied between 0-7.7 minutes. **b:** 15 picomole individual samples of the therapeutic OGN FLP and P=O impurity analysed at 1.2 ml/min. Comparison of water, strong IP-RP HPLC and HFIP modified IP-RP HPLC (using 80 mM HFIP) diluents. Gradient applied between 0-5.1 minutes.

## **6.4 Optimisation of offline 2D-LC and a reference mapping strategy for 2D-LC method development.**

Based on the orthogonality analysis and mobile phase compatibility studies, two workflows: (strong IP-RP)-(SAX) and (HFIP modified IP-RP)-(SAX) were used to develop an offline 2D-LC method to characterise the therapeutic OGN and the therapeutic OGN-conjugate and their associated manufacturing impurities. This work aimed to separate co-eluting or closely eluting impurities, which are difficult to characterise in 1D HPLC analysis. As previously described in Chapters 4 and 5, offline 2D-LC was used in conjunction with a reference mapping strategy and mass spectrometry analysis of the 1<sup>st</sup> dimension fractions to validate OGNs present in each fraction.

### **6.4.1 Offline (strong IP-RP)-(SAX) 2D-LC for the analysis of OGN therapeutics.**

The FLP of both unconjugated and conjugated GSK OGN therapeutic samples were mixed with 1.5% of each corresponding impurity within the sample mixture, resulting in the unconjugated FLP being analysed at 94% and the conjugated impurity at 92.5%. 1000 picomole samples were analysed in a 1<sup>st</sup> dimension of strong IP-RP HPLC and fractionated into six 100  $\mu$ L fractions corresponding to 30 second intervals. 20  $\mu$ L of each fraction was next analysed in a 2<sup>nd</sup> dimension of SAX-LC at pH 11.5 (see Figures 6.4 and 6.5), and reference OGNs (within a diluent matching the elution conditions of the 1<sup>st</sup> dimension, specifically- 5 mM TBuAA, 0.1  $\mu$ M Na<sub>4</sub> EDTA, 45% MeCN) were analysed alongside the fractions within the 2<sup>nd</sup> dimension to characterise the observed peaks. The offline 2D-LC analysis of the therapeutic OGN is shown in Figure 6.4a. The results show that peaks are observed in fractions 3-6 with the P=O impurity observed in fraction 3 and 4. The N-1, N-2 and N+1 impurities are difficult to characterise using reference OGNs due to low resolution with the FLP. A zoomed view of the overlaid chromatograms is shown in Figure 6.4b, showing fractions 3-5 alongside impurity references P=O, N-1 and N-2. The shortmers demonstrate low resolution with the P=O impurity, which makes characterisation of the P=O in 2<sup>nd</sup> dimension fractions difficult.

The offline 2D-LC analysis of the therapeutic OGN-conjugate is shown Figure 6.5a. The results show that no impurity can be correctly identified by the reference standard OGNs due to low resolution.

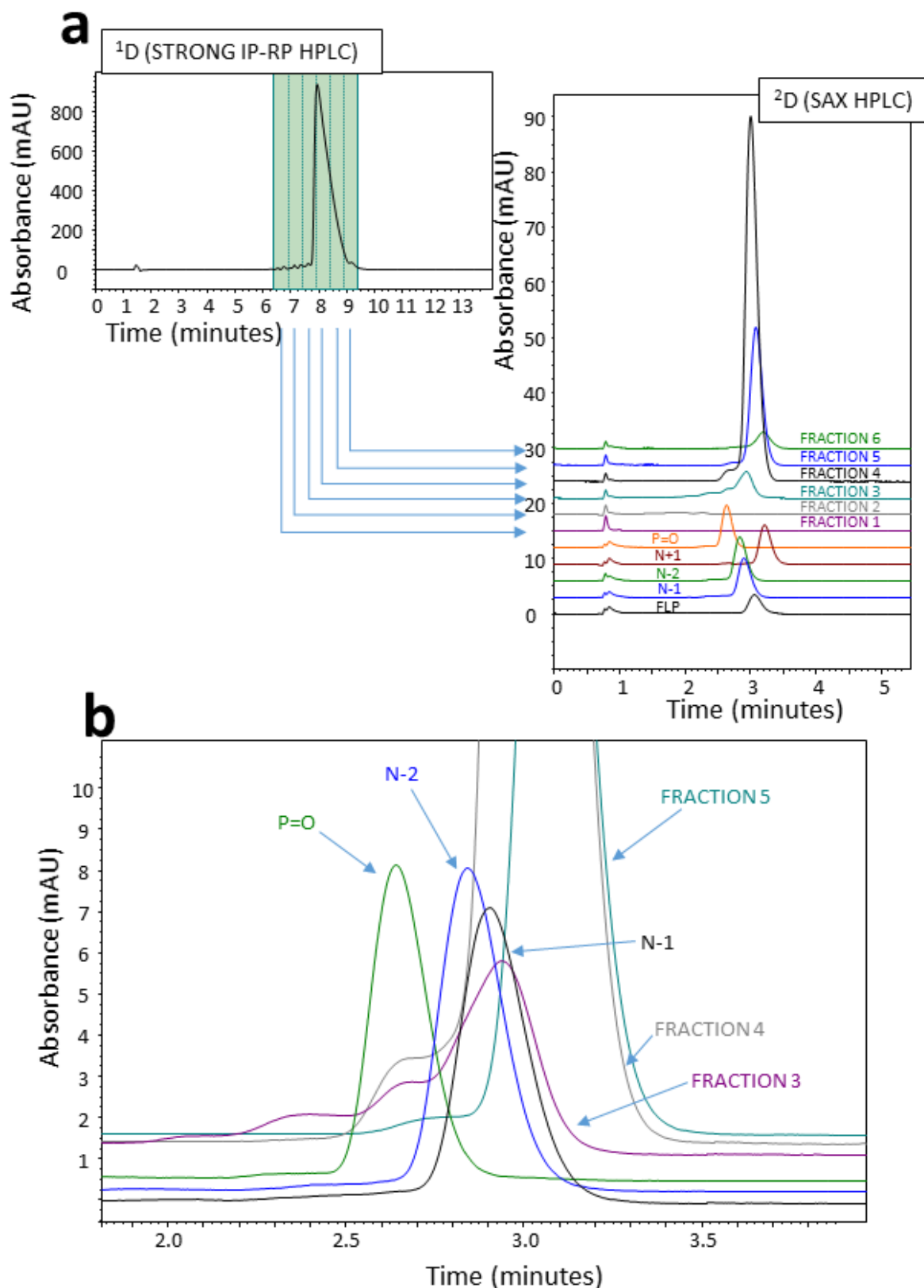


**Figure 6.4: Offline (strong IP-RP)-(SAX) 2D-LC analysis of 1000 picomole sample of the therapeutic OGN and its associated manufacturing impurities.** Impurity concentration added at 1.5% and FLP at 94%. Reference mapping using 15 picomole of reference OGNs was concurrently analysed in the 2<sup>nd</sup> dimension. **a:** 1<sup>st</sup> dimension analysis was performed using strong IP-RP HPLC using 5 mM TBuAA, 0.1  $\mu$ M Na<sub>4</sub> EDTA and 41.5-52% v/v MeCN gradient from 1-15 minutes. Analysed at 0.2 ml/min and 50 °C using a DNAPac RP column. Six 100  $\mu$ l fractions were collected from the 1<sup>st</sup> dimension. 20  $\mu$ l of each fraction was analysed in a 2<sup>nd</sup> dimension of SAX HPLC using a gradient of 20 mM Tris, 160-264 mM NaClO<sub>4</sub> pH 11.5 with 20% v/v MeCN from 0-5.1 minutes. Analysed at 1.2 ml/min and 30 °C using a DNAPac Pa200 Rs column. **b:** Zoomed view of 2<sup>nd</sup> dimension analysis.

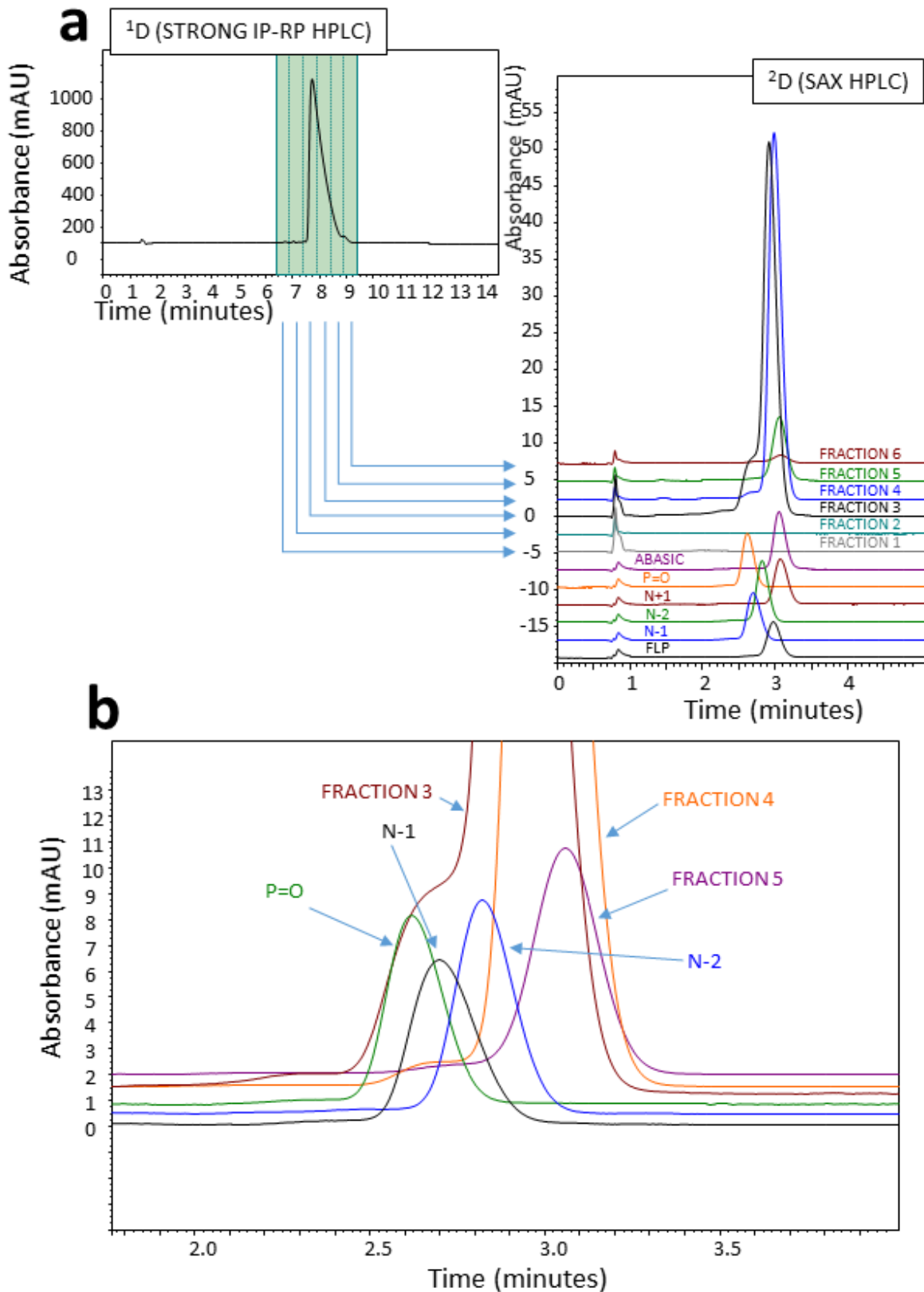


**Figure 6.5: Offline (strong IP-RP)-(SAX) 2D-LC analysis of 1000 picomole sample of the conjugated therapeutic OGN and its associated manufacturing impurities.** Impurity concentration added at 1.5% and FLP at 92.5%. Reference mapping using 15 picomole of reference OGNs was concurrently analysed in the 2<sup>nd</sup> dimension. **a:** 1<sup>st</sup> dimension analysis was performed by strong IP-RP HPLC using 5 mM TBuAA, 0.1  $\mu$ M Na<sub>4</sub> EDTA and 41.5-52% v/v MeCN gradient from 1-15 minutes. Analysed at 0.2 ml/min and 50 °C using a DNAPac RP column. Six 100  $\mu$ l fractions were collected from the 1<sup>st</sup> dimension. 20  $\mu$ l of each fraction was analysed in a 2<sup>nd</sup> dimension of SAX HPLC using a gradient of 20 mM Tris, 160-264 mM NaClO<sub>4</sub> pH 11.5 with 20% v/v MeCN from 0-5.1 minutes. Analysed at 1.2 ml/min and 30 °C using a DNAPac Pa200 Rs column. **b:** Zoomed view of 2<sup>nd</sup> dimension analysis.

The analytes are observed in fractions 3-6, however in fraction 3 there is low resolution leading to a loss of resolution of the initial peak. This results in the main peak appearing to have a shoulder. The abasic and N+1 impurity reference OGNs elute under the main peak and so identification of the impurities within sample is not possible. An enhanced view of the 2<sup>nd</sup> dimension separation is shown in Figure 6.5b. The Figure shows fractions 3-5 alongside reference OGNs N-1, N-2 and P=O. In this analysis, identification of the peaks using reference standards is inhibited due to loss of resolution and close elution of impurities to the main peak.

MS analysis of the 1<sup>st</sup> dimension fractions was also utilised to help identify impurities within the 2<sup>nd</sup> dimension and to identify OGNs within each fraction. Replicate 1000 picomole samples of the unconjugated and conjugated OGN samples from the 1<sup>st</sup> dimension (strong IP-RP HPLC) were fractionated and analysed by MS. A summary of the OGN identifications are shown in Tables 6.7 and 6.8 where OGNs have been observed in one or both replicate analyses. Example mass spectrum peak assignments are shown in Appendix 2 Figure A2.13 for the unconjugated and conjugated OGN therapeutic respectively. The ambiguity observed when performing 2D-LC analysis of these samples is mirrored within the mass spectrometry data. For both unconjugated and conjugated OGN samples, fractions 3 and/or 4 showed an early eluting peak that could potentially correspond to the P=O impurity. However, analysis by MS found that the fractions also contained the N-1, N-2 and FLP OGNs. This highlights that mapping the analyte peaks with reference OGNs is not possible under (strong IP-RP)-(SAX) 2D-LC conditions due to the close or co-elution of impurities to the FLP.

In summary, key impurities present in both sample sets were not fully identified using a (strong IP-RP)-(SAX) 2D-LC workflow due to lack of resolution of the impurities from the FLP. Collecting a smaller fraction sampling volume may overcome this challenge, however would require equipment adaptation from what was utilised for the analysis. In addition, generation of smaller fractions potentially leads to signal loss in the 2<sup>nd</sup> dimension due to sub the lower concentration of analyte collected in the individual fractions.

**Table 6.7: LC-MS identification OGN masses within each fraction of the 1<sup>st</sup> dimension analysis (strong IP-RP HPLC) of the therapeutic OGN and its associated manufacturing impurities added at 1.5% total sample concentration.**

<b>Fraction</b>	<b>OGN Observed Mass (Da)</b>	<b>OGN Theoretical Mass (Da)</b>	<b>Observed m/z of [M-4H] 4<sup>-</sup></b>	<b>Theoretical m/z of [M-4H] 4<sup>-</sup></b>	<b>Identity Assignment</b>
<b>1</b>	N/A	N/A	N/A	N/A	N/A
<b>2</b>	N/A	N/A	N/A	N/A	N/A
<b>3</b>	6532.0	6531.5	1631.980	1631.867	N-2
	6925.0	6924.8	1730.252	1730.192	N-1
	7328.2	7328.1	1831.030	1831.017	P=O
	7344.1	7344.2	1835.021	1835.042	FLP
<b>4</b>	7344.1	7344.2	1835.016	1835.042	FLP
	7328.1	7328.1	1831.008	1831.017	P=O
	6925.0	6924.8	1730.254	1730.192	N-1
	6532.0	6531.5	1631.979	1631.867	N-2
<b>5</b>	7344.1	7344.2	1835.014	1835.042	FLP
	7689.1	7689.5	1921.274	1921.367	N+1
	7328.1	7328.1	1831.013	1831.017	P=O
<b>6</b>	7344.1	7344.2	1835.016	1835.042	N
	7689.1	7689.5	1921.265	1921.367	N+1

**Table 6.8: LC-MS identification OGN masses within each fraction of the 1<sup>st</sup> dimension analysis (strong IP-RP HPLC) of the conjugated therapeutic OGN and its associated manufacturing impurities added at 1.5% total sample concentration.**

<b>Fraction</b>	<b>OGN Observed Mass (Da)</b>	<b>OGN Theoretical Mass (Da)</b>	<b>Observed m/z of [M-4H] 4<sup>-</sup></b>	<b>Theoretical m/z of [M-4H] 4<sup>-</sup></b>	<b>Identity Assignment</b>
<b>1</b>	N/A	N/A	N/A	N/A	N/A
<b>2</b>	N/A	N/A	N/A	N/A	N/A
<b>3</b>	8141.8	8141.3	2034.443	2034.317	N-2
	8518.9	8518.6	2128.710	2128.642	N-1
	8848.0	8847.8	2210.983	2210.942	P=O
	8863.7	8863.9	2214.927	2214.967	FLP
	9193.0	9193.2	2297.242	2297.292	N+1
<b>4</b>	8863.9	8863.9	2214.972	2214.967	FLP
	8848.0	8847.8	2210.983	2210.942	P=O
	9192.8	9193.2	2297.202	2297.292	N+1
	8730.9	8730.8	2181.705	2181.692	ABASIC
<b>5</b>	8863.9	8863.9	2214.955	2214.967	FLP
	9192.9	9193.2	2297.226	2297.292	N+1
	8847.9	8847.8	2210.959	2210.942	P=O
	8730.9	8730.8	2181.712	2181.692	ABASIC
<b>6</b>	9192.9	9193.2	2297.227	2297.292	N+1

#### **6.4.2 Offline (HFIP modified IP-RP)-(SAX) 2D-LC for the analysis of OGN therapeutics.**

In addition to the offline 2D-LC workflow described in section 6.4.1, an alternative approach using (HFIP modified IP-RP)-(SAX) 2D-LC was also performed to analyse the unconjugated and conjugated OGN samples. As described in section 6.4.1, the impurities were added 1.5% concentration and the FLP at 94% (therapeutic OGN) and 92.5% (therapeutic OGN-conjugate). 1000 picomole samples were first fractionated into four 120  $\mu$ L fractions within a 1<sup>st</sup> dimension analysis of HFIP modified IP-RP-LC. 20  $\mu$ L of each fraction was next analysed in a 2<sup>nd</sup> dimension of SAX-LC at pH 11.5 (see Figures 6.6 and 6.7). Reference OGNs were analysed alongside the fractions within the 2<sup>nd</sup> dimension to identify the peaks.

The 2D-LC analysis of the therapeutic OGN is shown in Figure 6.6a. The 1<sup>st</sup> dimension separation demonstrates increased resolution of the closely eluting impurities next to the FLP main peak in comparison to a strong IP-RP 1<sup>st</sup> dimension (see Figure 6.4a). These impurities can be separated from the main peak by targeted fractionation and this is shown in the SAX 2<sup>nd</sup> dimension where reference OGN mapping aligns the N-1 and N-2 OGN impurities with the peak of fraction 1 (Figure 6.6b). The P=O reference aligns with the 1<sup>st</sup> eluting peak of fraction 2 and 3. The N+1 reference OGN aligns to the main peak and so is unable to characterise the corresponding N+1 impurity within the separation. A zoomed view of the 2<sup>nd</sup> dimension separation is shown in Figure 6.6b highlighting where reference OGNs align to sample peaks.

The 2D-LC analysis of the therapeutic OGN-conjugate and its impurities is shown in Figure 6.7a. The results show the reduced resolution of the N-1 impurity from the FLP (as can be determined by observation of the reference OGN analysis). The 1<sup>st</sup> dimension separation shows a resolved impurity peak within fraction 1, which aligns with the N-2 reference OGN. Fraction 2 of the 2<sup>nd</sup> dimension shows an early eluting peak next to the main FLP peak, the peak aligns in between the P=O and N-1 reference OGNs and possibly contains a mixture of the two impurities. As with the previous sample set, the N+1 and abasic reference OGNs co-elute under the main FLP peak and so can't be used to characterise their corresponding impurities.

As described in section 6.4.1, MS analysis was also performed on fractions of the 1<sup>st</sup> dimension separation to validate the reference mapping strategy and identify OGNs within each fraction of the 1<sup>st</sup> dimension. Replicate 1000 picomole samples of the unconjugated and conjugated OGNs were fractionated in the 1<sup>st</sup> dimensions (HFIP modified IP-RP HPLC), analysed by MS and are summarised in Tables 6.9 and 6.10 (showing OGNs that were observed in one or both replicate analyses). The 1<sup>st</sup> dimension fractionations were optimised to facilitate the fractionation of the early eluting peaks in the separation. This would more accurately identify the OGNs those peaks correspond to. Example mass spectrum peak assignments are shown in Appendix 2 Figure A2.14 and A2.15 for the unconjugated and conjugated OGN therapeutic respectively, along with their corresponding 1<sup>st</sup> dimension fractionations. The MS data highlights that the reference mapping strategy was robust for determining what the early eluting peaks of the 1<sup>st</sup> dimension separation were. It also confirms where there are ambiguities in the reference mapping approach of later eluting impurities under these conditions. The main peak of the 1<sup>st</sup> dimension separation has co-eluting impurities N+1 and the abasic OGN.

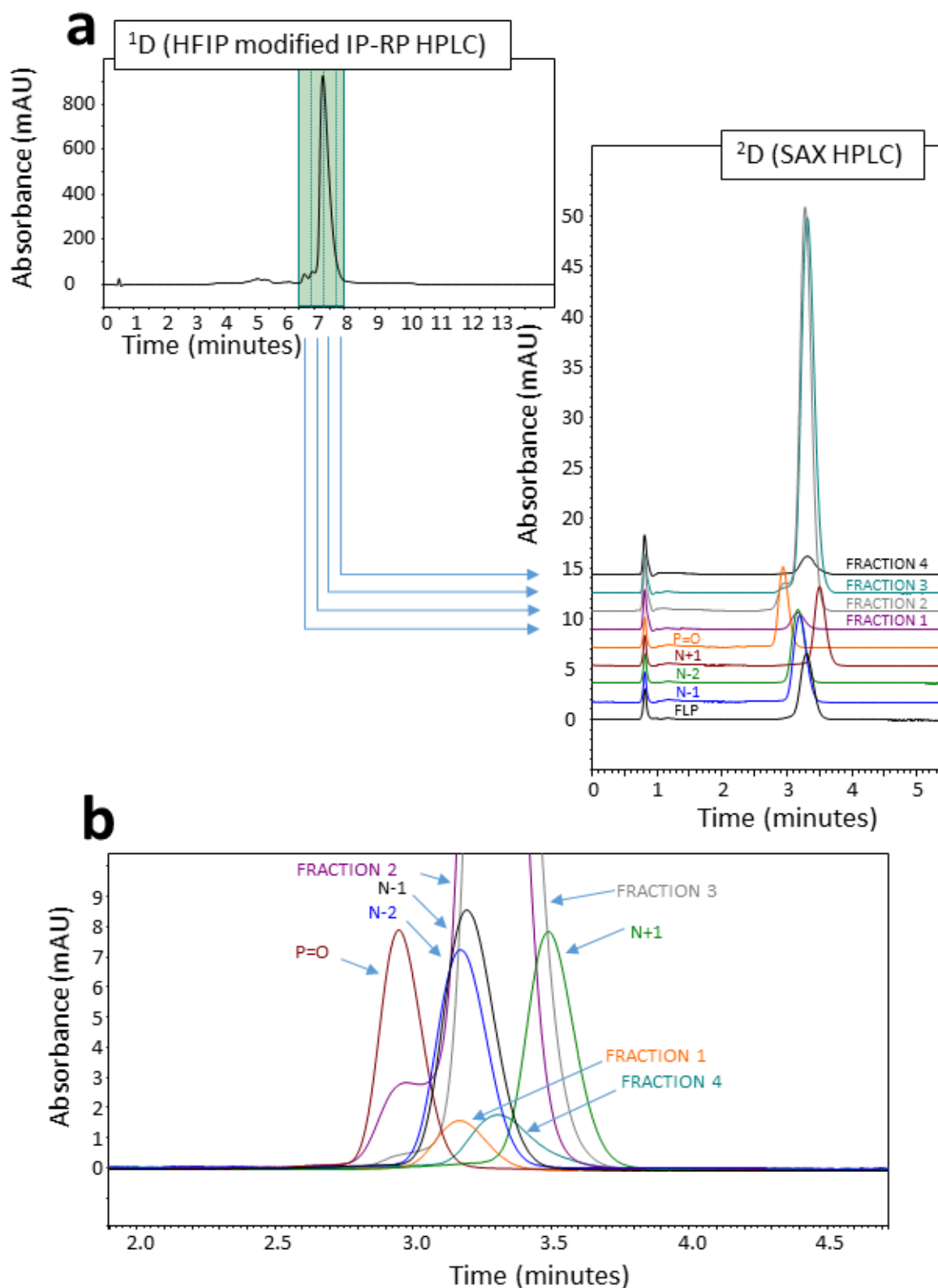


**Figure 6.6: Offline (HFIP modified IP-RP)-(SAX) 2D-LC analysis of 1000 picomole sample of the therapeutic OGN and its associated manufacturing impurities.** Impurity concentration added at 1.5% and FLP at 94%. Reference mapping using 15 picomole of reference OGNs was concurrently analysed in the 2<sup>nd</sup> dimension. **a:** 1<sup>st</sup> dimension analysis was performed by HFIP modified IP-RP HPLC using a gradient of 100 mM TEAA, 80 mM HFIP, 0.1 mM Na<sub>4</sub> EDTA and 16.25-21.25% v/v MeCN from 1-15 minutes. Analysed at 0.3 ml/min and 30 °C using an Accucore C18 column. Four 120 µl fractions were collected from the 1<sup>st</sup> dimension. 20 µl of each fraction was analysed in a 2<sup>nd</sup> dimension of SAX HPLC using a gradient of 20 mM Tris,

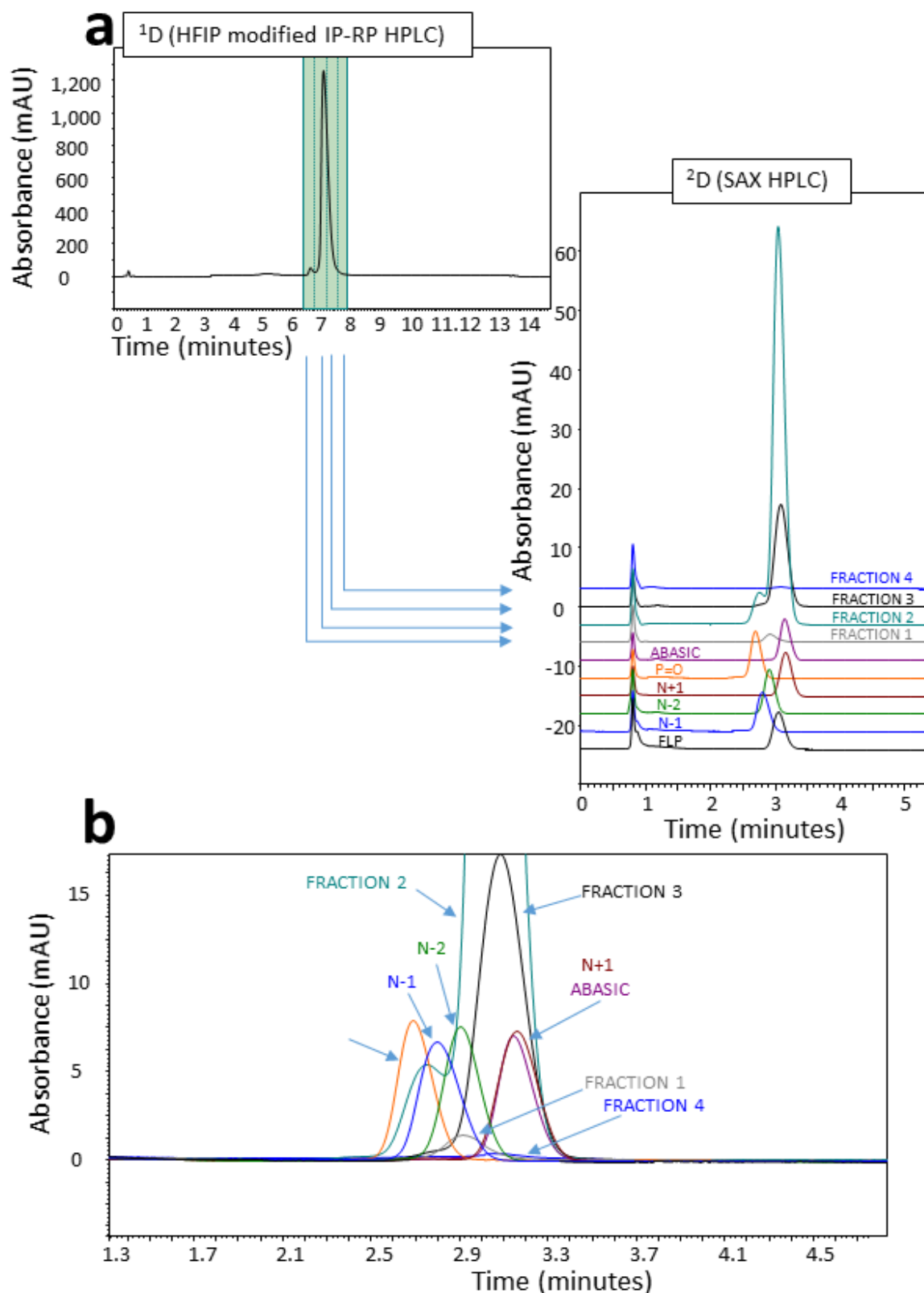


**Figure 6.7: Offline (HFIP modified IP-RP)-(SAX) 2D-LC analysis of 1000 picomole sample of the conjugated therapeutic OGN and its associated manufacturing impurities.** Impurity concentration added at 1.5% and FLP at 92.5%. Reference mapping using 15 picomole of reference OGNs was concurrently analysed in the 2<sup>nd</sup> dimension. **a:** 1<sup>st</sup> dimension analysis was performed by HFIP modified IP-RP HPLC using a gradient of 100 mM TEAA, 80 mM HFIP, 0.1 mM Na<sub>4</sub> EDTA and 16.25-21.25% v/v MeCN from 1-15 minutes. Analysed at 0.3 ml/min and 30 °C using an Accucore C18 column. Four 120 µl fractions were collected from the 1<sup>st</sup> dimension. 20 µl of each fraction was analysed in a 2<sup>nd</sup> dimension of SAX HPLC using a gradient of 20 mM Tris, 160-264 mM NaClO<sub>4</sub> pH 11.5 with 20% v/v MeCN from 0-5.1 minutes. Analysed at 1.2 ml/min and 30 °C using a DNAPac Pa200 Rs column. **b:** Zoomed view of 2<sup>nd</sup> dimension analysis.

Separation within a 1<sup>st</sup> dimension of HFIP modified IP-RP enabled separation of the N-1 and N-2 shortmer impurities from the unconjugated therapeutic OGN. This was confirmed by MS analysis. The resolution of impurities reduced when analysing the therapeutic OGN-conjugate as only the N-2 impurity resolved from the main peak. MS confirmed that the P=O, N+1 and abasic impurities (where present) co-eluted under the main peak of both FLP OGNs. These findings are not consistent with data from Chapter 5 where the P=O impurities (of PS model OGNs) were resolved under HFIP modified IP-RP HPLC conditions. This difference is likely to be a result of the alternate sequence and increased chemical complexity of the GSK OGN therapeutic compared to the PS model OGNs analysed in Chapter 5. The reduction in resolution of impurities from the FLP observed for the conjugated OGN compared to the unconjugated OGN again demonstrated the altered chemical complexity or the addition of terminal modifications also changes the selectivity of the impurities with the FLP.

**Table 6.9: LC-MS identification OGN masses within each fraction of the 1<sup>st</sup> dimension analysis (HFIP modified IP-RP HPLC) of the therapeutic OGN and its associated manufacturing impurities added at 1.5% total sample concentration.**

<b>Fraction</b>	<b>OGN Observed Mass (Da)</b>	<b>OGN Theoretical Mass (Da)</b>	<b>Observed m/z of [M-4H] 4<sup>-</sup></b>	<b>Theoretical m/z of [M-4H] 4<sup>-</sup></b>	<b>Identity Assignment</b>
1	6531.1	6531.5	1631.762	1631.867	N-2
2	6925.1	6924.8	1730.263	1730.192	N-1
3	7344.2	7344.2	1835.038	1835.042	FLP
	7328.3	7328.1	1831.067	1831.017	P=O
	7689.2	7689.5	1921.281	1921.367	N+1
4	7344.3	7344.2	1835.066	1835.042	FLP
	7328.3	7328.1	1831.065	1831.017	P=O
	7689.3	7689.5	1921.327	1921.367	N+1

**Table 6.10: LC-MS identification OGN masses within each fraction of the 1<sup>st</sup> dimension analysis (HFIP modified IP-RP HPLC) of the conjugated therapeutic OGN and its associated manufacturing impurities added at 1.5% total sample concentration.**

<b>Fraction</b>	<b>OGN Observed Mass (Da)</b>	<b>OGN Theoretical Mass (Da)</b>	<b>Observed m/z of [M-4H] 4<sup>-</sup></b>	<b>Theoretical m/z of [M-4H] 4<sup>-</sup></b>	<b>Identity Assignment</b>
1	8141.0	8141.3	2034.252	2034.317	N-2
2	8519.1	8518.6	2128.762	2128.642	N-1
	8864.2	8863.9	2215.030	2214.967	FLP
	8848.0	8847.8	2210.988	2210.942	P=O
3	8864.2	8863.9	2215.030	2214.967	FLP
	9193.3	9193.2	2297.308	2297.292	N+1
	8731.1	8730.8	2181.777	2181.692	ABASIC
4	N/A	N/A	N/A	N/A	N/A

In summary, a 2D-LC workflow using (HFIP modified IP-RP)-(SAX) was shown to be a better approach compared to (strong IP-RP)-(SAX) for the analysis of OGN therapeutics. In the 1<sup>st</sup> dimension, HFIP modified IP-RP demonstrated higher resolution of OGN impurities in comparison to strong IP-RP HPLC. Resolution of shorter impurities in the 1<sup>st</sup> dimension enabled analysis of the P=O impurity in the 2<sup>nd</sup> dimension for the unconjugated therapeutic OGN, resolution of impurities of the conjugated OGN was reduced and so a mixture of P=O and N-1 impurities was resolved in the 2<sup>nd</sup> dimension. Mass spectrometry analysis enabled identification of OGNs occupying each 1<sup>st</sup> dimension fraction and confirmed the identities of co-eluting OGNs in the early peak of the 2<sup>nd</sup> dimension SAX HPLC separation.

## Part C

### **6.5 Online heart-cut 2D-LC analysis of OGN therapeutics.**

The aim of performing offline 2D-LC analysis was to demonstrate that a 2D-LC method could resolve and identify OGNs that co-elute/closely elute under 1D-LC. Comparisons made between two

workflows in section 6.4 indicated that a workflow using (HFIP modified IP-RP)-(SAX) 2D-LC was most appropriate as it demonstrated capability to resolve shortmers and the phosphodiester impurity from the FLP. Further optimisation of the workflow was aimed at developing an online heart-cut 2D-LC method for the analysis of OGN therapeutics for an automated analysis approach. The HPLC equipment was set up as described in Chapter 2, Figure 2.2. Due to the 2<sup>nd</sup> dimension mobile phase conditions, the SAX column was incompatible with higher analysis temperatures and so for online 2D-LC work was connected outside the column oven. Analysis for online 2D-LC was performed at ambient temperature (~20°C).

Samples analysed in offline 2D-LC mode of section 6.4 were analysed by heart-cut online 2D-LC. The online method was developed with the aim of reproducing data obtained for the offline 2D-LC workflow in section 6.4.2. 1000 picomole samples were analysed of both the unconjugated and conjugated OGN therapeutic samples mixed with their associated manufacturing impurities added at 1.5% concentration. The samples were analysed under HFIP modified IP-RP HPLC conditions in a 1<sup>st</sup> dimension separation and fractionated into 3 \* 120 µL fractions. 20 µL of each fraction was then analysed in a 2<sup>nd</sup> dimension of SAX HPLC alongside 15 picomole samples of reference OGN samples for reference mapping. Two replicate analyses were performed for each sample for reproducibility (see Figures 6.9-6.11 and Appendix 2 for replicate chromatograms). The analysis of the therapeutic OGN and associated impurities is shown in Figures 6.8a & 6.9. The results show the analysis of the shortmer impurities from the 1<sup>st</sup> fraction (see Figure 6.9a) where the peak of fraction 1 aligns with the N-1, N-2 and FLP reference OGNs. Offline 2D-LC development studies in section 6.4 showed that the N-1 and N-2 impurities resolve from the FLP in the 1<sup>st</sup> dimension but co-elute in the second dimension, so the alignment of fraction 1 peak with the N-1, N-2 and FLP is to be expected. Fraction 2 2<sup>nd</sup> dimension analysis is shown in Figure 6.9b where two peaks are observed. The small early eluting peak aligns with the P=O reference OGN. The N+1 reference OGN resolution from the main peak is slightly increased at ambient temperature (in comparison with 30 °C during offline 2D-LC analysis), however, does not identify the N+1 impurity within the sample based upon UV detection. MS analysis identified the presence of the N+1 impurity within the sample in section 6.4.2, however its resolution from the FLP was not observed in the 2<sup>nd</sup> dimension analysis. The results of analysis of fraction 3 are shown in Figure 6.9c and mirror results obtained from fraction 2 analysis. The smaller, earlier eluting peak in Fraction 3 aligns with the P=O reference OGN. The data obtained here showing retention time alignment for the P=O and shortmer impurities shows that the 2D-LC method has the capacity to characterise 75% of the sample impurity cohort.

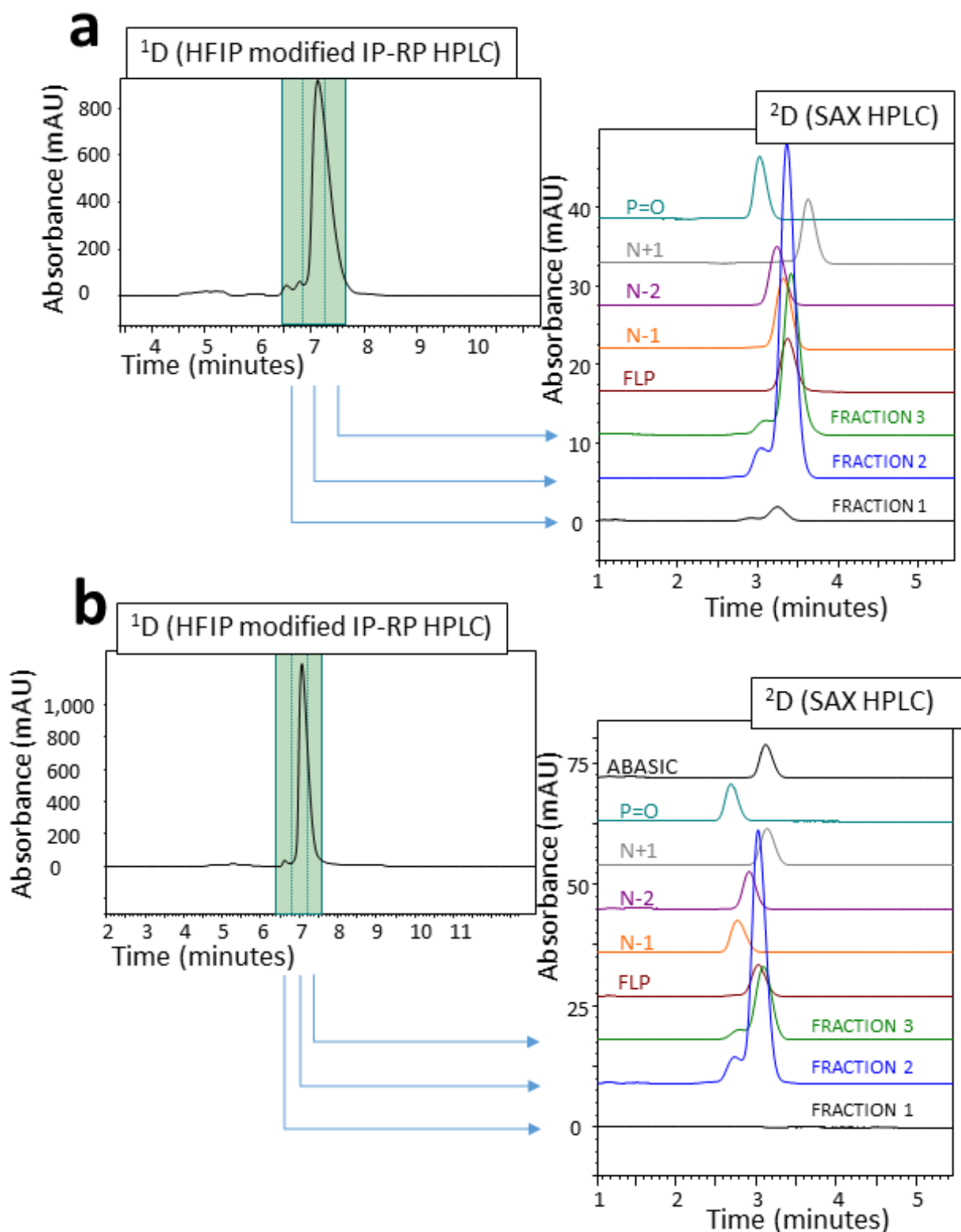


**Figure 6.8: Online heart-cut (HFIP modified IP-RP)-(SAX) 2D-LC analysis of 1000 picomole samples of OGN therapeutics and their associated manufacturing impurities.** Impurity OGNs concentrations added at 1.5%. Reference mapping using 15 picomole of reference OGNs was concurrently analysed in the 2<sup>nd</sup> dimension. 1<sup>st</sup> dimension analysis was performed by HFIP modified IP-RP HPLC using a gradient of 100 mM TEAA, 80 mM HFIP, 0.1 mM Na<sub>4</sub> EDTA and 16.25-21.25% v/v MeCN from 1-15 minutes. Analysed at 0.3 ml/min and 30 °C using an Accucore C18 column. Three 120 µl fractions were collected from the 1<sup>st</sup> dimension. 20 µl of each fraction was analysed in a 2<sup>nd</sup> dimension of SAX HPLC using a gradient of 20 mM Tris, 160-264 mM NaClO<sub>4</sub> pH 11.5 with 20% v/v MeCN from 0-5.1 minutes. Analysed at 1.2 ml/min and 30 °C using a DNAPac Pa200 Rs column. **a:** Analysis of the therapeutic OGN at 94%. **b:** Analysis of the conjugated therapeutic OGN at 92.5%.

Online 2D-LC analysis of the therapeutic OGN-conjugate and its associated manufacturing impurities is shown in Figure 6.8b and 2<sup>nd</sup> dimension analysis of each fraction is shown in Figure 6.10 a-c. Analysis was performed in replicate as previously described. Fraction 1 2<sup>nd</sup> dimension analysis is shown in Figure 6.10a. The peak aligned with the N-2 reference OGN and has lower peak area in comparison to the peak in fraction 1 of analysis of the therapeutic OGN. This is reflective of the lower concentration of OGN within the peak of the therapeutic OGN-conjugate where one impurity (N-1) has been resolved from the FLP peak (instead of both N-1 and N-2). Additionally, low level impurities present could result in increased sample loss during fractionation as a reflection of their low concentration.

Fraction 2 second dimension analysis (see Figure 6.10b) shows that two peaks were observed within this fraction with a smaller peak eluting before the main peak. Reference OGNs P=O and N-1 align with the early eluting peak, while the FLP, N+1 and abasic reference OGNs align with the main peak. The data is consistent with the offline 2D-LC analysis data (section 6.4.2) and the smaller earlier peak corresponds to a mixture of the P=O and N-1 impurities. In addition, the N+1 and abasic impurities cannot be identified due to their co-elution. The 2<sup>nd</sup> dimension analysis of fraction 3 (see Figure 6.10c) is the same as that observed for fraction 2. In summary, consistent with the offline 2D-LC analysis, resolution of OGN impurities from the FLP is observed to decrease for the analysis of the conjugated OGN therapeutic sample in respect to the unconjugated OGN therapeutic sample.

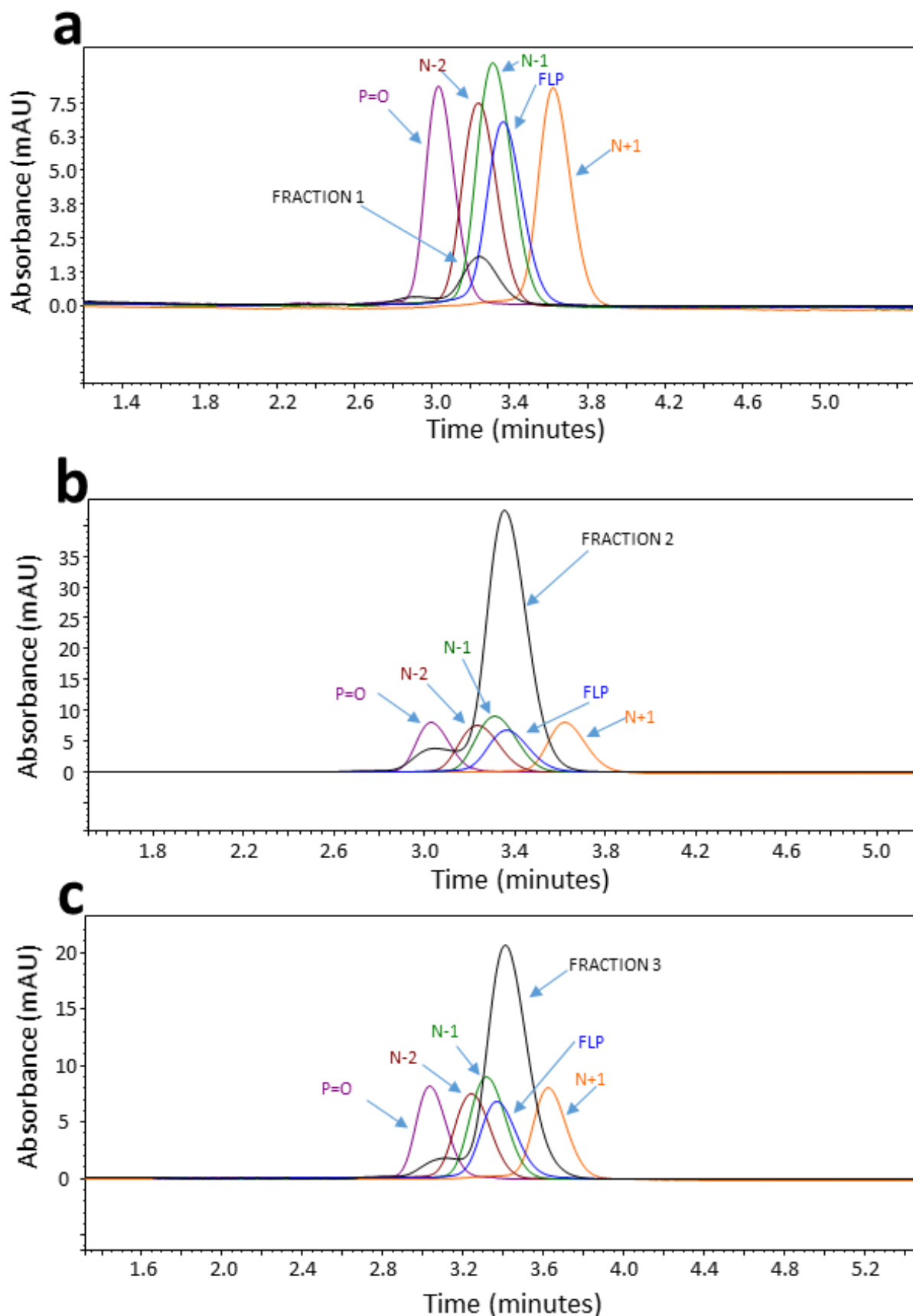


**Figure 6.9: Online heart-cut (HFIP modified IP-RP)-(SAX) 2D-LC analysis: Zoomed view of 2<sup>nd</sup> dimension analysis of the therapeutic OGN and its associated manufacturing impurities using SAX HPLC.** Reference mapping using 15 picomole of reference OGNs was concurrently analysed in the 2<sup>nd</sup> dimension. 2<sup>nd</sup> dimension analysis by SAX HPLC using a gradient of 20 mM Tris, 160-264 mM NaClO<sub>4</sub> pH 11.5 with 20% v/v MeCN from 0-5.1 minutes. Analysed at 1.2 ml/min and 30 °C using a DNAPac Pa200 Rs column. **a:** Analysis of fraction 1. **b:** Analysis of fraction 2. **c:** Analysis of fraction 3.

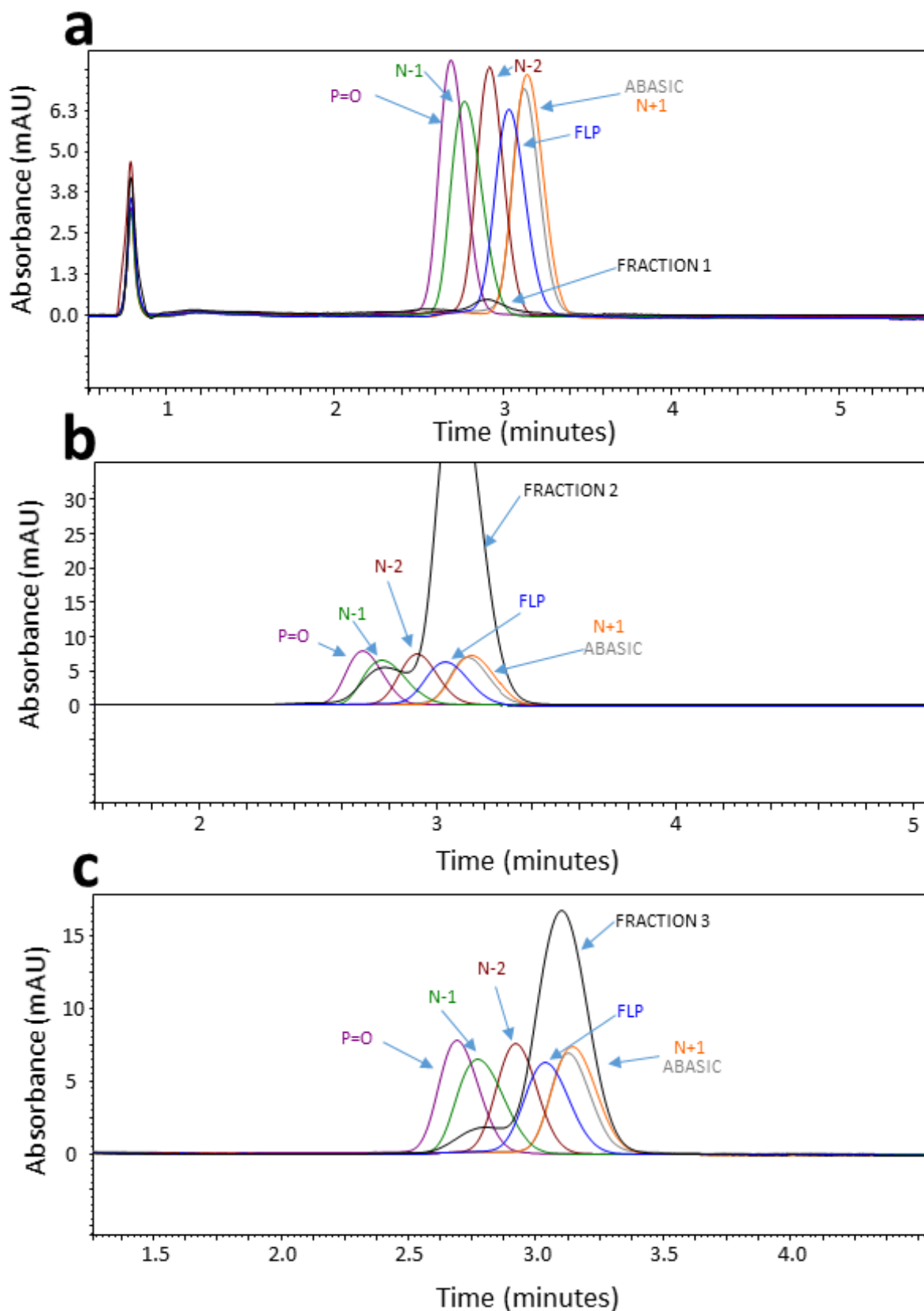


**Figure 6.10: Online heart-cut (HFIP modified IP-RP)-(SAX) 2D-LC analysis: Zoomed view of 2<sup>nd</sup> dimension analysis of the conjugated therapeutic OGN and its associated manufacturing impurities using SAX HPLC.** Reference mapping using 15 picomoles of reference OGNs was concurrently analysed in the 2<sup>nd</sup> dimension. 2<sup>nd</sup> dimension analysis by SAX HPLC using a gradient of 20 mM Tris, 160-264 mM NaClO<sub>4</sub> pH 11.5 with 20% v/v MeCN from 0-5.1 minutes. Analysed at 1.2 ml/min and 30 °C using a DNAPac Pa200 Rs column. **a:** Analysis of fraction 1. **b:** Analysis of fraction 2. **c:** Analysis of fraction 3

## 6.6 Conclusions.

As new OGN therapeutics continue to be developed with increasing levels of chemical modification to overcome some of the challenges of functionality, the increased chemical complexity can negatively impact efficiency of chromatographic separations. An online 2D-LC workflow was developed for analysis of an unconjugated and GalNac conjugated OGN therapeutic containing PS and 2'-O-MOE modifications.

Initial work focussed on the 1D HPLC analysis of the OGN therapeutics and their related manufacturing impurities under selected modes of chromatography. The results showed that a number of impurities co or closely elute to the FLP and could not be resolved by any single 1D-LC mode or 2D-LC combinations of these chromatographic modes. Other impurities could be resolved, but co-eluted with other impurities, creating a need for purification of co-eluting peaks in a 2<sup>nd</sup> dimension.

Size dependent separations were demonstrated within strong IP-RP HPLC and HFIP modified IP-RP HPLC, while sequence based separation mechanisms impacted selectivity in SAX HPLC. Orthogonality assessment showed that both strong IP-RP HPLC and HFIP modified IP-RP HPLC would lead to pseudo-orthogonal separations when combined with SAX HPLC in a 2D-LC workflow. Feasibility studies confirmed that there was compatibility of both eluting conditions in SAX HPLC conditions and retention was maintained. Offline 2D-LC workflows using (strong IP-RP)-(SAX) and (HFIP modified IP-RP)-(SAX) were performed to analyse samples of unconjugated and conjugated OGN therapeutics mixed with low levels of impurities. Due to broad peak shapes caused by chemical modification of the OGNs, a pseudo-orthogonal workflow was required, where size based separation mechanisms dominate in both dimensions, to maintain the peak shape of these OGN therapeutics.

A mapping strategy was performed using reference OGNs in conjunction with MS to identify the OGNs present in each fraction. MS analysis of the 1<sup>st</sup> dimension fractions proved to be crucial for understanding co-elution events in both workflows. Due to the increased chemical complexity of these OGN therapeutics (compared to the full PS OGN models), in particular the addition of the GalNac chemical conjugation to the OGN therapeutic, a reduction in resolution within the 2D-LC workflow was observed. This led to ambiguity during reference mapping as a result of co-elution and close elution and resulted in a higher dependency on MS analysis, which suggests that reference mapping alone is unsuitable for these OGN therapeutics.

Optimisation of online heart-cut 2D-LC demonstrated that the method could be performed in an automated approach. An online 2D-LC workflow of (HFIP modified IP-RP)-(SAX) was chosen for online 2D-LC development in respect of the higher resolution of shortmer impurities within the 1<sup>st</sup> dimension separation. This characteristic led to simpler separation space in the 2<sup>nd</sup> dimension. Analysis of the unconjugated OGN and its manufacturing impurities at 1.5% concentration resulted in successful identification of 75% of the impurity cohort using 2D-LC interfaced with a UV based retention time reference mapping strategy. Analysis of the conjugated OGN therapeutic and its associated manufacturing impurities under identical conditions did not yield the same results and the mapping strategy only identified 20% of the impurity cohort. This highlights the challenges of analysing these types of molecule by HPLC and how increasing chemical complexity (in this case, as a result of the conjugate molecule) reduces selectivity under HFIP modified IP-RP conditions.

It is important to remember that these results could be OGN specific (as the sequences for the conjugated and unconjugated OGN therapeutic samples were identical). The data from Chapter 5 shows that OGNs of different sequence demonstrate selectivity differences under identical chromatographic conditions. The selectivity changes seen under HFIP modified conditions within this Chapter suggest there is additional selectivity changes imparted from increased chemical complexity in respect to model PS OGNs analysed in Chapter 5 (where the N+1 impurity was resolved and identifiable by reference mapping).

The key novelty of this 2D-LC analytical method is that it focuses on reference mapping instead of MS detection to reduce the complexity of data analysis and experimental implementation. Automated 2D-LC methods enable the scientist/technician to 'plug and go' while potentially improving peak capacity through orthogonal separations. This approach was demonstrated to be of utility when analysing unmodified OGNs (see Chapter 4) and could also be appropriate for the analysis of OGN therapeutics with lower levels of hydrophobicity (where they are modified with different moieties, such as 2' -fluoro substitution), such as siRNAs.

For OGNs with high levels of chemical modification that imparts a higher hydrophobicity upon the molecule, chromatographic selectivity and efficiency reduces significantly in comparison to unmodified OGNs. This phenomenon leads to lower overall peak capacities in both 1D HPLC and 2D-LC and negatively impacts upon the capability of the reference mapping strategy to identify OGN impurities as resolved peaks. The aim of this approach was to develop an alternative approach to LC-MS and act as a standalone method of impurity characterisation. For the therapeutic OGN and the therapeutic OGN-conjugate, this approach was not able to identify all of the OGN impurity cohort, although some impurities were successfully mapped for the therapeutic OGN. The presence of a

GalNac conjugate reduced the capability of the mapping strategy further by reducing selectivity of impurities. The insight gained from this work is that the development of a single 2D-LC method for OGNs is not possible, due to differences in selectivity caused by sequence and chemical modification. Improvements in selectivity may be gained from further optimisation of analytical parameters; however, without retention prediction models for chemically complex OGNs, this must be performed in an OGN specific approach. This method could serve as a qualitative approach to tracking impurities during manufacturing optimisation, provided that the separations are optimised to the specific OGN sequence and chemical modification.

Further work could aim to analyse the extent of the mapping strategy capability to identify different types of OGN impurity across a range of analytes of differing sequence and conjugation. At present, it is difficult to conclude the level at which this approach would provide benefit in comparison to LC-MS as it has been performed on only one OGN sequence. Further optimisation of analytical parameters, such as stationary phase or mobile phase chemistry would potentially increase the ability to resolve co-eluting impurities (discussed in Chapter 7). However, due to the requirement for size based separations of fully PS OGNs, a truly orthogonal workflow would never be attained.

In respect to OGN therapeutics that are conjugated to delivery molecules, hydrophobicity based separation mechanisms may not be the most appropriate approaches. Increased potential hydrophobic interactions between the conjugate and the stationary phase may be the cause of steric hindrance effects during separations, or increased net hydrophobicity may reduce the hydrophobic differences between OGNs that differ by only 1 nucleotide, similar to the loss in resolution that is observed as OGN length increases due to a reduction in net chemical differences due to length [189]. Therefore, implementation of methods that reduce hydrophobic interactions (such as HILIC HPLC) may be more appropriate to resolve OGNs using their polar backbones.

## Chapter 7: Conclusions and future directions.

OGN therapeutics are versatile pharmaceutical agents that are used for treating a variety of diseases, including hereditary ATTR amyloidosis, hypercholesterolemia, spinal muscular dystrophy and age-related macular degeneration. OGN therapeutics are emerging as an important class of therapeutic agents, currently at a market value of \$2-2.5 billion with anticipated growth to \$8 billion by 2026. OGN therapeutics are synthetically manufactured and, as with all synthetic manufacturing processes, batches consist of both the target molecule and product related synthesis impurities. These OGN impurities are structurally and chemically very similar to the OGN target product. As regulatory guidelines continue to develop in respect to this emerging pharmaceutical class, improvements in analytical methods help to define impurity reporting thresholds. Analytical data feeds into regulatory governance, toxicology understanding and manufacturing optimisation strategies.

HPLC has been widely used to analyse OGN therapeutics, employing a multitude of different modes of separations. Increasing chemical complexity of modern generations of OGN therapeutic reduces chromatographic performance by reducing efficiency and resolution of OGN impurities. Therefore, improved analytical approaches, such as 2D-LC are required to increase analytical peak capacities through orthogonal separation mechanisms. Often, mass spectrometry (MS) analysis is coupled to chromatographic separations to characterise co-eluting OGNs; however, isobaric co-eluting analytes are not distinguished from each other and would benefit from improved selectivities generated from orthogonal separations. MS imparts additional expense and technical complexity to analytical methods and 2D-LC methods that reduce the requirement for MS analysis through reduction in co-elution combat the extra challenges of complexity, expense and additional equipment. The aim of this research was to optimise size and sequence dependent separations of OGNs and develop orthogonal 2D-LC methods for the characterisation of OGN therapeutics and their manufacturing impurities.

### 7.1 Summary of contribution to the field.

Initial work, presented in Chapter 3, optimised 1D HPLC OGN separations using a range of different chromatographic modes, including SAX, IP-RP and SEC in conjunction with model OGNs of varying

size, sequence or chemical modification (phosphorothioation). High resolution size and sequence based OGN separations were developed and optimised by manipulating temperature, flow rate and stationary or mobile phase chemistry.

Although size and sequence based separation mechanisms play a part in all chromatographic OGN separations, manipulation of analytical parameters could shift separation dominance towards either size or sequence basis. This involved reducing secondary interactions and resolution of PS diastereoisomers for size dependent separations and increasing secondary interactions or resolution of PS diastereoisomers for sequence dependent separations. Manipulation of size dependency was easier to achieve in IP-RP HPLC (in conjunction with using a strong IPR, such as TBuAA and the addition of HFIP to weak IP-RP mobile phases) where PS OGN PWHH was dramatically reduced following optimisation. Manipulating sequence dependency was easier to achieve in SAX HPLC as increases in mobile phase pH showed large selectivity changes in comparison to lower mobile phase pH. Within this work, further insight was gained into the mechanisms of OGN separations in conjunction with a range of modes of chromatography and chromatographic conditions. In IP-RP HPLC conditions specifically, it was demonstrated that changes to the mobile phase chemistry (using TBuAA vs TEAA:HFIP) could alter OGN impurity selectivity and a reduction in secondary interactions could be achieved with a relatively low concentration of HFIP modifier in the mobile phase.

Following the optimisation of size and sequence based OGN separations, 2D-LC workflows were developed by combining a variety of different orthogonal modes. 2D-LC methods that demonstrated orthogonality were optimised, resulting in an increase in peak capacity and resolution between the OGN impurities and the FLP. First, offline heart-cut 2D-LC was developed to optimise an OGN reference mapping (confirmed by MS analysis). Reference OGNs were analysed within the 2D-LC methods to identify OGN peaks in either the 1<sup>st</sup> or 2<sup>nd</sup> dimension separation. The heart-cut fractions of the 1<sup>st</sup> dimension were also analysed by MS to confirm the reference mapping. To conclude the method development, the 2D-LC methods were optimised to be performed in an online approach to demonstrate how automation of analytical methods reduces sample handling and analytical operational complexity.

Initially in Chapter 4, a 2D-LC method was developed for unmodified OGNs using (strong IP-RP in conjunction with TBuAA)-(SAX) HPLC. OGNs in each sample were accurately characterised using a UV retention time based reference mapping strategy integrated within the method. The 2D-LC method showed that increased peak capacity was obtained, which reduced OGN co-elution. The promise of this novel approach to reducing close and co-elution (i.e. resolution values below 1) is that it could be used for many types of OGN with low levels of chemical modification. The success of the

reference mapping strategy in characterising unmodified OGNs demonstrates that a reduction in the requirement for MS analysis can be obtained.

In Chapter 5, focus progressed to developing a targeted 2D-LC method for the analysis of PS OGNs and reduced co-elution of the P=O impurity and the FLP. The (strong IP-RP)-(HFIP modified IP-RP) 2D-LC method demonstrated mobile phase incompatibility in one direction, which was overcome by reversing analytical dimensions. The higher chemical complexity of PS OGNs resulted in lower resolution and chromatographic efficiency in comparison to unmodified OGNs. The reference mapping strategy was able to identify some of the OGN impurities present (such as shortmer and longmers along with P=O impurities). However, co-elution of OGNs in the 2<sup>nd</sup> dimension (FLP and P=O or the 5'-1 and 5'-1 P=O) demonstrated that the requirement for MS analysis remains for chemically modified OGNs. The novelty of using orthogonal separations such as the (IP-RP in conjunction with TEAA:HFIP)-(IP-RP in conjunction with TBUAA) 2D-LC method is that it simplifies the separation space prior to MS analysis, which can reduce the co-elution of isobaric OGN impurities. Further potential development of this method is discussed in section 7.2. The combination of TEAA:HFIP in the IP-RP conditions of the 1<sup>st</sup> dimension also demonstrated ability to resolve the P=O impurities from the FLP OGN. It could be argued that this is an improvement on many IP-RP conditions, where the P=O co-elutes with or closely elutes to the FLP.

In Chapter 6, a (HFIP modified IP-RP)-(SAX) 2D-LC analytical method was developed for the analysis of OGN therapeutics provided by GlaxoSmithKline. In addition to PS modification, these OGNs were additionally chemically modified with 2'-O-MOE and a GalNac conjugate. Increased chemical complexity resulted in further reduction in chromatographic efficiency and selectivity of impurities from the FLP. A targeted approach was applied to reduce co-elution in respect to the P=O, N-1 and N-2 impurities under SAX HPLC conditions. The most orthogonal workflow indicated that HFIP modified IP-RP could resolve some of these peaks in the 1<sup>st</sup> dimension, to reduce co-elution in the 2<sup>nd</sup> dimension of SAX HPLC. An online 2D-LC method was optimised for the unconjugated OGN and associated impurities. However, it was not possible to reproduce these results in respect to the conjugated OGN (identical OGN sequence/modifications). OGN GalNac conjugation resulted in reduced selectivity of the N-1 OGN under HFIP modified IP-RP conditions, which inhibited reduction in 2<sup>D</sup> co-elution. In all optimised modes of chromatography, the N+1 and abasic impurities co-eluted with the FLP. This prevented their characterisation within a 2D-LC method using reference mapping.

The results from Chapter 5 and 6 demonstrate the difficulty in developing chromatographic methods to analyse chemically modified OGNs. Online heart-cut 2D-LC was successfully optimised for the analysis of unmodified OGNs demonstrating reduction in co-elution, increased peak capacity and

characterisation of OGNs using UV based reference mapping. The LC-UV based reference mapping strategy was implemented to identify OGNs without the requirement for MS detection. As OGN chemical complexity increased, impurity resolution, selectivity and chromatographic efficiency reduced. Although optimisation of the chromatography was successfully performed to overcome broad peak shapes of PS OGNs (by focusing on using predominantly size dependent separations), this did not facilitate total orthogonality in 2D-LC workflows. In respect to workflow pseudo-orthogonality, targeted strategies were developed to reduce co-elution or identify specific impurities within the method. Although increases in peak capacities was achieved using 2D-LC, total characterisation of chemically modified OGN impurities using the reference mapping strategy alone was not achieved.

Previous studies have developed 2D-LC workflows for OGNs in conjunction with mass spectrometry for the analysis of OGNs. However, results presented in this thesis are the first 2D-LC methods that have been developed for the analysis of OGNs (and their associated manufacturing impurities) using UV based detection methods alone. 2D-LC methods that do not rely upon MS based detection have a number of potential advantages, including removing the requirement of expensive instrumentation and enabling increased throughput with simple operation and data analysis for manufacturing staff. The 2D-LC methods, which have been developed and optimised, would be best implemented during OGN manufacturing optimisation for impurity tracking. Furthermore, the 2D-LC methods could also be utilised symbiotically with 1D HPLC approaches to confirm or align with quantitative 1D HPLC data. The 2D-LC methods developed in the study also have potential further applications where complex mixtures of OGNs require analysis, such as RNase mapping experiments and separations of PCR associated OGNs.

## **7.2 Directions for future research.**

During 1D HPLC optimisations, challenges of low resolution, broad peak shapes and co-elution of OGN impurities and the FLP were observed. Chemically modified OGNs were more difficult to analyse compared to unmodified OGNs due to broad peak shapes, which was overcome by optimising analytical parameters and mobile phase chemistry. Further 2D-LC method development would utilise further optimised 1D HPLC separations of chemically modified OGNs in a range of modes, which are discussed below.

Using IP-RP HPLC, combinations of IPR have been demonstrated by Levin *et al.* to improve resolution of siRNA and associated impurities [112]. Potentially this approach could be used to prevent diastereoisomer resolution when using a weaker IPR, such as propylamine, with a stronger IPR, such as tributylamine for size based separations. It could be predicted that the stronger IPR would be more likely to create the stationary phase layer and the smaller IPR may interfere with the differential associations with the stationary phase by different conformations of diastereoisomer.

Using SAX HPLC, Roussis *et al.* used sodium bromide for analysis of chemically modified OGNs [322]. They reported the resolution of the P=O impurity, however, did not indicate how well resolved it was from the FLP peak. They also performed their analysis at high pH, presumably to inhibit secondary structure formation. To further understand size and sequence based separation for highly chemically modified OGNs, further investigation of high and low mobile phase pH with a wider range eluotropic salts (sodium bromide, sodium iodide and lithium perchlorate in comparison with sodium perchlorate) should be undertaken.

In this study, OGNs were analysed using a small range of stationary phases (DNAPac RP, DNAPac PA200 Rs, Accucore C18 and Advance BioSEC) that have previously been used to perform high resolution OGN separations. Further work for improving 2D-LC methods should focus on optimising 1D HPLC size and sequence based separations (with particular focus on chemically modified OGNs) using a wider range of alternative stationary phases. These optimised 1D separations that demonstrate higher resolution or selectivity of OGN impurities from the FLP would further increase peak capacity in a 2D-LC workflow. Studzińska *et al.* have analysed phosphorothioated OGNs using IP-RP in conjunction with stationary phases that have cholesterol bonded chemistries [200]. Although they used a lab made phase, a cholesterol based core shell stationary phase is available from Nacalai Tesque (Cosmocore 2.6Cholester). Which may provide alternate selectivity when analysing chemically modified OGNs in addition to good resolution due to core shell 2.6  $\mu\text{m}$  size particles of the stationary phase. Biba *et al.* analysed siRNA OGNs using phenyl-hexyl and amide bonded stationary phases, which may also provide alternative selectivity when analysing chemically modified OGNs [203]. The only caveat of using core shell technologies such as in the Ascentis Express Phenyl-Hexyl or Ascentis Express RP-Amide columns is low stability over time (limited to around 200 analyses), which increases the expense of the analytical method 5-10 fold. In addition, further alternative stationary phases that could be used include the Waters ACQUITY UPLC BEH Phenyl or Amide or XSelect CSH Phenyl-Hexyl XP columns, which could hold potential alternate selectivity characteristics for PS OGNs. Additionally, alternative SAX stationary phases for differential selectivity analysis are the Agilent PL-SAX column, BioMonolith QA or the Thermo Scientific ProSwift SAX 1S monolith.

The 2D-LC methods developed in this study coupled modes of SAX and IP-RP or IP-RP and IP-RP. SEC was not implemented within a 2D-LC workflow owing to low resolution of the mode. Roussis *et al.* showed that 2D-LC methods implementing SEC in the 1<sup>st</sup> dimension could be performed on unmodified OGNs as high resolution in the 1<sup>st</sup> dimension is not necessarily needed in 2D-LC [322]. However, the optimised SEC mobile phase (containing 30% v/v MeCN) for OGN therapeutics (which are commonly modified with PS bonds) would inhibit OGN retention in a 2<sup>nd</sup> dimension.

To further improve resolution under SEC HPLC conditions, an investigation into how pore size affects resolution of chemically modified OGNs could be performed. Although the addition of organic solvent to the mobile phase reduced PWHH, the OGN peaks remained broad and asymmetric-leading to low resolution (compared to IP-RP and SAX). In this study, SEC was performed using a stationary phase with 130 Å pore sizes, further studies using smaller pore size, such as Zenix-C SEC-80 (80 Å pores) or Waters BEH 125-SEC (125 Å pores) columns could potentially improve resolution further than 5 nucleotides.

The automated online 2D-LC methods developed for the analysis of chemically modified OGNs failed to fully resolve a full cohort of impurities within the OGN sample sets. To further develop the 2D-LC methods, reduction in sampling volume in the 1<sup>st</sup> dimension could be used to improve resolution in the 2<sup>nd</sup> dimension and prevent remixing in the 2<sup>nd</sup> dimension. Initial work aimed to maintain an accurate sample volume going into the 2<sup>nd</sup> dimension analysis (20 µL). The limitations of the equipment meant that fractionation volume could not be reduced below 70 µL, however, this could be overcome by using smaller sampling loop volume in the 2<sup>nd</sup> dimension. Alternatively, performing these methods on 2D-LC focused equipment (such as an Agilent Infinity 2D-LC) that contain a 1<sup>st</sup> dimension sample docking system would enable the entirety of a multitude of small volume fractions to be analysed in a 2<sup>nd</sup> dimension.

In this study, the 1<sup>st</sup> dimension column was overloaded to overcome dilution effecting sensitivity in the 2<sup>nd</sup> dimension. Capillary HPLC provides benefits of reduced sampling volume and increases in sensitivity [331, 332]. Therefore, by implementing capillary flow HPLC in the 2<sup>nd</sup> dimension of a 2D-LC method, a reduction in 1<sup>st</sup> dimension column overloading could be possible, which would facilitate higher resolution separations across a 2D-LC method.

2D-LC workflows using (strong IP-RP)-(HFIP modified IP-RP) developed in Chapter 5, were shown to be incompatible for 2D-LC due to the presence of the organic solvent within the eluent of the 1<sup>st</sup> dimension. To overcome this challenge in further method development, an alternative approach to reversing dimensions (as successfully developed in Chapter 5) is using active solvent modulation [333, 334]. This is a process of diluting the 1<sup>st</sup> dimension with 2<sup>nd</sup> dimension starting conditions to

increase retention in the 2<sup>nd</sup> dimension. This can be performed with a 2D-LC set up such as described by Koshel *et al.* (using T junctions) [321] or with an active solvent modulator in a 2D-LC machine, as described by Gargano *et al.* [333]. A rudimentary approach would be to mix 1<sup>st</sup> dimension fractions in a sample vial of 2<sup>nd</sup> dimension mobile phase (at a ratio of 1:4) and perform multiple injection analysis at low eluent conditions in the 2<sup>nd</sup> dimension to increase sensitivity, this is not possible with the HPLC configuration used. Alternatively, coupling capillary HPLC in the 2<sup>nd</sup> dimension may reduce the requirement to perform multiple injections.

The key novelty of a 2D-LC analytical method that relies on reference mapping instead of MS analysis is that it reduces the complexity of data analysis and experimental operation. Automated 2D-LC methods enable the scientist/technician to operate the instrumentation without significant user intervention while potentially improving peak capacity through orthogonal separations. The reference mapping strategy showed promise for OGNs with lower chemical complexity. However, efficiency was decreased as the chemical complexity of the OGN samples increased. This leads to the conclusion that, without improved 1D selectivity, MS characterisation of OGN impurities is required in both 2D-LC and 1D HPLC analysis.

The 2D-LC methods developed in this study were aimed at using UV detection and therefore many of the methods developed were not fully compatible with MS analysis. Therefore, future work could focus on the development of specific 2D-LC methods in conjunction with MS analysis. Previous studies have shown that a mobile phase consisting of 8.6 mM TEA: 100 mM HFIP is comparable to 100 mM TEAA in IP-RP chromatographic performance [240]. Therefore, it is proposed that by altering the HFIP concentration in combination with low TEA concentrations, comparable resolution and selectivity of OGN impurities (P=O impurities and the FLP) to the HFIP modified mobile phases (100 mM TEAA: 40-80 mM) used in this study could be achieved. This would also be beneficial with the 2D-LC method developed in Chapter 6 (for OGNs with additional modifications), where the analytical dimensions could be reversed with a HFIP modified IP-RP 2<sup>nd</sup> dimension that effectively de-salts the sample prior to MS analysis. Using MS compatible mobile phases could further improve characterisation of low concentration OGN impurities by increasing their resolution from high concentration analytes using 2D-LC increased peak capacity.

Many studies have demonstrated that HFIP is a good mobile phase additive to improve size based separations (see Chapter 1 section 1.3.2.3). Utilisation of HFIP as an IPR counter ion has demonstrated increased MS sensitivity due to improvement in ionisation efficiency [239]. Further studies investigating the combination of both HFIP and hexafluoromethylisopropanol (HFMIIP) with a range of different IPRs for analysis of chemically modified OGNs could be performed. In addition,

combining tributylamine, tetrabutylamine or cyclohexyldimethylamine with either HFIP or HFMP in low concentration to analyse retention of highly modified OGNs may facilitate improved size dependent separations.

Although analytical methods were developed for a range of OGNs, the diversity of chemically modified OGNs was limited in this study. Current understanding of retention behaviour of chemically modified OGNs and their related impurities is limited. Therefore, the development of analytical methods remain somewhat empirical without retention predictions. The results generated in this research demonstrate that the resolution and selectivity of the related manufacturing impurities varied depending on the OGNs analysed. This raises an interesting question of whether a generic 2D-LC method could be successfully developed for the analysis of therapeutic OGNs given the variability in chemical modifications and sequences. Therefore, further studies are needed to analyse a larger range of chemically modified therapeutic OGN samples (including PS, 2'-O-MOE, 2'-O-Me, LNA, 2'-F and conjugation complexities). In addition, further studies using the developed 2D-LC methods for the analysis of OGN therapeutics with lower levels of phosphorothioation, such as siRNA or antagomirs are required.

During 1D HPLC size and sequence dependent OGN separations were manipulated using changes in analysis temperature. Increases in temperature also demonstrated improvements in mass transfer and reduction in secondary structure formation. Supercritical fluid chromatography (SFC) is a mode of chromatography that transforms gases to a fluid state at supercritical temperature and pressure and implements these supercritical fluids within separations. It demonstrates NP and HILIC 'like' separation mechanisms and is becoming more popular with ionic analytes for achievement of alternative selectivities to those obtained in HPLC [335, 336]. The added benefit of SFC conditions is compatibility with MS analysis and greener chemistry approach (use of lower amounts of organic solvents). Previous studies have focused on peptide separations using SFC modified with water and mobile phase additives for analysis of polar analytes [336-338]. However, there have been no reports to date on OGN separations in conjunction with SFC, which opens avenues for future research into improved chromatographic methods for the analysis of OGNs. Therefore, future work using SFC in 1D and 2D HPLC is proposed for the analysis of OGNs and further 2D-LC method development. The higher hydrophobicity of PS OGNs may facilitate separations in SFC conditions when using ethyl pyridine or bare silica stationary phases and MeOH / H<sub>2</sub>O / CO<sub>2</sub> mobile phases. In addition, further studies to investigate the effect of additives such as ammonium acetate and HFIP in SFC OGN separations could be performed in an effort to improve selectivity and resolution of OGN impurities.

## Appendix 1: Methods supplements.

Code A1.1: Minimum convex hull calculation using the shoelace algorithm.

```
def PolygonArea(corners):  
    n = len(corners)  
    area = 0.0  
    for i in range(n):  
        j = (i + 1) % n  
        area += corners[i][0] * corners[j][1]  
        area -= corners[j][0] * corners[i][1]  
    area = abs(area) / 2.0  
    return area  
corners = [(2.0, 1.0), (4.0, 5.0), (7.0, 8.0)]
```

Corners values are the x,y co-ordinates of the periphery normalised retention values.

Table A1.1: Coefficient of peak area and retention time for HPLC columns.

Column	Retention time CV (%)	Peak Area CV (%)
DNAPac RP	0.10	1.41
Accucore 150 C18	0.16	1.03
DNAPac PA200 Rs	0.14	0.61

**Table A1.2: 2D-LC fraction sampling parameters between the 1<sup>st</sup> and second dimension separations.**

<b>2D-LC method</b>	<b>OGN sample</b>	<b>Sampling time window (minutes)</b>	<b>Sampling period (seconds)</b>	<b>Flow rate (mL/min)</b>
(strong IP-RP)-(SAX)	Test set 1	8-11	30	0.2
	Test set 2	8-11.5		
	1 <sup>st</sup> generation OGN and manufacturing impurities	7-10.5		
(HFIP modified IP-RP)-(Strong IP-RP)	Model A PS OGN set	8-11	30	0.2
	Model B PS OGN set	8-11		
(HFIP modified IP-RP)-(SAX)	GSK therapeutic OGN set	6.45-7.65	24	0.3
	GSK conjugated OGN therapeutic set	6.4-7.6		

## Appendix 2: Data Supplements

### A2.1 Chapter 3 data supplements.

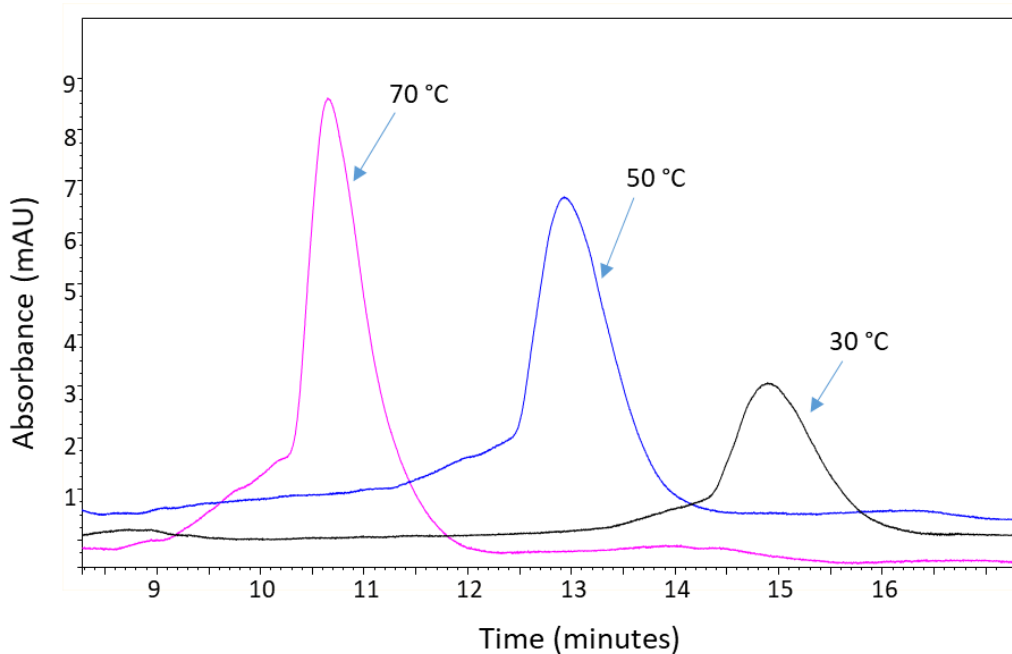


**Figure A2.1:** Weak IP-RP HPLC analysis of full PS 16-mer OGN at 30-70 °C. 30 picomole samples analysed using 100 mM TEAA, 0.1 mM Na<sub>4</sub> EDTA with 8.75-17.5%  $v/v$  MeCN on a DNA Pac RP column at 0.2 ml/min.

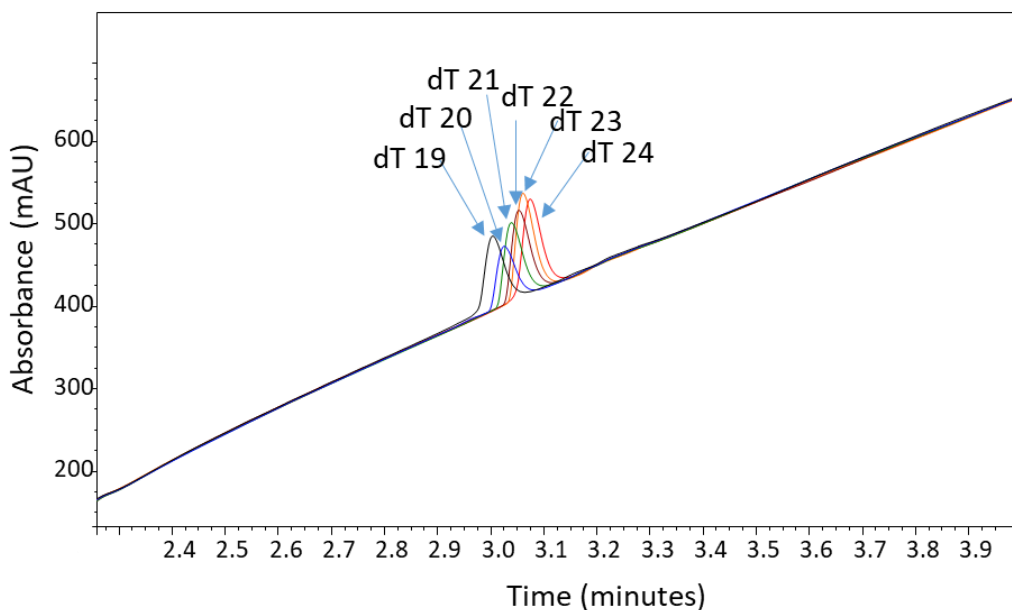


**Figure A2.2:** SAX HPLC analysis (Using NaSCN) of 19-24-mer dT OGNs at 30-70 °C. 50 picomole samples analysed using 50 mM ammonium phosphate pH 8.5 with 20%  $v/v$  MeCN under a gradient of 0-800 mM sodium thiocyanate. Analysed at 28°C and 1 ml/min on a DNAPac PA200 Rs column.

## A2.2 Chapter 4 data supplements.

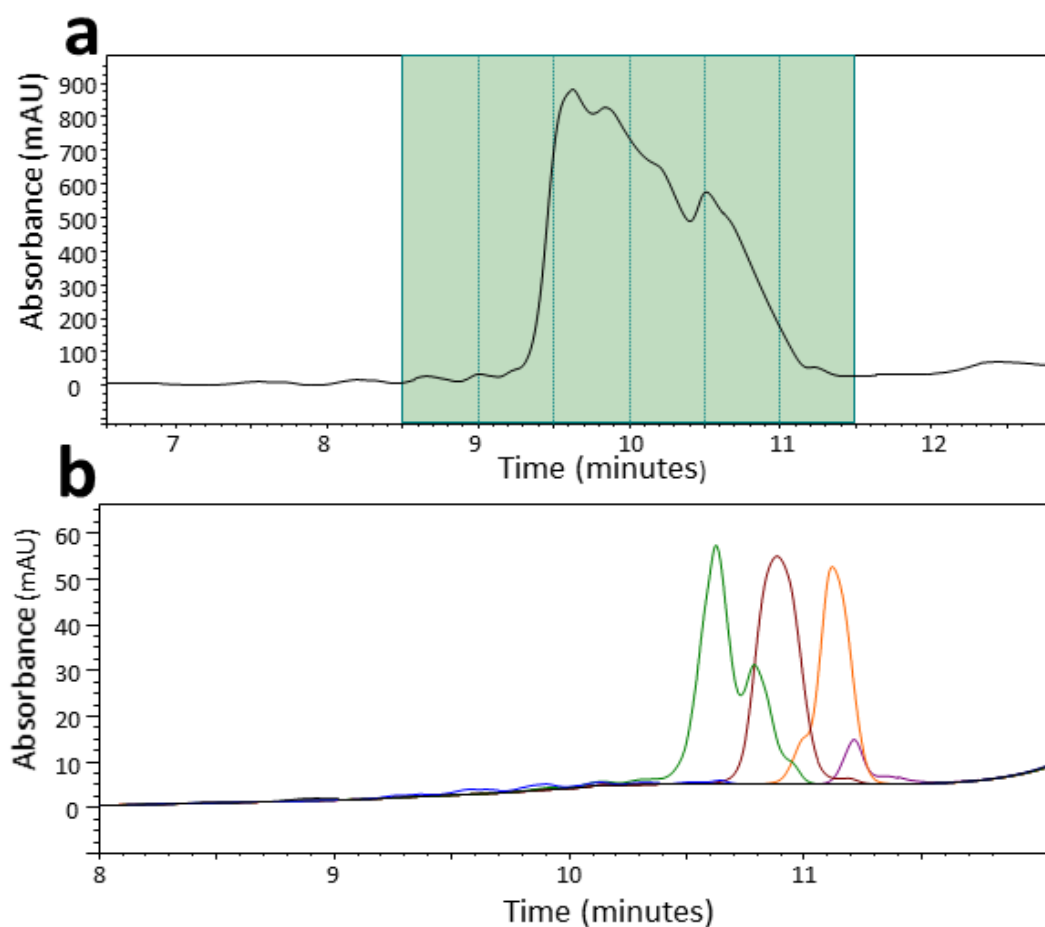


**Figure A2.3: Strong IP-RP HPLC analysis of 1650 picomole sample of 19-22-mer OGN size and sequence variants to calculate fractionation efficiency.** **a:** 5 mM TBuAA, 0.1  $\mu$ M Na<sub>4</sub>EDTA and 37.5-73% v/v MeCN gradient. Analysed at 0.2 ml/min at 60°C using a DNAPac RP column. 6\*100  $\mu$ l fractions were collected from the 1<sup>st</sup> separation. **b:** 5  $\mu$ l of each fraction was re-analysed in a 2<sup>nd</sup> dimension (under identical conditions). Black trace – fraction 1. Blue trace- fraction 2. Green trace- fraction 3. Brown trace – fraction 4. Orange trace – fraction 5. Purple trace – fraction 6.

**Table A2.1: Quality control calculations for fractionation efficiency and analysed fraction amount.** Strong IP-RP HPLC fractionation of 1650 picomoles of size and sequence OGN variant mixture, data in conjunctions with Figure A2.3.

	Replicate 1	Replicate 2	Average
Total area of sample (mAU*min)	1033.77	1036.27	1035.02
Relative area of fraction volume (%)	93.26	92.98	93.12
Original fraction volume ( $\mu$ l)	600	600	600
Amount of sample fractionated (picomole)	1538.79	1534.17	1536.48
Area of fraction volume (mAU*min)	964.08	963.49	963.78
Analysed fraction total area (mAU*min)	44.44	36.98	40.71
Analysed fraction volume ( $\mu$ l)	30	30	30
Analysed fraction total amount (picomole)	70.93	58.89	64.91
Estimated fraction total area (mAU*min)	888.80	739.68	814.24
Fractionation efficiency (%)	0.92	0.77	0.84

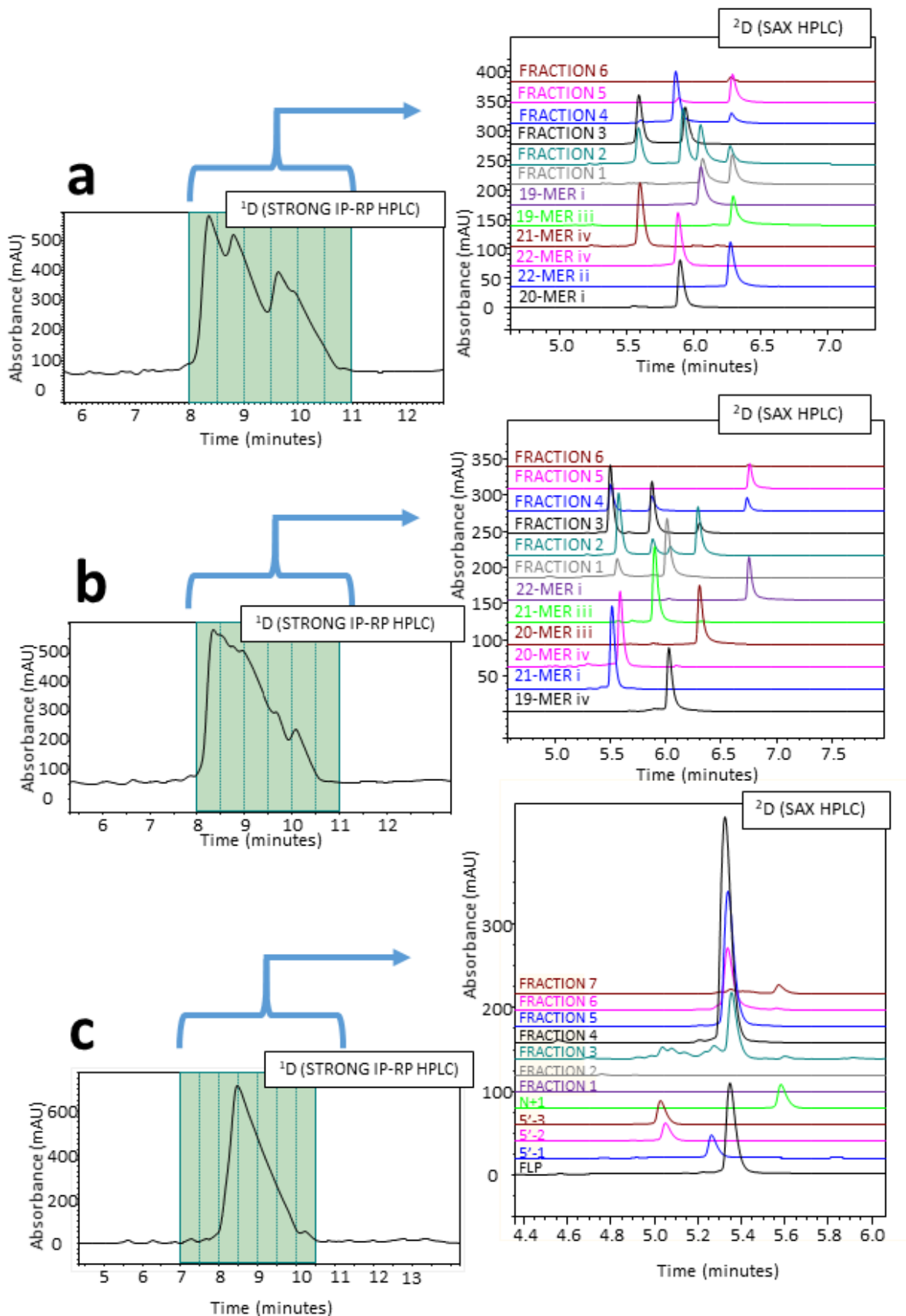


**Figure A2.4: Offline 2D-LC using strong IP-RP to SAX HPLC to analyse 1000 picomole samples of 19-22 mer size and sequence variant OGN mixture.** 1<sup>st</sup> dimension strong IP-RP HPLC under 5 mM TBuAA, 0.1  $\mu$ M Na<sub>4</sub> EDTA and 34.5-59% v/v MeCN gradient from 1-15 min. Analysis at 0.2 ml/min, 50 °C using a DNAPac RP column. 20  $\mu$ l of each fraction was reanalysed in the 2<sup>nd</sup> dimension using SAX HPLC. Analysis using 20 mM Tris, 80-160 mM NaClO<sub>4</sub> between 0-7.7 min and 160-320 mM NaClO<sub>4</sub> between 7.7-10.1 min pH 11.5 and 20% v/v MeCN. Analysis at 0.8 ml/min, 30 °C using a DNAPac PA200 Rs column. Reference OGNs analysed concurrently at 30 picomole sample amount. **a:** Test Set 1 (replicate 2). **b:** Test Set 2 (replicate 2). **c:** 1<sup>st</sup> generation OGN therapeutic (replicate 2).

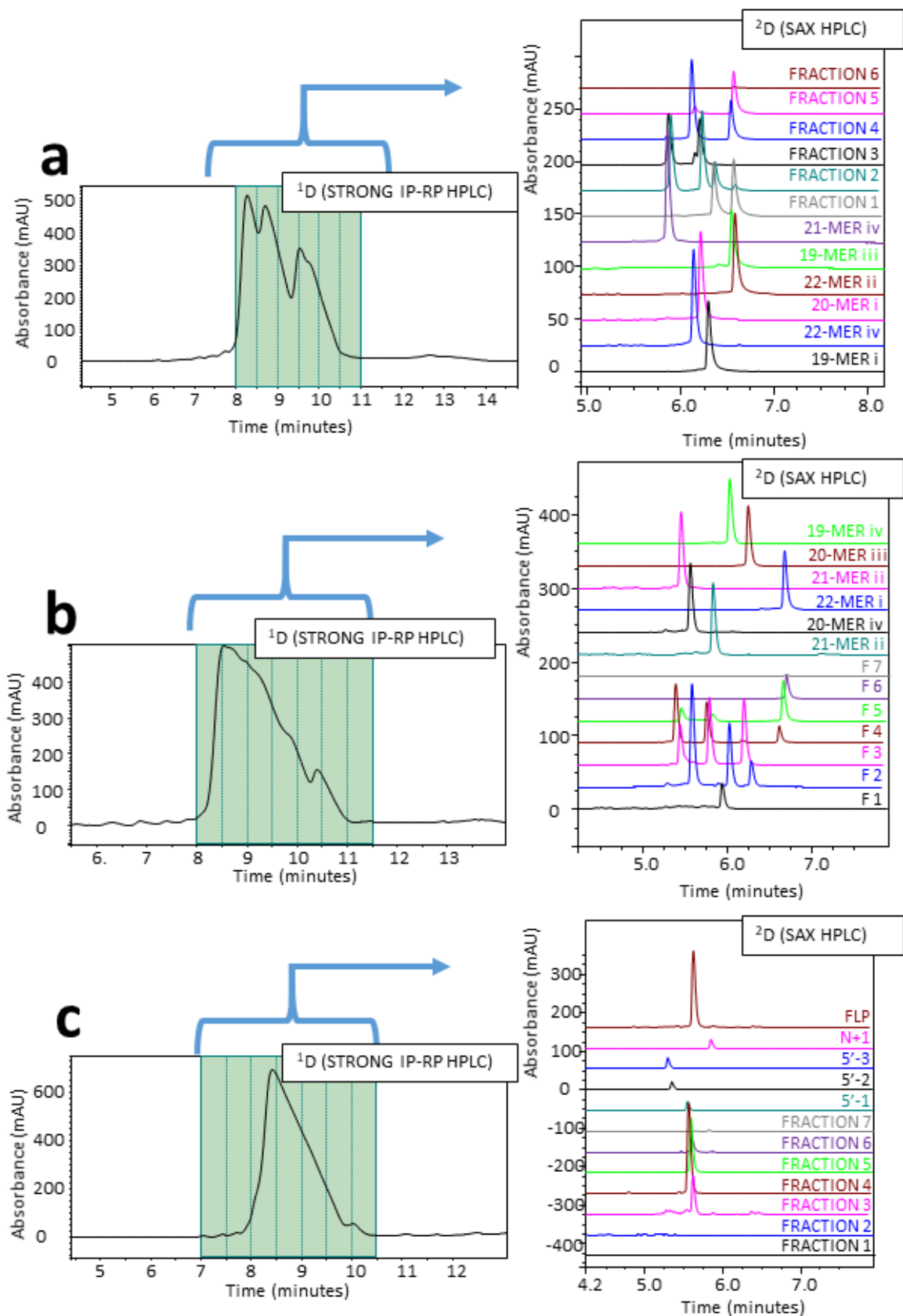


**Figure A2.5: Online 2D-LC analysis of OGNs using strong IP-RP to SAX HPLC.** <sup>1</sup>D separation under 5 mM TBuAA, 0.1 μM Na<sub>4</sub> EDTA and 34.5-59% v/v MeCN gradient from 1-15 min. Analysis at 0.2 ml/min, 50 °C using a DNAPac RP column. 100 μl Fractions were collected and then 20 μl of each was separated in a 2<sup>nd</sup> dimension under a gradient of 20 mM Tris, 80-160 mM NaClO<sub>4</sub> between 0-7.7 min and 160-320 mM NaClO<sub>4</sub> between 7.7-10.1 min pH 11.5 and 20% v/v MeCN. Analysis at 0.8 ml/min, ambient temperature using a DNAPac PA200 Rs column. **a:** Analysis of a 1000 picomole sample of 19-22 mer size and sequence variant OGN mixture (TEST SET 1- replicate 2). **b:** 1000 picomole sample of 19-22 mer size and sequence variant OGN mixture (TEST SET 2 replicate 2). **c:** 1000 picomole sample of 17-21 mer mixture of unmodified OGN and manufacturing impurities added at 1.5% of total concentration (replicate 2).

A2.3 Chapter 5 data supplements.

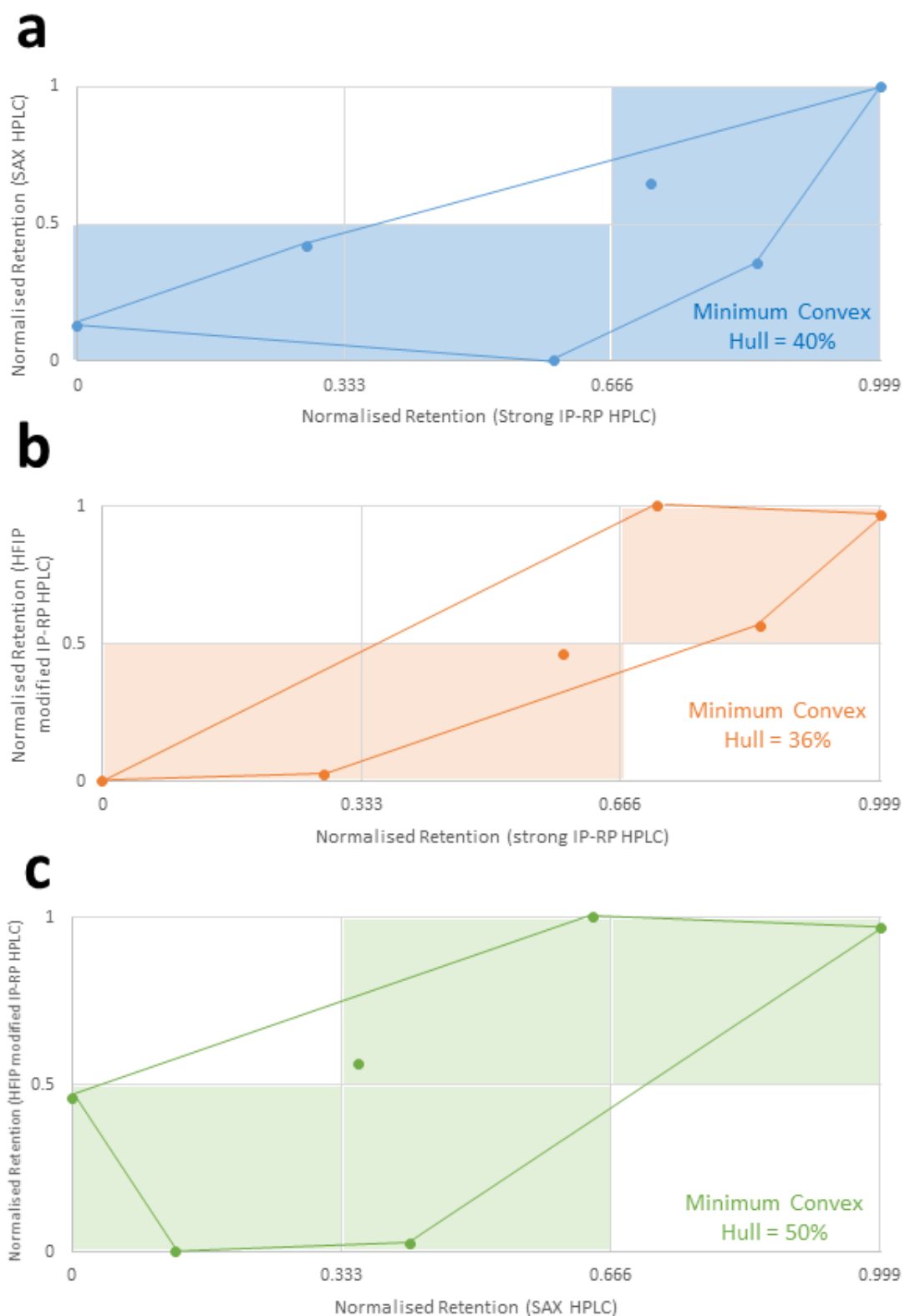
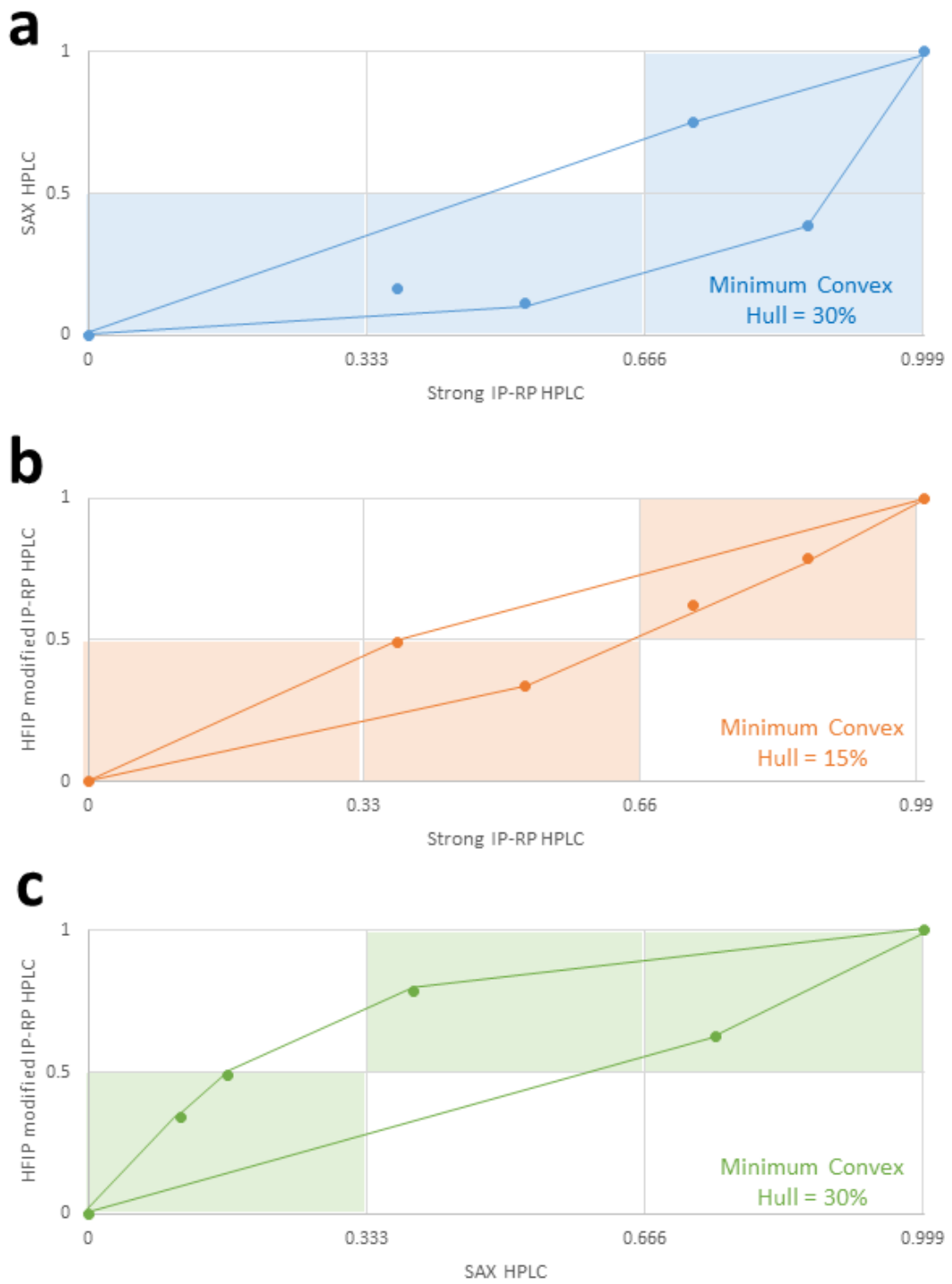
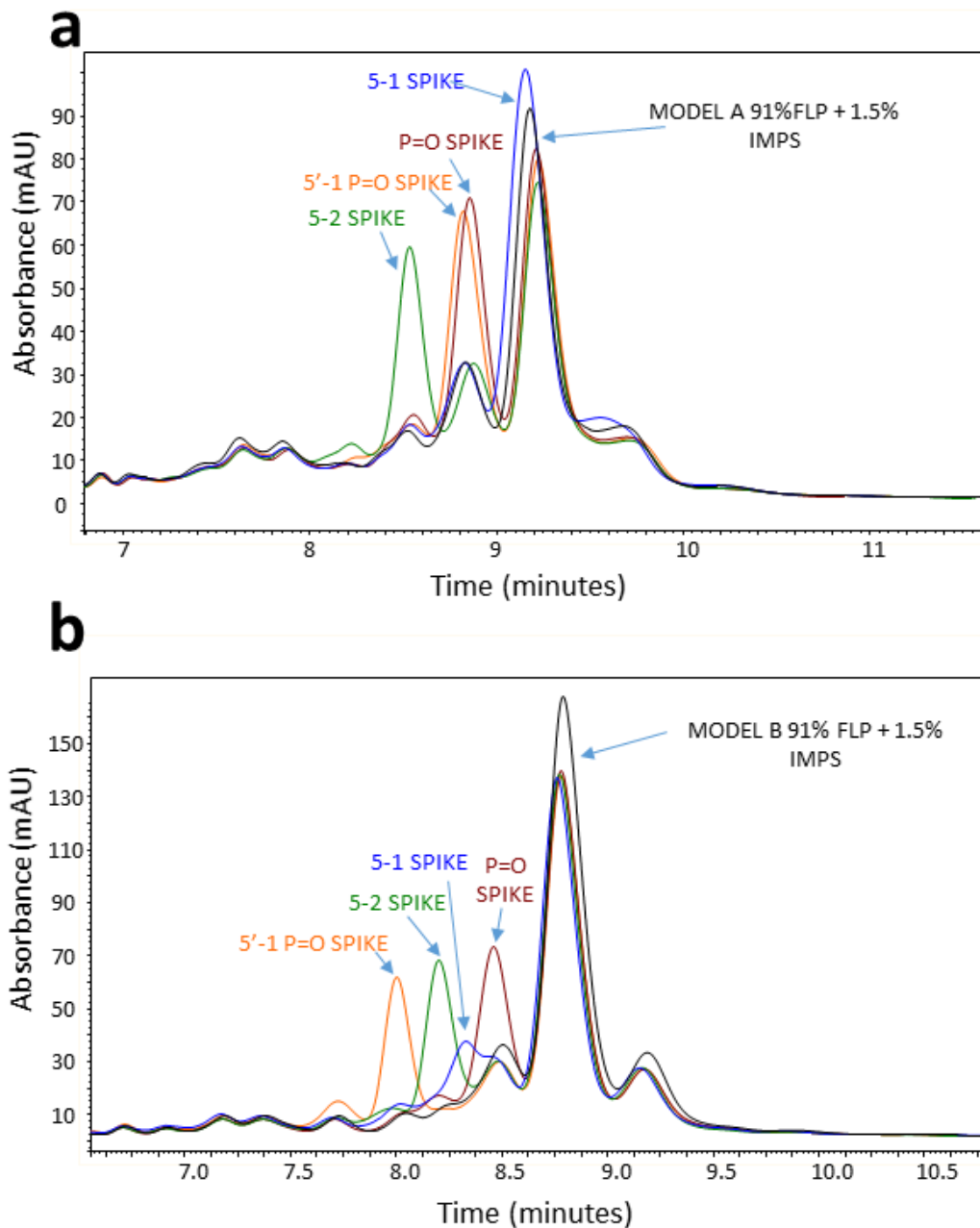


Figure A2.6: Minimum convex hull area of 2D-LC workflows for analysis of Model A PS OGN. a: Strong IP-RP – SAX 2D-LC. b: Strong IP-RP – HFIP modified IP-RP 2D-LC. c: HFIP modified IP-RP – SAX 2D-LC.



**Figure A2.7: Minimum convex hull area of 2D-LC workflows for analysis of Model B PS OGNs. a: Strong IP-RP – SAX 2D-LC. b: Strong IP-RP > HFIP modified IP-RP 2D-LC. c: HFIP modified IP-RP > SAX 2D-LC.**



**Figure A2.8: Spiking experiments analysis of PS OGNs using HFIP modified IP-RP HPLC.** 100 picomole sample with associated manufacturing impurities added at 1.5%. 20% sample volume spiked with highlighted impurities (5'-1, 5'-2, P=O and 5'-1 P=O). Analysed using HFIP modified IP-RP with 100 mM TEAA, 40 mM HFIP, 0.1 mM Na<sub>4</sub>EDTA and 11.25-17.5% v/v MeCN gradient from 1-15 min. Analysed at 0.2 ml/min and 75°C on a DNAPac RP column. **a:** Model A PS OGN. **b:** Model B PS OGN.

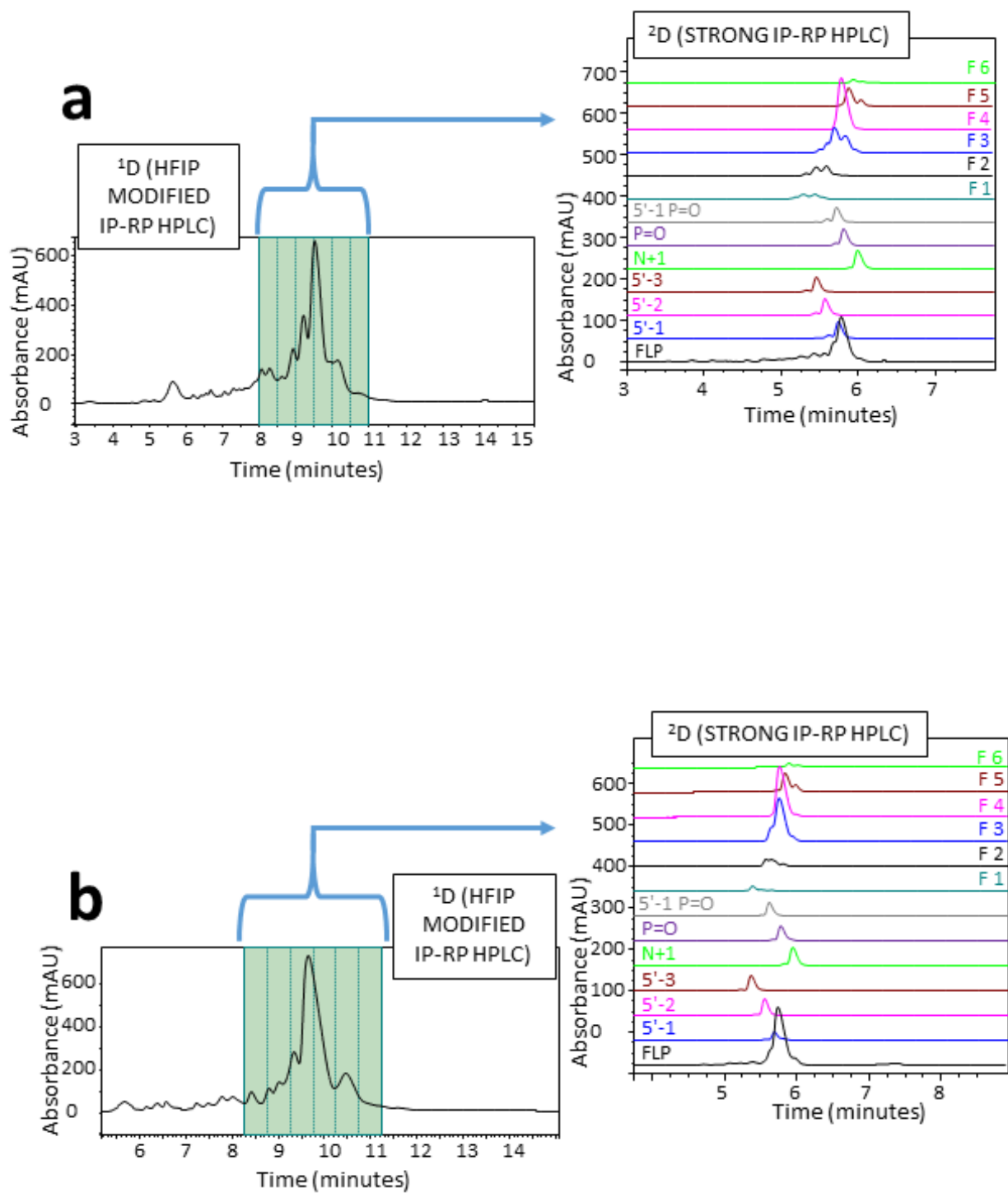


**Figure A2.9: Offline HFIP modified IP-RP to strong IP-RP 2D-LC analysis of Model A and B PS OGNs.** 1<sup>st</sup> dimension using 100 mM TEAA, 40 mM HFIP, 0.1 mM Na<sub>4</sub> EDTA and 11.25-17.5% v/v MeCN gradient from 1-15 min. 1000 picomole sample analysed at 0.2 ml/min and 75 °C and fractionated, using a DNAPac RP column. 2<sup>nd</sup> dimension using 5 mM TBuAA, 0.1 μM Na<sub>4</sub> EDTA and 34.5-59% v/v MeCN gradient from 1-15 min. Analysis at 0.2 ml/min and 50 °C using a DNAPac RP column. 15 picomole samples of reference OGNs were analysed in the 1<sup>st</sup> dimension to track elution order. **a:** Offline 2D-LC analysis of Model A PS OGN sample set with FLP at 91% sample amount and impurities at 1.5 % sample amount (replicate 2). **b:** Offline 2D-LC analysis of Model B PS OGN set with FLP at 91% sample amount and impurities at 1.5 % sample amount (replicate 2).

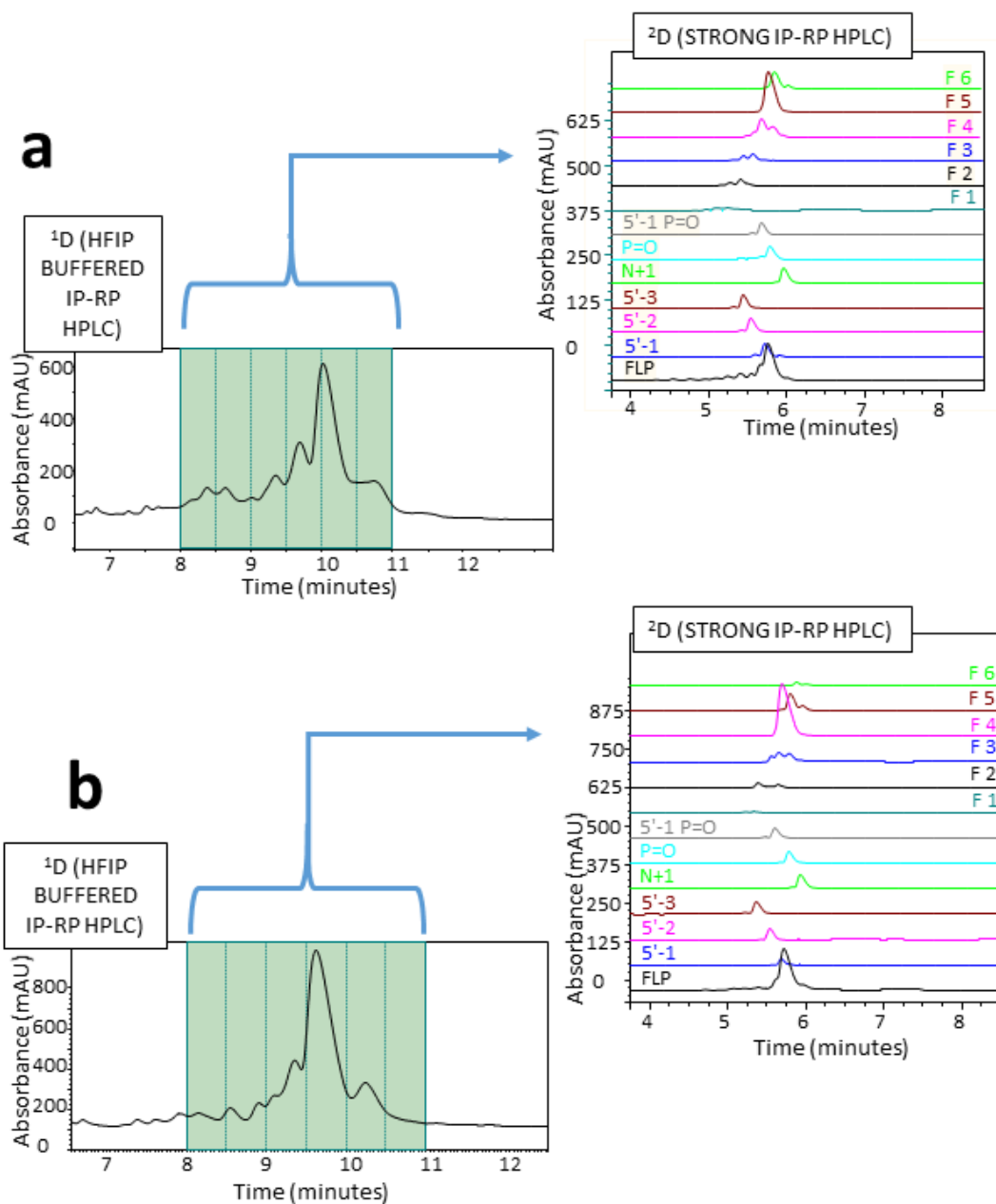


**Figure A2.10: Online heart-cut HFIP modified IP-RP to strong IP-RP 2D-LC analysis of PS OGN Model A and B samples (replicate 2).** 1<sup>st</sup> dimension HFIP modified IP-RP HPLC using 100 mM TEAA, 40 mM HFIP, 0.1 mM Na<sub>4</sub> EDTA and 11.25-17.5% v/v MeCN gradient from 1-15 min. 1000 picomole sample analysed at 0.2 ml/min, 75 °C and fractionated, using a DNAPac RP column. 2<sup>nd</sup> dimension strong IP-RP using 5 mM TBuAA, 0.1 μM Na<sub>4</sub> EDTA and 34.5-59% v/v MeCN gradient from 1-15 min. Analysis at 0.2 ml/min and 50 °C using a DNAPac RP column. 15 picomole samples of reference OGNs were analysed in the 1<sup>st</sup> dimension to track elution order. **a:** Online 2D-LC performed on Model A PS OGN sample set with FLP at 91% sample amount and impurities at 1.5 % sample amount (replicate 2). **b:** Online 2D-LC performed on Model B PS OGN sample set with FLP at 91% sample amount and impurities at 1.5 % sample amount (replicate 2).

## A2.4 Chapter 6 data supplements.

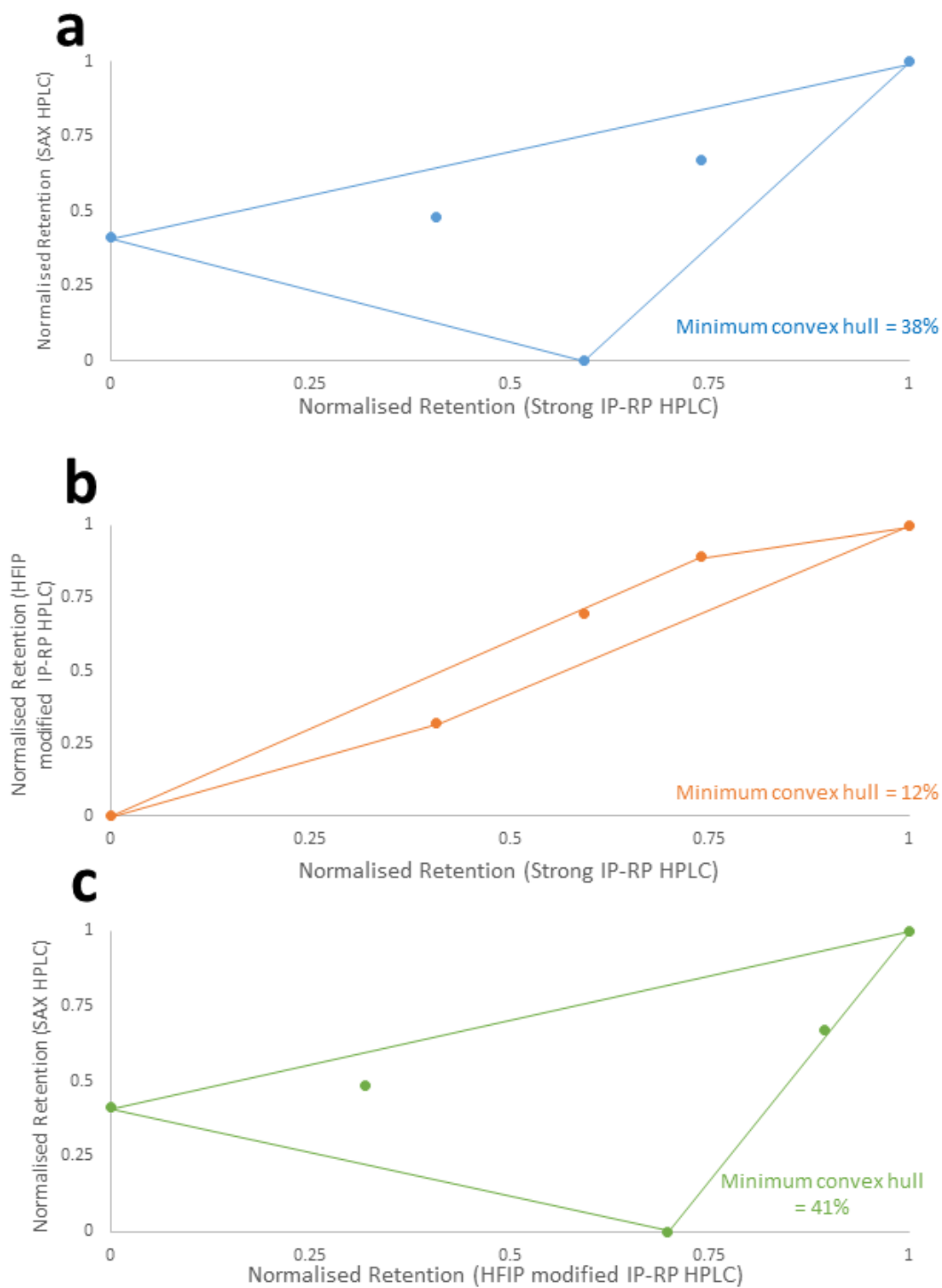


**Figure A2.11: Minimum convex hull area of 2D-LC workflows for analysis of the therapeutic OGN and its associated manufacturing impurities. a: Strong IP-RP – SAX 2D-LC. b: Strong IP-RP – HFIP modified IP-RP 2D-LC. c: HFIP modified IP-RP – SAX 2D-LC.**

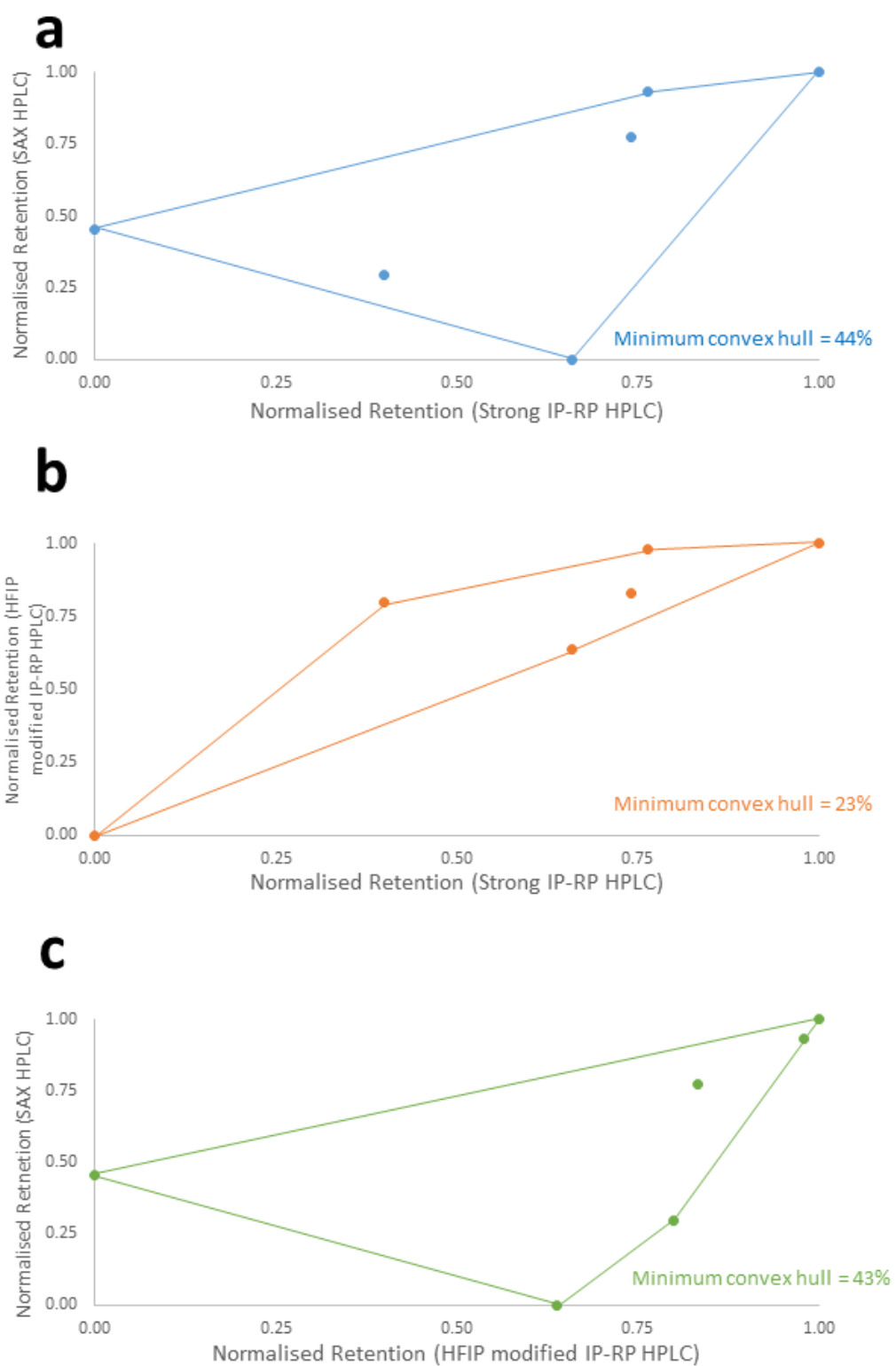


**Figure A2.12: Minimum convex hull area of 2D-LC workflows for analysis of the conjugated therapeutic OGN and its associated manufacturing impurities. a: Strong IP-RP – SAX 2D-LC. b: Strong IP-RP – HFIP modified IP-RP 2D-LC. c: HFIP modified IP-RP – SAX 2D-LC.**

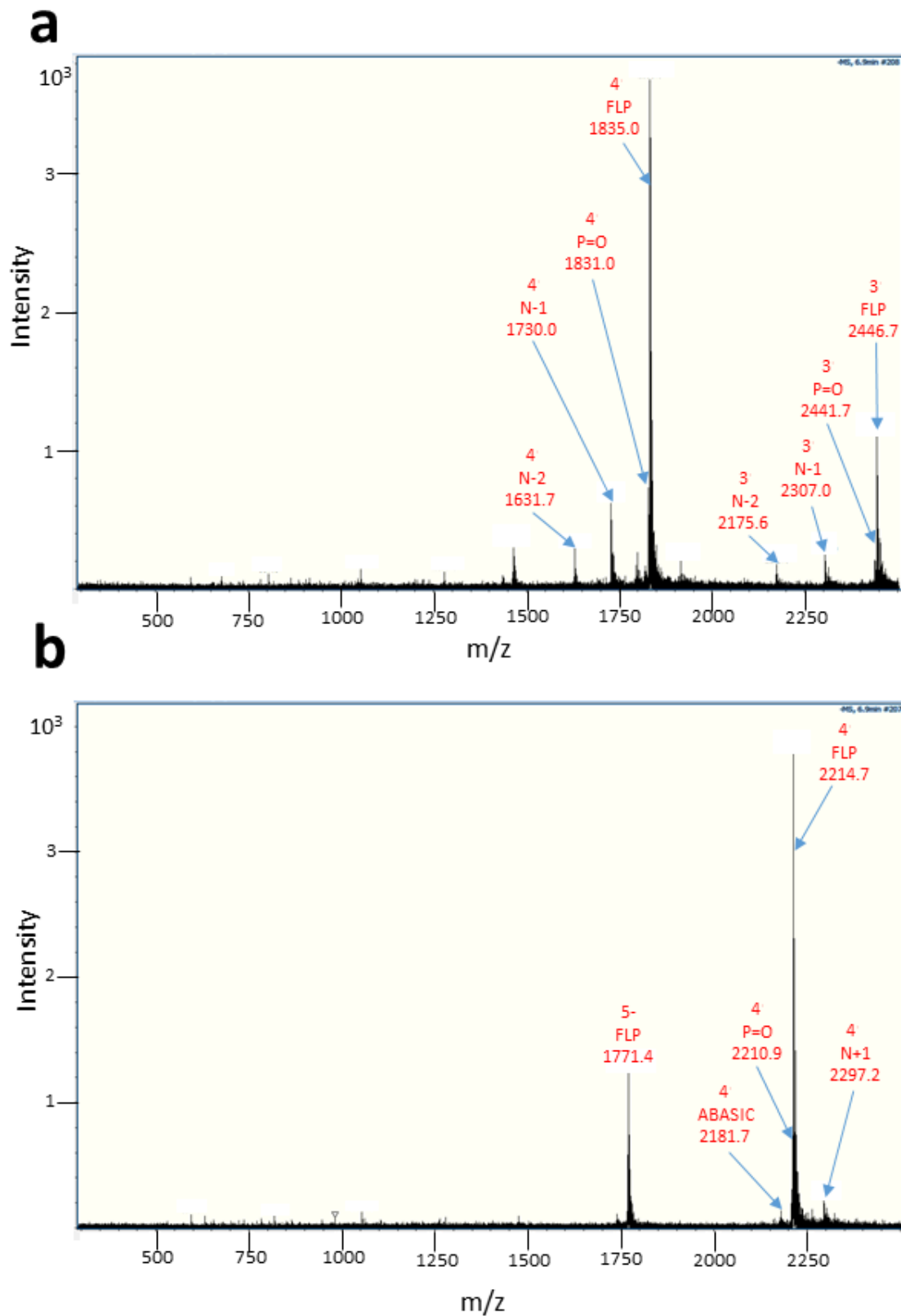


**Figure A2.13: Mass spectrometry analysis of fractions of a 1<sup>st</sup> dimension separation (fractionated under strong IP-RP HPLC conditions).** Shown here are example mass spectrums and OGN identifications. **a:** Analysis of the therapeutic OGN and associated manufacturing impurities using strong IP-RP-LC-MS, fraction 4. Mass spectrometry method is outlined in chapter 2. **b:** Analysis of the conjugated therapeutic OGN and associated manufacturing impurities using strong IP-RP-LC-MS, fraction 4. Mass spectrometry method is outlined in chapter 2.

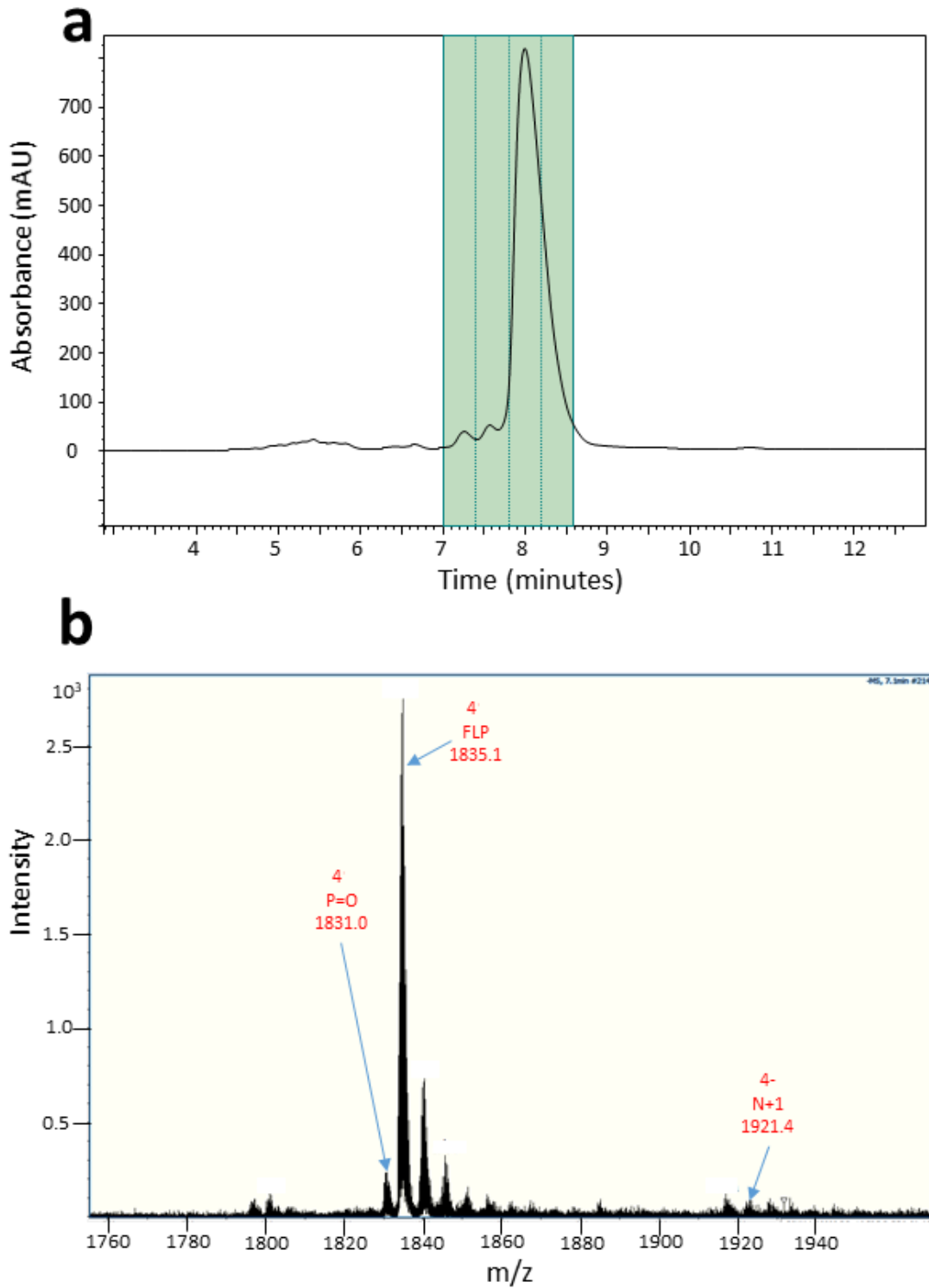


**Figure A2.14: MS analysis of fractions of the 1<sup>st</sup> dimension separation of the therapeutic OGN (fractionated under HFIP modified IP-RP HPLC conditions).** Shown here is the 1<sup>st</sup> dimension fractionation of the therapeutic OGN and its associated impurities with an example mass spectrum. **a:** 1<sup>st</sup> D fractionation was performed by HFIP modified IP-RP HPLC using 100 mM TEAA, 80 mM HFIP, 0.1 mM Na<sub>4</sub> EDTA and 16.25-21.25% v/v MeCN gradient from 1-15 minutes. Analysis performed at 0.3 ml/min and 30 °C using an Accucore C18 column. **b:** MS analysis of Fraction 3-method is outlined in chapter 2.

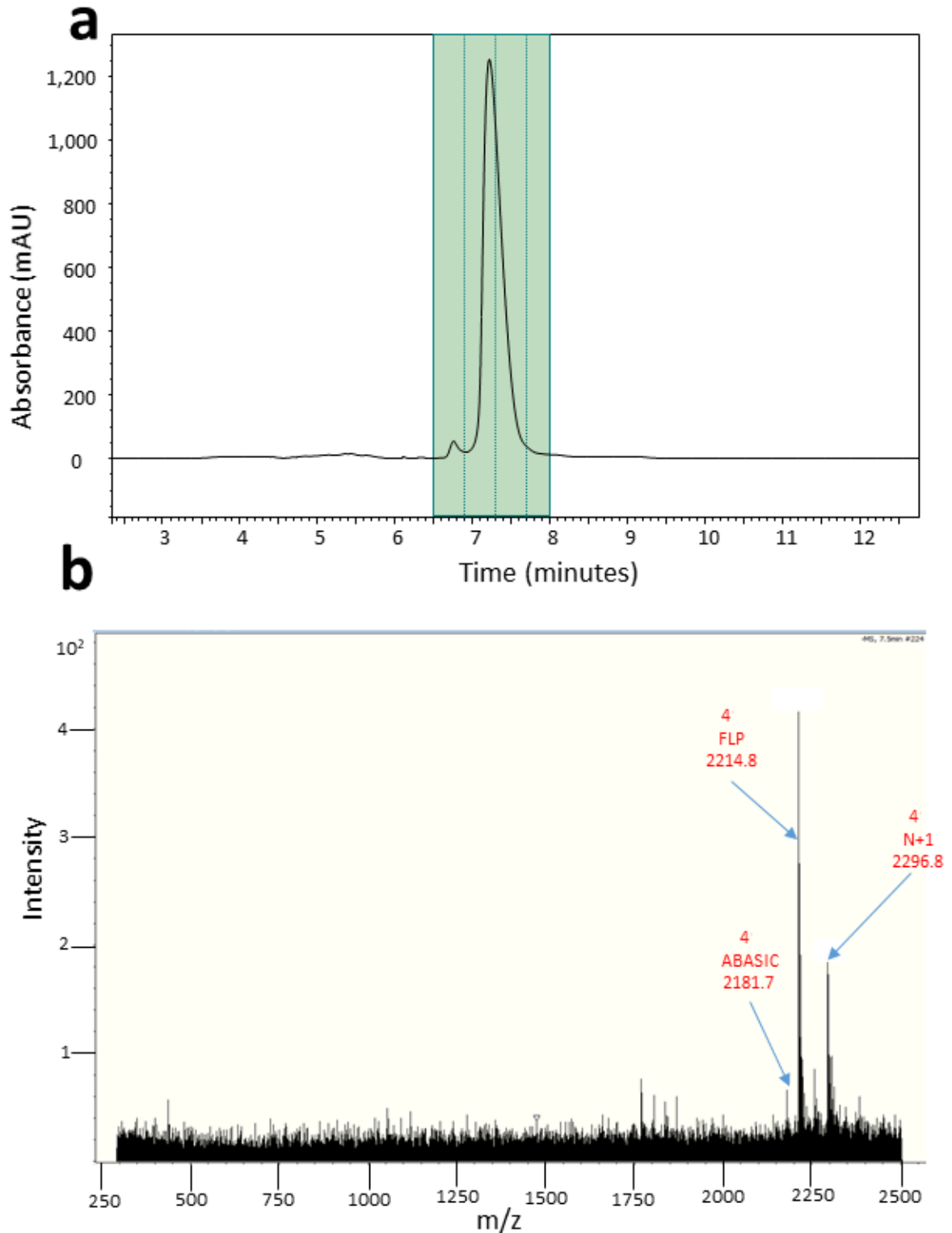


**Figure A2.15: MS analysis of fractions of the 1<sup>st</sup> dimension separation of the conjugated therapeutic OGN (fractionated under HFIP modified IP-RP HPLC conditions).** Shown here is the 1<sup>st</sup> dimension fractionation of the conjugated therapeutic OGN and its associated impurities with an example mass spectrum. **a:** 1<sup>D</sup> fractionation was performed by HFIP modified IP-RP HPLC using 100 mM TEAA, 80 mM HFIP, 0.1 mM Na<sub>4</sub> EDTA and 16.25-21.25% v/v MeCN gradient from 1-15 minutes. Analysis performed at 0.3 ml/min and 30 °C using an Accucore C18 column. **b:** MS analysis of Fraction 3-method is outlined in chapter 2.

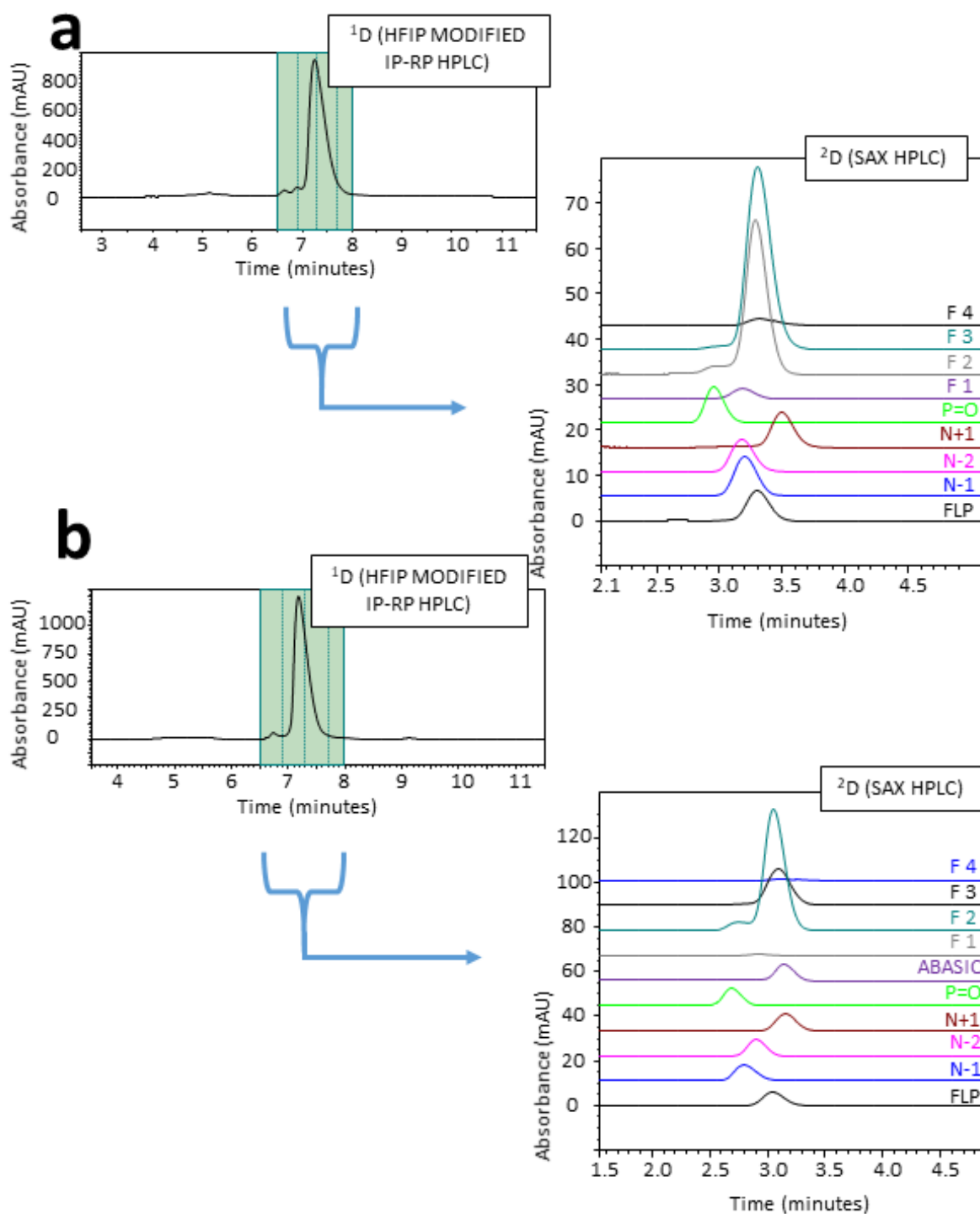


**Figure A2.16: Offline (HFIP modified IP-RP)-(SAX) 2D-LC analysis of 1000 picomole sample of OGN therapeutics and their associated manufacturing impurities (replicate 2).** Impurity concentration added at 1.5%. Reference mapping using 15 picomole of reference OGNs was concurrently analysed in the 2<sup>nd</sup> dimension. 1<sup>st</sup> dimension analysis was performed by HFIP modified IP-RP HPLC using a gradient of 100 mM TEAA, 80 mM HFIP, 0.1 mM Na<sub>4</sub> EDTA and 16.25-21.25% v/v MeCN from 1-15 minutes. Analysed at 0.3 ml/min and 30 °C using an Accucore C18 column. Four 120 µl fractions were collected from the 1<sup>st</sup> dimension. 20 µl of each fraction was analysed in a 2<sup>nd</sup> dimension of SAX HPLC using a gradient of 20 mM Tris, 160-264 mM NaClO<sub>4</sub> from 0-5.1 minutes. Analysed at 1.2 ml/min and 30 °C using a DNAPac Pa200 Rs column. **a:** Analysis of the therapeutic OGN (replicate 2). **b:** Analysis of the conjugated therapeutic OGN (replicate 2)..

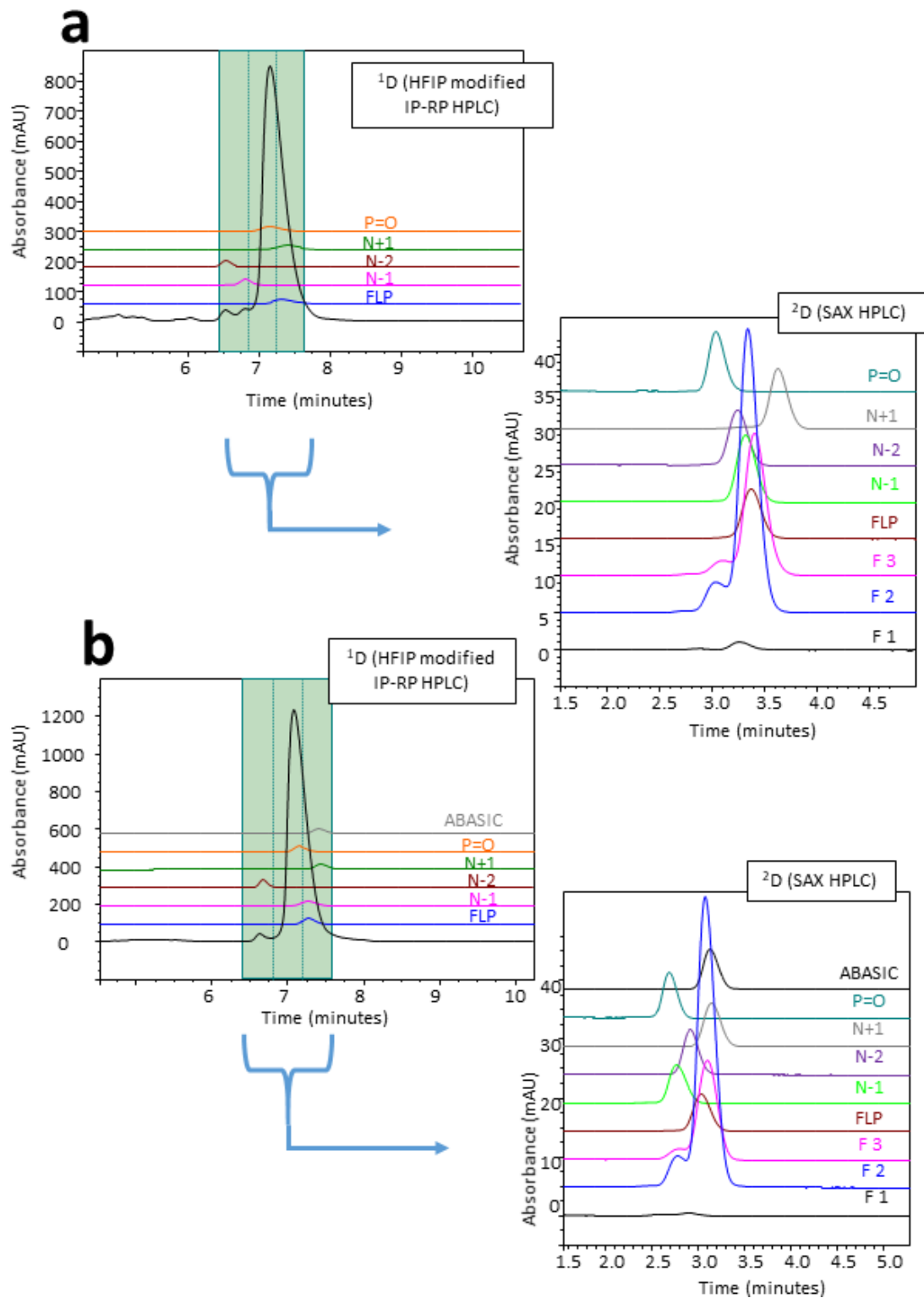


**Figure A2.17: Online heart-cut (HFIP modified IP-RP)-(SAX) 2D-LC analysis of 1000 picomole samples of OGN therapeutics and their associated manufacturing impurities (replicate 2).** Impurity OGNs concentrations added at 1.5%. Reference mapping using 15 picomole of reference OGNs was concurrently analysed in the 2<sup>nd</sup> dimension. 1<sup>st</sup> dimension analysis was performed by HFIP modified IP-RP HPLC using a gradient of 100 mM TEAA, 80 mM HFIP, 0.1 mM Na<sub>4</sub> EDTA and 16.25-21.25% v/v MeCN from 1-15 minutes. Analysed at 0.3 ml/min and 30 °C using an Accucore C18 column. Three 120 µl fractions were collected from the 1<sup>st</sup> dimension. 20 µl of each fraction was analysed in a 2<sup>nd</sup> dimension of SAX HPLC using a gradient of 20 mM Tris, 160-264 mM NaClO<sub>4</sub> pH 11.5 with 20% v/v MeCN from 0-5.1 minutes. Analysed at 1.2 ml/min and 30 °C using a DNAPac Pa200 Rs column. **a:** Analysis of the therapeutic OGN(replicate 2). **b:** Analysis of the conjugated therapeutic OGN (replicate 2).

## Bibliography.

- [1] B. D. Hames, *Biochemistry*, 4th ed. ed. New York NY: New York NY : Garland Science, c2011, (2011).
- [2] L. Miotke, H. Ji, A. Maity, K. Astakhova, and J. Brewer, "Enzyme- free detection of mutations in cancer DNA using synthetic oligonucleotide probes and fluorescence microscopy," *PLoS ONE*, vol. 10, no. 8, 2015, doi: 10.1371/journal.pone.0136720.
- [3] M. Konrad, "Plasmid DNA sequencing using highly degenerate oligonucleotides as primers," *Nucleic Acids Research*, vol. 18, no. 17, p. 5320, 1990, doi: 10.1093/nar/18.17.5320.
- [4] M. Trévisan, M. Schawaller, G. Quapil, E. Souteyrand, Y. Mérieux, and J.-P. Cloarec, "Evanescent wave fluorescence biosensor combined with DNA bio- barcode assay for platelet genotyping," *Biosensors and Bioelectronics*, vol. 26, no. 4, pp. 1631-1637, 2010, doi: 10.1016/j.bios.2010.08.038.
- [5] E. M. Southern, "Measurement of DNA length by gel electrophoresis," *Analytical Biochemistry*, vol. 100, no. 2, pp. 319-323, 1979, doi: 10.1016/0003-2697(79)90235-5.
- [6] S.-N. Park, Y. Lim, and J.-K. Kook, "Development of quantitative real-time PCR primers for detecting 42 oral bacterial species," *Archives of Microbiology*, vol. 195, no. 7, pp. 473-482, 2013, doi: 10.1007/s00203-013-0896-4.
- [7] A. East, A. Cheng, S. Lin, and J. Doudna, "RNA-programmed genome editing in human cells," *eLife*, vol. 2, no. 2, 2013, doi: 10.7554/eLife.00471.
- [8] R. J. Fernandes and S. S. Skiena, "Microarray synthesis through multiple- use PCR primer design," *Bioinformatics*, vol. 18, no. 1, pp. 128-135, 2002.
- [9] P. Chapdelaine, H.-K. My-Anh, R. R. Tremblay, and J. Y. Dube, "Southern blot analysis with synthetic oligonucleotides. Application to prostatic protein genes," *International Journal of Biochemistry*, vol. 22, no. 1, pp. 75-82, 1990, doi: 10.1016/0020-711X(90)90080-M.
- [10] H. Sommerfelt, A. M. Svennerholm, K. H. Kalland, B. I. Haukanes, and B. Bjorvatn, "Comparative study of colony hybridization with synthetic oligonucleotide probes and enzyme- linked immunosorbent assay for identification of enterotoxigenic Escherichia coli," *Journal of Clinical Microbiology*, vol. 26, no. 3, pp. 530-534, 1988.
- [11] C. A. Stein and D. Castanotto, "FDA- Approved Oligonucleotide Therapies in 2017," *Molecular Therapy*, vol. 25, no. 5, pp. 1069-1075, 2017, doi: 10.1016/j.ymthe.2017.03.023.
- [12] A. Khvorova and J. K. Watts, "The chemical evolution of oligonucleotide therapies of clinical utility," *Nature Biotechnology*, 2017, doi: 10.1038/nbt.3765.
- [13] J. M. Beierlein, L. M. McNamee, and F. D. Ledley, "As Technologies for Nucleotide Therapeutics Mature, Products Emerge," *Molecular Therapy - Nucleic Acids*, vol. 9, no. C, pp. 379-386, 2017, doi: 10.1016/j.omtn.2017.10.017.
- [14] F. Andrew, X. Siqun, K. M. Mary, A. K. Steven, E. D. Samuel, and C. M. Craig, "Potent and specific genetic interference by double- stranded RNA in *Caenorhabditis elegans*," *Nature*, vol. 391, no. 6669, p. 806, 1998, doi: 10.1038/35888.
- [15] M. L. Stephenson and P. C. Zamecnik, "Inhibition of Rous sarcoma viral RNA translation by a specific oligodeoxyribonucleotide," *Proceedings of the National Academy of Sciences of the United States of America*, vol. 75, no. 1, p. 285, 1978, doi: 10.1073/pnas.75.1.285.
- [16] B. M. Paterson, B. E. Roberts, and E. L. Kuff, "Structural gene identification and mapping by DNA-mRNA hybrid-arrested cell-free translation," *Proceedings of the National Academy of Sciences of the United States of America*, vol. 74, no. 10, p. 4370, 1977, doi: 10.1073/pnas.74.10.4370.
- [17] T. Wirth, N. Parker, and S. Ylä-Herttuala, "History of gene therapy," *Gene*, vol. 525, no. 2, pp. 162-169, 2013, doi: 10.1016/j.gene.2013.03.137.

- [18] L. Cong *et al.*, "Multiplex genome engineering using CRISPR/Cas systems," *Science (New York, N.Y.)*, vol. 339, no. 6121, pp. 819-823, 2013, doi: 10.1126/science.1231143.
- [19] Y. Weng *et al.*, "The challenge and prospect of mRNA therapeutics landscape," *Biotechnology Advances*, vol. 40, 2020, doi: 10.1016/j.biotechadv.2020.107534.
- [20] W. Brad Wan and P. P. Seth, "The Medicinal Chemistry of Therapeutic Oligonucleotides," *Journal of Medicinal Chemistry*, vol. 59, no. 21, pp. 9645-9667, 2016, doi: 10.1021/acs.jmedchem.6b00551.
- [21] A. M. Rossor, M. M. Reilly, and J. N. Sleight, "Antisense oligonucleotides and other genetic therapies made simple," *Practical Neurology*, vol. 18, no. 2, p. 126, 2018, doi: 10.1136/practneurol-2017-001764.
- [22] K. P. Anderson, M. C. Fox, V. Brown-Driver, M. J. Martin, and R. F. Azad, "Inhibition of human cytomegalovirus immediate- early gene expression by an antisense oligonucleotide complementary to immediate- early RNA," *Antimicrobial agents and chemotherapy*, vol. 40, no. 9, p. 2004, 1996.
- [23] M. A. Havens and M. L. Hastings, "Splice- switching antisense oligonucleotides as therapeutic drugs," *Nucleic acids research*, vol. 44, no. 14, p. 6549, 2016, doi: 10.1093/nar/gkw533.
- [24] D. Li, F. L. Mastaglia, S. Fletcher, and S. D. Wilton, "Precision Medicine through Antisense Oligonucleotide-Mediated Exon Skipping," *Trends in Pharmacological Sciences*, vol. 39, no. 11, pp. 982-994, 2018, doi: 10.1016/j.tips.2018.09.001.
- [25] L. Wan and G. Dreyfuss, "Splicing-Correcting Therapy for SMA," *Cell*, vol. 170, no. 1, pp. 5-5, 2017, doi: 10.1016/j.cell.2017.06.028.
- [26] Y.-A. Heo, "Golodirsen: First Approval," *Drugs*, vol. 80, no. 3, pp. 329-333, 2020, doi: 10.1007/s40265-020-01267-2.
- [27] J. Kim *et al.*, "Patient-Customized Oligonucleotide Therapy for a Rare Genetic Disease," *N Engl J Med*, vol. 381, no. 17, pp. 1644-1652, 2019, doi: 10.1056/NEJMoa1813279.
- [28] R. L. Juliano, "The delivery of therapeutic oligonucleotides," *Nucleic acids research*, vol. 44, no. 14, p. 6518, 2016, doi: 10.1093/nar/gkw236.
- [29] P. H. Hagedorn *et al.*, "Hepatotoxic Potential of Therapeutic Oligonucleotides Can Be Predicted from Their Sequence and Modification Pattern," *nucleic acid therapeutics*, vol. 23, no. 5, pp. 32-310, 2013, doi: 10.1089/nat.2013.0436.
- [30] T. P. Prakash *et al.*, "Targeted delivery of antisense oligonucleotides to hepatocytes using triantennary N-acetyl galactosamine improves potency 10-fold in mice," *Nucleic acids research*, vol. 42, no. 13, pp. 8796-8807, 2014, doi: 10.1093/nar/gku531.
- [31] C. Ammala *et al.*, "Targeted delivery of antisense oligonucleotides to pancreatic beta-cells," *Sci. Adv.*, vol. 4, no. 10, 2018, doi: 10.1126/sciadv.aat3386.
- [32] T. Yamamoto, M. Sawamura, F. Wada, M. Harada-Shiba, and S. Obika, "Serial incorporation of a monovalent GalNAc phosphoramidite unit into hepatocyte-targeting antisense oligonucleotides," *Bioorganic & Medicinal Chemistry*, vol. 24, no. 1, pp. 26-32, 2016, doi: 10.1016/j.bmc.2015.11.036.
- [33] S. T. Crooke, S. Wang, T. A. Vickers, W. Shen, and X.-H. Liang, "Cellular uptake and trafficking of antisense oligonucleotides," *Nature biotechnology*, vol. 35, no. 3, pp. 230-237, 2017, doi: 10.1038/nbt.3779.
- [34] J. P. Patrick, A. C. Amy, and J. H. Gregory, "Stable suppression of gene expression by RNAi in mammalian cells," *Proceedings of the National Academy of Sciences of the United States of America*, vol. 99, no. 3, p. 1443, 2002, doi: 10.1073/pnas.032652399.
- [35] D. Haussecker, "The Business of RNAi Therapeutics in 2012," *Molecular Therapy - Nucleic Acids*, vol. 1, no. C, 2012, doi: 10.1038/mtna.2011.9.
- [36] D. Adams *et al.*, "Patisiran, an RNAi Therapeutic, for Hereditary Transthyretin Amyloidosis," *The New England Journal of Medicine*, vol. 379, no. 1, pp. 11-21, 2018, doi: 10.1056/NEJMoa1716153.

- [37] R. Agami, "RNAi and related mechanisms and their potential use for therapy," *Current Opinion in Chemical Biology*, vol. 6, no. 6, pp. 829-834, 2002, doi: 10.1016/S1367-5931(02)00378-2.
- [38] S. C. Semple *et al.*, "Rational design of cationic lipids for siRNA delivery," *Nature Biotechnology*, vol. 28, no. 2, p. 172, 2010, doi: 10.1038/nbt.1602.
- [39] C. Alabi, A. Vegas, and D. Anderson, "Attacking the genome: emerging siRNA nanocarriers from concept to clinic," *Current Opinion in Pharmacology*, vol. 12, no. 4, pp. 427-433, 2012, doi: 10.1016/j.coph.2012.05.004.
- [40] W. Querbes *et al.*, "Direct CNS delivery of siRNA mediates robust silencing in oligodendrocytes," *Oligonucleotides*, vol. 19, no. 1, pp. 23-30, 2009.
- [41] M. E. Davis, "The First Targeted Delivery of siRNA in Humans via a Self-Assembling, Cyclodextrin Polymer-Based Nanoparticle: From Concept to Clinic," in *Mol. Pharm.* vol. 6, ed, 2009, pp. 659-668.
- [42] S. Kruspe and P. Giangrande, "Aptamer-siRNA Chimeras: Discovery, Progress, and Future Prospects," *Biomedicines*, vol. 5, no. 3, 2017, doi: 10.3390/biomedicines5030045.
- [43] S. M. Hoy, "Patisiran: First Global Approval," *Drugs*, vol. 78, no. 15, pp. 1625-1631, 2018, doi: 10.1007/s40265-018-0983-6.
- [44] T. Coelho *et al.*, "Safety and Efficacy of RNAi Therapy for Transthyretin Amyloidosis," *The New England Journal of Medicine*, vol. 369, no. 9, pp. 819-829, 2013, doi: 10.1056/NEJMoa1208760.
- [45] C. Tuerk and L. Gold, "Systematic Evolution of Ligands by Exponential Enrichment: RNA Ligands to Bacteriophage T4 DNA Polymerase," *Science*, vol. 249, no. 4968, pp. 505-510, 1990.
- [46] Y. Zheng, Y. Wang, and X. Yang, "Aptamer-based colorimetric biosensing of dopamine using unmodified gold nanoparticles," *Sensors & Actuators: B. Chemical*, vol. 156, no. 1, pp. 95-99, 2011, doi: 10.1016/j.snb.2011.03.077.
- [47] M. Yigit, D. Mazumdar, and Y. Lu, "MRI Detection of Thrombin with Aptamer Functionalized Superparamagnetic Iron Oxide Nanoparticles," *Bioconjugate Chemistry*, vol. 19, no. 2, p. 412, 2008, doi: 10.1021/bc7003928.
- [48] S. M. Nimjee, R. R. White, R. C. Becker, and B. A. Sullenger, "Aptamers as Therapeutics," in *Annu. Rev. Pharmacol. Toxicol.* vol. 57, ed, 2017, pp. 61-79.
- [49] E. W. Ng, D. T. Shima, P. Calias, E. T. Cunningham, D. R. Guyer, and A. P. Adamis, "Pegaptanib, a targeted anti-VEGF aptamer for ocular vascular disease," *Nature reviews drug discovery*, vol. 5, no. 2, pp. 123-132, 2006.
- [50] Z. Li and T. M. Rana, "Therapeutic targeting of microRNAs: current status and future challenges," in *Nat. Rev. Drug Discov.* vol. 13, ed, 2014, pp. 622-638.
- [51] M.-S. Song and J. J. Rossi, "The anti-miR21 antagomir, a therapeutic tool for colorectal cancer, has a potential synergistic effect by perturbing an angiogenesis-associated miR30," *Frontiers in genetics*, vol. 4, pp. 301-301, 2014, doi: 10.3389/fgene.2013.00301.
- [52] K. S. Frazier, "Antisense Oligonucleotide Therapies: The Promise and the Challenges from a Toxicologic Pathologist's Perspective," *Toxicologic Pathology*, vol. 43, no. 1, pp. 78-89, 2015, doi: 10.1177/0192623314551840.
- [53] M. Caskey *et al.*, "Synthetic double-stranded RNA induces innate immune responses similar to a live viral vaccine in humans," *The Journal of experimental medicine*, vol. 208, no. 12, pp. 2357-2366, 2011, doi: 10.1084/jem.20111171.
- [54] A. F. Radovic-Moreno *et al.*, "Immunomodulatory spherical nucleic acids," *Proceedings of the National Academy of Sciences*, vol. 112, no. 13, pp. 3892-3897, 2015.
- [55] I. Dotan *et al.*, "Ameliorating Active Ulcerative Colitis via an Orally Available Toll-Like Receptor-9 Modifier: A Prospective Open-Label, Multicenter Phase II Trial," *Digestive Diseases and Sciences*, vol. 61, no. 11, pp. 3246-3254, 2016, doi: 10.1007/s10620-016-4276-1.

- [56] J. Dalal. "Oligonucleotide Therapeutics Industry: Global Market Overview, Shares, Growth, Demand, market Size, Production, Types & Applications and Forecast Report 2026." <https://medium.com/@jyoti.d3007/oligonucleotide-therapeutics-industry-global-market-overview-shares-growth-demand-market-size-d20abba81f59> (accessed 2020 ).
- [57] [www.marketreportsworld.com](http://www.marketreportsworld.com). "GLOBAL OLIGONUCLEOTIDE THERAPEUTICS MARKET SIZE, STATUS AND FORECAST 2019-2025." <https://www.marketreportsworld.com/global-oligonucleotide-therapeutics-market-14088531> (accessed 2020 ).
- [58] A. M. Michelson and A. R. Todd, "Nucleotides part XXXII. Synthesis of a dithymidine dinucleotide containing a 3': 5'- internucleotidic linkage," *Journal of the Chemical Society (Resumed)*, pp. 2632-2638, 1955, doi: 10.1039/JR9550002632.
- [59] B. C. Froehler, P. G. Ng, and M. D. Matteucci, "Synthesis of DNA via deoxynucleoside H-phosphonate intermediates," *Nucleic Acids Research*, vol. 14, no. 13, pp. 5399-5407, 1986, doi: 10.1093/nar/14.13.5399.
- [60] P. J. Garegg, I. Lindh, T. Regberg, J. Stawinski, R. Strömberg, and C. Henrichson, "Nucleoside H-phosphonates. III. Chemical synthesis of oligodeoxyribonucleotides by the hydrogenphosphonate approach," *Tetrahedron Letters*, vol. 27, no. 34, pp. 4051-4054, 1986, doi: 10.1016/S0040-4039(00)84908-4.
- [61] H. Seliger, M. Holupirek, and H.-H. Görtz, "Solid-phase oligonucleotide synthesis with affinity-chromatographic separation of the product," *Tetrahedron Letters*, vol. 19, no. 24, pp. 2115-2118, 1978, doi: 10.1016/S0040-4039(01)94764-1.
- [62] S. Roy and M. Caruthers, "Synthesis of DNA/ RNA and Their Analogs via Phosphoramidite and H-Phosphonate Chemistries," in *Molecules* vol. 18, ed, 2013, pp. 14268-14284.
- [63] I. D. Technologies, "Chemical Synthesis and Purification of Oligonucleotides," Integrated DNA Technologies, Online, 2011. [Online]. Available: <https://www.idtdna.com/pages/docs/technical-reports/chemical-synthesis-of-oligonucleotides.pdf?sfvrsn=4>
- [64] F. Wincott *et al.*, "Synthesis, deprotection, analysis and purification of RNA and ribosomes," *Nucleic Acids Research*, vol. 23, no. 14, pp. 2677-2684, 1995, doi: 10.1093/nar/23.14.2677.
- [65] G. Zon, "Automated synthesis of phosphorus-sulfur analogs of nucleic acids-25 years on: potential therapeutic agents and proven utility in biotechnology," *New J. Chem.*, vol. 34, no. 5, pp. 795-804, 2010, doi: 10.1039/b9nj00577c.
- [66] A. H. S. Hall, J. Wan, E. E. Shaughnessy, B. Ramsay Shaw, and K. A. Alexander, "RNA interference using boranophosphate siRNAs: structure-activity relationships," *Nucleic acids research*, vol. 32, no. 20, pp. 5991-6000, 2004, doi: 10.1093/nar/gkh936.
- [67] V. Rait *et al.*, "Boranophosphate Nucleic Acids - A Versatile DNA Backbone," *Nucleosides and Nucleotides*, vol. 18, no. 6-7, pp. 1379-1380, 1999, doi: 10.1080/07328319908044721.
- [68] F. Eckstein, "Phosphorothioates, Essential Components of Therapeutic Oligonucleotides," *nucleic acid therapeutics*, vol. 24, no. 6, pp. 374-387, 2014, doi: 10.1089/nat.2014.0506.
- [69] U. Flierl *et al.*, "Phosphorothioate backbone modifications of nucleotide-based drugs are potent platelet activators," *The Journal of experimental medicine*, vol. 212, no. 2, pp. 129-137, 2015, doi: 10.1084/jem.20140391.
- [70] S. Agrawal, J. Tamsamani, and J. Y. Tang, "Pharmacokinetics, biodistribution, and stability of oligodeoxynucleotide phosphorothioates in mice," *Proceedings of the National Academy of Sciences*, vol. 88, no. 17, pp. 7595-7599, 1991.
- [71] C. M. Miller *et al.*, "Stabilin-1 and Stabilin-2 are specific receptors for the cellular internalization of phosphorothioate-modified antisense oligonucleotides (ASOs) in the liver," *Nucleic acids research*, vol. 44, no. 6, pp. 2782-2794, 2016, doi: 10.1093/nar/gkw112.
- [72] R. S. Geary, D. Norris, R. Yu, and C. F. Bennett, "Pharmacokinetics, biodistribution and cell uptake of antisense oligonucleotides," *Advanced Drug Delivery Reviews*, vol. 87, pp. 46-51, 2015, doi: 10.1016/j.addr.2015.01.008.

- [73] S. M. Freier and K.-H. Altmann, "The ups and downs of nucleic acid duplex stability: structure-stability studies on chemically-modified DNA: RNA duplexes," *Nucleic acids research*, vol. 25, no. 22, pp. 4429-4443, 1997.
- [74] D. Showkat Ahmad, T. Anamika, Q. Abid, and K. Manoj, "siRNAmoD: A database of experimentally validated chemically modified siRNAs," *Scientific Reports*, vol. 6, no. 1, 2016, doi: 10.1038/srep20031.
- [75] M. Boczkowska, P. Guga, and W. J. Stec, "Stereo-defined phosphorothioate analogues of DNA: relative thermodynamic stability of the model PS-DNA/DNA and PS-DNA/RNA complexes," *Biochemistry*, vol. 41, no. 41, pp. 12483-12487, 2002, doi: 10.1021/bi026225z.
- [76] M. Koziolkiewicz, A. Krakowiak, M. Kwinkowski, M. Boczkowska, and W. J. Stec, "Stereo-differentiation--the effect of P chirality of oligo(nucleoside phosphorothioates) on the activity of bacterial RNase H," *Nucleic acids research*, vol. 23, no. 24, pp. 5000-5005, 1995, doi: 10.1093/nar/23.24.5000.
- [77] I. Naoki *et al.*, "Control of phosphorothioate stereochemistry substantially increases the efficacy of antisense oligonucleotides," *Nature Biotechnology*, vol. 35, no. 9, 2017, doi: 10.1038/nbt.3948.
- [78] Y. Nukaga, N. Oka, and T. Wada, "Stereocontrolled Solid-Phase Synthesis of Phosphate/Phosphorothioate (PO/PS) Chimeric Oligodeoxyribonucleotides on an Automated Synthesizer Using an Oxazaphospholidine-Phosphoramidite Method," *The Journal of organic chemistry*, vol. 81, no. 7, p. 2753, 2016, doi: 10.1021/acs.joc.5b02793.
- [79] H. Jahns *et al.*, "Stereochemical bias introduced during RNA synthesis modulates the activity of phosphorothioate siRNAs," *Nature Communications*, vol. 6, no. 1, p. 6317, 2015, doi: 10.1038/ncomms7317.
- [80] D. Mutisya *et al.*, "Amides are excellent mimics of phosphate internucleoside linkages and are well tolerated in short interfering RNAs," *Nucleic acids research*, vol. 42, no. 10, pp. 6542-6551, 2014, doi: 10.1093/nar/gku235.
- [81] J. Summerton and D. Weller, "Morpholino antisense oligomers: design, preparation, and properties," *Antisense and Nucleic Acid Drug Development*, vol. 7, no. 3, pp. 187-195, 1997.
- [82] S. Cirak *et al.*, "Exon skipping and dystrophin restoration in patients with Duchenne muscular dystrophy after systemic phosphorodiamidate morpholino oligomer treatment: an open-label, phase 2, dose-escalation study," *The Lancet*, vol. 378, no. 9791, pp. 595-605, 2011, doi: 10.1016/S0140-6736(11)60756-3.
- [83] M. Egli *et al.*, "Probing the influence of stereoelectronic effects on the biophysical properties of oligonucleotides: comprehensive analysis of the RNA affinity, nuclease resistance, and crystal structure of ten 2'-O-ribonucleic acid modifications," *Biochemistry*, vol. 44, no. 25, pp. 9045-9057, 2005, doi: 10.1021/bi050574m.
- [84] L. Cummins *et al.*, "CHARACTERIZATION OF FULLY 2'-MODIFIED OLIGORIBONUCLEOTIDE HETERODUPLEX AND HOMODUPLEX HYBRIDIZATION AND NUCLEASE SENSITIVITY," *Nucleic Acids Res.*, vol. 23, no. 11, pp. 2019-2024, 1995, doi: 10.1093/nar/23.11.2019.
- [85] T. P. Prakash *et al.*, "Positional effect of chemical modifications on short interference RNA activity in mammalian cells," *Journal of medicinal chemistry*, vol. 48, no. 13, pp. 4247-4253, 2005, doi: 10.1021/jm050044o.
- [86] C. F. Bennett, "Pharmacological properties of 2'-O-methoxyethyl-modified oligonucleotides," *Antisense Drug Technology: Principles, Strategies, and Applications. 2nd ed.* Boca Raton, FL: CRC Press/Taylor & Francis Group, pp. 273-303, 2007.
- [87] C. Allerson *et al.*, "Fully 2'-Modified Oligonucleotide Duplexes with Improved in Vitro Potency and Stability Compared to Unmodified Small Interfering RNA," *Journal of Medicinal Chemistry*, vol. 48, no. 4, pp. 901-904, 2005, doi: 10.1021/jm049167j.
- [88] M. Manoharan *et al.*, "Unique gene-silencing and structural properties of 2'-fluoro-modified siRNAs," *Angewandte Chemie (International ed. in English)*, vol. 50, no. 10, pp. 2284-2288, 2011, doi: 10.1002/anie.201006519.

- [89] B. P. Monia *et al.*, "Evaluation of 2'-modified oligonucleotides containing 2'-deoxy gaps as antisense inhibitors of gene expression," *The Journal of biological chemistry*, vol. 268, no. 19, pp. 14514-14522, 1993.
- [90] R. Owczarzy, Y. You, C. L. Groth, and A. V. Tataurov, "Stability and mismatch discrimination of locked nucleic acid-DNA duplexes," *Biochemistry*, vol. 50, no. 43, pp. 9352-9367, 2011, doi: 10.1021/bi200904e.
- [91] S. Singh, P. Nielsen, A. A. Koshkin, and J. Wengel, "LNA (locked nucleic acids): synthesis and high-affinity nucleic acid recognition," *Chem. Commun.*, no. 4, pp. 455-456, 1998.
- [92] E. Swayze *et al.*, "Antisense oligonucleotides containing locked nucleic acid improve potency but cause significant hepatotoxicity in animals," *Nucleic Acids Research*, vol. 35, no. 2, pp. 687-700, 2007, doi: 10.1093/nar/gkl1071.
- [93] K. Lennox and M. Behlke, "A Direct Comparison of Anti-microRNA Oligonucleotide Potency," *An Official Journal of the American Association of Pharmaceutical Scientists*, vol. 27, no. 9, pp. 1788-1799, 2010, doi: 10.1007/s11095-010-0156-0.
- [94] K.-Y. Lin, R. Jones, and M. Matteucci, "Tricyclic 2'-deoxycytidine analogs: Syntheses and incorporation into oligodeoxynucleotides which have enhanced binding to complementary RNA," *Journal of the American Chemical Society*, vol. 117, no. 13, pp. 3873-3874, 1995, doi: 10.1021/ja00118a026.
- [95] A. Gutierrez, T. Terhorst, M. D. Matteucci, and B. Froehler, "5-Heteroaryl-2'-deoxyuridine analogs. Synthesis and incorporation into high-affinity oligonucleotides," *Journal of the American Chemical Society*, vol. 116, no. 13, pp. 5540-5544, 1994, doi: 10.1021/ja00092a003.
- [96] D. Chen, Z. Yan, D. Cole, and G. Srivatsa, "Analysis of internal (n-1)mer deletion sequences in synthetic oligodeoxyribonucleotides by hybridization to an immobilized probe array," *Nucleic Acids Research*, vol. 27, no. 2, p. 389, 1999, doi: 10.1093/nar/27.2.389.
- [97] atdbio. "SOLID-PHASE OLIGONUCLEOTIDE SYNTHESIS." <https://www.atdbio.com/content/17/Solid-phase-oligonucleotide-synthesis> (accessed 2016).
- [98] D. Capaldi *et al.*, "Quality Aspects of Oligonucleotide Drug Development: Specifications for Active Pharmaceutical Ingredients," *Therapeutic Innovation & Regulatory Science*, vol. 46, no. 5, pp. 611-626, 2012, doi: 10.1177/0092861512445311.
- [99] D. Capaldi *et al.*, "Impurities in Oligonucleotide Drug Substances and Drug Products," *nucleic acid therapeutics*, vol. 27, no. 6, pp. 39-322, 2017, doi: 10.1089/nat.2017.0691.
- [100] K. L. Fearon, J. T. Stults, B. J. Bergot, L. M. Christensen, and A. M. Raible, "Investigation of the 'n-1' impurity in phosphorothioate oligodeoxynucleotides synthesized by the solid-phase beta-cyanoethyl phosphoramidite method using stepwise sulfurization," *Nucleic acids research*, vol. 23, no. 14, p. 2754, 1995.
- [101] J. Temsamani, M. Kubert, and S. Agrawal, "Sequence identity of the n-1 product of a synthetic oligonucleotide," *Nucleic acids research*, vol. 23, no. 11, p. 1841, 1995.
- [102] A. T. Yeung and C. G. Miller, "A general method of optimizing automated DNA synthesis to decrease chemical consumption to less than half," *Analytical Biochemistry*, vol. 187, no. 1, pp. 66-75, 1990, doi: 10.1016/0003-2697(90)90418-9.
- [103] A. H. Krotz, P. G. Klopchin, K. L. Walker, G. S. Srivatsa, D. L. Cole, and V. T. Ravikumar, "On the formation of longmers in phosphorothioate oligodeoxyribonucleotide synthesis," *Tetrahedron Letters*, vol. 38, no. 22, pp. 3875-3878, 1997, doi: 10.1016/S0040-4039(97)00798-3.
- [104] M. Septak, "Kinetic studies on depurination and detritylation of CPG-bound intermediates during oligonucleotide synthesis," *Nucleic Acids Research*, vol. 24, no. 15, pp. 3053-3058, 1996.
- [105] A. A. Rodriguez, I. Cedillo, and A. K. McPherson, "Conversion of adenine to 5-amino-4-pyrimidinylimidazole caused by acetyl capping during solid phase oligonucleotide synthesis,"

- Bioorganic & Medicinal Chemistry Letters*, vol. 26, no. 15, pp. 3468-3471, 2016, doi: 10.1016/j.bmcl.2016.06.042.
- [106] A. A. Rodriguez, I. Cedillo, B. P. Mowery, H. J. Gaus, S. S. Krishnamoorthy, and A. K. McPherson, "Formation of the N(2)-acetyl-2,6-diaminopurine oligonucleotide impurity caused by acetyl capping," *Bioorganic & medicinal chemistry letters*, vol. 24, no. 15, pp. 3243-3246, 2014, doi: 10.1016/j.bmcl.2014.06.025.
- [107] D. C. Capaldi *et al.*, "Synthesis of High-Quality Antisense Drugs. Addition of Acrylonitrile to Phosphorothioate Oligonucleotides: Adduct Characterization and Avoidance," *Organic Process Research and Development*, vol. 7, no. 6, pp. 832-838, 2003, doi: 10.1021/op020090n.
- [108] W. B. Wan *et al.*, "Synthesis, biophysical properties and biological activity of second generation antisense oligonucleotides containing chiral phosphorothioate linkages," *Nucleic acids research*, vol. 42, no. 22, p. 13456, 2014, doi: 10.1093/nar/gku1115.
- [109] C. Scremin and G. Bonora, "LIQUID-PHASE SYNTHESIS OF PHOSPHOROTHIOATE OLIGONUCLEOTIDES ON POLYETHYLENE-GLYCOL SUPPORT," *Tetrahedron Lett.*, vol. 34, no. 29, pp. 4663-4666, 1993.
- [110] D. Yu *et al.*, "Stereo-enriched phosphorothioate oligodeoxynucleotides: Synthesis, biophysical and biological properties," *Bioorg. Med. Chem.*, vol. 8, no. 1, pp. 275-284, 2000, doi: 10.1016/S0968-0896(99)00275-8.
- [111] A. H. Krotz *et al.*, "Phosphorothioate oligonucleotides with low phosphate diester content: Greater than 99.9% sulfurization efficiency with "aged" solutions of phenylacetyl disulfide (PADS)," *Organic Process Research and Development*, vol. 8, no. 6, pp. 852-858, 2004, doi: 10.1021/op040208v.
- [112] D. S. Levin, B. T. Shepperd, and C. J. Gruenloh, "Combining ion pairing agents for enhanced analysis of oligonucleotide therapeutics by reversed phase- ion pairing ultra performance liquid chromatography ( UPLC)," *Journal of Chromatography B*, vol. 879, no. 19, pp. 1587-1595, 2011, doi: 10.1016/j.jchromb.2011.03.051.
- [113] J. K. Frederiksen and J. A. Piccirilli, "Separation of RNA Phosphorothioate Oligonucleotides by HPLC," *Methods in Enzymology*, vol. 468, pp. 289-309, 2009, doi: 10.1016/S0076-6879(09)68014-9.
- [114] S. Seiffert *et al.*, "Characterization of side reactions during the annealing of small interfering RNAs," *Analytical Biochemistry*, vol. 414, no. 1, pp. 47-57, 2011, doi: 10.1016/j.ab.2011.02.040.
- [115] M. A. Morgan, S. A. Kazakov, and S. M. Hecht, "Phosphoryl migration during the chemical synthesis of RNA," *Nucleic acids research*, vol. 23, no. 19, p. 3949, 1995.
- [116] R. Kanasty, J. R. Dorkin, A. Vegas, and D. Anderson, "Delivery materials for siRNA therapeutics," *Nature materials*, vol. 12, no. 11, pp. 967-977, 2013, doi: 10.1038/nmat3765.
- [117] T. National Information Center on Health Services Research and Health Care, "International Conference on Harmonisation; guidance on Q6A specifications: test procedures and acceptance criteria for new drug substances and new drug products: chemical substances. Notice," *Federal register*, vol. 65, no. 251, pp. 83041-83063, 2000.
- [118] T. National Information Center on Health Services Research and Health Care, "International Conference on Harmonisation; guidance on specifications: test procedures and acceptance criteria for biotechnological/biological products. Notice. Food and Drug Administration, HHS," *Federal register*, vol. 64, no. 159, pp. 44928-44935, 1999.
- [119] M. Sapru, "CMC Regulatory Considerations for Oligonucleotide Drug Products: FDA Perspective

", ed. Online

2017.

- [120] A. Wake, "Characterization and impurity analysis of oligonucleotide therapeutics," *Pharmaceutical Technology*, vol. 41, no. 1, pp. 30-33, 2017.
- [121] I. E. W. Group, "Impurities: Guideline for residual solvents Q3C (R6)" "Impurities: Guideline for residual solvents Q3C (R6).", " ed: International Council for Harmonisation Geneva, 2016.
- [122] I. C. o. H. o. T. R. f. R. o. P. f. H. use, "Guideline for Elemental Impurities Q3D," ed, 2014.
- [123] U. F. a. D. Administration, "Naming of drug products containing salt drug substances; guidance for industry; availability," *Silver Spring: Center for Drug Evaluation and Research, US Food and Drug Administration*, 2015.
- [124] C. Chaix, C. Minard-Basquin, T. Delair, C. Pichot, and B. Mandrand, "Oligonucleotide synthesis on maleic anhydride copolymers covalently bound to silica spherical support and characterization of the obtained conjugates," *Journal of Applied Polymer Science*, vol. 70, no. 12, pp. 2487-2497, 1998, doi: 10.1002/(SICI)1097-4628(19981219)70:12<2487::AID-APP22>3.0.CO;2-H.
- [125] G. Huang and T. R. Krugh, "Large- scale purification of synthetic oligonucleotides and carcinogen- modified oligodeoxynucleotides on a reverse- phase polystyrene ( PRP- 1) column," *Analytical Biochemistry*, vol. 190, no. 1, pp. 21-25, 1990, doi: 10.1016/0003-2697(90)90127-U.
- [126] M. Smith, "Characterisation of a modified oligonucleotide together with its synthetic impurities using accurate mass measurements," *Rapid Communications in Mass Spectrometry*, vol. 25, no. 4, pp. 511-525, 2011, doi: 10.1002/rcm.4886.
- [127] Z. Cui, J. A. Theruvathu, A. Farrel, A. Burdzy, and L. C. Sowers, "Characterization of synthetic oligonucleotides containing biologically important modified bases by matrix- assisted laser desorption/ ionization time-of- flight mass spectrometry," *Analytical Biochemistry*, vol. 379, no. 2, pp. 196-207, 2008, doi: 10.1016/j.ab.2008.04.031.
- [128] A. Alving, "Improving Oligonucleotide Analysis," *Biopharm International*, vol. 32, no. 9, pp. 40-43, 2019.
- [129] C. L. Clark, P. K. Cecil, D. Singh, and D. M. Gray, "CD, absorption and thermodynamic analysis of repeating dinucleotide DNA, RNA and hybrid duplexes [d/r(AC)]<sub>12</sub>[d/r(GT/U)]<sub>12</sub> and the influence of phosphorothioate substitution," *Nucleic acids research*, vol. 25, no. 20, pp. 4098-4105, 1997, doi: 10.1093/nar/25.20.4098.
- [130] J. W. Jaroszewski, V. Clausen, J. S. Cohen, and O. Dahl, "NMR investigations of duplex stability of phosphorothioate and phosphorodithioate DNA analogues modified in both strands," *Nucleic Acids Research*, vol. 24, no. 5, pp. 829-834, 1996, doi: 10.1093/nar/24.5.829.
- [131] J. Santalucia Jr, "A unified view of polymer, dumbbell, and oligonucleotide DNA nearest-neighbor thermodynamics," *Proceedings of the National Academy of Sciences, USA*, vol. 95, no. 4, pp. 1460-1465, 1998.
- [132] H. Oberacher and F. Pitterl, "On the use of ESI- QqTOF- MS/ MS for the comparative sequencing of nucleic acids," *Biopolymers*, vol. 91, no. 6, pp. 401-409, 2009, doi: 10.1002/bip.21156.
- [133] U. Pielers, W. Zürcher, M. Schär, and H. E. Moser, "Matrix- assisted laser desorption ionization time-of- flight mass spectrometry: a powerful tool for the mass and sequence analysis of natural and modified oligonucleotides," *Nucleic acids research*, vol. 21, no. 14, p. 3191, 1993.
- [134] R. Matthiesen and F. Kirpekar, "Identification of RNA molecules by specific enzyme digestion and mass spectrometry: software for and implementation of RNA mass mapping," *Nucleic acids research*, vol. 37, no. 6, pp. e48-e48, 2009, doi: 10.1093/nar/gkp139.

- [135] B. Bergot and G. Zon, "SEPARATION OF SYNTHETIC PHOSPHOROTHIOATE OLIGONUCLEOTIDES FROM PHOSPHODIESTER-DEFECT SPECIES BY STRONG-ANION EXCHANGE HPLC," *Ann. N.Y. Acad. Sci.*, vol. 660, pp. 310-312, 1992.
- [136] M. Smith and T. Beck, "Quantitation of a low level coeluting impurity present in a modified oligonucleotide by both LC-MS and NMR," *Journal of pharmaceutical and biomedical analysis*, vol. 118, pp. 34-40, 2016, doi: 10.1016/j.jpba.2015.10.019.
- [137] Q. Zhang *et al.*, "Recent Methods for Purification and Structure Determination of Oligonucleotides," in *Int. J. Mol. Sci.* vol. 17, ed, 2016.
- [138] T. Brown, D. Kizza, M. Kiezel-Tsugunova, and A. Wake, "ANALYTICAL STRATEGIES FOR QUALITY CONTROL OF OLIGONUCLEOTIDE THERAPEUTICS," Intertek Group PLC, Online: [www.intertek.com](http://www.intertek.com), 2018. [Online]. Available: <https://www.intertek.com/knowledge-education/oligonucleotide-therapeutics-analytical-strategies-wp/>
- [139] M. P. Latham, D. J. Brown, S. A. McCallum, and A. Pardi, "NMR Methods for Studying the Structure and Dynamics of RNA," vol. 6, ed. Weinheim, 2005, pp. 1492-1505.
- [140] L. A. Dedionisio and D. H. Lloyd, "Capillary gel electrophoresis and antisense therapeutics analysis of DNA analogs," vol. 735, ed, 1996, pp. 191-208.
- [141] K. Grodowska and A. Parczewski, "ANALYTICAL METHODS FOR RESIDUAL SOLVENTS DETERMINATION IN PHARMACEUTICAL PRODUCTS," *ACTA POL. PHARM.*, vol. 67, no. 1, pp. 13-26, 2010.
- [142] Q. Tu, E. N. Guidry, F. Meng, T. Wang, and X. Gong, "A high-throughput flow injection inductively coupled plasma mass spectrometry method for quantification of oligonucleotides," *Microchemical Journal*, vol. 124, pp. 668-674, 2016, doi: 10.1016/j.microc.2015.10.011.
- [143] A. C. McGinnis, B. Chen, and M. G. Bartlett, "Chromatographic methods for the determination of therapeutic oligonucleotides," *Journal of Chromatography B*, vol. 883-884, pp. 76-94, 2012, doi: 10.1016/j.jchromb.2011.09.007.
- [144] J. Gerstner, P. Pedroso, J. Morris, and B. Bergot, "Gram-scale purification of phosphorothioate oligonucleotides using ion-exchange displacement chromatography," *Nucleic Acids Research*, vol. 23, no. 12, pp. 2292-2299, 1995, doi: 10.1093/nar/23.12.2292.
- [145] B. Noll *et al.*, "Purification of Small Interfering RNA Using Nondenaturing Anion-Exchange Chromatography," *nucleic acid therapeutics*, vol. 21, no. 6, pp. 383-393, 2011, doi: 10.1089/nat.2011.0317.
- [146] Amersham\_Biosciences. "Oligonucleotide purification by ion exchange chromatography:process development, optimization and scale-up." [https://www.gelifesciences.com/gehcls\\_images/GELS/Related%20Content/Files/1314729545976/litdoc18116179\\_20161013220213.pdf](https://www.gelifesciences.com/gehcls_images/GELS/Related%20Content/Files/1314729545976/litdoc18116179_20161013220213.pdf) (accessed 4 Jan 2017).
- [147] K. Ashman, A. Bosserhoff, and R. Frank, "High-speed preparative reversed-phase high-performance liquid chromatography of synthetic oligonucleotides," *Journal of Chromatography A*, vol. 397, no. C, pp. 137-140, 1987, doi: 10.1016/S0021-9673(01)84996-7.
- [148] W. H. Pearson, D. A. Berry, P. Stoy, K.-Y. Jung, and A. D. Sercel, "Fluorous affinity purification of oligonucleotides," *The Journal of organic chemistry*, vol. 70, no. 18, pp. 7114-7122, 2005, doi: 10.1021/jo050795y.
- [149] Y. Igata, N. Saito-Tarashima, D. Matsumoto, K. Sagara, and N. Minakawa, "A 'catch and release' strategy towards HPLC-free purification of synthetic oligonucleotides by a combination of the strain-promoted alkyne-azide cycloaddition and the photocleavage," *Bioorganic & Medicinal Chemistry*, vol. 25, no. 21, pp. 5962-5967, 2017, doi: 10.1016/j.bmc.2017.09.014.
- [150] I. H. T. Guideline, "Impurities in new drug substances Q3A (R2)," in *Proceedings of the International Conference on Harmonization of Technical Requirements for Registration of Pharmaceuticals for Human Use, Geneva, Switzerland*, 2006, vol. 25.

- [151] B. Noll, S. Seiffert, H.-P. Vornlocher, and I. Roehl, "Characterization of small interfering RNA by non- denaturing ion- pair reversed- phase liquid chromatography," *Journal of Chromatography A*, vol. 1218, no. 33, pp. 5609-5617, 2011, doi: 10.1016/j.chroma.2011.06.057.
- [152] G. D. Christian, *Analytical chemistry*, Seventh edition / Gary D. Christian, University of Washington, Purnendu K. (Sandy) Dasgupta, University of Texas at Arlington, Kevin A. Schug, University of Texas at Arlington. ed. Hoboken, NJ : John Wiley and Sons, Inc., 2014, 2014.
- [153] L. R. Snyder, *Practical HPLC method development*, Second edition. ed. Hoboken, NJ : John Wiley & Sons, Inc., 1997, 1997.
- [154] C. G. Huber, "Micropellicular stationary phases for high- performance liquid chromatography of double- stranded DNA," *Journal of Chromatography A*, vol. 806, no. 1, pp. 3-30, 1998, doi: 10.1016/S0021-9673(97)01124-2.
- [155] Biorad. "Ion Exchange Chromatography." <http://www.bio-rad.com/en-uk/applications-technologies/liquid-chromatography-principles/ion-exchange-chromatography> (accessed 3 January, 2017).
- [156] J. V. Bonilla and G. S. Srivatsa, *Handbook of analysis of oligonucleotides and related products [electronic resource]*. Boca Raton, FL: Boca Raton, FL : CRC Press, 2011, 2011.
- [157] J. R. Thayer, G. Gendeh, S. Rao, D. Jamieson, C. A. Pohl, and Y. Agroskin, "Performance Improvements for High Resolution Anion-Exchange Oligonucleotide Separations Using Small Particle Substrates," Thermo Scientific, USA, 2013.
- [158] W. Wieder, C. P. Bisjak, C. W. Huck, R. Bakry, and G. K. Bonn, "Monolithic poly(glycidyl methacrylate- co -divinylbenzene) capillary columns functionalized to strong anion exchangers for nucleotide and oligonucleotide separation," *Journal of Separation Science*, vol. 29, no. 16, pp. 2478-2484, 2006, doi: 10.1002/jssc.200600146.
- [159] R. R. Deshmukh, J. E. Miller, P. De Leon, W. E. Leitch II, D. L. Cole, and Y. S. Sanghvi, "Process development for purification of therapeutic antisense oligonucleotides by anion- exchange chromatography," *Organic Process Research and Development*, vol. 4, no. 3, pp. 205-213, 2000, doi: 10.1021/op990091o.
- [160] Y. Baba, M. Fukuda, and N. Yoza, "Computer-assisted retention prediction system for oligonucleotides in gradient anion-exchange chromatography," *Journal of Chromatography A*, vol. 458, pp. 385-394, 1988.
- [161] Y. Baba and M. K. Ito, "Optimization of gradients in anion-exchange separations of oligonucleotides using computer-assisted retention prediction and a high-performance liquid chromatographic simulation system," *Journal of Chromatography A*, vol. 485, no. C, pp. 647-655, 1989, doi: 10.1016/S0021-9673(01)89170-6.
- [162] M. A. Strege and A. L. Lagu, "ANION-EXCHANGE CHROMATOGRAPHY OF DNA RESTRICTION FRAGMENTS," *Journal Of Chromatography*, vol. 555, no. 1-2, pp. 109-124, 1991.
- [163] M. Bunček *et al.*, "Unusual chromatographic behavior of oligonucleotide sequence isomers on two different anion exchange HPLC columns," *Analytical Biochemistry*, vol. 348, no. 2, pp. 300-306, 2006, doi: 10.1016/j.ab.2005.10.047.
- [164] M. Bunček *et al.*, "Retention Behavior of Oligonucleotides on a Glycidyl Methacrylate- Based DEAE-Modified Sorbent," *Chroma*, vol. 62, no. 5, pp. 263-269, 2005, doi: 10.1365/s10337-005-0620-x.
- [165] N. L. Krajnc *et al.*, "Purification of large plasmids with methacrylate monolithic columns," *Journal of Separation Science*, vol. 32, no. 15-16, pp. 2682-2690, 2009, doi: 10.1002/jssc.200900260.
- [166] A. Sabarudin, J. Huang, S. Shu, S. Sakagawa, and T. Umemura, "Preparation of methacrylate-based anion- exchange monolithic microbore column for chromatographic separation of DNA fragments and oligonucleotides," *Analytica Chimica Acta*, vol. 736, pp. 108-114, 2012, doi: 10.1016/j.aca.2012.05.039.

- [167] F. I. Raynaud *et al.*, "Pharmacokinetics of G3139, a phosphorothioate oligodeoxynucleotide antisense to bcl-2, after intravenous administration or continuous subcutaneous infusion to mice," *Journal of Pharmacology and Experimental Therapeutics*, vol. 281, no. 1, pp. 420-427, 1997.
- [168] R. Stribling, "High-performance liquid chromatography of oligoguanylates at high pH," *Journal of Chromatography A*, vol. 538, no. 2, pp. 474-479, 1991, doi: 10.1016/S0021-9673(01)88872-5.
- [169] J. R. Thayer, V. Barreto, S. Rao, and C. Pohl, "Control of oligonucleotide retention on a pH-stabilized strong anion exchange column," *Analytical Biochemistry*, vol. 338, no. 1, pp. 39-47, 2005, doi: 10.1016/j.ab.2004.11.013.
- [170] X. Yang, R. P. Hodge, B. A. Luxon, R. Shope, and D. G. Gorenstein, "Separation of Synthetic Oligonucleotide Dithioates from Monothiophosphate Impurities by Anion- Exchange Chromatography on a Mono- Q Column," *Analytical Biochemistry*, vol. 306, no. 1, pp. 92-99, 2002, doi: 10.1006/abio.2001.5694.
- [171] J. R. Thayer, Y. Wu, E. Hansen, M. D. Angelino, and S. Rao, "Separation of oligonucleotide phosphorothioate diastereoisomers by pellicular anion- exchange chromatography," *Journal of Chromatography A*, vol. 1218, no. 6, pp. 802-808, 2011, doi: 10.1016/j.chroma.2010.12.051.
- [172] G. P. G. Grant and A. E. m. p. u. e. Popova, "Diastereomer characterizations of nitroxide-labeled nucleic acids," *Biochemical and Biophysical Research Communications*, vol. 371, no. 3, 2008, doi: 10.1016/j.bbrc.2008.04.088.
- [173] G. S. Srivatsa, P. Klopchin, M. Batt, M. Feldman, R. H. Carlson, and D. L. Cole, "Selectivity of anion exchange chromatography and capillary gel electrophoresis for the analysis of phosphorothioate oligonucleotides," *Journal of Pharmaceutical and Biomedical Analysis*, vol. 16, no. 4, pp. 619-630, 1997, doi: 10.1016/S0731-7085(97)00180-5.
- [174] J. R. Thayer, S. Rao, N. Puri, C. A. Burnett, and M. Young, "Identification of aberrant 2'–5' RNA linkage isomers by pellicular anion exchange chromatography," *Analytical Biochemistry*, vol. 361, no. 1, pp. 132-139, 2007, doi: 10.1016/j.ab.2006.10.032.
- [175] G. Scott, "Depurination During Trityl-on Purification.," ed. Online: Phenomenex, 2007.
- [176] J. Thayer, S. Rao, C. Pohl, Y. Wu, and M. Angelino, "Pellicular anion-exchange chromatography applied to RNAi assays for monitoring strand stoichiometry and RNA stability," 2011.
- [177] A. Romanovskaya, L. P. Sarin, D. H. Bamford, and M. M. Poranen, "High- throughput purification of double- stranded RNA molecules using convective interaction media monolithic anion exchange columns," *Journal of Chromatography A*, 2012, doi: 10.1016/j.chroma.2012.12.050.
- [178] S. Yamamoto, M. Nakamura, C. Tarmann, and A. Jungbauer, "Retention studies of DNA on anion- exchange monolith chromatography: Binding site and elution behavior," *Journal of Chromatography A*, vol. 1144, no. 1, pp. 155-160, 2007, doi: 10.1016/j.chroma.2007.01.025.
- [179] D. Sýkora, F. Svec, and J. M. J. Fréchet, "Separation of oligonucleotides on novel monolithic columns with ion-exchange functional surfaces," *Journal of Chromatography A*, vol. 852, no. 1, pp. 297-304, 1999, doi: 10.1016/S0021-9673(99)00004-7.
- [180] J. R. Thayer, K. J. Flook, A. Woodruff, S. Rao, and C. A. Pohl, "New monolith technology for automated anion- exchange purification of nucleic acids," *Journal of Chromatography B*, vol. 878, no. 13, pp. 933-941, 2010, doi: 10.1016/j.jchromb.2010.01.030.
- [181] J. R. Thayer, N. Puri, C. Burnett, M. Hail, and S. Rao, "Identification of RNA linkage isomers by anion exchange purification with electrospray ionization mass spectrometry of automatically desalted phosphodiesterase- II digests," *Analytical Biochemistry*, vol. 399, no. 1, pp. 110-117, 2010, doi: 10.1016/j.ab.2009.11.009.
- [182] A. J. Bourque and A. S. Cohen, "Quantitative analysis of phosphorothioate oligonucleotides in biological fluids using direct injection fast anion-exchange chromatography and capillary

- gel electrophoresis," *Journal of Chromatography B: Biomedical Sciences and Applications*, vol. 662, no. 2, pp. 343-349, 1994, doi: 10.1016/0378-4347(94)00207-X.
- [183] S. Chen, M. X. Qian, J. Brennan, and J. Gallo, "Determination of antisense phosphorothioate oligonucleotides and catabolites in biological fluids and tissue extracts using anion-exchange high-performance liquid chromatography and capillary gel electrophoresis," *J. Chromatogr. B*, vol. 692, no. 1, pp. 43-51, 1997.
- [184] C. E. Tucker, L.-S. Chen, M. B. Judkins, J. A. Farmer, S. C. Gill, and D. W. Drolet, "Detection and plasma pharmacokinetics of an anti-vascular endothelial growth factor oligonucleotide-aptamer (NX1838) in rhesus monkeys," *Journal of Chromatography B: Biomedical Sciences and Applications*, vol. 732, no. 1, pp. 203-212, 1999, doi: 10.1016/S0378-4347(99)00285-6.
- [185] V. Arora, D. C. Knapp, M. T. Reddy, D. D. Weller, and P. L. Iversen, "Bioavailability and Efficacy of Antisense Morpholino Oligomers Targeted to c-myc and Cytochrome P-450 3A2 Following Oral Administration in Rats," vol. 91, ed, 2002, pp. 1009-1018.
- [186] G. R. Devi, V. Arora, D. L. Weller, P. L. Iversen, T. M. Beer, and C. L. Corless, "In vivo bioavailability and pharmacokinetics of a c-MYC antisense phosphorodiamidate morpholino oligomer, AVI-4126, in solid tumors," *Clinical Cancer Research*, vol. 11, no. 10, pp. 3930-3938, 2005, doi: 10.1158/1078-0432.CCR-04-2091.
- [187] A. C. McGinnis, B. S. Cummings, and M. G. Bartlett, "Ion exchange liquid chromatography method for the direct determination of small ribonucleic acids," *Analytica Chimica Acta*, vol. 799, pp. 57-67, 2013, doi: 10.1016/j.aca.2013.08.040.
- [188] M. J. Dickman, "Effects of sequence and structure in the separation of nucleic acids using ion pair reverse phase liquid chromatography," *Journal of Chromatography A*, vol. 1076, no. 1, pp. 83-89, 2005, doi: 10.1016/j.chroma.2005.04.018.
- [189] M. Gilar *et al.*, "Ion-pair reversed-phase high-performance liquid chromatography analysis of oligonucleotides:: Retention prediction," *Journal of Chromatography A*, vol. 958, no. 1, pp. 167-182, 2002, doi: 10.1016/S0021-9673(02)00306-0.
- [190] C. Horvath, W. Melander, I. Molnar, and P. Molnar, "Enhancement of retention by ion-pair formation in liquid chromatography with nonpolar stationary phases," *Anal. Chem.*, vol. 49, no. 14, pp. 2295-2305, 1977, doi: 10.1021/ac50022a048.
- [191] J. H. Knox and R. A. Hartwick, "Mechanism of ion-pair liquid chromatography of amines, neutrals, zwitterions and acids using anionic heteroions," *Journal of Chromatography A*, vol. 204, pp. 3-21, 1981, doi: 10.1016/S0021-9673(00)81633-7.
- [192] B. A. Bidlingmeyer and F. V. Warren Jr, "Effect of ionic strength on retention and detector response in reversed-phase ion-pair liquid chromatography with ultraviolet-absorbing ion interaction reagents," *Analytical Chemistry*<sup>®</sup>, vol. 54, no. 13, pp. 2351-2356, 1982.
- [193] Á. Bartha and J. Ståhlberg, "Electrostatic retention model of reversed-phase ion-pair chromatography," *Journal of Chromatography A*, vol. 668, no. 2, pp. 255-284, 1994, doi: 10.1016/0021-9673(94)80116-9.
- [194] G. Slim and M. J. Gait, "Configurally defined phosphorothioate-containing oligoribonucleotides in the study of the mechanism of cleavage of hammerhead ribozymes," *Nucleic acids research*, vol. 19, no. 6, p. 1183, 1991.
- [195] C. G. Huber, P. Oefner, E. Preuss, and G. Bonn, "HIGH-RESOLUTION LIQUID-CHROMATOGRAPHY OF DNA FRAGMENTS ON NONPOROUS POLY(STYRENE-DIVINYLBENZENE) PARTICLES," *Nucleic Acids Research*, vol. 21, no. 5, pp. 1061-1066, 1993.
- [196] M. Gilar and E. S. P. Bouvier, "Purification of crude DNA oligonucleotides by solid-phase extraction and reversed-phase high-performance liquid chromatography," *Journal of Chromatography A*, vol. 890, no. 1, pp. 167-177, 2000, doi: 10.1016/S0021-9673(00)00521-5.
- [197] P. J. Oefner, "Allelic discrimination by denaturing high-performance liquid chromatography," *Journal of Chromatography B: Biomedical Sciences and Applications*, vol. 739, no. 2, pp. 345-355, 2000, doi: 10.1016/S0378-4347(99)00571-X.

- [198] C. G. Huber, G. K. Bonn, and P. J. Oefner, "Rapid and accurate sizing of DNA fragments by ion-pair chromatography on alkylated nonporous poly(styrene-divinylbenzene) particles," *Analytical Chemistry*, vol. 67, no. 3, pp. 578-585, 1995.
- [199] K. Kawamura, K. Ikoma, Y. Maruoka, and H. Hisamoto, "Separation Behavior of Short Oligonucleotides by Ion-Pair Reversed-Phase Capillary Liquid Chromatography Using a Silica-Based Monolithic Column Applied to Simple Detection of SNPs," *Chromatographia*, vol. 78, no. 7, pp. 487-494, 2015, doi: 10.1007/s10337-015-2855-5.
- [200] S. Studzińska, K. Krzemińska, M. Szumski, and B. Buszewski, "Application of a cholesterol stationary phase in the analysis of phosphorothioate oligonucleotides by means of ion pair chromatography coupled with tandem mass spectrometry," *Talanta*, vol. 154, pp. 270-277, 2016, doi: 10.1016/j.talanta.2016.03.082.
- [201] C. L. Wysoczynski, S. C. Roemer, V. Dostal, R. M. Barkley, M. E. A. Churchill, and C. S. Malarkey, "Reversed-phase ion-pair liquid chromatography method for purification of duplex DNA with single base pair resolution," *Nucleic acids research*, vol. 41, no. 20, pp. e194-e194, 2013, doi: 10.1093/nar/gkt815.
- [202] S. M. McCarthy, M. Gilar, and J. Gebler, "Reversed-phase ion-pair liquid chromatography analysis and purification of small interfering RNA," *Analytical Biochemistry*, vol. 390, no. 2, pp. 181-188, 2009, doi: 10.1016/j.ab.2009.03.042.
- [203] M. Biba, C. J. Welch, J. P. Foley, B. Mao, E. Vazquez, and R. A. Arvary, "Evaluation of core-shell particle columns for ion-pair reversed-phase liquid chromatography analysis of oligonucleotides," *Journal of Pharmaceutical and Biomedical Analysis*, vol. 72, pp. 25-32, 2013, doi: 10.1016/j.jpba.2012.09.007.
- [204] S. Studzińska, L. Pietrzak, and B. Buszewski, "The Effects of Stationary Phases on Retention and Selectivity of Oligonucleotides in IP-RP-HPLC," *Chromatographia*, vol. 77, no. 23, pp. 1589-1596, 2014, doi: 10.1007/s10337-014-2766-x.
- [205] T. Hill and J. W. Mayhew, "CONVENIENT PURIFICATION OF TRITYLATED AND DETRITYLATED OLIGONUCLEOTIDES UP TO 100-MER," *Journal Of Chromatography*, vol. 512, pp. 415-431, 1990.
- [206] E. D. Close *et al.*, "Nucleic acid separations using superficially porous silica particles," *Journal of Chromatography A*, vol. 1440, pp. 135-144, 2016, doi: 10.1016/j.chroma.2016.02.057.
- [207] N. M. Djordjevic, F. Houdiere, P. Fowler, and F. Natt, "HPLC Separation of Oligonucleotides in Isocratic and Temperature-Programming Mode," *Analytical Chemistry*, vol. 70, no. 9, pp. 1921-1925, 1998.
- [208] C. G. Huber and A. Krajete, "Analysis of nucleic acids by capillary ion-pair reversed-phase HPLC coupled to negative-ion electrospray ionization mass spectrometry," *Analytical chemistry*, vol. 71, no. 17, pp. 3730-3739, 1999, doi: 10.1021/ac990378j.
- [209] J. M. Devaney, J. E. Girard, and M. A. Marino, "DNA microsatellite analysis using ion-pair reversed-phase high-performance liquid chromatography," *Analytical chemistry*, vol. 72, no. 4, p. 858, 2000.
- [210] C. G. Huber, A. Premstaller, W. Xiao, H. Oberacher, G. K. Bonn, and P. J. Oefner, "Mutation detection by capillary denaturing high-performance liquid chromatography using monolithic columns," *Journal of Biochemical and Biophysical Methods*, vol. 47, no. 1, pp. 5-19, 2001, doi: 10.1016/S0165-022X(00)00147-0.
- [211] Y. Baba, "Prediction of the behaviour of oligonucleotides in high-performance liquid chromatography and capillary electrophoresis," *Journal of Chromatography B: Biomedical Sciences and Applications*, vol. 618, no. 1, pp. 41-55, 1993, doi: 10.1016/0378-4347(93)80026-Z.
- [212] M. Gilar and U. D. Neue, "Peak capacity in gradient reversed-phase liquid chromatography of biopolymers: Theoretical and practical implications for the separation of oligonucleotides," *Journal of Chromatography A*, vol. 1169, no. 1, pp. 139-150, 2007, doi: 10.1016/j.chroma.2007.09.005.

- [213] S. P. Waghmare, P. Pousinis, D. P. Hornby, and M. J. Dickman, "Studying the mechanism of RNA separations using RNA chromatography and its application in the analysis of ribosomal RNA and RNA:RNA interactions," *Journal of Chromatography A*, vol. 1216, no. 9, pp. 1377-1382, 2009, doi: 10.1016/j.chroma.2008.12.077.
- [214] M. Gilar, "Analysis and Purification of Synthetic Oligonucleotides by Reversed-Phase High-Performance Liquid Chromatography with Photodiode Array and Mass Spectrometry Detection," *Analytical Biochemistry*, vol. 298, no. 2, pp. 196-206, 2001, doi: 10.1006/abio.2001.5386.
- [215] A. Premstaller, H. Oberacher, and C. G. Huber, "High-performance liquid chromatography-electrospray ionization mass spectrometry of single- and double-stranded nucleic acids using monolithic capillary columns," *Analytical chemistry*, vol. 72, no. 18, pp. 4386-4393, 2000, doi: 10.1021/ac000283d.
- [216] M. J. Dickman and D. P. Hornby, "Enrichment and analysis of RNA centered on ion pair reverse phase methodology," *RNA*, vol. 12, no. 4, pp. 691-696, 2006, doi: 10.1261/rna.2278606.
- [217] A. Azarani and K. H. Hecker, "RNA analysis by ion- pair reversed- phase high performance liquid chromatography," *Nucleic acids research*, vol. 29, no. 2, p. E7, 2001.
- [218] S. L. Gelhaus, W. R. LaCourse, N. A. Hagan, G. K. Amarasinghe, and D. Fabris, "Rapid purification of RNA secondary structures," *Nucleic acids research*, vol. 31, no. 21, p. e135, 2003.
- [219] S. Gelhaus and W. LaCourse, "Separation of modified 2'-deoxyoligonucleotides using ion-pairing reversed-phase HPLC.," vol. 820, ed: *Journal of Chromatography B*, 2005, pp. 157-163.
- [220] B. Mayr, G. Hoelzl, K. Eder, M. Buchmeiser, and C. Huber, "Hydrophobic, Pellicular, Monolithic Capillary Columns Based on Cross- Linked Polynorbornene for Biopolymer Separations," *Analytical Chemistry (Washington)*, vol. 74, no. 23, pp. 6080-6087, 2002, doi: 10.1021/ac025919a.
- [221] W. J. Stec, G. Zon, and B. Uznański, "Reversed- phase high- performance liquid chromatographic separation of diastereomeric phosphorothioate analogues of oligodeoxyribonucleotides and other backbone- modified congeners of dna," *Journal of Chromatography A*, vol. 326, pp. 263-280, 1985, doi: 10.1016/S0021-9673(01)87452-5.
- [222] L. Li, T. Leone, J. P. Foley, and C. J. Welch, "Separation of small interfering RNA stereoisomers using reversed-phase ion-pairing chromatography," *Journal of Chromatography A*, vol. 1500, pp. 84-88, 2017, doi: 10.1016/j.chroma.2017.04.008.
- [223] J. M. Schuette, D. L. Cole, and G. S. Srivatsa, "Development and validation of a method for routine base composition analysis of phosphorothioate oligonucleotides," *Journal of Pharmaceutical and Biomedical Analysis*, vol. 12, no. 11, pp. 1345-1353, 1994, doi: 10.1016/0731-7085(94)00099-9.
- [224] M. Biba, C. J. Welch, and J. P. Foley, "Investigation of a new core– shell particle column for ion- pair reversed- phase liquid chromatography analysis of oligonucleotides," *Journal of Pharmaceutical and Biomedical Analysis*, vol. 96, pp. 54-57, 2014, doi: 10.1016/j.jpba.2014.03.029.
- [225] S. Studzińska and B. Buszewski, "Evaluation of ultrahigh- performance liquid chromatography columns for the analysis of unmodified and antisense oligonucleotides," *Anal Bioanal Chem*, vol. 406, no. 28, pp. 7127-7136, 2014, doi: 10.1007/s00216-014-7959-5.
- [226] W. Xiong, J. Glick, Y. Lin, and P. Vouros, "Separation and sequencing of isomeric oligonucleotide adducts using monolithic columns by ion-pair reversed-phase nano-HPLC coupled to ion trap mass spectrometry," *Analytical chemistry*, vol. 79, no. 14, pp. 5312-5321, 2007.
- [227] K. J. Fountain, M. Gilar, Y. Budman, and J. C. Gebler, "Purification of dye- labeled oligonucleotides by ion- pair reversed- phase high- performance liquid chromatography,"

- Journal of Chromatography B*, vol. 783, no. 1, pp. 61-72, 2003, doi: 10.1016/S1570-0232(02)00490-7.
- [228] G. Hölzl, H. Oberacher, S. Pitsch, A. Stutz, and C. G. Huber, "Analysis of biological and synthetic ribonucleic acids by liquid chromatography-mass spectrometry using monolithic capillary columns," *Analytical chemistry*, vol. 77, no. 2, pp. 673-680, 2005, doi: 10.1021/ac0487395.
- [229] S. G. Roussis, M. Pearce, and C. Rentel, "Small alkyl amines as ion-pair reagents for the separation of positional isomers of impurities in phosphate diester oligonucleotides," *Journal of Chromatography A*, vol. 1594, pp. 105-111, 2019, doi: 10.1016/j.chroma.2019.02.026.
- [230] A. McKeown, P. Shaw, and D. Barrett, "Retention behaviour of an homologous series of oligodeoxythymidilic acids using reversed-phase ion-pair chromatography," *Chromatographia*, vol. 55, no. 5, pp. 271-277, 2002, doi: 10.1007/BF02491658.
- [231] R. Erb, K. Leithner, A. Bernkop-Schnürch, and H. Oberacher, "Phosphorothioate Oligonucleotide Quantification by  $\mu$ - Liquid Chromatography- Mass Spectrometry," *AAPS J*, vol. 14, no. 4, pp. 728-737, 2012, doi: 10.1208/s12248-012-9381-2.
- [232] C. Rentel, J. Dacosta, S. Roussis, J. Chan, D. Capaldi, and B. Mai, "Determination of oligonucleotide deamination by high resolution mass spectrometry," *Journal of Pharmaceutical and Biomedical Analysis*, vol. 173, pp. 56-61, 2019, doi: 10.1016/j.jpba.2019.05.012.
- [233] L. Gong, "Comparing ion-pairing reagents and counter anions for ion-pair reversed-phase liquid chromatography/electrospray ionization mass spectrometry analysis of synthetic oligonucleotides," *Rapid Communications in Mass Spectrometry*, vol. 29, no. 24, pp. 2402-2410, 2015, doi: 10.1002/rcm.7409.
- [234] Z. J. Lin, W. Li, and G. Dai, "Application of LC-MS for quantitative analysis and metabolite identification of therapeutic oligonucleotides," *Journal of Pharmaceutical and Biomedical Analysis*, vol. 44, no. 2, pp. 330-341, 2007, doi: 10.1016/j.jpba.2007.01.042.
- [235] M. J. Dickman, M. J. Conroy, J. A. Grasby, and D. P. Hornby, "RNA footprinting analysis using ion pair reverse phase liquid chromatography," *RNA*, vol. 8, no. 2, pp. 247-251, 2002.
- [236] C. Kurata *et al.*, "Characterization of high molecular weight impurities in synthetic phosphorothioate oligonucleotides," *Bioorganic & Medicinal Chemistry Letters*, vol. 16, no. 3, pp. 607-614, 2006, doi: 10.1016/j.bmcl.2005.10.051.
- [237] S. G. Roussis, C. Koch, D. Capaldi, and C. Rentel, "Rapid oligonucleotide drug impurity determination by direct spectral comparison of ion-pair reversed-phase high-performance liquid chromatography electrospray ionization mass spectrometry data," *Rapid Communications in Mass Spectrometry*, vol. 32, no. 14, pp. 1099-1106, 2018, doi: 10.1002/rcm.8125.
- [238] A. Apffel, J. A. Chakel, S. Fischer, K. Lichtenwalter, and W. S. Hancock, "New procedure for the use of high-performance liquid chromatography-electrospray ionization mass spectrometry for the analysis of nucleotides and oligonucleotides," *Journal of Chromatography A*, vol. 777, no. 1, pp. 3-21, 1997.
- [239] B. Chen, S. Mason, and M. Bartlett, "The Effect of Organic Modifiers on Electrospray Ionization Charge-State Distribution and Desorption Efficiency for Oligonucleotides," *The official journal of The American Society for Mass Spectrometry*, vol. 24, no. 2, pp. 257-264, 2013, doi: 10.1007/s13361-012-0509-5.
- [240] K. J. Fountain, M. Gilar, and J. C. Gebler, "Analysis of native and chemically modified oligonucleotides by tandem ion-pair reversed-phase high-performance liquid chromatography/electrospray ionization mass spectrometry," *Rapid Communications in Mass Spectrometry*, vol. 17, no. 7, pp. 646-653, 2003, doi: 10.1002/rcm.959.
- [241] Y. Zou, P. Tiller, I. W. Chen, M. Beverly, and J. Hochman, "Metabolite identification of small interfering RNA duplex by high-resolution accurate mass spectrometry," *Rapid*

- Communications in Mass Spectrometry*, vol. 22, no. 12, pp. 1871-1881, 2008, doi: 10.1002/rcm.3561.
- [242] M. Beverly, K. Hartsough, and L. Machemer, "Liquid chromatography/electrospray mass spectrometric analysis of metabolites from an inhibitory RNA duplex," *Rapid Communications in Mass Spectrometry*, vol. 19, no. 12, pp. 1675-1682, 2005, doi: 10.1002/rcm.1972.
- [243] G. Dai, X. Wei, Z. Liu, S. Liu, G. Marcucci, and K. K. Chan, "Characterization and quantification of Bcl-2 antisense G3139 and metabolites in plasma and urine by ion-pair reversed phase HPLC coupled with electrospray ion-trap mass spectrometry," *Journal of Chromatography B*, vol. 825, no. 2, pp. 201-213, 2005, doi: 10.1016/j.jchromb.2005.05.049.
- [244] P. Deng, X. Chen, G. Zhang, and D. Zhong, "Bioanalysis of an oligonucleotide and its metabolites by liquid chromatography–tandem mass spectrometry," *Journal of Pharmaceutical and Biomedical Analysis*, vol. 52, no. 4, pp. 571-579, 2010, doi: 10.1016/j.jpba.2010.01.040.
- [245] S. Franzoni *et al.*, "Development and validation of a bioanalytical method for quantification of LNA-i-miR-221, a 13-mer oligonucleotide, in rat plasma using LC–MS/MS," *Journal of Pharmaceutical and Biomedical Analysis*, vol. 150, pp. 300-307, 2018, doi: 10.1016/j.jpba.2017.12.027.
- [246] J. Farand and M. Beverly, "Sequence confirmation of modified oligonucleotides using chemical degradation, electrospray ionization, time-of-flight, and tandem mass spectrometry," *Analytical chemistry*, vol. 80, no. 19, p. 7414, 2008, doi: 10.1021/ac8011158.
- [247] V. B. Ivleva, Y. Q. Yu, and M. Gilar, "Ultra-performance liquid chromatography/tandem mass spectrometry (UPLC/MS/MS) and UPLC/MSE analysis of RNA oligonucleotides," *Rapid Communications in Mass Spectrometry*, vol. 24, no. 17, pp. 2631-2640, 2010.
- [248] V. Ivleva, "UPLC/UV MS Analysis of Phosphorothioate Oligonucleotides

" Waters Corporation, Online: [www.waters.com](http://www.waters.com), 2008. [Online]. Available:

- <https://www.waters.com/webassets/cms/library/docs/720002621en.pdf>
- [249] S. Li, D.-D. Lu, Y.-L. Zhang, and S.-Q. Wang, "An Improved Ion- Pair Reversed Phase LC Method for Analysis of Major Impurities of Phosphorothioate Oligonucleotide Cantide," *Chroma*, vol. 72, no. 3, pp. 215-223, 2010, doi: 10.1365/s10337-010-1655-1.
- [250] I. Nikcevic, T. K. Wyrzykiewicz, and P. A. Limbach, "Detecting low- level synthesis impurities in modified phosphorothioate oligonucleotides using liquid chromatography– high resolution mass spectrometry," *International Journal of Mass Spectrometry*, vol. 304, no. 2-3, pp. 98-104, 2011, doi: 10.1016/j.ijms.2010.06.001.
- [251] Z. Huang, S. Jayaseelan, J. Hebert, H. Seo, and L. Niu, "Single- nucleotide resolution of RNAs up to 59 nucleotides by high- performance liquid chromatography," *Analytical Biochemistry*, 2012, doi: 10.1016/j.ab.2012.12.011.
- [252] C.-Y. Lin, Z. Huang, W. Jaremko, and L. Niu, "High- performance liquid chromatography purification of chemically modified RNA aptamers," *Analytical Biochemistry*, vol. 449, pp. 106-108, 2014, doi: 10.1016/j.ab.2013.12.022.
- [253] C.-H. Liu *et al.*, "The analysis of major impurities of lipophilic- conjugated phosphorothioate oligonucleotides by ion- pair reversed- phase HPLC combined with MALDI- TOF- MS," *Anal Bioanal Chem*, vol. 403, no. 5, pp. 1333-1342, 2012, doi: 10.1007/s00216-012-5935-5.
- [254] L. Gong and J. S. O. McCullagh, "Comparing ion-pairing reagents and sample dissolution solvents for ion-pairing reversed-phase liquid chromatography/electrospray ionization mass spectrometry analysis of oligonucleotides," *Rapid Communications in Mass Spectrometry*, vol. 28, no. 4, pp. 339-350, 2014, doi: 10.1002/rcm.6773.
- [255] S. Studzińska, R. Rola, and B. Buszewski, "The impact of ion-pairing reagents on the selectivity and sensitivity in the analysis of modified oligonucleotides in serum samples by

- liquid chromatography coupled with tandem mass spectrometry," *Journal of Pharmaceutical and Biomedical Analysis*, vol. 138, no. 2, pp. 146-152, 2017, doi: 10.1016/j.jpba.2017.02.014.
- [256] S. Studzińska, R. Rola, and B. Buszewski, "Development of a method based on ultra high performance liquid chromatography coupled with quadrupole time-of-flight mass spectrometry for studying the in vitro metabolism of phosphorothioate oligonucleotides," *Analytical and Bioanalytical Chemistry*, vol. 408, no. 6, pp. 1585-1595, 2016, doi: 10.1007/s00216-015-9266-1.
- [257] L. Gong, "Comparing ion- pairing reagents and counter anions for ion- pair reversed- phase liquid chromatography/ electrospray ionization mass spectrometry analysis of synthetic oligonucleotides," *Rapid Communications In Mass Spectrometry*, vol. 29, no. 24, pp. 2402-2410, 2015, doi: 10.1002/rcm.7409.
- [258] B. T. Rivera, M, "Optimization of Mobile Phase Composition for the Analysis of Synthetic Oligonucleotides using a Clarity Oligo-XT Column

" P phenomenex, Online: [www.phenomenex.com](http://www.phenomenex.com), 2016. [Online]. Available:

<https://phenomenex.blob.core.windows.net/documents/eafe1cff-8899-4dba-b967-7d719b110bc6.pdf>

- [259] N. Elzahar, N. Magdy, A. El-Kosasy, and M. Bartlett, "Degradation product characterization of therapeutic oligonucleotides using liquid chromatography mass spectrometry," *Analytical and Bioanalytical Chemistry*, vol. 410, no. 14, pp. 3375-3384, 2018, doi: 10.1007/s00216-018-1032-8.
- [260] B. Basiri, H. Hattum, W. Dongen, M. Murph, and M. Bartlett, "The Role of Fluorinated Alcohols as Mobile Phase Modifiers for LC-MS Analysis of Oligonucleotides," *The official journal of The American Society for Mass Spectrometry*, vol. 28, no. 1, pp. 190-199, 2017, doi: 10.1007/s13361-016-1500-3.
- [261] Sepax, "Oligonucleotide Separation on Zenix™ SEC and Proteomix® SAX," Online, 2010. Accessed: 24/01/2017. [Online]. Available: [https://www.sigmaaldrich.com/content/dam/sigma-aldrich/docs/Supelco/Application\\_Notes/1/sepax\\_Oligonucleotides.pdf](https://www.sigmaaldrich.com/content/dam/sigma-aldrich/docs/Supelco/Application_Notes/1/sepax_Oligonucleotides.pdf)
- [262] E. Largy and J.-L. Mergny, "Shape matters: size- exclusion HPLC for the study of nucleic acid structural polymorphism," *Nucleic acids research*, vol. 42, no. 19, p. e149, 2014, doi: 10.1093/nar/gku751.
- [263] P. J. Lukavsky and J. D. Puglisi, "Large- scale preparation and purification of polyacrylamide-free RNA oligonucleotides," *RNA*, vol. 10, no. 5, pp. 889-893, 2004, doi: 10.1261/rna.5264804.
- [264] C. W. Scales *et al.*, "Corona- stabilized interpolyelectrolyte complexes of SiRNA with nonimmunogenic, hydrophilic/ cationic block copolymers prepared by aqueous RAFT polymerization," *Macromolecules*, vol. 39, no. 20, pp. 6871-6881, 2006, doi: 10.1021/ma061453c.
- [265] I. Kim, S. A. McKenna, E. Viani Puglisi, and J. D. Puglisi, "Rapid purification of RNAs using fast performance liquid chromatography ( FPLC)," *RNA (New York, N.Y.)*, vol. 13, no. 2, p. 289, 2007.
- [266] Y. H. Chionh *et al.*, "A multidimensional platform for the purification of non- coding RNA species," *Nucleic acids research*, vol. 41, no. 17, p. e168, 2013, doi: 10.1093/nar/gkt668.
- [267] C.-B. Liu *et al.*, "Radiolabeling morpholinos with 90Y, 111In, 188Re and 99mTc," *Nuclear Medicine and Biology*, vol. 30, no. 2, pp. 207-214, 2003, doi: 10.1016/S0969-8051(02)00389-X.
- [268] R. R. Alieva, E. G. Zavyalova, V. N. Tashlitsky, and A. M. Kopylov, "Quantitative characterization of oligomeric state of G-quadruplex antithrombin aptamers by size

- exclusion HPLC," *Mendeleev Communications*, vol. 29, no. 4, pp. 424-425, 2019, doi: 10.1016/j.mencom.2019.07.023.
- [269] A. Shimoyama, A. Fujisaka, and S. Obika, "Evaluation of size- exclusion chromatography for the analysis of phosphorothioate oligonucleotides," *Journal of Pharmaceutical and Biomedical Analysis*, vol. 136, pp. 55-65, 2017, doi: 10.1016/j.jpba.2016.12.036.
- [270] C. Timothy Wehr and S. R. Abbott, "High- speed steric exclusion chromatography of biopolymers," *Journal of Chromatography A*, vol. 185, pp. 453-462, 1979, doi: 10.1016/S0021-9673(00)85621-6.
- [271] M. B. Beverly, "Applications of mass spectrometry to the study of siRNA," vol. 30, ed. Hoboken, 2011, pp. 979-998.
- [272] S. Studzińska, "Review on investigations of antisense oligonucleotides with the use of mass spectrometry," *Talanta*, vol. 176, pp. 329-343, 2018, doi: 10.1016/j.talanta.2017.08.025.
- [273] S. Banerjee and S. Mazumdar, "Electrospray Ionization Mass Spectrometry: A Technique to Access the Information beyond the Molecular Weight of the Analyte," *Int. J. Anal. Chem.*, vol. 2012, no. 2012, 2012, doi: 10.1155/2012/282574.
- [274] J.-P. Antignac, K. de Wasch, F. Monteau, H. De Brabander, F. Andre, and B. Le Bizec, "The ion suppression phenomenon in liquid chromatography–mass spectrometry and its consequences in the field of residue analysis," *Analytica chimica acta*, vol. 529, no. 1, pp. 129-136, 2005, doi: 10.1016/j.aca.2004.08.055.
- [275] S. A. McLuckey and S. Habibi-Goudarzi, "Decompositions of multiply charged oligonucleotide anions," *Journal of the American Chemical Society*, vol. 115, no. 25, 1993.
- [276] Z. Wang, K. Wan, R. Ramanathan, J. Taylor, and M. Gross, "Structure and fragmentation mechanisms of isomeric T- rich oligodeoxynucleotides: A comparison of four tandem mass spectrometric methods," *J Am Soc Mass Spectrom*, vol. 9, no. 7, pp. 683-691, 1998, doi: 10.1016/S1044-0305(98)00178-0.
- [277] J. Tromp and S. Schürch, "Gas- phase dissociation of oligoribonucleotides and their analogs studied by electrospray ionization tandem mass spectrometry," *J Am Soc Mass Spectrom*, vol. 16, no. 8, pp. 1262-1268, 2005, doi: 10.1016/j.jasms.2005.03.024.
- [278] F. Erni and R. W. Frei, "Two-dimensional column liquid chromatographic technique for resolution of complex mixtures," *Journal of Chromatography A*, vol. 149, no. C, pp. 561-569, 1978, doi: 10.1016/S0021-9673(00)81011-0.
- [279] M. M. Bushey and J. W. Jorgenson, "Automated Instrumentation for Comprehensive Two-Dimensional High-Performance Liquid Chromatography of Proteins," *Analytical Chemistry*, vol. 62, no. 2, pp. 161-167, 1990, doi: 10.1021/ac00201a015.
- [280] P. W. Carr, Stoll, and D.R, *Two-Dimensional Liquid Chromatography. Principles, practical implementation and applications*.

Primer. Online: [www.Agilent.com](http://www.Agilent.com)

Agilent

Technologies

2015

- [281] P. Schoenmakers, P. Marriott, and J. Beens, "Nomenclature and conventions in comprehensive multidimensional chromatography," *LC GC Eur.*, vol. 16, no. 6, pp. 335-339, 2003.

- [282] P. J. Marriott, P. Schoenmakers, and Z. Y. Wu, "Nomenclature and conventions in comprehensive multidimensional chromatography- an update," *LC GC Europe*, vol. 25, no. 5, 2012.
- [283] U. D. Neue, "Theory of peak capacity in gradient elution," *Journal of Chromatography A*, vol. 1079, no. 1-2, pp. 153-161, 2005, doi: 10.1016/j.chroma.2005.03.008.
- [284] E. Grushka, "Chromatographic Peak Capacity and the Factors Influencing It," *Analytical Chemistry*, vol. 42, no. 11, pp. 1142-1147, 1970, doi: 10.1021/ac60293a001.
- [285] S. A. Cohen and M. R. Schure, *Multidimensional liquid chromatography: theory and applications in industrial chemistry and the life sciences*. John Wiley & Sons, 2008.
- [286] K. Horie *et al.*, "Calculating optimal modulation periods to maximize the peak capacity in two-dimensional HPLC," *Analytical chemistry*, vol. 79, no. 10, pp. 3764-3770, 2007, doi: 10.1021/ac062002t.
- [287] D. R. Stoll, J. D. Cohen, and P. W. Carr, "Fast, comprehensive online two-dimensional high performance liquid chromatography through the use of high temperature ultra-fast gradient elution reversed-phase liquid chromatography," *Journal of Chromatography A*, vol. 1122, no. 1-2, pp. 123-137, 2006, doi: 10.1016/j.chroma.2006.04.058.
- [288] D. R. Stoll and P. W. Carr, "Two-Dimensional Liquid Chromatography: A State of the Art Tutorial," *Analytical chemistry*, vol. 89, no. 1, pp. 519-531, 2017, doi: 10.1021/acs.analchem.6b03506.
- [289] J. M. Davis and J. C. Giddings, "Statistical Theory of Component Overlap in Multicomponent Chromatograms," *Analytical Chemistry*, vol. 55, no. 3, pp. 418-424, 1983, doi: 10.1021/ac00254a003.
- [290] P. Marriott, P. D. Morrison, R. Shellie, M. S. Dunn, E. Sari, and D. Ryan, "Multidimensional and comprehensive - Two-dimensional gas chromatography," *LC GC Eur.*, vol. 16, no. 12A, pp. 23-31, 2003.
- [291] B. Pirok, D. Stoll, and P. Schoenmakers, "Recent Developments in Two-Dimensional Liquid Chromatography: Fundamental Improvements for Practical Applications," *Anal. Chem.*, vol. 91, no. 1, pp. 240-263, 2019, doi: 10.1021/acs.analchem.8b04841.
- [292] B. W. J. Pirok, A. F. G. Gargano, and P. J. Schoenmakers, "Optimizing separations in online comprehensive two-dimensional liquid chromatography," vol. 41, ed, 2018, pp. 68-98.
- [293] D. Li, C. Jakob, and O. Schmitz, "Practical considerations in comprehensive two-dimensional liquid chromatography systems (LCxLC) with reversed-phases in both dimensions," *Analytical and Bioanalytical Chemistry*, vol. 407, no. 1, pp. 153-167, 2015, doi: 10.1007/s00216-014-8179-8.
- [294] J. C. Giddings, "Two-dimensional separations: concept and promise," *Analytical chemistry*, vol. 56, no. 12, pp. 1258A-1260A, 1984, doi: 10.1021/ac00276a717.
- [295] R. Murphy, M. Schure, and J. Foley, "Effect of sampling rate on resolution in comprehensive two-dimensional liquid chromatography," *Analytical Chemistry*, vol. 70, no. 8, pp. 1585-1594, 1998, doi: 10.1021/ac971184b.
- [296] M. R. Schure and J. M. Davis, "Orthogonal separations: Comparison of orthogonality metrics by statistical analysis," *Journal of Chromatography A*, vol. 1414, pp. 60-76, 2015, doi: 10.1016/j.chroma.2015.08.029.
- [297] M. R. Schure and J. M. Davis, "Orthogonality measurements for multidimensional chromatography in three and higher dimensional separations," *Journal of Chromatography A*, vol. 1523, pp. 148-161, 2017, doi: 10.1016/j.chroma.2017.06.036.
- [298] Z. Liu, D. G. Patterson, and M. Lee, "GEOMETRIC APPROACH TO FACTOR-ANALYSIS FOR THE ESTIMATION OF ORTHOGONALITY AND PRACTICAL PEAK-CAPACITY IN COMPREHENSIVE 2-DIMENSIONAL SEPARATIONS," *Anal. Chem.*, vol. 67, no. 21, pp. 3840-3845, 1995, doi: 10.1021/ac00117a004.

- [299] I. Dioumaeva, S.-B. Y. Choi, B. D. Jones, and R. Arora, "Understanding Orthogonality in Reversed-Phase Liquid Chromatography for Easier Column Selection and Method Development," Agilent

Technologies

Online: [www.Agilent.com](http://www.Agilent.com)

2010

[Online]. Available: <https://www.agilent.com/cs/library/applications/SI-02425.pdf>

- [300] S. C. Rutan, J. M. Davis, and P. W. Carr, "Fractional coverage metrics based on ecological home range for calculation of the effective peak capacity in comprehensive two-dimensional separations," *Journal of Chromatography A*, vol. 1255, pp. 267-276, 2012, doi: 10.1016/j.chroma.2011.12.061.
- [301] P. J. Slonecker, X. Li, T. H. Ridgway, and J. G. Dorsey, "Informational orthogonality of two-dimensional chromatographic separations," *Analytical chemistry*, vol. 68, no. 4, pp. 682-689, 1996, doi: 10.1021/ac950852v.
- [302] M. Gilar, P. Olivova, A. E. Daly, and J. C. Gebler, "Orthogonality of separation in two-dimensional liquid chromatography," *Analytical chemistry*, vol. 77, no. 19, pp. 6426-6434, 2005, doi: 10.1021/ac050923i.
- [303] B. S. Pirok, D. Multidimensional Separations (MOREPEAKS)

Overview

of 2D-LC literature

[Online] Available: <http://www.multidlc.org/literature/2DLC-Applications>

- [304] H. Zhao *et al.*, "An improved 2D-HPLC-UF-ESI-TOF/MS approach for enrichment and comprehensive characterization of minor neuraminidase inhibitors from Flos Lonicerae Japonicae," *Journal of Pharmaceutical and Biomedical Analysis*, vol. 175, 2019, doi: 10.1016/j.jpba.2019.07.006.
- [305] C.-L. Yao *et al.*, "Global profiling combined with predicted metabolites screening for discovery of natural compounds: Characterization of ginsenosides in the leaves of Panax notoginseng as a case study," *Journal of Chromatography A*, vol. 1538, pp. 34-44, 2018, doi: 10.1016/j.chroma.2018.01.040.
- [306] T. Sajic, E. Varesio, I. Szanto, and G. Hopfgartner, "Comparison of fractionation strategies for offline two-dimensional liquid chromatography tandem mass spectrometry analysis of proteins from mouse adipose tissue," *Analytical Biochemistry*, vol. 484, pp. 122-132, 2015, doi: 10.1016/j.ab.2015.05.015.
- [307] S. Schiesel, M. Lämmerhofer, and W. Lindner, "Comprehensive impurity profiling of nutritional infusion solutions by multidimensional off-line reversed-phase liquid chromatography×hydrophilic interaction chromatography–ion trap mass-spectrometry and charged aerosol detection with universal calibration," *Journal of Chromatography A*, vol. 1259, pp. 100-110, 2012, doi: 10.1016/j.chroma.2012.01.009.

- [308] A. Ndiripo and H. Pasch, "Comprehensive Analysis of Oxidized Waxes by Solvent and Thermal Gradient Interaction Chromatography and Two-Dimensional Liquid Chromatography," *Analytical chemistry*, vol. 90, no. 12, pp. 7626-7634, 2018, doi: 10.1021/acs.analchem.8b01480.
- [309] B. W. J. Pirok *et al.*, "Characterization of Dye Extracts from Historical Cultural-Heritage Objects Using State-of-the-Art Comprehensive Two-Dimensional Liquid Chromatography and Mass Spectrometry with Active Modulation and Optimized Shifting Gradients," *Analytical chemistry*, vol. 91, no. 4, pp. 3062-3069, 2019, doi: 10.1021/acs.analchem.8b05469.
- [310] J. Wang *et al.*, "Analysis of tartary buckwheat (*Fagopyrum tataricum*) seed proteome using offline two-dimensional liquid chromatography and tandem mass spectrometry," *Journal of Food Biochemistry*, vol. 43, no. 7, pp. n/a-n/a, 2019, doi: 10.1111/jfbc.12863.
- [311] G. Jin *et al.*, "Synthesis and chromatographic evaluation of phenyl/tetrazole bonded stationary phase based on thiol-epoxy ring opening reaction," *Journal of Separation Science*, vol. 41, no. 4, pp. 856-867, 2018, doi: 10.1002/jssc.201701125.
- [312] Y. Sun, X. Cai, J. Cao, Z. Wu, and D. Pan, "Effects of 1,8-cineole on Carbohydrate Metabolism Related Cell Structure Changes of Salmonella," *Frontiers in microbiology*, vol. 9, no. MAY, pp. 1078-1078, 2018, doi: 10.3389/fmicb.2018.01078.
- [313] H. O. Ghareeb and W. Radke, "Characterization of cellulose acetates according to DS and molar mass using two-dimensional chromatography," *Carbohydrate Polymers*, vol. 98, no. 2, pp. 1430-1437, 2013, doi: 10.1016/j.carbpol.2013.07.061.
- [314] Z. Long *et al.*, "A novel two-dimensional liquid chromatography - Mass spectrometry method for direct drug impurity identification from HPLC eluent containing ion-pairing reagent in mobile phases," *Analytica Chimica Acta*, vol. 1049, pp. 105-114, 2019, doi: 10.1016/j.aca.2018.10.031.
- [315] M. Suto, H. Kawashima, and N. Suto, "Heart-cutting two-dimensional liquid chromatography combined with isotope ratio mass spectrometry for the determination of stable carbon isotope ratios of gluconic acid in honey," *Journal of Chromatography A*, vol. 1608, 2019, doi: 10.1016/j.chroma.2019.460421.
- [316] C. Armutcu, E. Özgür, T. Karasu, E. Bayram, L. Uzun, and M. Çorman, "Rapid Analysis of Polycyclic Aromatic Hydrocarbons in Water Samples Using an Automated On-line Two-Dimensional Liquid Chromatography," *An International Journal of Environmental Pollution*, vol. 230, no. 10, pp. 1-11, 2019, doi: 10.1007/s11270-019-4306-7.
- [317] Q. Li, F. Lynen, J. Wang, H. Li, G. Xu, and P. Sandra, "Comprehensive hydrophilic interaction and ion- pair reversed- phase liquid chromatography for analysis of di- to deca-oligonucleotides," *Journal of Chromatography A*, vol. 1255, pp. 237-243, 2012, doi: 10.1016/j.chroma.2011.11.062.
- [318] A. Goyon and K. Zhang, "Characterization of Antisense Oligonucleotide Impurities by Ion-Pairing Reversed-Phase and Anion Exchange Chromatography Coupled to Hydrophilic Interaction Liquid Chromatography/Mass Spectrometry Using a Versatile Two-Dimensional Liquid Chromatography Setup," *Analytical chemistry*, vol. 92, no. 8, pp. 5944-5951, 2020.
- [319] P. Álvarez Porebski and F. Lynen, "Combining liquid chromatography with multiplexed capillary gel electrophoresis for offline comprehensive analysis of complex oligonucleotide samples," *Journal of Chromatography A*, vol. 1336, pp. 87-93, 2014, doi: 10.1016/j.chroma.2014.02.007.
- [320] C. Anacleto, R. Ouye, and N. Schoenbrunner, "Orthogonal ion pairing reversed phase liquid chromatography purification of oligonucleotides with bulky fluorophores," *Journal of Chromatography A*, vol. 1329, pp. 78-82, 2014, doi: 10.1016/j.chroma.2013.12.072.
- [321] B. Koshel, R. Birdsall, and W. Chen, "Two-dimensional liquid chromatography coupled to mass spectrometry for impurity analysis of dye-conjugated oligonucleotides," *Journal of Chromatography B*, vol. 1137, 2020, doi: 10.1016/j.jchromb.2019.121906.

- [322] S. G. Roussis, I. Cedillo, and C. Rentel, "Two-dimensional liquid chromatography-mass spectrometry for the characterization of modified oligonucleotide impurities," *Analytical Biochemistry*, vol. 556, pp. 45-52, 2018, doi: 10.1016/j.ab.2018.06.019.
- [323] K. R. Wijeweera and S. R. Kodituwakku, "A simple algorithm for calculating the area of an arbitrary polygon," *Ruhuna Journal of Science*, vol. 8, no. 1, pp. 67-75, 2017, doi: 10.4038/rjs.v8i1.27.
- [324] J. Rozenski. "Mongo Oligo Mass Calculator v2.08." The RNA Institute, College of Arts and Sciences, State University of New York at Albany.  
<https://mods.rna.albany.edu/masspec/Mongo-Oligo> (accessed).
- [325] J. Baek, J. Thayer, S. Lin, and X. Liu, "Separation of Mixed-Base Oligonucleotides Using a High-Resolution, Reversed Phase Chromatography Column.," Thermo Scientific,  
<https://tools.thermofisher.com/content/sfs/brochures/AN-21476-LC-Mixed-Base-Oligonucleotides-AN21476-EN.pdf>, 2016.
- [326] A. Murakami, Y. Tamura, H. Wada, and K. Makino, "Separation and Characterization of Diastereoisomers of Antisense Oligodeoxyribonucleoside Phosphorothioates," *Analytical Biochemistry*, vol. 223, no. 2, pp. 285-290, 1994, doi: 10.1006/abio.1994.1586.
- [327] R. G. Pearson, "Hard and Soft Acids and Bases," *Journal of the American Chemical Society*, vol. 85, no. 22, pp. 3533-3539, 1963, doi: 10.1021/ja00905a001.
- [328] R. Bischoff and L. W. McLaughlin, "Chemically synthesized hydrophobic anion-exchange high-performance liquid chromatography supports used for oligonucleotide resolution by mixed mode chromatography," *Journal of Chromatography A*, vol. 270, no. C, pp. 117-126, 1983, doi: 10.1016/S0021-9673(01)96356-3.
- [329] P. Hong and K. J. Fountain, "Method Development for Size-Exclusion Chromatography of Monoclonal Antibodies and Higher Order Aggregates," Online: Waters Corporation, 2011. [Online]. Available: <https://www.waters.com/webassets/cms/library/docs/720004076en.pdf>
- [330] D. Bhattacharyya, G. Mirihana Arachchilage, and S. Basu, "Metal cations in G-quadruplex folding and stability," *Frontiers in chemistry*, vol. 4, p. 38, 2016.
- [331] F. Zappacosta, M. Huddleston, R. Karcher, and V. Gelfand, "Improved sensitivity for phosphopeptide mapping using capillary column HPLC and microionspray mass spectrometry: Comparative phosphorylation site mapping from gel-derived proteins," *Analytical Chemistry*, vol. 74, no. 13, pp. 3221-3231, 2002, doi: 10.1021/ac025538x.
- [332] J. Zhang, Y. Liu, A. Jaquins-Gerstl, Z. Shu, A. C. Michael, and S. G. Weber, "Optimization for speed and sensitivity in capillary high performance liquid chromatography. The importance of column diameter in online monitoring of serotonin by microdialysis," *Journal of Chromatography A*, vol. 1251, pp. 54-62, 2012, doi: 10.1016/j.chroma.2012.06.002.
- [333] A. F. G. Gargano, M. Duffin, P. Navarro, and P. J. Schoenmakers, "Reducing Dilution and Analysis Time in Online Comprehensive Two-Dimensional Liquid Chromatography by Active Modulation," *Analytical chemistry*, vol. 88, no. 3, pp. 1785-1793, 2016, doi: 10.1021/acs.analchem.5b04051.
- [334] D. R. Stoll, K. Shoykhet, P. Petersson, and S. Buckenmaier, "Active Solvent Modulation: A Valve-Based Approach To Improve Separation Compatibility in Two-Dimensional Liquid Chromatography," *Analytical chemistry*, vol. 89, no. 17, pp. 9260-9267, 2017, doi: 10.1021/acs.analchem.7b02046.
- [335] L. T. Taylor, "Packed column supercritical fluid chromatography of hydrophilic analytes via water-rich modifiers," *Journal of Chromatography A*, vol. 1250, pp. 196-204, 2012, doi: 10.1016/j.chroma.2012.02.037.
- [336] J. Zheng, J. D. Pinkston, P. H. Zoutendam, and L. T. Taylor, "Feasibility of supercritical fluid chromatography/mass spectrometry of polypeptides with up to 40-mers," *Analytical chemistry*, vol. 78, no. 5, pp. 1535-1545, 2006, doi: 10.1021/ac052025s.
- [337] J. A. Blackwell and R. W. Stringham, "Effect of Mobile Phase Components on the Separation of Polypeptides Using Carbon Dioxide-Based Mobile Phases," *Journal of High Resolution*

*Chromatography*, vol. 22, no. 2, pp. 74-78, 1999, doi: 10.1002/(SICI)1521-4168(19990201)22:2<74::AID-JHRC74>3.0.CO;2-9.

- [338] M. A. Patel, F. Riley, M. Ashraf-Khorassani, and L. T. Taylor, "Supercritical fluid chromatographic resolution of water soluble isomeric carboxyl/amine terminated peptides facilitated via mobile phase water and ion pair formation," *Journal of Chromatography A*, vol. 1233, pp. 85-90, 2012, doi: 10.1016/j.chroma.2012.02.024.